

City Research Online

City St George's, University of London

Citation: Bansod, P. (1973). A transient numerical method for computing the flow about ducted bodies in supersonic freestreams. (Unpublished Doctoral thesis, The City University)

This is the accepted version of the paper.

This version of the publication may differ from the final published version. To cite this item please consult the publisher's version.

Permanent repository link: https://openaccess.city.ac.uk/id/eprint/38348/

Copyright and Reuse: Copyright and Moral Rights remain with the author(s) and/or copyright holders. Copies of full items can be used for personal research or study, educational, or not-for-profit purposes without prior permission or charge, unless otherwise indicated, provided that the authors, title and full bibliographic details are credited, a hyperlink and/or URL is given for the original metadata page and the content is not changed in any way. For full details of reuse please refer to City Research Online policy.

City Research Online: http://openaccess.city.ac.uk/ publications@citystgeorges.ac.uk

A TRANSIENT NUMERICAL METHOD FOR COMPUTING THE FLOW ABOUT DUCTED BODIES IN SUPERSONIC FREESTREAMS

P. BANSOD, B.Sc.(Hons), D.I.C., M.Sc.(Eng).

The Department of Aeronautics,

The City University,

London EC1V 4PB

September 1973

59

(A Thesis submitted for the degree of Doctor of Philosophy).

THE CITY UNIVERSITY LIBRARY,
ST. JOHN STREET, LONDON, E.C.1.

CONTENTS

Chapter		Page
	TITLE	
	ACKNOWLEDGEMENTS	1.
	ABSTRACT	2.
	NOTATION	3.
Chapter 1	INTRODUCTION	6.
1.1.	Introduction	7.
1.2.	Statement of the Problem	7.
1.3.	General Characteristics of Flow about Blunt and Ducted bodies in Supersonic Flow.	8.
Chapter 2	SURVEY OF RELEVANT NUMERICAL METHODS	14.
2.1.	Transient Numerical Methods	15.
2.2.	Relaxation Methods	27.
2.3.	The Method of Direct Integrals	29.
2.4.	The Selection of a Numerical Method	31.
2.5.	A Brief Review of Transient Finite Difference Methods applied to Transonic Flow Problems	32.
Chapter 3	APPLICATION OF THE TRANSIENT FINITE DIFFERENCE METHOD	38.
3.1.	Finite Difference Methods for the Interior Points	39.
3.2.	Treatment of Boundary Points	44.
3.3.	Initial Values for Mesh A and Mesh B	58.
3.4.	Differences in the Computational Proceedures between the SUBIB and SUPIB Problem	60.
Chapter 4	DISCUSSION OF RESULTS	62.
4.1.	Supersonic Internal Boundary Results	63.
4.2.	Subsonic Internal Boundary Results	67.
4.3.	Comments on Computational Efficiency	75.
Chapter 5	CONCLUSIONS AND RECOMMENDATIONS FOR FUTURE WORK	80.
5.1.	Conclusions	81.
5.2.	Recommendations for Future Work	82.

Contents continued...

Chapter		Page
	REFERENCES	85.
	FIGURES (1) to (42)	98.
	APPENDICES	144.
Appendix A	Definitions and Derivations of Expressions for Inlet Drag	145.
Appendix B	Some Mathematical Aspects of the Numerical Solution of Hyperbolic Equations	149.
Appendix C	Derivation of the Characteristic and Compatibility Equations for Two and Three Independent Variables	159.
Appendix D	The Computer Program	166.

ACKNOWLEDGEMENTS

The author gratefully acknowledges the advice and encouragement received from his supervisor Dr. M.M. Freestone. This research benefited considerably through numerous interesting discussions over a period of three years.

Thanks are also due to [redacted] for her patience and care in typing this thesis.

The financial support for this research was obtained through a City University Research Studentship.

ABSTRACT

A transient finite-difference method was developed to compute the transonic flow about blunt lipped ducted bodies in supersonic free streams. Moretti's second order accurate and explicit method was adapted for the computation of the interior regions and a transient method of characteristics was used at the boundaries. The flow velocity at the internal boundary of the ducted body was subsonic or supersonic as required. For the subsonic internal boundary case, the internal boundary was specially treated so as to enable the mass flow ratio and/or the axial velocity component to be prescribed.

Results were presented for the Mach number range $1.82 \leq M_\infty \leq 3.0$. Three inlet shapes were investigated for axisymmetric and two-dimensional flows: two circular section inlets and a symmetric elliptic section. The external drag, cowl drag, additive drag and total pressure recovery were also calculated.

Computer Programs were written in FORTRAN for use on CDC 6600 and CDC 7600 digital computers.

NOTATION

a — speed of sound

ACCT — accumulative time step $\sum \Delta T$

BOA — radial position of inlet surface node point, Mesh A

BOB — radial position of inlet surface node point, Mesh B

BOC — ordinate of inlet surface, Mesh C

C_{DADD} — additive drag coefficient

C_{DCOWL} — cowl drag coefficient

C_{DEXT} — external drag coefficient

CPU — Central Processor Unit Time (seconds)

CFL — Courant-Freidrichs-Lewy stability condition

C_p — pressure coefficient, $(p-p_\infty)/(\frac{1}{2}\gamma p_\infty M_\infty^2)$

Co-ordinate directions in the computational planes:-

ZA YA — Mesh A

ZB YB — Mesh B

Z X — Mesh C

CONCRIT — convergence criterion based on the movement of the bow shock in the time increment ΔT

D — detachment distance between inlet surface and shock wave or axis of symmetry

D_{ADD} — additive drag

$\frac{D}{Dt}$ — $\frac{\partial}{\partial t} + (\underline{Q} \cdot \nabla)$

E — internal energy

g — denotes any dependent variable

H — highlight height (defined in Fig 4)

j — set equal to unity for axisymmetric flow or equal to zero for two dimensional flow

k — number of time steps

K_{RUN} — total number of time steps

MOC — method of characteristics

$\dot{m}$ mass flow rate

MFR mass flow ratio (see Fig.4)

M Mach number

N number of strip using the Method of Direct Ingegrals

p pressure (non-dimensional) normalized with respect to $\bar{p}_\infty$

P $\log_e$ (p)

P_R total pressure recovery

P_O total pressure

$\underline{Q}$ local velocity of the air stream

R $\log_e$ (ρ)

R_H non-dimensional radius of the circular inlet lip (see Fig 4)

R_S radius of curvature of the bow shock

S entropy function ($S = P - \gamma R$)

SH radial position of the shock node point

SHX radial position of the axis node point

SUBIB Subsonic Internal Boundary

SUPIB Supersonic Internal Boundary

SF safety factor

t, T non-dimensional time in physical and computational planes respectively; normalized with respect to $H (\bar{\rho}_\infty / \bar{p}_\infty)^{\frac{1}{2}}$

t_H non-dimensional inlet thickness (see Fig 4)

Velocity components:-

(normalized with respect to $\bar{a}_\infty / \sqrt{\gamma}$)

u, v radial $\overset{(r)}{\wedge}$ and angular $\overset{(\theta)}{\wedge}$ velocity components for Mesh A and Mesh B

U, V ξ and η components for the MOC and also x, y components (Appendix C)

W radial shock velocity

Greek Symbols

α (a) characteristic surface

(b) angle between the radial line and the tangent to the inlet surface and

(c) angle of incidence (Table 1)

γ ratio of specific heats

Δ (a) increment

(b) shock detachment distance (Fig (3)(a) and Fig (4))

ϵ computational efficiency parameter

θ_A angle θ for the radial line passing through point A (see Fig 15, a constant)

θ_B angle θ for the radial line BE ($\theta_B = \theta_B(t)$, $\theta_B = \theta_E$)

θ_C angle θ for the radial line passing through point C (a constant)

$\Delta\theta_A$ angular mesh width for Mesh A

$\Delta\theta_B$ angular mesh width for Mesh B

$\bar{\theta}$ parametric angle used in the MOC

μ Mach angle

ρ density (non-dimensional), normalized with respect to $\bar{\rho}_\infty$

σ (a) angle between the radial line and the tangent to the bow shock

(b) $\theta_B - \theta_A$ or $\theta_C - \theta_B$

ψ (a) angle between the tangent to the inlet surface and the free-stream direction

(b) angle between the tangent to the shock wave and to the free-stream direction

ϕ_i value of $\bar{\theta}$ in the $T_o + \Delta T$ plane

ϕ small perturbation potential (relaxation method)

λ ratio of semi-major to semi-minor axis of ellipse

Suffices

∞ freestream conditions

$(\ )_N$ $T_o + \Delta T$ plane

Superscripts

$(\overline{\ \ })$ physical variable

CHAPTER 1

INTRODUCTION

1.1. Introduction

In recent years there has been a resurgence of interest in transonic aircraft. In the United States this interest has been encouraged in the case of commercial aircraft by the environmentalist lobby regarding the sonic boom created by supersonic transports. It is known that aircraft flying in the stratosphere up to Mach numbers of 1.2 do not usually create a sonic boom at sea level. This is due to the attenuation of the bow shock wave because the speed of sound is smaller in the stratosphere than at sea-level. Ref (1) to Ref (6) are papers devoted to the preliminary design study of the next generation of transonic aircraft. These papers evaluate the technical feasibility of aircraft flying in the range $0.9<M_\infty<1.2$. At slightly higher Mach numbers in the range $1.4<M_\infty<1.6$, consideration is also being given to asymmetric wing configurations pioneered by Jones, Ref (6). Aircraft designed to cruise at $M_\infty<1.5$ could use Pitot air-intakes because the total pressure recovery P_R, is approximately equal to that occurring through a normal shock at the same M_∞(see Ref (104), Fig (7)) and is within acceptable limits. Aircraft cruising in the Mach number range $2.0<M_\infty<3.0$, normally use additional compression surfaces such as centre-bodies and movable ramps to enhance their pressure recovery performance Fig (1) (b) and (c). Due to local flow separation effects on sharp inlets at subsonic Mach numbers, most inlets are usually blunted to improve their subsonic performance. An example of this can be found in Ref (7). Dobson Ref (8), reported that rounded inlet lips can give a drag reduction as compared to sharp inlet lips at $M_\infty = 1.5$. The work presented in this thesis is devoted to the prediction of the flow about two-dimensional and axisymmetric blunt lipped air inlets in supersonic freestreams: essentially ducted bodies.

1.2. Statement of the Problem

Fig (2) shows a sketch of a high by-pass ratio engine immersed in a supersonic air-stream. The problem is to predict the flow about a region of this configuration bounded by the bow shock D E and the cowl lip. The

computation is terminated at a convenient subsonic boundary C F internally and a supersonic boundary A D externally. The regions down-stream of boundaries A D and C F are not computed in this work. Refs(9), (10) and (11) use the method of characteristics (MOC) to compute supersonic flow about two dimensional and axisymmetric sharp lipped inlets. Once the flow properties on A D are known, such methods could be used to compute the supersonic flow downstream of A D. The flow upstream of the bow shock is assumed to be uniform i.e. the effects of centre bodies or compression ramps such as shown in Fig (1) (b) and (c) are neglected. The two dimensional inlet (a), is within the scope of this work. The gas flow (air) in the region of computation is taken to be ideal, inviscid and adiabatic, with a specific heat ratio of 1.4. The computational method is required to compute the position and shape of the bow shock D E and all the flow variables within boundaries D E, E F, C F and A C. The free-stream Mach number M_∞ and the inlet geometry will be specified. When the internal flow at boundary C F is subsonic the problem will be referred to as the Subsonic Internal Boundary Problem, abbreviated as SUBIB. In this case the mass flow or axial velocity across C F is also specified. When the internal flow is supersonic the problem will be referred to as the Supersonic Internal Boundary Problem, abbreviated as SUPIB. The mass flow is not then specified but is calculated as part of the solution.

1.3. General Characteristics of Flow about Blunt and Ducted Bodies in Supersonic Air-streams

In the last two decades the experimental study of the flow about blunt shaped axisymmetric and two-dimensional bodies has received much attention; Refs (12), (13), (14), (15) and (16). The main features of ideal gas flow about blunt bodies, often referred to as the detached shock wave problem, are well known. There are qualitative similarities in the flow characteristics about blunt bodies and blunt lipped ducted bodies immersed in supersonic streams. It is the purpose of this section to present a simple physical model for the supersonic flow about ducted bodies, based

on the experimental and theoretical studies made by other workers in this field.

For typical blunt bodies with elliptical or hemispherical forebodies, Fig (3) (a), we note the following:-

a) The detached shock wave position varies with both shape of the body and free stream, Mach number. If λ is defined as the ratio of major to minor axis of the ellipse ($\lambda = 1$ for a spherical cap or circle),for a given Mach number M_∞, the shock detachment distance Δ(defined in Fig.(3) (a)), increases with increasing bluntness i.e. with decreasing λ. For a given forebody shape, Δ increases with decreasing M_∞.

b) The region behind the detached shock wave is divided into a subsonic region and a supersonic region. Fig (3) (a) shows a sonic line (a contour of Mach number = 1.0) which spans the region between the bow shock wave and the body surface.

c) On the cylindrical afterbody A - $\acute{A}$, the freestream pressure is reached asymptotically with distance away from the junction with the forebody. In the Mach number range $1<M_\infty<3$, most blunt bodies with parallel afterbodies such as the hemisphere cylinder, have junction pressures less than the asymptotic afterbody pressures, i.e. an over expansion occurs . A recompression shock occurs in the region immediately down stream of the point A thus enabling the asymptotic pressures to be reached further downstream on the afterbody. The recompression region varies in intensity depending on the free stream Mach number and λ. At Mach number greater than 3, Traugott Ref (16), noticed that junction pressures were higher than the asymptotic limit i.e. under expansions occured.In this case no shock waves downstream of the junction were noticed.

From the point of view of numerical analysis, the geometry of the sonic line is of some importance. A study of some of the features of the flow in the vicinity of the sonic line has been presented in Refs.(16), (17) and (18). Some numerical methods incur difficulties in the region of the sonic line which are related to the fact that the sonic line is a boundary across

which the mathematical nature of the basic partial differential equations governing the steady flow change; they are elliptic in the subsonic region and hyperbolic in the supersonic region.

Hayes and Probstein Ref (19) derived simple analytical expressions which contribute towards the understanding of the sonic line geometry at the point of its intersection with the shock wave and the body surface. Fig (3)(b) illustrates the details of the flow in the vi cinity of the sonic line. The angle w_b which the sonic line makes with the body is usually acute for spherical forebodies at low Mach numbers. At higher Mach numbers exceeding 2.5, w_b could be obtuse especially for bodies which have a large radius of curvature.

At the sonic point on the bow shock, the shock makes an angle ψ_s with the free stream direction. If the radius of curvature of the shock R_s is approximately constant up to the sonic point, then the distance of the sonic point above the axis, is proportional to $R_s \cos\{\psi_s\}$. Albone Ref (69) shows a curve of ψ_s against M_∞. From a minimum value of about 62° at about Mach 1.7, the variation of ψ_s is very rapid as M_∞ approaches unity, at which point $\psi_s = 90^\circ$. As y_s increases with M_∞ tending towards unity, the radius of curvature R_s must increase rapidly so that the product $R_s \cos\{\psi_s\}$ must increase. These effects as noted above have been observed experimentally and are manifested by bow waves with larger values of Δ and larger radii of curvature as M_∞ is reduced.

In the region downstream of the sonic line, the flow is supersonic and hence the disturbances propagate along characteristic lines. The Mach lines are locally tangential to the characteristic lines and make angles $\mu = \pm \sin^{-1}(1/M)$ with the flow direction. Downstream of the sonic line, the Mach lines and hence the characteristics are nearly normal to the flow direction. It is possible for them to intersect the sonic line and hence influence the upstream subsonic region. The locus of points representing

the furthest down stream points from which this can happen is sketched in Fig (3)(b) and is called the Limiting Characteristic. In Fig (2) when terminating the region of computation at boundary A D, it is necessary to include the limiting charactertistic within the computed region so that points on the supersonic boundary A D do not influence the upstream region.

Molder Ref (18), shows (using intrinsic co-ordinates) that the ratio of the two characteristic strengths is negative when the local Mach number is unity. Thus the expansion waves emanating from the supersonic region reflect off the sonic line as compression waves which cause a rise in pressure on the afterbody A - Á. These compression waves originating from the sonic line can often coalesce to form a recompression shock as observed experimentally by Traugott Ref (16). At low Mach numbers the sonic line extends further away from the axis and thus there are more expansion waves reflected as compression waves and hence a stronger recompression shock is possible at lower Mach numbers.

Due to the weakening of the shock wave with respect to distance away from the axis, the streamlines which intersect the sonic line have an increasing value of total pressure with distance from the body surface, Fig (3)(b). In situations such as this, Hunt Ref (17) showed that it is possible (with $M_\infty > 1.6$) for the sonic line to generate expansion waves which weaken the shock just down stream of the sonic point on the shock. The bow shock is also weakened by expansion waves emanating from the body surface. These waves in turn reflect back towards the afterbody as compression waves.

When using the blunt body flow as a model for understanding the flow about blunt lipped ducted bodies the effect of mass flow through the internal boundary C F Fig (4), needs to be taken into account. The mass flow is conventionally defined in terms of the mass flow ratio MFR, which is the ratio of the mass flow through the internal boundary C F (Fig (4)(a))to the mass flow through a hypothetical streamtube bounded by the line P L. L is the leading edge of the cowl.

$$\text{Thus MFR} = \int_F^C \frac{\bar{v}_i\,\bar{\rho}_i\,(2\pi y)^j}{\bar{U}_\infty\,\bar{\rho}_\infty\,\pi\,(H)^{1+j}}\,dy$$

$$= \int_F^C \left(\frac{\bar{v}_i}{\bar{U}_\infty}\right)\left(\frac{\bar{\rho}_i}{\bar{\rho}_\infty}\right)\frac{(2y)^j}{(H)^{1+j}}\,dy \qquad \text{——(1)}$$

Point L is at a unit distance (H=1) above the axis of symmetry hence if Q - S is the stagnation streamline, the distance of Q above the axis of symmetry is in fact the MFR for two dimensional flow and equal to $\sqrt{\text{MFR}}$ for axisymmetric flow. With MFR equal to unity there is no spillage of air mass and the stagnation streamline intersects the leading edge L. In this case the shock wave is very close to the leading edge. With a sharp inlet the shock wave is usually attached at unit MFR. If M_∞ is kept constant and the MFR reduced, the stagnation point moves towards point C. The axial velocity component v_i can be calculated using a method which will be outlined later. Hence MFR = 0 corresponds to v_i=0 along F-C. In this case the axis of symmetry and F-C comprise the stagnation streamline. For a given M_∞ and cowl lip geometry, Δ is largest when MFR is zero. The position of the point of intersection Q with the bow shock varies with the MFR hence the stagnation streamline (body surface included) is not necessarily the streamline of maximum entropy as is the case with the blunt body problem. In practice the MFR varies between 0.6 and 0.8 for most engine operating conditions.

Figs (5)(a) and (b) show the flow about ducted bodies with supersonic and subsonic internal boundaries. Conjectured positions of the stagnation streamline Q-S, the sonic line and the limiting characteristic are also shown. Since the MFR influences the bow shock wave shape and stagnation point position, the sonic line, limiting characteris tic and the recompression region must also be correspondingly affected. The general flow characteristics observed with blunt bodies can only be qualitatively carried over to the ducted body case even with the same lip section geometry and M_∞ .

In the case of the SUBIB problem, specification of the MFR, M_∞ and lip geometry, define a unique flow field. This is not necessarily true for the SUPIB problem. Consider the flow about sharp lipped inlets with supersonic internal flow, Fig (6)(a) and (b) reproduced from Chernyi Ref (20).

Case (a) is realized by approaching the final M_∞ gradually from low values of velocity. Case (b) is realized if the same body is first rapidly brought up to a high velocity and then the velocity gradually decreased to the same M_∞ as case (a). Using one dimensional theory Ferri Ref (21) explains this phenomenon. A similar situation is possible with blunt lipped inlets. The continuosly curved shock case (c) corresponds to the detached shock of case (a). Corresponding to case (b), the blunt lip inlet in case (d) attempts to swallow the shock and produces a Mach interaction at the axis. Hence two solutions are possible for the same lip geometry and freestream conditions, depending on the starting conditions or in terms of numerical analysis 'Initial Conditions'.

Regarding the SUPIB problem, only the solutions for case (c) with the continuously curved shock have been attempted in this thesis.

In summary, there is a fair deal of similarity between the supersonic flow about blunt bodies and ducted blunt lipped bodies. Bearing in mind the remarks about the entropy on the body surface, the MFR, and the starting conditions for the SUPIB problem, there is evidence to believe that numerical methods which have been successfully applied to the blunted body would achieve similar accuracy when applied to the ducted body problem. In the next chapter four numerical methods are presented and their ability to predict transonic flow fields is discussed.

CHAPTER 2

SURVEY OF RELEVANT NUMERICAL METHODS

In the introduction it was shown that the flow about ducted bodies immersed in supersonic flow, involves subsonic and supersonic flows adjacent to one another. If the gas is assumed to be steady, inviscid, compressible and adiabatic the partial differential equations governing the flow are elliptic in the subsonic regions and hyperbolic in the supersonic regions. This feature is often referred to as a mixed flow problem or a transonic flow problem. Cole Ref (22) and more recently Yoshihara Ref (23) reviewed analytical and numerical methods for the transonic supercritical aerofoil problem. Serra Ref (88) contains an extensive review of transonic flow in nozzles. The detached shock wave occurring in the present problem makes it similar to theblunt body problem, i.e. a blunt body in a supersonic freestream. However as it can be seen from Fig (5) the problem involves both internal and external flows. Numerical methods for both internal flows (nozzles and ducts) and external flows (blunt bodies and aerofoils) are of relevance here particularly from the point of view of the variety of boundaries which occur in the present problem.

2.1. Transient Numerical Methods

The numerical approach to most steady state transonic flow problems is simplified by considering the fluid motion to be variant with time. The steady state is reached assymptotically in time. Adopting this point of view the governing equations of motions (see Ashley and Landahl, Ref (120)) are as follows:-

Equation of Continuity

$$\frac{D\bar{\rho}}{Dt} + \bar{\rho}\nabla.(\underline{Q}) = 0 \qquad - (2)$$

Momentum Equation

$$\frac{D\underline{Q}}{Dt} + \frac{1}{\bar{\rho}}\nabla\bar{p} = 0 \qquad - (3)$$

Conservation of Entropy (along a particle path)

$$\frac{D\bar{S}}{Dt} = 0 \qquad - (4)$$

The advantage of the time dependent or transient method is that the

above equations are hyperbolic throughout the regions of interest. This homogeneity in the nature of the partial differential equations, gives transient numerical method its powerful simplicity when applied to transonic flow problems.

The solution of the above equations presents itself as an Initial Value Problem. The equations are numerically integrated with respect to time. Fig.(7) depicts a flow diagram which shows the sequence of computation for a typical transient numerical method. The first time step of the solution starts from a set of initial conditions which are estimated using empirical formulae and also incorporate some fixed boundary conditions such as upstream Mach number. A time step Δt is computed from the given data the size of which is governed by a stability condition which is discussed later. Variables on the boundaries and the interior regions are integrated with respect to time t by a numerical solution of equations (2) to (4). Hence new values of variables in the $t_o + \Delta t$ plane are produced from those in the initial t_o plane. These values are checked against previous values in the t_o plane and if the values are found to be invariant with time (within given limits of accuracy) the solution is assumed to have converged and the computation is terminated. If the convergence criterion is not satisfied the new values in the $t_o + \Delta t$ are reset to form initial values in the t_o plane for the next time step, and the whole process is repeated until convergence is obtained.

The two widely accepted numerical methods for solving the equations (2) to (4) are, (1) The Transient Method of Characteristics (MOC) and (2) Transient Finite-Difference Methods.

2.1.1. The Method of Characteristics (MOC) for Transient Two-Dimensional and Axisymmetric Flows

The classical theory of the MOC is adequately covered by Courant and Hilbert Ref (24) and papers by Rusanov Ref (25) and Sauerwein Ref (31). Special applications to fluid dynamic problems are found in Ferri Ref (26), Fox Ref (27) and Von Mises Ref (28).

Equations (2) to (4) can be expressed alternatively using tensors in the form (see Ref (31)),

$$A_{ijk} \frac{\partial u_k}{\partial x_i} + B_j = 0 \qquad - (5)$$

which represent a set of quasi-linear partial differential equations (i.e. the highest order of derivatives to appear are only in the first degree). u_k represents the dependent variables and x_i the independent variables A_{ijk} and B_j are functions of u_k and x_i. Consider a transformation to a new set of co-ordinates α_m : equation (5) can now be expressed as,

$$A_{ijk} \frac{\partial u_k}{\partial \alpha_m} \frac{\partial \alpha_m}{\partial x_i} + B_j = 0$$

If α_1 = constant is the characteristic surface i.e. a surface along which discontinuities in the derivatives $\frac{\partial u_k}{\partial \alpha_1}$ propagate, then α_1 is given by the condition, (see Appendix C)

$$\det \left\{ A_{ijk} \frac{\partial \alpha_1}{\partial x_i} \right\} = 0$$

Typically for the case of cylindrical co-ordinates $\alpha_1 = \alpha_1(x,y,t)$ and u_k with $k = 1,2,3$ represents the dependent variables U, V and P respectively. The local Mach cone is illustrated in Fig (8)(b). If O Q is a particle path then from the geometry of the figure it can be seen that the Mach cone has the following equation,

$$(U\,dt - dx)^2 + (V\,dt - dy)^2 = (a\,dt)^2$$

which is satisfied by

$$dx = (U + a\cos\bar{\theta})\,dt \qquad (a)$$

$$dy = (V + a\sin\bar{\theta})\,dt \qquad (b) \qquad - (6)$$

where $\bar{\theta}$ (a parametic angle) is a function of t. At point Q, Fig (9)(b) the Mach cone is tangential to the Mach conoid. The lines of contact between the characteristic surface and the Mach conoid in Fig (9)(a) are called bi-characteristics.

Partial differential equations can be derived (Appendix C equation (C-32)) which hold along these bi-characteristics and take the form,

$$\frac{\partial P}{\partial t} + \frac{\gamma \cos\bar{\theta}}{a}\frac{\partial U}{\partial t} + \frac{\gamma \sin\bar{\theta}}{a}\frac{\partial V}{\partial t}$$

$$= -\gamma\left\{\frac{\partial U}{\partial x}\sin^2\bar{\theta} + \frac{\partial V}{\partial y}\cos^2\bar{\theta} - \sin\bar{\theta}\cos\bar{\theta}\left(\frac{\partial U}{\partial x} + \frac{\partial V}{\partial y}\right) + j\frac{V}{y}\right\} \quad - (7)$$

Equation (7) holds along bi-characteristics defined by equation (6) and can be used to relate dependent variables in the $t_o + \Delta t$ plane to known conditions in the initial time plane t_o. Thus the MOC produces a solution for equations (2) to (4) by solving equation (7). Additional equations are produced by varying $\bar{\theta}$ hence integrating along a different bi-characteristic each time. Usually three or more bi-characteristics are used along with equation (4) to solve for the four dependent variables and some derivatives occurring in the $t_o + \Delta t$ plane.

The developement of a Mach conoid in the increasing time direction can be understood by observing a ripple in a moving stream. The ripple changes shape with time and also moves in the general direction of the current. The Mach conoid can be imagined to be a three-dimensional envelope of the ripples formed if the origin of the disturbance was at point Q (Fig 9(b)) in the $t_o + \Delta t$ plane. For any t = constant plane, where $t > t_o + \Delta t$ the 'Region of Influence' defines the boundary of the region which is influenced by disturbances orginating at Q.

The same characteristic conoid extends to the initial time plane t_o. The 'Domain of Dependence' is a region in the t_o = constant plane. This region contains points such as A which have Q within their respective 'Regions of Influence'. Hence points outside the boundaries of the Domain of Dependence cannot influence point Q.

Courant, Freidrichs and Lewy Ref (29) determined a stability condition (CFL condition) for linear hyperbolic equations. This condition states that the stability of the differencing scheme is assured if the 'Domain of Dependence' of the differential equations is contained within the 'Domain of Dependence' of the difference scheme. This is illustrated in Fig (10) for polar and cartesian co-ordinates. A-B-C-D define the 'Domain of Dependence' of the difference scheme in the t_o plane, P - Q and Q - R

are bi-characteristics. Both these schemes satisfy the CFL condition. The nine node points centred about point 0 are used in interpolation routines to evaluate the flow properties at P and R.

P - Q and Q - R are two of the infinite number a bi-characteristics that can be chosen. This freedom of choice of the directions of integration and consequently the differential equations themselves, has given rise to a variety of successful schemes. The literature on the MOC for three independent variables is extensive. Sauerwein Ref (30) Chushkin Ref (33) and more recently Ransom Ref (34) are examples of papers which contain reviews on the subject. However the three independent variable MOC are often plagued with stability problems. Leigh and Hui Ref (35) showed that apart from the CFL condition a more stringent von Neumann stability condition is also required. The von Neumann condition (discussed in Appendix B) governs the manner in which interpolations in the initial time plane to are carried out and also the difference scheme used to integrate equation (7).

Sauerwein solves the problem of unsteady flow about a circular cylinder at Mach 5. The problem inherent in most MOC schemes is that the unequal time steps are used at each point in the initial time plane. Hence Sauerwein (1967) uses orthogonal polynomials to give a second degree least squares fit for three independent variables, (x,y,t). The work shows considerable complexity and programming effort. The scheme is first order accurate in Δt (i.e. leading truncation errors are $0(\Delta t^2)$).

Carriere and Capelier Ref (36), Brunk and Haack Ref (37) and Osnaghi and Macchi Ref (38) used natural co-ordinate systems (i.e.parallel and normal to the local flow direction). Carriere and Capelier attempted to compute the flow about an aerofoil at Mach 0.4 but the computation was terminated due to prohibitive computational time. Osnaghi and Macchi solved a variety of internal isentropic flow problems. The co-ordinate system was stretched so as to give a fine mesh size in the regions of interest and a coarse mesh in the upstream direction where prescribed boundaries

occurred. Of particular interest is the solution for the flow field occurring when the primary and secondary flow meet separated by a slip stream in the exhaust of a high by-pass fan jet. The subsonic boundaries are treated by the MOC rather like the interior points, however one variable (pressure) was specified. Good agreement with experimental results was observed.

Butler Ref (39) made a significant contribution by introducing a second order accurate scheme. Equation (7) was integrated using a modified Euler method. In this method the coefficients of the time derivatives and the terms on the right hand side were averaged over the time interval The computation of each point is repeated until a convergence limit is satisfied thus insuring the error is of second order. Unlike most other workers, Butler allowed for the deviation in geometry between the Mach cone and the characteristic conoid in determining the co-ordinates of the base of each bi-characteristic in the t_o plane. This refinement increased the overall accuracy of the solution. Butler proposed a scheme for treating shock fronts in unsteady flow moving into uniform and non-uniform flow. The schemes involve integration along four and eight bi-characteristics respectively. Richardson Ref (40) presents a simplified account of Butler's work. Elliot Ref (41), whose work is also reported in Ref (40), proposed a modification of Butler's methods for unsteady shock fronts which uses only one bi-characteristic. Ransom Ref (34) adapted Butler's scheme to compute three-dimensional supersonic flow in nozzles and inlets (internal flow only).

2.1.2. Transient Finite Difference Methods

Before describing the difference schemes, attention needs to be drawn to the two basic forms of the differential equations associated with inviscid, compressible and adiabatic flow: the conservation form and the non-conservation form. Derivations of general expressions for the conservation form in arbitary curvilinear co-ordinate systems are given in Anderson Ref (42). These equations in two dimensional cartesian co-ordinates

can be expressed as follows:-

Conservation of Mass

$$\frac{\partial \bar{\rho}}{\partial t} + \frac{\partial(\bar{\rho}\bar{u})}{\partial x} + \frac{\partial(\bar{\rho}\bar{v})}{\partial y} = 0 \qquad (a)$$

Conservation of 'x' momentum

$$\frac{\partial(\bar{\rho}\bar{u})}{\partial t} + \frac{\partial(\bar{\rho}\bar{u}^2 + \bar{p})}{\partial x} + \frac{\partial(\bar{\rho}\bar{u}\bar{v})}{\partial y} = 0 \qquad (b) - (8)$$

Conservation of 'y' momentum

$$\frac{\partial(\bar{\rho}\bar{v})}{\partial t} + \frac{\partial(\bar{\rho}\bar{u}\bar{v})}{\partial x} + \frac{\partial(\bar{\rho}\bar{v}^2 + \bar{p})}{\partial y} = 0 \qquad (c)$$

Conservation of Energy

$$\frac{\partial}{\partial t}\left[\bar{E} + \bar{\rho}\left(\frac{\bar{u}^2+\bar{v}^2}{2}\right)\right] + \frac{\partial}{\partial x}\left[\bar{u}\left(\bar{E} + \bar{p} + \bar{\rho}\left(\frac{\bar{u}^2+\bar{v}^2}{2}\right)\right)\right] + \frac{\partial}{\partial y}\left[\bar{v}\left(\bar{E} + \bar{p} + \bar{\rho}\left(\frac{\bar{u}^2+\bar{v}^2}{2}\right)\right)\right] = 0 \qquad - (d)$$

(where $\bar{E}$ is the internal energy)

Each spatial derivative contains terms which are conserved through a normal shock (shock normal to the direction of differentiation). Hence the equations are said to be in Conservation form. As quantities such as mass, momentum and energy are conserved in each spatial direction, the Rankine - Hugoniot relations are satisfied automatically. It is advantageous to use the Conservation form of equations in situations where the position of embedded shock waves is not known a priori.

The Non-Conservative form can be obtained by expanding terms in equations (8) as follows:-

$$\frac{\partial \bar{\rho}}{\partial t} + \bar{u}\frac{\partial \bar{\rho}}{\partial x} + \bar{\rho}\frac{\partial \bar{u}}{\partial x} + \bar{\rho}\frac{\partial \bar{v}}{\partial y} + \bar{v}\frac{\partial \bar{\rho}}{\partial y} = 0 \qquad (a)$$

$$\frac{\partial \bar{u}}{\partial t} + \bar{u}\frac{\partial \bar{u}}{\partial x} + \bar{v}\frac{\partial \bar{u}}{\partial y} + \frac{1}{\bar{\rho}}\frac{\partial \bar{p}}{\partial x} = 0 \qquad (b) - (9)$$

$$\frac{\partial \bar{v}}{\partial t} + \bar{u}\frac{\partial \bar{v}}{\partial x} + \bar{v}\frac{\partial \bar{v}}{\partial y} + \frac{1}{\bar{\rho}}\frac{\partial \bar{p}}{\partial y} = 0 \qquad (c)$$

Instead of expanding the energy equation, (8d), the Conservation of entropy along a particle path, equation (4), can be used to provide the fourth equation

$$\frac{\partial \bar{S}}{\partial t} + \bar{u}\frac{\partial \bar{S}}{\partial x} + \bar{v}\frac{\partial \bar{S}}{\partial y} = 0 \qquad (d) - (9)$$

The finite difference solution of equations (8) and (9) can be split up into two parts: the computation of interior points and the computation of boundary points. However there are some boundary evaluation procedures which allow the boundary points to be treated as interior points depending on the nature of the boundary.

2.1.3. Difference Schemes for Interior Points

It is often convenient to non-dimensionalize the dependent variables in equations (8) and (9) and transform the physical plane into a computational plane which is a unit square as shown in Fig (12). The differential equations are then integrated with respect to time T if initial values in the T_o computational plane are known. Schemes in which the new values in the $T_o + \Delta T$ plane are directly dependent on the initial values in the T_o plane, are called Explicit difference schemes. Such schemes require no iteration when the equations are integrated from one time plane (or level) to another. The present work is concerned only with explicit schemes for the interior points. Fig (13) shows the basic elements of a finite difference scheme. The Z and Y computational co-ordinates are broken up into m and n mesh lengths. A solution is sought for each interior point such as A. Hence, if g_{ij}^{k} is any dependent variable at point A, a second order Taylor series expansion gives:-

$$g_{ij}^{k+1} = g_{ij}^{k} + \left(\frac{\partial g}{\partial T}\right)_{ij}^{k} \Delta T + \frac{1}{2}\left(\frac{\partial^2 g}{\partial T^2}\right)_{ij}^{k} \Delta T^2 + \cdots + O(\Delta T)^3 \qquad - (10)$$

where k denotes the time level and (i,j) is any general point as defined in Fig (13). From equations (8) and (9) it can be seen that the time derivatives can be obtained explicitly in terms of the space derivatives which are evaluated as shown in Fig (13) for point (i,j).

Four difference schemes which have found wide applications in the field of transonic aerodynamics are described below using for simplicity a one dimensional linear equation of the form,

$$\frac{\partial g}{\partial T} + \frac{\partial g}{\partial Z} = 0 \qquad - (11)$$

Most difference schemes are based on evaluating the first three terms of the Taylor's series expansion, equation (10). Hence they are second

order accurate with a truncation error of the order of $\left[(\Delta T)^2, (\Delta Z_i)^2\right]$ (see Appendix B).

2.1.3.1. Moretti Scheme

This scheme was originally defined in a paper by Moretti and Abbett Ref (64) and involves a direct substitution of the time derivatives in terms of central spatial differences defined in Fig (13). For any point i,

$$\left(\frac{\partial q}{\partial T}\right)_i^k = -\left(\frac{\partial q}{\partial Z}\right)_i^k \approx -\left(q_{i+1}^k - q_{i-1}^k\right)/(2\Delta Z) \qquad - (12a)$$

$$\left(\frac{\partial^2 q}{\partial T^2}\right)_i^k = -\left(\frac{\partial^2 q}{\partial Z \partial T}\right)_i^k = -\left(\frac{\partial^2 q}{\partial T \partial Z}\right)_i^k = \left(\frac{\partial^2 q}{\partial Z^2}\right)_i^k$$
$$\approx \left(q_{i+1}^k + q_{i-1}^k - 2q_i^k\right)/(\Delta Z)^2 \qquad - (12b)$$

Hence substituting (12a) and (12b) into (11),

$$q_i^{k+1} = q_i^k - \left(q_{i+1}^k - q_{i-1}^k\right)\Delta T/(2\Delta Z) + \left(q_{i+1}^k + q_{i-1}^k - 2q_i\right)\Delta T^2/(2\Delta Z^2) \qquad - (13)$$

The Moretti scheme is second order accurate and uses the non-conservative form of equations. The time step is restricted by the CFL condition.

2.1.3.2. Lax-Wendroff (2-Step)

The conservative form of the equations are used in this scheme.

1st. Step

$$\bar{q}_i = \frac{1}{2}\left(q_{i-1}^k + q_{i+1}^k\right) + \left(\frac{\partial q}{\partial T}\right)_i^k \Delta T \qquad - (14a)$$

here $\left(\frac{\partial q}{\partial T}\right)_i^k$ is as defined in (12a).

2nd. Step

$$q_i^{k+1} = q_i^k + \frac{\Delta T}{2}\left\{\left(\frac{\partial q}{\partial T}\right)_i^k + \left(\overline{\frac{\partial q}{\partial T}}\right)_i\right\} \qquad - (14b)$$

where $\left(\overline{\frac{\partial q}{\partial T}}\right)_i = -\left\{\left(\bar{q}_{i+1} - \bar{q}_{i-1}\right)/(2\Delta Z)\right\}$

There are several versions of the Lax-Wendroff scheme. The particular version presented here is due to Barnwell Ref (77) and (78). Barnwell used this scheme to calculate the supersonic flow about blunt bodies with sharp corners. Embedded shock waves were smeared through several mesh lengths due to the 'artificial viscosity' terms occurring in the truncation errors of the difference scheme. Often stabilizing terms have to be added which take the form of fourth order terms. The nature of these terms and the largest permissible size of ΔT are determined by a von Neumann stability analysis (see Appendix (B)).

2.1.3.3. MacCormack Scheme

This scheme was first reported by MacCormack Ref (43) and is similar to the two step version of the Lax-Wendroff scheme but it uses forward and backward differences (see Fig (13)) for the spatial derivatives.

1st.Step

$$\left(\frac{\partial g}{\partial T}\right)_i^k = -\left(g_{i+1}^k - g_i^k\right)/(\Delta Z)$$

$$\bar{g}_i = g_i^k + \left(\frac{\partial g}{\partial T}\right)_i^k \Delta T \qquad \text{- (15a)}$$

2nd. Step

$$g_i^{k+1} = g_i^k + \frac{\Delta T}{2}\left\{\left(\frac{\partial g}{\partial T}\right)^k + \left(\overline{\frac{\partial g}{\partial T}}\right)_i\right\} \qquad \text{- (15b)}$$

where

$$\left(\overline{\frac{\partial g}{\partial T}}\right)_i = -\left(\bar{g}_i - \bar{g}_{i-1}\right)/(\Delta Z)$$

MacCormack originally used this scheme with the equations in conservation form. The author has used the MacCormack scheme for the supersonic blunt body problem by modifying a program originally written by Albone Ref (69). The Non-Conservative form of the equations were used. No noticeable difference was observed when these results were compared with those obtained using the Moretti scheme. The MacCormack scheme retains the second order accuracy of the Moretti scheme and eliminates the need to evaluate $\left(\frac{\partial^2 g}{\partial T^2}\right)$ which in a multi-dimensional problem is algebraically complex.

2.1.3.4. Godunov Scheme

This scheme uses the conservation form of the equations of motion. The flow field is discretized into many small cells which vary in shape and size depending on the complexities of the flow geometry and the accuracy required. The scheme works in terms of dependent variables g_{ij}^k which are located at the centre of each cell rather than the nodes at the corners of each cell as shown in Fig (13). The cell boundaries have constant values of dependent variables along them. The common boundary between two adjacent cells is considered to be analogous to a diaphragm in the solution of a shock tube problem. If the diaphragm is removed, a wave pattern is established in the tube which consists of a contact surface, compression and expansion waves. The flow properties on the boundary are determined by identifying the region in which the diaphragm exists. This involves an

iterative procedure; and the formulae used in this shock tube analogy are given in Godunov Ref (75) and Garner Ref (99).

If g_{ij}^{k} denotes the mass, momentum components or energy at the centre of the cell in the initial time plane, then

$$q_{ij}^{k+1} = q_{ij}^{k} + \Delta T\Big\{(\text{Influx of g into cell in } \Delta T) - (\text{efflux of g out of cell in } \Delta T)\Big\}_{ij} \quad - (16)$$

The Godunov scheme is first order accurate in the sense that it evaluates only the first two terms of the Taylor series expansion equation (10). It is the least accurate of the difference schemes considered so far and has a truncation error which is $O(\Delta Z, \Delta T)$. The one dimensional analogy is only accurate when the cell boundary is oriented normal to the predominant direction of flow.

The survey of difference schemes does not include other well known schemes such as Lax, Rusanov, and Richtmyer. These schemes have been evaluated by other workers in Refs (45), (46), (47), (49) and(54) primarily for their shock calculating capabilities.

2.1.4. Evaluation of Boundary Points in Transient Finite Difference Methods

Boundary evaluating procedures of interest here are those which have the same order of accuracy as the difference schemes for the interior points. They should also be capable of interpreting the correct nature of the boundary points.

The Reflection Method

Using this method, solid boundary or axis of symmetry points can be calculated by having an extra row of grid points. If the grid lines are normal and parallel to the boundary this extra row of points which is situated within the boundary is also parallel to it. Variables on the extra row are set equal to those on the interior grid line immediately adjacent to the boundary i.e. they are reflected at the boundary. This imposes a condition of zero normal derivative for all dependent variables except the vertical velocity component which is reflected anti-symmetrically to insure zero normal velocity at the solid boundary or axis of symmetry. When the

grid lines are not parallel and normal to the boundary, the same principle applies but in this case interpolation is required to determine the reflected values at each boundary point. An illustration of this method is given in Burstein Ref (51).

Transient MOC for Boundary Points

In an attempt to combine the coding simplicity of the finite difference methods with the accuracy of the MOC, schemes have been developed which apply to most boundaries of practical interest. The boundary points are evaluated using the transient MOC by integrating the compatibility equations (written interms of a local co-ordinate system, ξ, η Fig (14)) along characteristics which originate in the initial time plane To, point G in Fig (14). As the interior node points of the finite difference grid are known in the initial time plane, interpolation procedures are used to evaluate the flow properties at point G. In practice this invloves an iterative procedure. Other supplementary expressions depending on the nature of the boundary can be incorporated conveniently into the iterative process and can serve to reduce the number of compatibility equations needed. Examples of this technique can be found in papers by Kentzer Ref (52) Elliot Ref (41) and Moretti (53).

For highly curved boundaries the reflection principle requires a fine mesh to obtain acceptable accuracy (see for example, the throat regions of nozzles, Serra Ref (88) and transonic aerofoil surfaces, Singleton Ref (82)). Singleton's results were unsatisfactory; comparing Singleton's work with that of Magnus and Yoshihara Ref (81) who also used a variation of the Lax-Wendroff scheme for the interior points but the MOC for the aerofoil surface, Singleton's problems appear to arise from the use of the reflection principle on the aerofoil surface. Abbett Ref (100) conducted a survey of twenty-five solid boundary evaluation methods for two-dimensional steady supersonic flow. Schemes using the MOC or based on the use of the compatibility equation (see Kentzer Ref (52)), proved to be superior to the reflection method for a simple compression and expansion problem.

The Lax-Wendroff scheme appears to be a convenient method for calculating embedded shock waves but it is considered wasteful for computing the position of bow shock waves. Bow shock waves are smeared over several mesh lengths due to the effects of artificial viscosity (see Appendix (B)). A fine mesh is needed to confine the shock to acceptable limits. Examples of smeared bow shock waves can be found in Burstein Ref (72) and Bohachevsky Ref (66). Barnwell Refs (77) and(78),who used the Lax-Wendroff method for the interior points, elected to use the transient MOC for the boundary points which includes a detached bow shock wave. The bow shock wave was treated as a sharp moving discontinuity across which the Rankine-Hugoniot conditions hold. Distinct shock waves shapes were calculated for axisymmetric and asymmetric problems.

2.2. Relaxation Methods

Rapid advances have been made recently in the numerical solution of transonic supercritical flows about slender bodies and aerofoils. One of the most successful approaches in this field appears to be through the numerical solution of the transonic small perturbation potential equation (see Refs(56) to (60)) which in cylindrical co-ordinates takes the form (see Ref (60)),

$$\left[(1-M_\infty) - M_\infty^2(\gamma+1)\phi_z\right]\phi_{zz} + \frac{1}{Y}(Y\phi_Y)_Y = 0 \qquad - (17)$$

where ϕ_z and ϕ_Y are the perturbation velocities along the Z and Y directions. The boundary conditions at large distances from the body surface take the simple form $\phi_z = \phi_Y = 0$. However with circulation arising with an aerofoil at incidence, Krupp Ref (58) found this method unsuitable and a special analytical solution was developed for the far field solution. On the surface of the body, the flow tangency condition is given by the first order expression,

$$\lim_{Y\to 0}\left(Y\phi_Y\right) = Y\frac{\partial Y}{\partial Z}$$

Steger and Lomax Ref (59), used co-ordinates which insured that the body surface was one side of the computational grid and thus improved the accur-

acy of the solution for blunt nosed aerofoils at incidence.

The solution of equation (17) presents itself, as a'Boundary Value Problem' and the Relaxation method is used to compute ϕ at each node point of a finite difference grid. When the local Mach number is supersonic the coefficient of ϕ_{zz} is negative and equation (17) is hyperbolic. When it is positive, the local flow is subsonic and hence this equation is elliptic. Thus by examining the sign of this coefficient the differencing scheme was varied so as to suit the local nature of the partial differential.

Consider the numerical solution of equation (17) in a rectangular region Fig (13). $Z_i = i\Delta Z$, $Y_j = j\Delta Y$ and $\phi_{ij} = \phi(Z_i, Y_j)$

; where $i = 1, 2 \cdots i_{max}$ and $j = 1, 2 \cdots j_{max}$

Boundary conditions are given along Y_1 , Y_{jmax} and Z_1 and Z_{imax}

Along any i^{th} column the unknown perturbation potential values are,

$$\vec{\phi}_i = \begin{bmatrix} \phi_{i,2} \\ \phi_{i,3} \\ \vdots \\ \phi_{i,j_{max-1}} \end{bmatrix} \qquad - (18)$$

The solution of equation (17) can be expressed as

$$\vec{A}_j \vec{\phi}_i = \vec{F}_i \qquad - (19)$$

where $\vec{F}_i$ is a column vector similar to $\vec{\phi}_i$. Equation (19) represents a i_{max-2} matrix equations. $\vec{A}_j$ is a (j max - 2) square matrix each element being a function of ϕ_{ij} , ϕ_{ij-1} and ϕ_{ij+1}

The relaxation technique is given by

$$\vec{\phi}_i^{k+1} = \vec{\phi}_i^{k} + \omega_i \left(\vec{\phi}_i - \vec{\phi}_i^{k} \right) \qquad - (20)$$

where k is the iteration count and $\vec{\phi}_i$ is the intermediate solution of equation (19) which is given by a direct algorthim and ω_i is a diagonal matrix of relaxation parameters.

One of the most attractive features of the Relaxation method is its ability to compute weak shock waves which develop within the computational field without any special treatment. Bailey Ref (60) used this method to

compute the flow about slender bodies at Mach numbers up to 1.2. Detached shock waves with subsonic regions behind them, compare well with the experimental results. Hence it appears that the relaxation method which has seen successful applications in the field of supercritical flows about aerofoils, can also be used for detached shock waves problems.

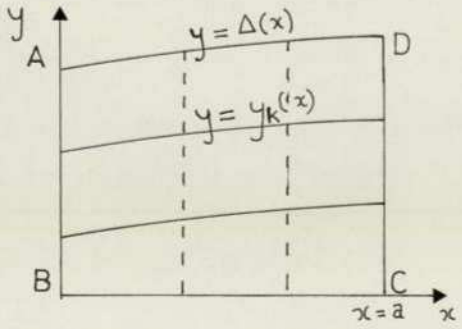
Some workers in this field have used the process of graphic interaction during the computation in order to improve the choice of relaxation parameters ω_i . This was done to improve the convergence of the solution and also to avoid instability. It is not clear whether this interaction was optional or a necessity: if it was a necessity then it would limit the usage of the relaxation method.

2.3. The Method of Direct Integrals

Dorodnitsyn Ref (61) presented a method of solving non linear partial differential equation of the type

$$\frac{\partial P_i}{\partial x} + \frac{\partial Q_i}{\partial y} = L_i$$

where $P_i = P_i(x, y, \bar{u}, \bar{v}, \bar{\rho}, \bar{p})$, $Q_i = Q_i(x, y, \bar{u}, \bar{v}, \bar{\rho}, \bar{p})$ and $L_i = L_i(x, y, \bar{u}, \bar{v}, \bar{\rho}, \bar{p})$. As the steady conservation form of the gas dynamic equation can be written in the above form, the Method of Direct Integrals presents a means of solving many transonic problems. A full account of Dorodnitsyn's method is presented in Ref (62) and (63) and so only a brief outline will be given here. For two dimensional and axisymmetric problems , $i = 1, 2 \cdots 4$ i.e. there are four dependent variables and as many equations.



A-B-C-D represents the domain in which the solution is required. The domain is divided into N curvilinear strips by drawing equidistant lines $y = y_k(x)$ for $0 \leq y \leq \Delta(x)$. Then the above system of equations

is integrated along any arbitrary line x = constant from y = 0 to the boundary of each of the strips. Since there are 4 partial differential equations there are 4N equations of the form

$$\frac{d}{dx}\int_0^{y_k(x)} P_i\, dy - \frac{d(y_k)}{dx}(P_i)_k + (Q_i)_k - (Q_i)_{y=0} = \int_0^{y_k(x)} L_i\, dy$$

where k = 1,2...N, and on the k^{th} line

$$y = y_k(x) = \Delta(x)\left[N-(k-1)\right]/N$$

Thus four boundary conditions are required on each line with an additional condition at $y = \Delta(x)$ if this boundary is not known in advance.

The integrals are now approximated by interpolation polynomials of the form

$$P_i = \sum_{m=0}^{N} a_m(x)\, y^m \qquad i = 1, 2, \ldots 4$$

similarly for Q_i and L_i. Coefficients a_m are linearly dependent on the function P_i on the strip boundaries. This innovation by Dorodnitsyn is an important step, as it reduces the solution of 4 non-linear partial differential equations to the solution of 4N simultaneous ordinary differential equations.

Hayes and Probstein Ref (19) applied the one strip method to the supersonic blunt body problem. With some algebraic manipulation the 4 conservation equations are reduced to two working equations which are integrated along lines from the body to the detached shock wave. The curve $y = \Delta(x)$ now corresponds to the shock wave. A sonic point singularity occurs on the body surface. This singularity is removed using an iterative process by re-estimating of the shock detachment distance Δ and integration of the ordinary differential equation until the solution passes smoothly through the sonic point.

Since the conservation form of the equations are used, embedded shock waves could be calculated using this method. A disadvantage of the method lies in the degree of arbitrariness in the choice of the interpolation functions. Convergence of the method can only be checked by increasing the number of strips, N. Unfortunately the solution increases in complexity as the value of N is increased because the number of boundary

conditions on the boundaries of each strip and the number of ordinary differential equations increase proportionately. Hence checking convergence could involve writing new computer codes for higher values of N. This problem does not occur with most finite difference methods where the mesh size is altered merely by using different data. However Belotserkovski Ref (62) contains results for $1 \leq N \leq 6$ for blunt body flows. For a free stream Mach number of 1.15, 6 strips were used. Results for a sphere in supersonic flow compared well with experimental observation made by Xerikos and Anderson Ref (13).

2.4. The Selection of a Numerical Method

The selection of a numerical method is guided by:-

a) Accuracy of the method illustrated by successful applications in other relevant problems.

b) Computational efficiency defined in terms of computer storage requirements and executing time i.e. Central Processor Unit (CPU) time.

c) Conceptional simplicity and program development time.

Butler's transient MOC appears to be the most accurate of the numerical schemes surveyed. This is borne out by Ransom Ref (34) who used a similar scheme with three dimensional supersonic flow and compared his results with source flow for which the exact analytical results were known. However Roesner Ref (55) who computed unsteady flow in three dimensional ducts using both a transient finite difference method and a transient MOC, commented that the program development times of the latter were larger.

In terms of computational efficiency the relaxation method is attractive. Execution times ranging from $\frac{1}{3}$ to $\frac{1}{5}$ of the transient finite difference schemes have been reported, by Wear Ref (58) for the nozzle problem and Murman Ref (56) for the supercritical aerofoil problem. The only drawback appears to be its limited range of application in the supersonic range. Only results with $M_\infty \leq 1.2$ have been reported due to the assumption of isentropic flow which limits the calculation to weak bow shocks and embedded shocks.

The transient finite-difference method is conceptionally simple and shorter development times were expected due to the explicit nature of the solution. Also starting from any realistic initial conditions a unique solution could be obtained. Convergence to a unique solution could also be checked by varying the mesh size. This could not be done as conveniently using the method of Direct Integrals. The literature on transient finite difference methods revealed that ad hoc boundary point evalution schemes could be developed which possessed comparable accuracy in relation to the difference schemes for interior points. An economic handling of boundary points could give better overall computational efficiency. Hence the transient finite-difference method was selected for the present problem.

2.5. A Brief Review of Transient Finite Difference Methods Applied to Transonic Flow Problems.

Fig (11) depicts four broad categories of transonic flow problems. Table 1 lists most of the recent major contributions in each of these categories with essential data in the form of M_∞ , surface geometry and schemes for interior and boundary points.

There appears to be a wealth of information related to the Blunt Body problem, Internal Flows and Supercritical Flows. The Ducted Body problem, however, appears to be a more recent field of investigation and has the least number of contributions. Workers appear to have been divided in their choice of schemes for interior points mainly between schemes which use the conservation form of equations (Lax-Wendroff, Lax and Godunov) and those which use the non-conservation form (Moretti). The Lax-Wendroff scheme or variations of it appear to be most widely used of all schemes. It is also interesting to note that Moretti's method has been used successfully in all four categories. The transient MOC is widely used as a means of implementing the boundary conditions. Mason Ref (16) reported an improvement in the results obtained after the use of the transient MOC for the body and bow shock points of the Blunt Body problem (as compared with

TABLE 1

APPLICATIONS OF TRANSIENT FINITE DIFFERENCE METHODS TO TRANSONIC FLOW PROBLEMS FIG (11)(a) BLUNT BODY PROBLEM.

REF.	M_∞	Surface Geometry	Scheme for Interior Points	Scheme for Boundary Points
(64)	4.0	Blunted Wedge	Moretti	MOC (Moretti)
(65)	8.0	Ellipsoid cone $\lambda = 1.5$, $\alpha = 20^\circ$ and 30°	"	"
(69)	$1.1 \leq M_\infty \leq 3.05$	Sphere, Sphere cone ellipsoids (only axisymmetric flow)	"	"
(70)	4.0	Unit circle with a 4:1 gradient after body.	Lax-Wendroff	"
(71)	3.0, 4.0 4.44 15.0	Concave nosed Blunt Body	Moretti	"
(66)	8, 29	Flat faced step and cylinder	Lax	Reflection
(67)	4, 28 and 29	Apollo vehicle $\alpha = 20^\circ$	"	"
(68)	4.63	Large angle cones (mass injection)	"	"
(72)	4.3	Flat faced cylinder	Lax-Wendroff	"
(73)	6		"	"
(74)	2.99, 3.97 4.9, 4.0	Sphere, Sphere-cone, hemisphere-cylindrical flare	Lax	Shock wave - special method using Rankine-Hugoniot relations, Body points - reflection
(75)	4.0	Sphere	Godunov	Godunov
(76)	10, 20 29	Sphere and 60° blunted cone	Godunov	MOC (Similar to Moretti)
(77)	$1.79 \leq M_\infty \leq 2.81$	Flat faced cylinder, sharp and rounded shoulders, 60° sphere cone, 30° truncated cone and truncated cone cylinder	Lax-Wendroff	MOC (bi-characteristics)

TABLE 1 (Continued)

Blunt Body Problem Fig (11)(a)

Ref.	M_∞	Surface Geometry	Interior points	Boundary points
(78)	2.49, 2.81 4.63 and 3.0	Apollo vehicle $\alpha = 22^\circ$, spherical cap cylinder, $\alpha = 15^\circ$; sphere cone, $\alpha = 10^\circ$, 20° and prolate spherical.	Lax-Wendroff	MOC (bi-characteristics)
(79)	4, 8	Parabolic cylinder blunted wedge, sphere cone and circle	Moretti	MOC (Moretti)
(80)	2.81, 3 and 4	Flat faced cylinder (mass injection) and circle	Fluid in cell scheme	reflection
(117)	4	axsy. flow spherical cap	Moretti	MOC at all boundaries
SUPERCRITICAL FLOWS FIG (11)(b)				
(81)	0.72 0.786	NACA 64A410, $\alpha = 4^\circ$ Quasi elliptic (Dutch NLR)	Lax-Wendroff	Unsteady wave theory reduces normal velocity on aerofoil surface to zero. Prescribed boundary at ∞ using stretched co-ordinates.
(82)	.704 0.5	Niewland aerofoil	Lax-Wendroff	reflection
(84)	0.56 0.91 0.80	isolated bowtail symmetric aerofoil and axisymmetric conical forebody	MacCormack	Moretti's method for embedded shocks and stretched co-ordinates for boundaries at infinity.
(85)	0.85	sharp leading edge aerofoils and bodies of revolution	Richtmyer	upstream boundaries specified and reflection for the body surface
(86)	0.8, 0.9 and 0.95	Axisymmetric flows: sphere, sphere cone with circular base and ellipsoid	indegenous based on the MOC (implicit)	—
(83)	0.6	aerofoil in nozzle flow not super critical; provisional results for Ref (84)	Moretti	Moretti

TABLE 1 (Continued)

Fig (11)(c) Internal Flows

Ref	Surface Geometry	Scheme for Interior Points	Scheme for Boundary Points
(87)	45^{o}-15 conical nozzle small throat radius of curvature	Moretti	MOC(Moretti) for surface points, stretched co-ordinate used for subsonic boundary.
(88)	2-D hyperbolic nozzle and curved channel. Circular arc nozzle, Anular turbofan passage, 45^{o}-15^{o} Conical nozzle with small throat radius of curvature	Lax-Wendroff	Reflection on nozzle surface and MOC for subsonic upstream boundary.
(89)	turbine blade passages	Lax-Wendroff	Upstream and downstream boundaries stretched.
(90)	Combustion camber of 2-D rocket	Lax-Wendroff	Reflection on body surface; MOC used on subsonic partial specified boundary
(91)	Axisymmetric nozzles with and without centre bodies, small throat radius of curvature.	Lax-Wendroff	Parabolic extrapolation at all boundaries
(92)	Convergent nozzle	Moretti	Stretched co-ordinate system for upstream boundary; MOC (Moretti) used for jet boundary and linear interpolation at wall surface.
(93)	Convergent nozzles	Lax-Wendroff	Parabolic extrapolation; upstream boundaries held constant.
(94)	Turbomachinery blade passages	One step, first order scheme in conservation form	wall conditions based on interior point; subsonic boundary - forward or backward differences.
(96)	"	two step method equations in conservation form. Finite elements used.	upstream boundaries specified.
(95)	Sonic jets and jets impinging on normal wall	Lax-Wendroff	Reflection on wall and least squares quadratic extrapolation solution for down stream jet boundary.

TABLE 1 (Continued)

Fig (11)(d) Ducted Bodies in Supersonic Flow

Ref	M_∞	Surface Geometry	Interior Points	Boundary Points
(97)	2.81, 4 8.33	Circular section lip 2-D and toroidal flow; elliptic and square sections with rounded corners	Moretti	MOC (Moretti)
(98)	8.33	Circular section toriod	Moretti	MOC (Moretti)
(99)	0.9, 0.799 2.0	Centre bodies with sharp lips (M_∞ = 2.0) and blunted tips	Godunov	Godunov and second order extrapolation

the results obtained using the Godunov scheme at the boundaries).

D'Souza Ref (97) made a major contribution to the ducted body problem by computing hypersonic flow about blunt lipped ducted bodies with supersonic internal boundaries. The Moretti scheme for both interior and boundary points was used. Results were presented for continuously curved shocks as well as Mach interaction at the axis of symmetry as shown in Figs (6)(c) and (d). However, the internal boundaries were always supersonic. Excellent comparisons with experiment were achieved for freestream flow normal to a toroid and also for two parallel circular cylinders shown in Fig (6).

Garner Ref (99) computed the flow about inlets with centrebodies using the Godunov scheme. A sharp lipped inlet was considered at $M_\infty = 2.0$. Four hours of computing time was required to solve this problem on an IBM 360/65. D'Souza's program required about 20 minutes on an IBM 360/75 for a two dimensional blunt lipped inlet at $M_\infty = 8.33$. Garner's larger computational time was possibly due to the larger physical space and consequently more computational cells required by the computational scheme. This was necessary as the bow shock was not treated as a sharp discontinuity but evolved within the computational grid as part of the solution, (section 2.1.3.4). Garner's results produced unsatisfactory comparisons with experiment in the region of the inlet lip. This can be attributed to the first order accuracy of the Godunov scheme which was used.

The author's preliminary results were presented in Ref (98). Two methods of treating the subsonic internal method were outlined. In the next chapter a detailed account of the more successful of these methods is presented along with details of the computational procedures for other boundary points and the interior points.

CHAPTER 3

APPLICATION OF THE TRANSIENT FINITE DIFFERENCE METHOD

We now proceed to describe in detail the computational procedures used to obtain the flow field about ducted bodies with uniform supersonic upstream conditions.

Moretti's second order accurate method is applied to compute the interior points. Moretti's method for the boundary points is also adapted to meet the requirements of the present problem. The explanation of computational procedures which follow are given with the SUBIB problem in mind. However, most of the discussion applies also to the SUPIB problem. Hence the few differences between the methods for the SUBIB problem and the SUPIB problem are referred to at the end of the chapter.

3.1. Finite Difference Methods for the Interior Points

3.1.1. Equations of Motion in Toroidal and polar co-ordinates

Referring to Fig (15), the governing equations of motion can be written in terms of polar (two-dimensional) or toroidal (axisymmetric) co-ordinates with the origin at O. The equations of motion in non-dimensional form are as follows:-

Continuity Equations

$$\frac{\partial R}{\partial t} + \frac{\partial u}{\partial r} + u\frac{\partial R}{\partial r} + \frac{u}{r} + \frac{1}{r}\frac{\partial v}{\partial \theta} + \frac{v}{r}\frac{\partial R}{\partial \theta} + j\frac{(u\sin\theta + v\cos\theta)}{(H + r\sin\theta)} = 0 \qquad - (21)$$

Momentum Equations

$$\frac{\partial u}{\partial t} + u\frac{\partial u}{\partial r} + \frac{v}{r}\frac{\partial u}{\partial \theta} - \frac{v^2}{r} + \frac{1}{\rho}\frac{\partial P}{\partial r} = 0 \qquad - (22)$$

$$\frac{\partial v}{\partial t} + u\frac{\partial v}{\partial r} + \frac{v}{r}\frac{\partial v}{\partial \theta} + \frac{uv}{r} + \frac{1}{r\rho}\frac{\partial P}{\partial \theta} = 0 \qquad - (23)$$

Conservation of Entropy along a particle Path

$$\frac{\partial S}{\partial t} + u\frac{\partial S}{\partial r} + \frac{v}{r}\frac{\partial S}{\partial \theta} = 0 \qquad - (24)$$

When j = 0 the equations represent two dimensional flow in polar co-ordinates and when j = 1 they represent axisymmetric flow in toroidal co-ordinates.

The origin O is at a distance H (which is the 'highlight' height) above the axis of symmetry. The non-dimensional dependent variables are defined as follows:-

$$R = \log_e(\bar{\rho}/\bar{\rho}_\infty) \quad , \quad P = \log_e(\bar{p}/\bar{p}_\infty) \quad , \quad S = P - \gamma R$$

$$v = \frac{\bar{v}}{\bar{a}_\infty}\sqrt{\gamma} \qquad \text{and} \qquad u = \frac{\bar{u}}{\bar{a}_\infty}\sqrt{\gamma}$$

The non-dimensional independent variables are given by,

$$t = \frac{\bar{t}}{H}\sqrt{\frac{\bar{p}_\infty}{\bar{\rho}_\infty}} \quad \text{and} \quad r = \bar{r}/H$$

H defines the length scale. Hence the lip geometry and shock radial position are defined relative to H. For convenience H is set equal to unity for all the work presented in this thesis.

3.1.2. Equations of Motion in Computational Planes

Following in the same spirit as shown in Fig (12), the computed physical region given by A-D-E-F-C-B-A in Fig (15), is transformed into two computational rectangular planes; designated as Mesh A and Mesh B. Mesh A represents A D E B and Mesh B B E F C. This division into two computational regions insures that a radial line B E, always passes through the point of intersection between the bow shock wave D E and the axis of symmetry E F. Hence the computed position of the point E is well defined. The transformations are effected by the following equations:-

Mesh A

$$Z = ZA = \frac{r - BOA(\theta)}{SH(\theta,t) - BOA(\theta)}, \qquad \text{and} \quad T = t \qquad - (25a)$$

$$Y = YA = \frac{\theta - \theta_A}{\theta_B(t) - \theta_A}$$

Mesh B

$$Z = ZB = \frac{r - BOB(\theta)}{SHX(\theta) - BOB(\theta)}, \qquad \text{and} \quad T = t \qquad - (25b)$$

$$Y = YB = \frac{\theta - \theta_B(t)}{\theta_C - \theta_B(t)}$$

It can be seen from equations (25)(a) and (b) that the body surface at r = BOA (θ) or BOB(θ) is mapped into the line Z = 0. Similarly the shock and axis points represented by SH(θ,t) and SHX(θ) respectively are mapped into the line Z = 1. During the process of computation, the shock D E starts from an assumed shape and position and moves upstream or downstream as dictated by the numerical method and boundary conditions. This movement causes a change in the angular extend of each mesh as θ_A and θ_C have constant values. Hence $\theta_B(t)$ is a function of time. Although the shock moves in physical space, its position in the computational mesh

is fixed at Z = 1. Mesh A and Mesh B retain their convenient rectangular shapes regardless of the change of co-ordinates experienced by the boundaries in the physical plane. Fig (16) shows the corresponding Z = constant and Y = constant curves as they occur in the physical plane. A desirable feature of the transformation appears to be its ability to concentrate node points in the region of the body surface where more rapid variations in flow properties are expected.

Using the chain rule for partial derivatives, the derivatives of dependent variables in terms of r, θ and t can now be expressed in terms of the computing co-ordinate directions Z, Y, and T using equations (25)(a) and (b). Thus the equations of motion for Mesh A and B in the computational plane are given by:-

Continuity Equation

$$\frac{\partial R}{\partial T} + B\frac{\partial R}{\partial Z} + A\frac{\partial R}{\partial Y} + \frac{1}{D}\frac{\partial u}{\partial Z} + \frac{C}{rD}\frac{\partial v}{\partial Z} + \frac{1}{ra}\frac{\partial v}{\partial Y} + \frac{u}{r} + j\frac{(u\sin\theta + v\cos\theta)}{(H + r\sin\theta)} = 0 \qquad - (26)$$

Momentum Equation

$$\frac{\partial u}{\partial T} + B\frac{\partial u}{\partial Z} + A\frac{\partial u}{\partial Y} - \frac{v^2}{r} + \frac{b}{Dp}\frac{\partial P}{\partial Z} = 0 \qquad - (27)$$

$$\frac{\partial v}{\partial T} + B\frac{\partial v}{\partial Z} + A\frac{\partial v}{\partial Y} + \frac{uv}{r} + \frac{Cb}{rDp}\frac{\partial P}{\partial Z} + \frac{b}{rap}\frac{\partial P}{\partial Y} = 0 \qquad - (28)$$

Conservation of Entropy along a Particle Path

$$\frac{\partial S}{\partial T} + B\frac{\partial S}{\partial Z} + A\frac{\partial S}{\partial Y} = 0 \qquad - (29)$$

For Mesh A

$$\alpha = \alpha(t) = \theta_B(t) - \theta_A$$

$$A = \frac{1}{\alpha}\left(\frac{v}{r} - YA\frac{\partial \alpha}{\partial T}\right)$$

$$B = \frac{1}{D}\left(u + \frac{vC}{r} - WZ\right) \qquad - (30)$$

$$C = (Z-1)\frac{\partial BOA}{\partial \theta} - Z\frac{\partial SH}{\partial \theta}$$

$$D = SH - BOA$$

For Mesh B

$$\alpha = \alpha(t) = \theta_C - \theta_B(t)$$

$$A = \frac{1}{\alpha}\left(\frac{v}{r} + (1 - YB)\frac{\partial \alpha}{\partial T}\right) \qquad - (31)$$

$$B = \frac{1}{D}\left(u + \frac{vC}{r}\right)$$

$$C = (Z-1)\frac{\partial BOB}{\partial \theta} - Z\frac{\partial SHX}{\partial \theta}, \quad D = SHX - BOB$$

3.1.3. Difference Scheme for Interior Points

Moretti's second order difference scheme is utilized for the interior points. Using this scheme which was briefly described in section (2.1.3.1.), chapter 2. Equations (26) to (28) for Mesh A and B can be integrated as follows:-

$$R_{ij}^{k+1} = R_{ij}^{k} + \left(\frac{\partial R}{\partial T}\right)_{ij}^{k} \Delta T + \frac{1}{2}\left(\frac{\partial^2 R}{\partial T^2}\right)_{ij}^{k} \Delta T^2 \quad (a)$$

$$u_{ij}^{k+1} = u_{ij}^{k} + \left(\frac{\partial u}{\partial T}\right)_{ij}^{k} \Delta T + \frac{1}{2}\left(\frac{\partial^2 u}{\partial T^2}\right)_{ij}^{k} \Delta T^2 \quad (b)$$

$$v_{ij}^{k+1} = v_{ij}^{k} + \left(\frac{\partial v}{\partial T}\right)_{ij}^{k} \Delta T + \frac{1}{2}\left(\frac{\partial^2 v}{\partial T^2}\right)_{ij}^{k} \Delta T^2 \quad (c) \qquad - (32)$$

$$S_{ij}^{k+1} = S_{ij}^{k} + \left(\frac{\partial S}{\partial T}\right)_{ij}^{k} \Delta T + \frac{1}{2}\left(\frac{\partial^2 S}{\partial T^2}\right)_{ij}^{k} \Delta T^2 \quad (d)$$

Referring to Fig (13),(i,j)represents any interior node point where the computational mesh could represent either Mesh A or Mesh B. As this is an explicit scheme, the values of the dependent variables at the k + 1 time step depend only on those for the k time step. The time derivatives are replaced by space derivatives which is demonstrated for equation (29) as follows: -

$$\left(\frac{\partial S}{\partial T}\right)_{ij}^{k} = -\left(B\frac{\partial S}{\partial Z} + A\frac{\partial S}{\partial Y}\right)_{ij}^{k} \qquad - (33)$$

$$\left(\frac{\partial^2 S}{\partial T^2}\right)_{ij}^{k} = -\left(\frac{\partial B}{\partial T}\frac{\partial S}{\partial Z} + B\frac{\partial^2 S}{\partial Z \partial T} + \frac{\partial A}{\partial T}\frac{\partial S}{\partial Y} + A\frac{\partial^2 S}{\partial Y \partial T}\right)_{ij}^{k} \qquad - (34)$$

If there are no discontinuities in the flow

$$\frac{\partial^2 S}{\partial Z \partial T} = \frac{\partial^2 S}{\partial T \partial Z} \quad \text{and} \quad \frac{\partial^2 S}{\partial Y \partial T} = \frac{\partial^2 S}{\partial T \partial Y}$$

hence by differentiating equation (33) with respect to Z and Y,

$$\frac{\partial^2 S}{\partial Z \partial T} = -\left(\frac{\partial B}{\partial Z}\frac{\partial S}{\partial Z} + B\frac{\partial^2 S}{\partial Z^2} + \frac{\partial A}{\partial Z}\frac{\partial S}{\partial Y} + A\frac{\partial^2 S}{\partial Y \partial Z}\right)_{ij}^{k} \qquad - (35)$$

$$\text{and } \frac{\partial^2 S}{\partial Y \partial T} = -\left(\frac{\partial B}{\partial Y}\frac{\partial S}{\partial Z} + B\frac{\partial^2 S}{\partial Z \partial Y} + \frac{\partial A}{\partial Y}\frac{\partial S}{\partial Y} + A\frac{\partial^2 S}{\partial Y^2}\right)_{ij}^{k} \qquad - (36)$$

Substituting equations (35) and (36) into equation (34), $\left(\frac{\partial^2 S}{\partial T^2}\right)_{ij}^{k}$ is obtained in terms of spatial derivatives. The spatial derivatives of S with respect to Y and Z are now evaluated using central differences as shown in Fig (13). In a similar manner $\left(\frac{\partial R}{\partial T}\right)_{ij}^{k}$, $\left(\frac{\partial^2 R}{\partial T^2}\right)_{ij}^{k}$, $\left(\frac{\partial u}{\partial T}\right)_{ij}^{k}$, $\left(\frac{\partial^2 u}{\partial T^2}\right)_{ij}^{k}$ $\left(\frac{\partial v}{\partial T}\right)_{ij}^{k}$ and $\left(\frac{\partial^2 v}{\partial T^2}\right)_{ij}^{k}$ are evaluated and eliminated from equation (32).

3.1.4. Stability Condition

The time step ΔT is governed by the C F L stability condition which

was described in section (2.1.1), chapter 2. A simple expression for the C.F.L. condition for the present problem can be derived by analogy to the case of quasi one dimensional compressible flow for which the characteristics slopes are given by, $\frac{dx}{dt} = U + a$, $\frac{dx}{dt} = U - a$ and $\frac{dx}{dt} = U$, the latter being the equation of a particle path (U is the velocity in the x direction and a is the speed of sound).

Consider Fig (8)(a) where, P, Q, R are the node points. Hence P R is the domain of dependence of the difference scheme with Δx as the mesh width. The left running characteristic $U + a$ and the right running characteristic $U - a$ from points R and P respectively (assumed to be straight lines) intersect at point S. Hence at point S, the domain of dependence of the difference scheme coincides with the domain of dependence of the differential equations. In order to satisfy the C.F.L. condition at the new time level $t_o + \Delta t$, Q' must be contained within region P S R. If a larger time step were used and Q' were situated at Q", Q" would now be influenced by disturbances originating from points such as E. Since E is not situated within P Q R, it is not accounted for by the difference equation which involve nodes P, Q and R. Hence the need to restrict the time step Δt becomes apparent. If Δx is constant or varies insignificantly during each time step, the C.F.L. condition at Q' is satisfied if $\left(\Delta x/\Delta t\right) \geq |U + a|$

and $\left(\Delta x/\Delta t\right) \geq |U - a|$ or $\Delta t \leq \frac{\Delta x}{|U| + a}$

For the present problem,

$$\Delta t = \frac{\Delta x}{SF(|Q| + a)} \qquad - (37)$$

where Δx = minimum of (Δr, $r \Delta \theta$) for a particular node point (see Fig (10)(b)) and SF is the safety factor (>1) used to make the stability condition more severe because the C.F.L. condition was originally (Ref (29)) derived for linear hyperbolic partial differential equations, where as in the present problem the equations are non-linear. A value of SF = 1.5 appears to have been used by most workers using the Moretti scheme and it

is also used in the present problem.

Equation (37) is evaluated at each node point and the minimum value is selected as the time step size for which all the node points are integrated.

3.2. Treatment of Boundary Points

3.2.1. Inter Mesh Boundary B E

As the position of the bow shock wave is not known a priori, the angular extent of Mesh A and Mesh B are also not known. Hence, the angular Mesh widths $\Delta\theta_A$ and $\Delta\theta_B$ are unlikely to be equal. In order to evaluate angular derivatives of the form $\frac{\partial R}{\partial \theta}$ and $\frac{\partial^2 R}{\partial \theta^2}$ or $\frac{\partial R}{\partial Y}$ and $\frac{\partial^2 R}{\partial Y^2}$, an extra row of points is used for each computational grid. These are shown in Fig (15) as B' E' and B" E". B' E' is the extra row of points for Mesh A. B' E' protrudes into Mesh B and the points on it including the boundary points are evaluated using linear interpolation along the Z = constant lines which are illustrated in Fig(16). Only the first three rows of Mesh B are involved in this interpolation. B' E' occurs as a Y = constant line in Mesh B. Points on the extra row B" E" of mesh B are evaluated in a similar manner. Excluding points B and E, the points on B E are evaluated as interior points for Mesh A and Mesh B at each time step. The final values at B E for each time step are obtained by averaging the values at B E obtained with B E as part of Mesh A and as part of Mesh B.

Ideally when $\Delta\theta_A = \Delta\theta_B$ no interpolation is required as the extra mesh points of Mesh A and B overlap exactly rows of points in each mesh. Since only three rows of each mesh are used in the interpolation, the interpolations were most accurate when $0.5 \leq \left(\Delta\theta_A / \Delta\theta_B\right) \leq 2.0$. In subsequent computations it was observed that if this inequality was not satisfied, unstable results occurred. This was remedied by changing the angular mesh size of Mesh A and B and restarting the computation.

3.2.2. Supersonic Boundary C F

In Fig (5)(b) the angular position of boundary A D is selected so as to include the sonic line and the limiting charactistic within the

computed region. The dependent variables on A D are calculated by linearly extrapolating values on the two adjacent rows of node points. If suffix j = n corresponds to the 'Y' position of A D and i corresponds to any Z position of a node point, then the following expression is used:-

$$g(i,n) = 2g(i,n-1) - g(i,n-2) \qquad - (38)$$

The errors associated with this linear extrapolation do not propagate upstream as the flow is locally supersonic and A D is situated downstream of the limiting characterisitic.

3.2.3. The Application of Moretti's Method for Calculating Boundary Points

3.2.3.1. A General Comment on Butler's Scheme

Consider a segment of any boundary P-Q-R in Fig (14). The unsteady equations of motion in ξ - η co-ordinates at Q can be written as follows:-

$$\frac{\partial P}{\partial T} + U\frac{\partial P}{\partial \xi} + \gamma\frac{\partial U}{\partial \xi} + \gamma\frac{\partial V}{\partial \eta} + V\frac{\partial P}{\partial \eta} + j\frac{\gamma V_c}{y} = 0 \qquad - (39)$$

$$\frac{\partial U}{\partial T} + U\frac{\partial U}{\partial \xi} + \frac{a^2}{\gamma}\frac{\partial P}{\partial \xi} + V\frac{\partial U}{\partial \eta} = 0 \qquad - (40)$$

$$\frac{\partial V}{\partial T} + U\frac{\partial V}{\partial \xi} + V\frac{\partial V}{\partial \eta} + \frac{a^2}{\gamma}\frac{\partial P}{\partial \eta} = 0 \qquad - (41)$$

Equations (39), (40) and (41) correspond to equations (C-9), (C-6) and (C-7) of Appendix C. The ξ - η co-ordinates replace the axisymmetric cylindrical co-ordinates written in the x and y co-ordinate directions respectively. U and V are now the velocity components in the ξ and η directions respectively. In equation (39) Vc is velocity normal to the axis of symmetry and y is the distance from the axis.

The characteristic equations in ξ - η co-ordinates are given by

$$\frac{\partial \xi}{\partial T} = U + a\cos\bar{\theta} \qquad (a)$$

and

$$\frac{\partial \eta}{\partial T} = V + a\sin\bar{\theta} \qquad (b) \qquad - (42)$$

If the origin is at point Q in the To + ΔT plane of Fig (14), the co-ordinates of a disturbance in the To plane which reaches Q along any bi-characteristic 'i' can be found as follows:-

$$\xi_i(T_o+\Delta T) = \xi_i(T_o) + \left(\frac{\partial \xi}{\partial T}\right)_{\text{average}} \Delta T = 0$$

where

$$\left(\frac{\partial \xi}{\partial T}\right)_{\text{average}} = \frac{1}{2}\left\{\left(\frac{\partial \xi}{\partial T}\right)_{T_o} + \left(\frac{\partial \xi}{\partial T}\right)_{T_o+\Delta T}\right\}$$

hence $\xi_i(T_o) = -\left(\frac{\partial \xi}{\partial T}\right)\Delta T$ - (43)

$$\xi_i(T_o) = -\frac{\Delta T}{2}\left\{U_N + a_N\cos\phi_i + U_i + a_i\cos\bar{\theta}_i\right\} \quad (a)$$

similarly - (44)

$$\eta_i(T_o) = -\frac{\Delta T}{2}\left\{V_N + a_N\sin\phi_i + V_i + a_i\sin\bar{\theta}_i\right\} \quad (b)$$

$\bar{\theta}$ is a parameter angle and ϕ_i is the value of $\bar{\theta}_i$ at the To + ΔT plane. Suffix N distinguishes dependent variables and their functions in the To + ΔT plane from those in the initial time plane To. The value of $\bar{\theta}_i$ in the To plane is given by

$$\bar{\theta}_i = \phi_i + \Delta T\left\{-\sin\phi_i\left(\frac{\partial a}{\partial \xi}\right)_i + \cos\phi_i\left(\frac{\partial a}{\partial \eta}\right)_i + \cos^2\phi_i\left(\frac{\partial U}{\partial \eta}\right)_i - \sin\phi_i\cos\phi_i\left(\frac{\partial U}{\partial \xi} - \frac{\partial V}{\partial \eta}\right)_i - \sin^2\phi_i\left(\frac{\partial V}{\partial \xi}\right)_i\right\} \quad - (45)$$

The general compatibility equation which holds along any bi-characteristic 'i' is given by

$$\frac{\partial P}{\partial T} + \frac{\gamma}{a}\cos\bar{\theta}_i\frac{\partial U}{\partial T} + \frac{\gamma}{a}\sin\bar{\theta}_i\frac{\partial V}{\partial T} = -\gamma\left\{\frac{\partial U}{\partial \xi}\sin^2\bar{\theta}_i + \frac{\partial V}{\partial \eta}\cos^2\bar{\theta}_i - \sin\bar{\theta}_i\cos\bar{\theta}_i\left(\frac{\partial U}{\partial \xi} + \frac{\partial V}{\partial \eta}\right) + j\frac{V_c}{y}\right\} \quad - (46)$$

Integrating equation (46) gives,

$$\left(P_N - P_i\right) + K_1\left(U_N - U_i\right) + K_2\left(V_N - V_i\right) = \frac{\Delta T}{2}\left(RHS_N + RHS_{T_o}\right) \quad - (47)$$

here K_1 and K_2 are the time averaged coefficients of $\frac{\partial U}{\partial T}$ and $\frac{\partial V}{\partial T}$ in equation (46). R H S is the right hand side of equation (46) and is also averaged over time interval Δ T. It may appear that only three bi-characteristics i = 1,2,3 are needed to evaluate the three unknown P_N, V_N and U_N in the To + ΔT plane. Unfortunately, derivatives of the dependent variables occur in the term RHS_N and hence more bi-characteristics are needed in order to eliminate them. Usually at least 4 bi-charactistics are needed along with the condition of invariance of entropy along a particle path, which is used to evaluate S_N and hence provide a fifth relation of the form $P_N - \gamma R_N = S_N$. The co-ordinates at the base of each bi-characteristic ξ_i and η_i are transformed into co-ordinates of the computational To plane, point G_i Fig (14). An accurate interpolation procedure is required at each point Gi so as to maintain the overall second

order accuracy of the scheme. Once the dependent variables and their derivatives are calculated at G_i, equation (47) can be solved. An iterative procedure is required involving equations (43) to (47) The iteration is continued until a convergence criterion is satisfied after which the next boundary point is evaluated.

3.2.3.2. Simplifications Suggested by Moretti

Clearly Butler's method involves considerable computational effort for each boundary point. The complexities of the method are associated with the formulation of the MOC in three independent variables. Moretti Ref (105) proposed that by judicious orientation of the $\xi - \eta$ co-ordinate system Fig (14), such that the η direction is parallel to the predominent direction of flow relative to the boundary point, the derivatives of the dependent variables with respect to η can be assumed to be constant during the integrated time interval ΔT. This assumption appears feasible as an appreciable change in the derivatives $\frac{\partial q}{\partial \eta}$ can only occur as a consequence of an abrupt spreading of streamlines in the ξ direction during the time interval ΔT. This approach has also seen successful application with three dimensional steady supersonic flow, Dash Ref (106). Dash used reference planes, the orientation of which were chosen so that the primary flow variations occurred within them while the co-ordinate normal to them described the local cross flow. The governing equations were written in this reference co-ordinate system with the terms representing the derivatives normal to the reference planes treated as 'forcing terms'. The characteristic directions are thus of the two dimensional system in the reference plane and the compatibility equations differ from those of the two dimensional system due to the inclusion of the cross-derivative terms. Using this technique, Dash calculated the supersonic flow in a three dimensional Nozzle Exhaust System.

The derivatives of the form $\frac{\partial q}{\partial \eta}$ in equations (39), (40) and (41) are assumed to be independent of T and can therefore be taken over to the right hand side.

$$\frac{\partial P}{\partial T} + U\frac{\partial P}{\partial \xi} + \gamma\frac{\partial U}{\partial \xi} = -\left(\gamma\frac{\partial V}{\partial \eta} + V\frac{\partial P}{\partial \eta} + j\frac{\gamma V_c}{y}\right) \quad - (47)$$

$$\frac{\partial U}{\partial T} + U\frac{\partial U}{\partial \xi} + \frac{a^2}{\gamma}\frac{\partial P}{\partial \xi} = -\left(V\frac{\partial V}{\partial \eta}\right) \quad - (48)$$

$$\frac{\partial V}{\partial T} + U\frac{\partial V}{\partial \xi} = -\left(V\frac{\partial V}{\partial \eta} + \frac{a^2}{\gamma}\frac{\partial P}{\partial \eta}\right) \quad - (49)$$

These equations now comprise a set of quasi-linear hyperbolic partial differential equations in two independent variables, ξ and T.

The characteristic and corresponding compatibility equations are given by,

$$\frac{d\xi}{dT} = U + a \quad \text{along which} \quad - (50)$$

$$\frac{dP}{dT} + \frac{\gamma}{a}\frac{dU}{dT} = -\left(\gamma\frac{\partial V}{\partial \eta} + V\frac{\partial P}{\partial \eta} + \frac{V\gamma}{a}\frac{\partial U}{\partial \eta} + j\frac{\gamma V_c}{y}\right)_{T_0} = RHS1 \quad - (51)$$

holds, and

$$\frac{d\xi}{dT} = U - a \quad \text{along which} \quad - (52)$$

$$\frac{dP}{dT} - \frac{\gamma}{a}\frac{dU}{dT} = -\left(\gamma\frac{\partial V}{\partial \eta} + V\frac{\partial P}{\partial \eta} - \frac{V\gamma}{a}\frac{\partial U}{\partial \eta} + j\frac{\gamma V_c}{y}\right)_{T_0} = RHS2 \quad - (53)$$

holds.

Along a particle path $\frac{d\xi}{dT} = U \quad - (54)$

$$\frac{dS}{dT} = -\left(V\frac{\partial S}{\partial \eta}\right)_{T_0} \quad - (55)$$

Integrating Equations (50) and (52) gives,

$$\xi_1 = -\frac{\Delta T}{2}\left(U_N + a_N + U_1 + a_1\right) \quad - (56)$$

and $$\xi_2 = -\frac{\Delta T}{2}\left(U_N - a_N + U_2 - a_2\right) \quad - (57)$$

In practice, improved results were obtained by allowing a translation in the η direction for locating the point G in Fig (14). Equations (50) and (52) can be regarded as special cases of equation (42)(a) where $\bar{\theta} = \frac{\pi}{2}$ and $\frac{3\pi}{2}$ respectively. For these values of $\bar{\theta}$, $\frac{d\eta}{dT} = V$ hence

$$\eta_1 \text{ or } \eta_2 = -(V)\Delta T \quad - (58)$$

Integrating equation (51) and (53) gives

$$P_N + \frac{\gamma}{\bar{a}}U_N = P_1 + \frac{\gamma}{\bar{a}_1}U_1 + (RHS1)\Delta T \quad - (59)$$

$$P_N - \frac{\gamma}{\bar{a}}U_N = P_2 - \frac{\gamma}{\bar{a}_2}U_2 + (RHS2)\Delta T \quad - (60)$$

where $\bar{a}_i = (a_i + a_N)/2 \quad \text{for } i = 1, 2$

Equations (56) to (60) comprise a simpler set of working equations as compared to Butler's equations (43) to (47). Besides, the above formulation involves only two characteristics and consequently much less iteration in the initial time plane is required.

The method of integrating equations (59) and (60) is known as a modified Euler's method which has been shown in standard texts such as Ref (101) to be second order accurate. The coefficients of the derivatives $\frac{dU}{dT}$ are averaged over the time interval ΔT. The ξ_i co-ordinates are evaluated in the first iteration by setting a_n and a_i equal to the value of a at point Q Fig (14) in the To time plane. As the iterative method proceeds, more accurate estimates of the characteristic slopes are made and the estimates of the co-ordinates of point G_i improve. As in the case of Butler's scheme, the iteration is continued until a convergence criterion is satisfied.

3.2.3.4. Evaluation of Body Surface and Axis of Symmetry Boundary Points

The orientation of the $\xi - \eta$ co-ordinates is shown in Fig (17) for the body points at Q_3 and the axis points at Q_5. At Q_3 and Q_5 the $\xi - \eta$ co-ordinates are normal and tangential to the boundary. Since the localized co-ordinates have their origin at the boundary points to be evaluated in the To + ΔT plane, the origin of the disturbance reaching the boundary points Q must originate from a point in the To plane. Also the correct characteristic needs to be taken into account so as to insure that the point involved viz. G_1 is within the computational grid. For Q_3 and Q_5,

$$\eta_1 = -(V)\,\Delta T$$

where V is the tangential velocity at Q_3 and Q_5.

In order that the characteristic should originate from within the computational mesh at To, from equation (43) it can be seen that must be >0. Hence $\frac{d\xi}{dT} = U + a$ is the required characteristic and $\frac{d\xi}{dT}$ equation (59) the corresponding compatibility equation.

$$\xi_1 = -\frac{\Delta T}{2}\left\{U_N + a_N + U_1 + a_1\right\}$$

As U_N is zero on the axis and body surface,

$$\xi_1 = -\frac{\Delta T}{2}\left\{a_N + U_1 + a_1\right\}$$

Equation (59) reduces to,

$$P_N = P_1 + \frac{\gamma}{a_1} U_1 + (RHS1)\Delta T$$

P_1, U_1, a_1 and the η derivatives of RHS1 are evaluated at G_1 in Fig (14).

Details of the interpolation routines used at point G_1 are given in Appendix (B). These interpolation procedures were selected so as to avoid instability at the boundary points. The time step ΔT was governed by the C F L condition.

Successive values of $\left(\frac{d\xi}{dT}\right)_{average}$ were compared and their differences were incorporated into a Newton-Raphson iterative procedure where by improved values of $\left(\frac{d\xi}{dT}\right)_{average}$ were obtained until a convergence crition was statisfied. If ℓ denotes the iteration step,

$$\left| \left[\left(\frac{d\xi}{dT}\right)^{\ell+1}_{average} - \left(\frac{d\xi}{dT}\right)^{\ell}_{average}\right]\left(\frac{\Delta T}{a_N}\right) \right| \leq 10^{-5}$$ was used

as the convergence criterion for body and axis points. This value was established after some numerical experimentation and was found to give results with acceptable accuracy. A value of (10^{-5}) was also used by D'Souza Ref (97) and Albone Ref (69). In most computations performed, ΔT was of the order of 10^{-3}, (T is dimensionless).

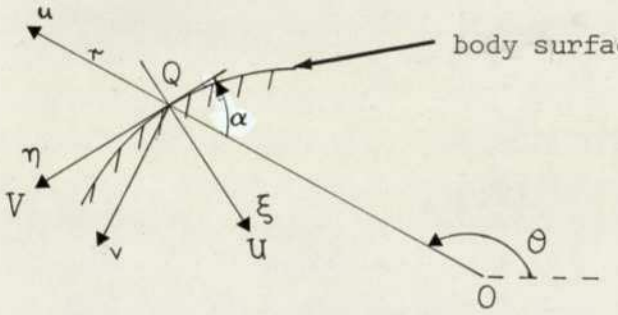
The entropy on the body surface was assumed to be constant and equal to the value on the stagnation streamline of it passed through a normal shock at the given M_∞. Later, an alternative method was developed. Referring to Fig (4)(a) the co-ordinates of point Q, which is the point of intersection of the bow shock wave with the stagnation streamline can be calculated if the MFR is known. Knowing the values of entropy on adjacent shock wave points, the entropy at Q (S_q) was calculated by linear interpolation. The minimum velocity point on the body surface was located and the value of entropy at this point was set equal to S_q. As the inlet surface is a particle path, the entropy at other body node points in the To + ΔT plane was obtained by tracing the particle path and thus locating its position in the To plane where the entropy distribution is known. This was given by $\eta = -(V)\Delta T$, where η here represents the distance travelled by the particle in time ΔT from its position in the To plane so as to reach Q in Fig (14) at To + ΔT. The entropy was evaluated at this point in the To plane and was equal to the required value at point Q in the To + ΔT plane. This method was explicit and was repeated at each time step.

Since the axis of symmetry E F of Fig (16) is also a particle path, the entropy on the axis points was evaluated by a process similar to the body points.

Having evaluated P_N and S_N, R_N for the body and axis points was given by $R_N = (P_N - S_N)/\gamma$. This leaves only V_N to be calculated as U_N is zero for axis and body points. V_N was calculated by applying the MacCormack scheme (see section (2.1.3.3), chapter 2) to equation (41)

$$\frac{\partial V}{\partial T} = -\left(V\frac{\partial V}{\partial \eta} + \frac{a^2}{\gamma}\frac{\partial P}{\partial \eta} \right) \qquad - (61)$$

In this case, equation (61) refers to the tangential momentum equation with its origin at Q in the To plane. This method is demonstrated for the body points of mesh A but similar expressions for the body points of Mesh B and the axis points can also be derived.



The derivatives are expressed in terms of the computational co-ordinates

$$\frac{\partial P}{\partial \eta} = \frac{\sin\alpha}{BOA(\theta_B - \theta_A)}\left(\frac{\partial P}{\partial Y}\right)$$

$$\frac{\partial V}{\partial \eta} = \frac{\sin\alpha}{BOA(\theta_B - \theta_A)}\left(\frac{\partial u}{\partial Y}\cos\alpha + \frac{\partial v}{\partial Y}\sin\alpha\right)$$

Hence equation (61) becomes

$$\left(\frac{\partial V}{\partial T}\right)_{T_o} = -\frac{\sin\alpha}{BOA(\theta_B - \theta_A)}\left[V\left(\frac{\partial u}{\partial Y}\cos\alpha + \frac{\partial v}{\partial Y}\sin\alpha\right) + \frac{a^2}{\gamma}\frac{\partial P}{\partial Y}\right] \qquad - (62)$$

Derivatives with respect to Z do not occur in equation (62). The Y derivatives can be evaluated using forward or backward differnces, Fig (13).

1st Step.

$$\overline{V}(j) = V(j) + \left(\frac{\partial V}{\partial T}\right)_{T_o}\Delta T \qquad - (63)$$

2nd Step

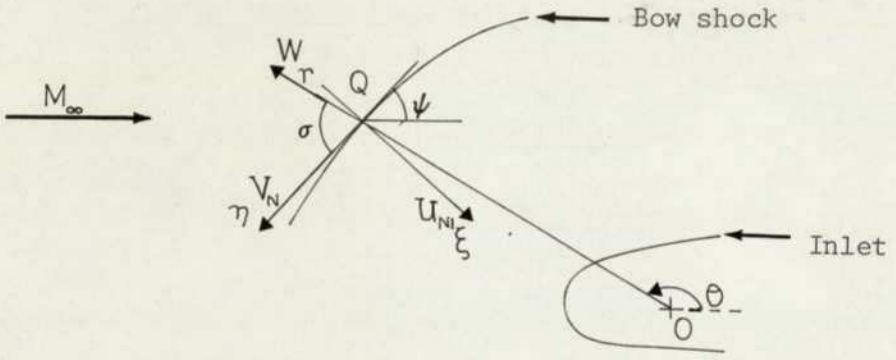
$$V_N(j) = V(j) + \left\{ \left(\frac{\partial V}{\partial T}\right)_{T_o} + \overline{\left(\frac{\partial V}{\partial T}\right)} \right\}\frac{\Delta T}{2} \qquad -(64)$$

where $\left(\overline{\frac{\partial V}{\partial T}}\right) = \frac{-\sin\alpha}{BOA(\theta_B-\theta_A)}\left[\overline{V}(j)\left(\frac{\partial \bar{u}}{\partial Y}\cos\alpha + \frac{\partial \bar{v}}{\partial Y}\sin\alpha\right)+\frac{a_N^2}{\gamma}\frac{\partial P_N}{\partial Y}\right]$ - (65)

The Y derivatives occurring in $\left(\frac{\partial V}{\partial T}\right)_{T_o}$ are evaluated using forward differences and those occurring in $\left(\overline{\frac{\partial V}{\partial T}}\right)$ are evaluated using backward differences. In equation (65) a_N and P_N are the converged values and are obtained using the MOC at the point Q. $\bar{u}$ and $\bar{v}$ are obtained by resolving $\overline{V}(j)$ in the r and θ directions (see sketch above). Hence the second step of the above scheme can only be completed after the P_N, R_N and S_N are computed using the MOC in conjunction with the entropy evaluation procedure.

3.2.3.5. Method of Evaluating Points on the Moving Bow Shock D E

The bow shock D E in Fig (17) is treated as a moving discontinuity. The dependent variables downstream of this bow shock can be obtained using the Rankine-Hugoniot shock relations for a moving shock wave (reproduced from Albone, Ref (69).)



$$U_{NI} = \frac{(\gamma-1)(M_\infty\sqrt{\gamma}\sin\psi + W\sin\sigma)^2 + 2\gamma}{(\gamma-1)(M_\infty\sqrt{\gamma}\sin\psi + W\sin\sigma)} - W\sin\sigma \qquad - (66)$$

$$\rho_N = \frac{M_\infty\sqrt{\gamma}\sin\psi + W\sin\sigma}{U_{NI} + W\sin\sigma} \qquad - (67)$$

$$P_N = \frac{(\gamma-1) - (\gamma+1)\rho_N}{(\gamma-1)\rho_N - (\gamma+1)} \qquad - (68)$$

$$V_N = -M_\infty\sqrt{\gamma}\cos\psi \qquad - (69)$$

It appears from equations (66) to (69) that radial shock speed W and the shock wave shape in terms of ψ and σ are required in order to evaluate the required dependent variables downstream of the shock. The computation starts from an assumed shock shape $SH(T_o)$ and shock velocity W. The new shock shape is given by,

$$SH(T_o + \Delta T) = SH(T_o) + W\Delta T \qquad - (70)$$

(For subsequent calculations, SH (To) is the calculated shock position and W the new estimate of shock speed).

Before the start of the shock evaluation routine, equation (70) is evaluated for each shock point Q. The sketch above represents the (To + ΔT) physical plane with the origin of the ξ-η co-ordinates at the point Q which is to be evaluated. The problem thus reduces to evaluating the shock velocity W which was assumed for the very first iteration, to be equal to the most recently computed one for a particular point. W is computed using an iterative procedure involving the MOC similar to the body and axis points.

Since the ξ co-ordinate direction is locally normal to the shock wave, the normal component of velocity U downstream of the shock is less than the speed of sound a. As $\xi_2(T_o) = -\left\{\left(\frac{d\xi}{dT}\right)_{T_o} + \left(\frac{d\xi}{dT}\right)_{T_o+\Delta T}\right\}\frac{\Delta T}{2}$. $\left(\frac{d\xi}{dT}\right)$ must be < 0 so that $\xi_2(T_o)$ is positive (Fig (17), Q1, Q2) and lies within the computational mesh. Hence $\left(\frac{d\xi}{dT}\right)$ = U - a is the required characteristic. As in the case of the body points $\eta_2(T_o) = -(V)\Delta T$ and $\xi_2(T_o) = -\frac{1}{2}\left\{U_N - a_N + U_2 - a_2\right\}\Delta T$. Using $\xi_2(T_o)$ and $\eta_2(T_o)$ the co-ordinates of point G_2 in Fig (14) are located. To start the iterative process $\xi_2(T_o)$ is set equal to $-(U - a)\Delta T$ where U and a are the normal component of velocity and speed of sound at Q in the T_o plane. This enables the compatibility equation (53) to be integrated,

$$U_{N2} = -\bar{a}\left\{P_N + P_2 - \frac{\gamma}{\bar{a}}U_2 + (RHS2)\Delta T\right\}$$

where P_2, U_2 and RHS2 are evaluated at G_2 using an iterpolation routine similar to the body points. P_N and ρ_N (which are also required for $\bar{a}$) are evaluated using the Rankine-Hugoniot relations (67) and (68). The normal velocity component U_{N1} is also evaluated using (66). The fraction $(U_{N2} - U_{N1}) / U_{N1}$ is used as an error function in a Newton-Raphson iteration procedure which enables a better estimate of W to be made. Thus the Rankine-Hugoniot relations and the compatibility equation are again evaluated and the process is repeated until the following convergence criterion is satisfied:-

$$\left| \frac{U_{N2} - U_{N1}}{U_{N1}} \right| < 10^{-5}$$

3.2.3.6. Evaluation of Subsonic Boundary C F

It would be convenient to treat boundary C F as a specified boundary such that the MFR could be set a priori by a particular choice of P, ρ, U and V at C F and held constant throughout the computation. Unfortunately specified boundaries in a transient computational procedure are not conducive to a stable computation if they are situated at a finite distance from the region of interest. When disturbances (changes in flow quantities due to the time dependency of the system) from the interior points reach the subsonic boundary they are reflected back into the computed region if the values are specified on the boundary. This is because there is no mechanism for absorbing the disturbances. Sharp peaks in the distribution of dependent variables occur and the computation soon becomes unstable (Moretti, Ref (53)).

Subsonic boundaries occur in other transonic flow problems such as supercritical flow over aerofoils and bodies of revolution and also flows in nozzles. Schemes have been developed by other workers in conjunction with the transient numerical method, for treating such subsonic boundaries with considerable success. Two promising methods have emerged and will be referred to as Scheme 1 and Scheme 2.

Scheme 1: Co-ordinate Stretching Method

A suitable transformation can be used to position the specified boundary at 'Infinity'. In Fig (18) this involves the equations of motion for the internal flow. As the computation is completed in a finite number of time steps, the disturbances originating from Mesh B would not reach the specified boundary which is at infinity. The physical axisymmetric cylindrical co-ordinates x and y are defined in Fig (18). The x - co-ordinate direction is stretched and two possible transformations are

$$X = \frac{x}{x + C} \qquad \text{(a)} \qquad \text{- (71)}$$

or

$$X = 1 - e^{-(xC)} \qquad \text{(b)}$$

and for the y direction,

$$Z = \frac{y}{BOC} \qquad - (72)$$

The above transformations, transform the semi-infinite region associated with the flow downstream of C F into a convenient unit computational Mesh C Fig (18)(b). In equation (71), C is a constant and X and Z are the computation co-ordinate directions. It can be seen from equation (71)(a) and (b), that as x tends to $+\infty$ X tends to 1. X = 1 at G' H' corresponds to the specified boundary in the computational mesh. X = 0 corresponds to x = 0 which is the entry plane. If BOC = BOC (x) is the ordinate of the inlet lip i.e. along C-C' then Z = 0 corresponds to the axis of symmetry and Z = 1 corresponds to C-C'.

The non-conservative equations (9) of chapter 2 can be rewritten in terms of computation co-ordinates of Mesh C using the above transformations. The interior and boundary points for Mesh C could then be evaluated using the same methods as indicated for Mesh A and B. At C F extra rows of Mesh points would be required so as to enable similar interpolation routines to that shown for intermesh boundary B E (section (3.2.1) to be used.

Migdal Ref (87) and Brown Ref (92) have used the stretching concept to prescribe upstream subsonic conditions for a convergent divergent and a convergent nozzle problem respectively. If this method were used for the present problem, the subsonic conditions giving the required MFR could be prescribed at G' H' in Fig (18)(b) and held constant throughout the computation. However considerable computation effort would be required for Mesh C which would have about the same number of node points as Mesh A or B. Moreover problems of matching the polar or toroid co-ordinates to the stretched two-dimensional or axisymmetric cylindrical co-ordinates were expected. Hence it was decided to persue an alternative course and use the MOC on boundary C F which would not require an extra grid system such as Mesh C.

Scheme 2 Evaluation of Subsonic Boundary C F using the Transient MOC

Fig (17) shows the orientation of the ξ - η co-ordinate system for the subsonic boundary C F. The method used was similar to those used for

the body, axis of symmetry and shock points. In this case however all three characteristics were used, i.e. $\frac{d\xi}{dT} = U + a$, $U - a$ and U. By using the first two characteristics, their corresponding compatibility equations could be evaluated using a similar iterative process described for other boundary points. This provided two simultaneous equations (59) and (60) which were solved in order to obtain P_N and U_N. S_N was obtained by integrating equation (55) along $\frac{d\xi}{dT} = U$ as follows:-

$$S_N = S(T_0) - \left(\nu \frac{\partial S}{\partial \eta}\right)_{T_0} \Delta T \qquad - (73)$$

and as before $R_N = (P_N - S_N)/\gamma$

The iterative process was continued until values of P_N and U_N from two consecutive iterations, l and $l + 1$, satisfied the following convergence criterion:-

$$\left| \left(P_N^{l+1} - P_N^{l} \right) / P_N^{l} \right| < 10^{-6} \quad \text{and} \quad \left| \left(U_N^{l+1} - U_N^{l} \right) / U_N^{l} \right| < 10^{-6}$$

Having calculated the converged values of P_N, R_N and U_N, the axial velocity V_N was calculated using the integral expression for the MFR equation (1), chapter 1. V_N was assumed constant along C F and hence can be expressed as:-

$$\bar{v} = (MFR) \Big/ \int_F^C \left(\frac{\bar{\rho}}{\rho_\infty}\right) \frac{(2y)^j}{U_\infty} \, dy$$

$$V_N = \frac{\sqrt{\gamma}}{a_\infty} \bar{v} = (MFR \sqrt{\gamma} M_\infty) \Big/ \int_F^C e^{R_N} (2y)^j \, dy \qquad - (74)$$

as $R_N = \log_e \left(\frac{\bar{\rho}}{\rho_\infty}\right)$

Using equation (74) it is possible to specify the MFR and calculate the axial velocity V_N. Thus the method outlined here for C F, calculates three variables R_N, P_N and U_N using the MOC and the fourth variable V_N using equation (74). Hence all four dependent variables were allowed to vary during the computation, with V_N constrained by the mass flow requirement which was achieved by specifying the MFR. For axially symmetric flows Equation (74) was not used due to stability problems. V_N was set equal to a constant calculated value using a one dimensional approximation described below in Section 3.3.

The original proposals for the subsonic boundary (Ref (98))required the η direction of the $\xi - \eta$ co-ordinate system to be parallel to C F in Fig (17). However preliminary computations were unsuccessful. By merely changing the orientation of the ($\xi - \eta$) co-ordinate system so that the η direction was parallel to the axis of symmetry, stable results were obtained. Since the flow in the vicinity of C F is predominantly in the axial direction, this choice of the η direction satisfied the requirement of Moretti's method (Section 3.2.3.2.) i.e. that the η direction should be parallel to the predominant direction of the local flow.

The transient MOC has been used by Bucher Ref (90) for the subsonic boundary occurring in the computation of the flow in the combustion chamber of a rocket engine. Serra Ref (88) also used the same method for the subsonic boundary occurring in a convergent divergent nozzle flows. Serra specified the pressure and computed the other dependent variables using the MOC. Both Serra and Bucher used the Lax-Wendroff Scheme for the interior points.

In the present work, the manner in which the flow variables are calculated at the subsonic boundary does not take into account the influence of the inlet geometry downstream of C F(see Fig (2)). The condition of uniformity in the axial velocity along C F does not cause a serious loss of generality. However this method is best suited for inlets with constant diameter internal ducts wherein uniform axial velocities would eventually occur at some distance downstream of C F for a specified mass flow requirement.

3.3. Initial Values for Mesh A and Mesh B

The computation starts with the estimation of initial values for Mesh A and Mesh B of Fig (15). The shape and position of the bow shock and the dependent variables between the shock, axis of symmetry and body surface are required. These initial estimates can only be expected to be rough approximations of the desired steady flow.

Subsonic boundary C F

It is assumed that the internal mass flow which is bounded by the stagnation streamline and the axis of symmetry passes through a region of the bow shock which is normal to the axis of symmetry. Hence for the given M_∞ , the downstream Mach number M_2 is calculated from the steady state Rankine-Hugoniot relations for a normal shock. Assuming the internal flow is isentropic and one-dimensional the ratio of the stream tube areas

$$(A/A_{sonic}) = \frac{1}{M}\left[\frac{1 + \frac{\gamma-1}{2} M^2}{\frac{\gamma+1}{2}}\right]^{(\gamma+1)/(2(\gamma-1))}$$

(given by Houghton, Ref (102).)

From Fig (4)(a) it can be seen that A = MFR for 2-dimensional flow and $A = \sqrt{MFR}$ for axisymmetric flow, if A is set equal to y_Q.

At the subsonic boundary C F, A_{C_F} is known. M_{C_F} can be calculated iteratively (or obtained from tables) using the above area - Mach number formula in terms of (A_{C_F} / A_{sonic}). Knowing M_{C_F} and the total pressure behind the normal shock which is assumed constant for the isentropic internal flow, all the other variables at C F can now be estimated. For the axisymmetric computations the axial velocity (which was calculated in this manner), was kept constant throughout the computations allowing the other variables to be calculated using the MOC. In order to check the validity of the one-dimensional approximation, comparisons were made with experimental results. Fig (19)(a) shows a comparison between the experimental and theoretical Mach number M_{C_F}. The experimental Mach number is in fact the average Mach number measured by a pitot-static rake at a station within the sharp lipped inlet for $M_\infty = 1.2$. The second comparison is between static pressure coefficients Fig (19)(b). The experimental static pressure coefficient is for a point C ($\theta = 270$) on a circular sectional inlet at $M_\infty = 1.82$. There

is good agreement with the Mach numbers for the sharp lipped Pitot-Inlet for a range of MFR. However a comparison of static pressure coefficients show larger discrepancies. This is due to the two dimensional effects which exist in the region of inlet lip. Thus the one dimensional approximation appears to predict a lower C_{pC} or higher axial velocity for MFR < 0.8. The variation of C_{pC} with MFR appears to follow the same trend as the experimental results and is adequate for an initial estimate of flow quantities for the subsonic boundary C F.

Bow Shock Wave Fig (20) (a)

An initial estimate of shock stand-off distance is made by studying previous numerical computations for similar shapes, M_∞ and MFR. Alternatively the estimate is guided by shock stand off data available for supersonic blunt body flows. The bow shock is assumed to be normal up to a distance of unity above the axis of symmetry. This implies that the stagnation streamline is parallel to the axis and the stagnation point corresponds to $\theta = 180^\circ$ on the inlet surface. Above this stagnation streamline, the shock is assumed to take the shape of a hyperbola with an asymptote to the a Mach line with a slope of $\tan(\mu)$; μ is the Mach angle. Knowing the shock shape and M_∞, the flow variables downstream are computed using the Rankine-Hugoniot Relations. The initial shock velocity is set equal to zero for all points.

Body and Axis of Symmetry Points Figs (20)(b) and (c)

On the body surface the pressure distribution is given by Newtonian impact theory, from the stagnation point at $\theta = 180^\circ$ to the external supersonic boundary at point A. The velocity components are given by an assumption of the Mach number at point A. The Mach number is linearly interpolated between the stagnation point and point A. A similar linear interpolation is carried out between the stagnation point and the point C where the flow variables are computed using the one dimensional approximation described above. The entropy on the body and axis points are set

equal to the normal shock entropy for the given M_∞ . The other variables on the axis of symmetry are estimated by linear interpolation between the shock point E and point F, Fig (20)(a).

Interior Points

Once the initial values on the boundary points have been estimated for Mesh A and Mesh B, the flow variables at the interior points are obtained by linear interpolation between the body points and the shock and axis of symmetry points along each Z co-ordinate in the computational plane. As can be seen from Fig (20)(a) this interpolation is adequate and gives a realistic variation of flow directions above and below the stagnation streamline which divides the internal and external flow. Fig (20)(b) and (c) give examples of the variation of Mach number and pressure for the interior and boundary points along Z = constant lines in the computational plane.

3.4. Differences in the Computational Procedures between the SUBIB and SUPIB Problem

Fig (21) shows the physical and computation planes for the SUPIB problem. These are very similar to the SUBIB problem, Fig (15) excepting that in Fig (21) the boundary C F in the physical plane is at an angular position $\theta > 270^\circ$ so as to allow the flow to reach supersonic speeds internally.

Most of the computational techniques for the interior points and boundary points are almost the same as those used for the SUBIB problem and only the chief differences are indicated here. As the internal flow is supersonic, use is made of the expected sonic conditions near the minimum cross-sectional area on the body and axis points, when specifying initial conditions.

When evaluating the tangential component of velocity for the body and axis of symmetry, a first order method using equation (63) was used and was found sufficient to insure stability. However in this case the spatial derivatives were replaced by central differences when $\left(\frac{\partial V}{\partial T}\right)_{T_0}$ was evaluated.

The evaluation of the boundary points on C F was considerably simplified.

The linear interpolation equation (38) was used to evaluate the flow variables from the two adjacent rows of points. Thus the MFR or axial velocity was not specified at C F but was determined as part of the solution.

3.5. Summary (Refer to the Flow Diagram in Appendix (D).)

The computation starts with the specification of initial values. The first stable time step is computed. Next the boundary points are computed in the following order:-

Shock points, Axis points, body points and finally the subsonic boundary points. The interior points for Mesh A and B are then evaluated. The second steps of the MacCormack scheme for the body and axis points follow next. The computation for the first time step is concluded with the new values of the dependent variables at each grid point being reset to initial values in preparation for the next time step and finally the extra mesh points for Mesh A and Mesh B are evaluated.

Depending on the output frequency parameters which are read in with the data cards, at this stage the program can either return directly to the begining to start the next time step or list variables on the boundaries and or interior points and compute and list other variables such as the drag coefficients. Storage of results on Magnetic-Tape is also optional. The process is repeated for each time step until the computation is terminated after a certain number of time steps is reached.

Appendix (D) contains a complete listing of a computer program written in FORTRAN for the SUBIB problem. Running instructions and a list of the main identifiers are also provided. The computations were performed on CDC 6600 and CDC 7600 digital computers at the University of London Computer Centre.

CHAPTER 4

DISCUSSION OF RESULTS

Initially a computer program was developed to solve the SUPIB problem. Since the SUBIB problem involved the same scheme for the interior points and similar schemes for the boundary points, it was first necessary to check the SUPIB results before incorporating these schemes into the computer program for the SUBIB problem.

Most of the results presented in this chapter are for Inlets A, B and C, details for which are given in Fig (4).

4.1. Supersonic Internal Boundary Results

The flow about an axisymmetric inlet for a free stream Mach number of 2 was computed. The inlet lip had a circular section with $R_H = 0.35$ (similar to Inlet A of Fig (4)).

Fig (22) shows a flow direction plot for the converged results. The mesh boundaries are defined by A-B-C the inlet surface, D-E the shock, E-F the axis of symmetry and A-D and C-F are external and internal supersonic boundaries. Each arrow corresponds to a node point, hence the node density for Mesh A can be specified as 10 x 20 i.e.10 mesh divisions in the radial direction and 20 divisions in the θ direction. Similarly for Mesh B the node density is 10 x 10. These numbers do not include the extra mesh points for each mesh at B-E.

The point Q is the intercept in a meridian plane of the stagnation streamline (represented by a broken line) and the bow shock wave. The ordinate y_Q is given in terms of the mass flow ratio MFR (for axisymmetric flow),

$$\text{MFR} = \frac{y_Q^2 \pi U_\infty \rho_\infty}{H^2 \pi U_\infty \rho_\infty} = \left(y_Q / H\right)^2 .$$

H is the distance of the origin O above the axis of symmetry E F. The MFR was calculated at C-F using an expression similar to equation (1), chapter 1 and in this case had a value of 0.44. Hence $y_Q = H\sqrt{\text{MFR}}$. It is interesting to note that the position of Q calculated in this manner agrees well with the estimated position of the stagnation streamline obtained by studying the flow direction plot.

The corresponding Mach number contours for the same physical region

are given in Fig (23). The stagnation streamline divides the flow into two regions: the external flow and the internal flow. For the external flow, the Mach number contours are similar to those reported for the supersonic blunt body results, given by Moretti Ref (64). The internal flow Mach countours bear a resemblance to those reported by Serra Ref (88) for convergent-divergent nozzle flows. The external sonic line makes an acute angle with the inlet surface and intercepts the shock wave downstream of the sonic point on the body. This is similar to the sonic line shape for spherical blunt bodies at $M_\infty < 2.5$ (see Chapter 1, section 1.3 and Fig (3) (a)). The external and internal computational boundaries A-D and C-F have been placed well downstream of the sonic lines so as to justify the use of the simple extrapolation method described in section 3.2.2. chapter 3.

Fig (24) shows the pressure and Mach number distribution for the body shock and axis of symmetry points. In Fig (24) (a) the angular position of the stagnation point is located at M = 0. The angular position for this stagnation point agrees with the angular position for the maximum pressure in Fig (24)(b). There is a noticeable discontinuity in the slope of the Mach number and pressure curves (corresponding to the shock and axis points) at θ_E (see Fig (22)), from where the axis points commence. The flow variables at point E were known exactly from the normal shock relations as the bow shock is normal to the axis of symmetry at point E. A comparison of the computed pressure p with that obtained from the exact Rankine-Hugoniot relations (for steady flow) at $M_\infty = 2.0$ showed an error of 2%. This was attributed to the shock point E having a positive radial velocity W of the order of 10^{-2} when the computation was finally terminated. If W was $\leq 10^{-3}$ (as was the case for all the other points), the steady state conditions, given by W = 0 in Equations (66) to (69) chapter 3 would have been more accurately obtained.

Using the Moretti scheme for the body surface points the entropy cannot be calculated merely by tracing the particle path along the surface of the body. This is because the scheme does not have any mechanism by which the

time dependent entropy on the stagnation streamline can proceed beyond the stagnation point on the body surface. Hence the particle tracing method would merely re-distribute an initial distribution of entropy or alternatively, if it were initially assumed constant it would remain so for the rest of the calculation. Two possible methods for computing the entropy which were discussed in section 3.2.3.4. chapter 3 will now be described in relation to Figs (22) and (25).

Method 1 assumes that the entropy is constant on the surface and equal to that obtained from the normal shock relations for the given M_∞. This assumption implies that the stagnation streamline in the final steady state passes through a region of the bow shock which is normal to the free stream direction. The validity of this assumption can be checked by observing the position of point Q in Fig (22) in relation to the local slope of the bow shock.

Method 2 calculates the MFR at each time step and hence the co-ordinates of point Q are obtained as explained above. The entropy at point Q is obtained using values from the adjacent node points. The node point with the minimum value of velocity is then located on the inlet surface and the entropy at this point is set equal to the calculated value at point Q. For the other points the entropy is calculated by tracing the particle path.

Fig (25)(a) shows the variation of entropy on the inlet surface (using method 2) at k = 300, 600 and 1200. Initially the maximum fluctuations occur in the region of the stagnation point. These fluctuations then reduce with increasing k and at k = 1200, the entropy is almost constant on the inlet surface; a variation of $\pm$ 0.8% about the mean value was noticed at k = 1200. The mean value of entropy did not differ significantly from the normal shock value (shown by a broken line in Fig (25)(a)) i.e. the value set using Method 1.

Also shown in Fig (25)(a) is the variation of entropy behind the bow shock at k = 1200. The variation of entropy is smooth until the angular position corresponding to point E is reached where again as in the case of

the pressure and Mach number results of Fig (24), a discontinuity in the slope of the entropy curve is noticed.However for other points on the axis, the entropy is almost constant. This is to be expected as the axis of symmetry is a particle path with a constant value of entropy on it (in the steady state) which is equal to the normal shock value.

Fig (25)(b) compares the values of entropy computed using Method 1 and Method 2 at two different time steps, k = 600 and k = 1200. The results correspond to the column of grid points of Mesh A and Mesh B for which Z = 0.5 (where Z = 0 on the Inlet surface and Z = 1 for the shock and axis of symmetry node points). At k = 600 large fluctuations are noticed in the vicinity of the stagnation point and there is a noticeable difference between Method 1 and Method 2. However for the converged results at k = 1200, these differences are small. The transient behavior of the results for Method 1 and Method 2 were different, but the converged results for pressure and Mach number were essentially the same. Differences in the fourth significant figure were noticed for the inlet surface pressure results, when the two methods were compared. Hence this justifies the use of Method 1 for most of the other results presented in this chapter as Method 2 was developed later.*

Comments regarding the value of entropy on the body surface have been made by Bohachevsky (67),Shifrin Ref (114) and Ladyshenkii Ref (115). Bohachevsky who computed the flow about axisymmetric bodies at incidence noticed that the maximum entropy streamline which passed through the normal region of the bow shock wave, did not wet the body surface. Studying Fig (22), a similar observation can be made. In the steady state the axis of symmetry is a maximum entropy streamline. The streamlines formed subsequently above the axis of symmetry have a decreasing value of entropy, as the bow shock gets weaker. This can be seen by observing the entropy curve for the shock wave in Fig (25)(a); for $\theta < \Theta_E$ ($\Theta_E = \Theta_B$) i.e. proceding away from the axis of symmetry the entropy decreases behind the bow shock. However for this particular case, the converged value of the stagnation

*(Provided the shock is nearly normal to the stagnation streamline).

streamline entropy was only 0.4% less than the exact normal shock entropy at $M_\infty = 2.0$.

To check the accuracy of the method, comparisons were made with the experimental results produced by D'Souza Ref (97). Fig (26) shows the pressure distribution for the flow about a toroid with $R_H = 0.5$ at $M_\infty = 8.33$. The comparison shows a good agreement with the experimental and numerical results produced by D'Souza who also used a transient numerical method.

4.2. Subsonic Internal Boundary Results

In this section, results for the SUBIB problem are presented. As outlined in chapter 3, section (3.2.3.6), the node points on boundary C F of Fig (15) needed to be specially treated so as to enable the axial velocity or the MFR to be specified.

4.2.1. Axisymmetric Flow

In this case the axial velocity was specified at boundary C F and held constant throughout the computation. Hence the MFR which involved pressures and densities did not correspond to a preset fraction. In practice values of the actual MFR calculated differed by not more than $\pm$ 10% of the preset value which was used to calculate the axial velocity at C F using a one-dimensional approach . (This was described in section (3.3), chapter 3).

Initially the flow about Inlet B at $M_\infty = 2.81$ was calculated. The effect of reducing the mesh size for the same boundary conditions, was studied. The two node densities for the coarse and fine mesh sizes were, 5 x 10 (Mesh A), 5 x 4 (Mesh B) and 10 x 20 (Mesh A), 10 x 8 (Mesh B) respectively. Thus by reducing the mesh size by half, the total number of node points was increased by a factor of four, from 70 node points to 280 nodes.

Flow direction plots for both mesh sizes are presented in Fig (27). An uneven distribution of shock points occurs towards the axis of symmetry for both node densities. This is attributed to the inaccuracies incurred

due to the one dimensional unsteady MOC which was used to calculate the shock velocity in conjunction with the Rankine-Hugoniot relations. It will be recalled, referring to Fig (17) that the Moretti's one dimensional unsteady approach works best when η direction is parallel to the local direction of the flow so as to justify the assumption that the derivatives with respect to η in the compatibility equation (equation (53), Chapter 3), are constant with respect to time. In the case of the shock points the predominant direction of flow at Q_2 appraoches the ξ direction rather than the η direction, for points near the axis of symmetry. This can be checked by referring to Fig (27). However as the bow shock gets weaker at increasing distance away from the axis of symmetry, the tangential component of velocity at the bow shock (see equation (69), Chapter 3) is larger so that the local flow direction approaches a direction parallel to the η direction at point Q_1 in Fig (17). This would explain why the irregularities in shock shape subside with increasing distance from the axis of symmetry in Fig (27).

The possibility of the shock points being affected by the disturbances originating from the subsonic boundary C-F cannot be ruled out. The shock shape for the SUPIB problem Fig (22) appears to be more smooth compared to the shock shapes presented in Fig (27). Since the boundary C-F in Fig (22) is supersonic, disturbances cannot propagate upstream from any point on it. Hence Fig (22) presents a shock shape uninfluenced by any inaccuracies originating from the treatment of boundary C-F. However for both the SUPIB and SUBIB problem results (including those to be discussed below), the shock points near the axis of symmetry always took longer to converge compared to the shock points nearer point D, (Fig (27)).

Fig (28)(a) and (b) compare Mach number and pressure distribution on the inlet surface for the two node densities. Reducing the mesh size improves the pressure results in the region of the stagnation point for a value of θ corresponding to M = 0.

Fig (29) shows the transient behaviour of the normal pressure drag, total pressure and shock movement convergence criterion. The results are

plotted against the computational time T. The accumulative computational time for the complete computation is defined as,

$$ACCT = \sum_{k=1}^{K_{RUN}} \Delta T$$

where K_{RUN} is the maximum number of time steps. 750 time steps were required for the coarse mesh and 1500 for the fine mesh. Both the coarse and fine mesh solutions were started with the same initial conditions and appear to converge at about the same value of ACCT $\approx$ 6.0. Thus it appears that for the same initial conditions and boundary conditions such as M_∞ , MFR and body shape, the value of T for which the solution approaches the steady state, is almost independent of the node density. The increment ΔT reduced in size as the mesh size in the computational plane (and hence the phsyical plane) was reduced, consequently a larger number of time steps k was required to reach the value of T for which convergence occurred.

The common feature of the curves presented in Fig (29), is that the fluctuations reduce in amplitude as the steady state is reached. The cowl drag coefficient is defined as follows

$$C_D = \int_{\theta_A}^{\theta_C} \frac{C_p r \sin\psi (2y)^j}{\sin(\theta-\psi)} d\theta$$

(derived in Appendix A) and involves the integration of the pressure coefficient on the inlet surface and hence Fig(29)(a) is a good measure of the overall transient behaviour of the pressure distribution on the inlet surface.

The pressure recovery was calculated at the subsonic boundary C-F using the following expression:-

$$P_R = \frac{1}{CF} \int_F^C \left(\frac{\bar{P}_o}{\bar{P}_{o\infty}}\right) dy$$

where P_0 is the total pressure P_R represents the ratio of average value of the total pressure on boundary C-F to the freestream tot al pressure. Since the calculation of $\left(\frac{\bar{P}_o}{\bar{P}_{o\infty}}\right)$ at each node point on C-F involved all four dependent variables, the transient behaviour of P_R (Fig (29)(b))is

a good indication of the manner in which the flow quantities on C-F converge. For comparison the value of P_R was calculated for which the ratio was set equal to the normal shock value for the given free stream Mach number of 2.81. This value of P_R is the lowest expected value for the given M_∞. The fine mesh values of P_R in Fig (29)(b) converge to a larger value of P_R which is to be expected as the bow shock calculated for this case (see Fig (27)) is not strictly a normal shock. The coarse mesh results show a lower value of P_R compared to the normal shock P_R and hence must be affected by the larger truncation errors.

The shock velcities appeared to be the most sensitive parameters regarding the approach of the steady state conditions. A parameter which was effectively a measure of the overall shock movement served as a useful convergence criterion (abbreviated as CONCRIT; defined in Fig (29)(c)). For most cases CONCRIT $\leq 5 \times 10^{-5}$ was sufficient to ensure that the solution had converged. This condition was obtained for both the coarse and fine mesh results in Fig (29) (c).

In Fig (30) a comparison is made between experimental results reported by Gibbings Ref (104) and numerical results for a circular lipped axisymmetric inlet at M_∞ = 1.82 and MFR = 0.58. Numerical results are presented for Inlet B with R_H = 0.25, Fig (30)(a). The details of the inlet geometry used in the experiment are given in Fig (30) (b). The circular lip radius was given by R_H = 0.0935 i.e. the Inlet B had a lip radius more than 2.5 times as large as that of the experimental results. The bow shock for Inlet B is presented but the corresponding experimental results were not available. Fig (30)(c) shows a comparison of C_p as a function of θ. The experimental values of C_p at MFR of 0.58 were obtained by interpolation from the given table of C_p values at different values of MFR for M_∞ = 1.82 Since the external afterbody lies downstream of the supersonic region (at $\theta = 97.4^\circ$), its shape has no influence on the given results. The major differences result from the comparitive thickness of the two inlets.

Since the internal contraction for Inlet B is much larger, the mean internal velocity at $\theta = 270^{\circ}$ or C-F is expected to be larger (for the same MFR and M_{∞}). Hence lower values of C_p are obtained towards the subsonic boundary C-F.

An attempt was made to repeat the numerical calculations with R_H = 0.0935 so as to enable a closer comparison with experiment to be made. Large negative shock velocities were observed in the region near the axis of symmetry after which the results soon became unstable. These instabilities appear to have been caused by the limitations of the one-dimensional unsteady MOC treatment for the shock points which was discussed earlier in relation to the uneven distribution of shock points observed in Fig (27).

To conclude the presentation of the axisymmetric flow results, the flow about an elliptic Inlet with major to minor axis ratio of 1.5 (Inlet C), was computed. The free-stream Mach number was 2.81. The flow direction plot for the converged results are given in Fig (31). The position of point Q obtained from the calculated value of the MFR, agrees well with the conjectured position of the stagnation streamline (shown by a broken line) obtained by studying the flow direction plot. The converged MFR in this case was equal to 0.594. Fig (32) shows the Mach number contours for Inlet C. The subsonic boundary C-F was observed to have $\pm$ 1% variation in Mach number about the mean Mach number. Hence the subsonic boundary was almost a constant Mach number line.

Fig (33) gives the Mach number and pressure distribution on the surface of Inlet C, behind the bow shock and on the axis of symmetry. The variations of pressure and Mach number in the region of the stagnation point appears to be more rapid than that in Fig (28)(a) and (b) for Inlet B which had a circular section and the same thickness t_H = 0.5. These results required 1500 time steps to converge and about the same computer

Central Processor Unit (CPU) time as the results for Inlet B.

Figs (31) to (33) demonstrate the computer program's expected ability to calculate the flow about an arbitrary inlet shape whose contour is specified using an analytical expression with the origin at point O in Fig (31). Inlet shapes which have discontinuities in curvature which occur in the supersonic region are unlikely to be treated successfully by the present method. This is because embedded shocks are often known to occur when a supersonic expansion is arrested by an abrupt change in curvature (see Traugott Ref (16) and Barnwell Ref (77)).

4.2.2. Two Dimensional Flow Results

Two dimensional computations were performed for Inlet A for a free stream Mach number range $2 \leq M_\infty \leq 3$ were calculated at a constant MFR of 0.6. At $M_\infty = 2.5$, results were also produced for different mass flow ratios in the range $0.5 \leq MFR \leq 0.9$. For these two-dimensional case studies, the treatment of the subsonic boundary C-F enabled the MFR for a preset fraction to be obtained. The subsonic axial velocity component was constant along C-F but it changed from one time step to another, until the results finally converged.

Fig (34) shows the flow direction plot about Inlet A at $M_\infty = 2.81$ and MFR = 0.6. Once again, as was observed with the axisymmetric results, the conjectured position of the stagnation streamline (broken line) agrees with the position of point Q which was obtained from MFR; i.e. $y_Q = MFR \times H = 0.6H$.

Fig (35) is an example of the variations of the Mach number and pressure distribution through Mesh A and Mesh B for the above case. Results are presented for Z = constant lines, going up in increments of 0.2 from the body surface to the shock points and axis of symmetry. Oscillations are seen to occur in the Mach number distribution for the axis of symmetry These oscillations were seen to increase in amplitude as the node density was increased from 10 x 15 (Mesh A), 10 x 7 (Mesh B) to the present case 15 x 20 (Mesh A), 15 x 10 (Mesh B). To try to alleviate this problem, the

convergence criterion for the MOC at axis points was reduced by an order of magnitude and the second order accurate MacCormack scheme was used for computing the axial velocity (section (3.2.3.4) Chapter 3). Both these modifications made no significant improvements to the converged results. In Fig (34) it can be seen that the subsonic internal flow in Mesh B (bounded by B-E-C-F) suffers a reduction in streamtube area as boundary C-F is approached and hence the Mach number is expected to increase. However for the low mass flow ratio cases, the flow is forced to decelerate due to the boundary conditions at C-F which demand a lower mass flow for the same M_∞ and body inlet shape. The oscillations of Mach number on the axis of symmetry appear to be the reaction of the numerical scheme to the conflicting requirements of a decelerating flow in a contracting subsonic stream tube. This problem was investigated further by plotting the Mach number at each node point on the axis of symmetry for different values of MFR and a constant $M_\infty = 2.5$. Fig (36) shows that the oscillations reduce as the MFR is increased i.e. as the mean Mach number at the subsonic boundary increases above the value immediately behind the shock (at $Y_B = 0$). For the SUPIB problem where no boundary conditions were imposed internally, the flow accelerated to supersonic Mach numbers and no oscillations were noticed for the Mach number distribution on the axis of symmetry (see Fig (24)(a)).

In Fig (35)(a), it can be seen that the oscillations are confined to the axis of symmetry and do not spread across the mesh. Wehofer and Moger Ref (93) reported severe oscillations in time-dependent solution of nozzle flow problems. To prevent the solution from becoming unstable they used a smoothing process in the subsonic region where they imposed constant upstream conditions. In the present problem, no smoothing process was used; the oscillations remained bounded as convergence was reached asymptotically in time.

Fig (37) shows the variation of bow shock position and shape with MFR at $M_\infty = 2.5$. As the MFR is increased the bow shock detachment distance

reduces. Alternatively Fig (38) shows a reduction in the shock detachment distance when M_∞ is increased at a constant MFR of 0.6. This trend is similar to the reduction of shock detachment distance for a blunt body in a supersonic stream of increasing M_∞ .

Fig (39) shows the variation of Mach number and static pressure coefficient on the surface of Inlet A for MFR = 0.5, 0.7 and 0.9 at M_∞ = 2.5. In Fig (39)(a) the stagnation point which occurs at M = 0 moves away from the leading edge which is at $\theta = 180^\circ$ as the MFR is decreased. Ideally if the MFR were zero, the stagnation point would be situated at $\theta = 270^\circ$.

Fig (39)(b) shows the corresponding variation of C_p for different values of MFR at constant M_∞ . Irregularities in C_p values for MFR = 0.5 are seen to occur. A closer examination of results revealed that this was caused by the stagnation point occurring adjacent to the node point corresponding to the inter mesh boundary at B in Fig (15).

Fig (40) shows the variation of M_∞ and C_p on the surface of Inlet A for M_∞ = 2.0, 2.5 and 3.0 a a constant MFR of 0.6. Due to an increase in free stream total pressure (as M_∞ increases), an increase in the subsonic boundary Mach number (Fig (40)(a) $\theta = 270^\circ$) is noticed for the same mass flow requirement. The corresponding C_p results show an expected increase in stagnation pressure as M_∞ is increased.

The drag coefficients for Inlet A are presented in Fig (41). Expressions for the Cowl Drag, Additive Drag and External Drag are derived in Appendix (A). Briefly, the Cowl Drag is the axial component of the force obtained by integrating the static pressure on the surface of the cowl. The Additive Drag is the drag associated with the integration of pressures on the stagnation streamline from the bow shock to the stagnation point on the inlet surface. Additive Drag occurs due to the spillage of mass flow when the inlet is operating at Mass Flow Ratios less than unity. The External Drag is the sum of the Additive Drag and the Cowl Drag associated with the external flow. The External Drag is effectively the resultant drag force acting on the inlet and its coefficient $C_{D_{EXT}}$ is comparable

to the C_D obtained by wind tunnel force measurements (neglecting the skin friction drag and allowing for base pressure effects).

Fig (41)(a) shows the Drag coefficients plotted against M_∞ at a MFR = 0.6. C_{DEXT} increases gradually due to the effect of wave drag which increases as M_∞ increases. (The wave drag is also known to increase with M_∞ for low fineness ratio (length to diameter ratio) axisymmetric blunt body at supersonic speeds). As M_∞ increases the shock detachment distance reduces and the length of the stagnation streamline shortens, consequently there is a reduction in C_{DADD}.

Fig (41)(b) shows the drag coefficients plotted against MFR for a constant value of M_∞ equal to 2.5.

Referring to the sketch in Fig (41) the Additive Drag can be defined as,

$$C_{DADD} = \frac{2}{\gamma M_\infty^2 H^{(j+1)}} \int_{y_Q}^{y_S} (p-1)(2y)^j \, dy$$

where p is the static pressure acting on the stagnation streamline. As the MFR tends to unity, the difference between y_S and y_Q tends to zero, i.e. at MFR = 1 the stagnation streamline is nearly parallel to the axis of symmetry and the shock detachment distance is small. Hence the magnitude of the above integral reduces in size as the MFR approaches unity. In Fig (41)(b) C_{DADD} shows the expected trend as the MFR approaches unity. Since C_{DEXT} is dependent on C_{DADD}, there is a corresponding decrease in C_{DEXT}.

4.3. Comments on Computational Efficiency

Fig (42) shows the variation of time step k and Central Processor Unit Time (CPU, CDC 6600 digital computer) in seconds, as a function of computational time T. The data presented in Fig (42) corresponds to the results for the two mesh sizes presented earlier in Figs (27) to (29). Fig (42)(a) shows that by halving the mesh size for computational co-ordinates, the number of time steps required for convergence approximately doubles. The relationship between the two values of CPU at the converged

value of T is not as simple, i.e. halving the mesh size does not necessarily double the CPU time for the same value of ACCT (assuming the same initial conditions were used). The interior points for each computational region, Mesh A or Mesh B, are computed using an explicit scheme and hence invlove the same number of arithmetic operations for each time step k. The CPU time for each interior point at any value of k is independent of the node density. The boundary points however involve iterative processes which could vary with k (in the initial stages of the computation) and more significantly with the node density. The latter point can be demonstrated by defining a computational efficiency parameter ϵ as follows:-

$$\epsilon = \frac{\text{CPU (seconds)}}{K_{RUN} \text{ X (total number of node points)}} .$$

(Note, the computational efficiency effectively reduces with an increase in the value of parameter ϵ). ϵ gives the average value of CPU seconds per node point per time step. The relationship between CPU and k (for a given node density) is almost linear as both CPU and k are nearly linearly dependent on T as shown in Figs(42)(a) and (b). Hence for a given node density, the number of CPU seconds per time step is almost constant. If ϵ were defined for the two node densities presented in Fig (42), the fine mesh gives $\epsilon = 2.1 \times 10^{-3}$ and for the coarse mesh $\epsilon = 9.92 \times 10^{-3}$. The coarse mesh results show a reduction in computational efficiency partly because a larger number of iterations are required at the boundary points because of the larger truncation errors and also because the number of boundary points is a bigger percentage of the total number of node points.

The definition of ϵ does not take into account the rate of convergence of the scheme. For example, although the coarse mesh results show an increase in ϵ, only half as many time steps are required for convergence. This is due to the larger average time step size as compared to that in the fine mesh results. For a given node density, schemes which could produce stable solutions with a larger time step size would be expected to converge

faster.

Table (2) lists the node density, K_{RUN}, CPU seconds and other relevant information for some case studies. For items (1) to (5) the computations were performed on the CDC 7600 digital computer. The CPU value equivalent to the CDC 6600 digital computer were obtained approximately by multiplying by a factor of 4. ϵ for the SUPIB results, items (11) and (12) give values of 1.94×10^{-3} and 1.89×10^{-3} respectively. For comparison item (13) gives a set of typical data for the supersonic blunt body problem of Ref (69) which gives a value of $\epsilon = 1.14 \times 10^{-3}$.

Computations were usually terminated when CONCRIT was of the order of 5×10^{-5}. However in some cases a less severe criterion with CONCRIT 15×10^{-3} also produced acceptable results. In general for both the SUPIB and SUBIB problems it was noticed that as M_∞ was lowered, the accumulative computational time ACCT increased in size, hence more time steps were required to achieve convergence.

TABLE 2

Item No.	M_∞	MFR	Inlet Shape	Node Density MxNA MxNB	k	ACCT	CONCRIT (X 10-5)	CPU 6600 (Secs)	CPU 7600 (Secs)
1.	2.0	0.6	Inlet A 2-D	10 x 18 10 x 9	2500	18.12	14.6	1168*	292+
2.	2.25	0.6	"	10 x 18 10 x 9	2000	14.19	6.5	956*	239+
3.	2.50	0.6	"	10 x 18 10 x 8	2000	13.53	13.55	900*	225+
4.	2.75	0.6	"	10 x 18 10 x 8	2000	13.12	4.93	904*	226+
5.	3.00	0.6	"	10 x 18 10 x 8	2000	12.53	9.29	908*	227+
6.	2.81	0.59	Inlet C (Axsy)	10 x 20 10 x 8	1500	6.8	0.4	888+	222*
7.	2.81	0.49	Inlet A (Axsy)	10 x 18 10 x 6	1500	9.75	0.07	885+	221*
8.	2.81	0.39	Inlet A (Axsy)	10 x 18 10 x 6	1500	9.59	1.06	774+	193*
9.	2.81	0.59	Inlet B (Axsy)	10 x 20 10 x 8	1500	5.88	2.4	891+	222*

Continued overleaf/

TABLE 2 continued...

Item No	M_∞	MFR	Inlet Shape	Node Density MxNA MxNB	k	ACCT	CONCRIT ($\times 10^{-5}$)	CPU 6600 (Secs)	CPU 7600 (Secs)
10.	2.81	0.59	Inlet B (Axsy)	5 x 10 5 x 4	750	6.00	2.9	522+	130*
11.	2.0	0.44	(SUPIB) See Fig (22)	10 x 20 10 x 10	1200	8.95	2.1	684+	171*
12.	8.33	0.369	(SUPIB) Circular section R_H = 0.5	10 x 20 10 x 15	800	1.94	2.7	531+	142*
13.	2.0	—	(Blunt Body) circle 2-D	12 x 12	1200	25.5	2.88	197+	49*

+ Actual

* Equivalent (Approx)

CHAPTER 5

CONCLUSIONS AND RECOMMENDATIONS FOR FUTURE WORK

5.1. Conclusions

A transient finite difference method was developed to compute the supersonic flow about ducted bodies with supersonic and subsonic internal boundaries. From the results presented in chapter 4 the following conclusions were drawn:-

1) Moretti's method for the interior points required only the CFL stability condition to be imposed so as to obtain a simple explicit and second order accurate method. Node points at the intermesh boundary B E, were treated as interior points and did not cause any stability problems provided the following inequality was satisfied.

$$0.5 \leq (\Delta\theta_A / \Delta\theta_B) \leq 2.0$$

where $\Delta\theta_A$ and $\Delta\theta_B$ are the angular mesh increments for Mesh A and Mesh B respectively.

2) The boundary points had a strong influence on the stability and computational efficiency. The one-dimensional unsteady approach greatly simplified the treatment of the boundary points and reduced the computational effort required.

3) The main contribution of the work is the development of a scheme for treating the subsonic internal boundary. The MFR for two-dimensional flow and the axial velocity in the case of axisymmetric flow could be specified*. The unsteady MOC used at this boundary avoided the need to use a co-ordinated stretching method which would have reduced the computational efficiency and increased the storage requirements.

4) For the SUPIB problem, two examples of results for circular sectional inlets were presented: the first at $M_\infty = 2.0$ and the second for $M_\infty = 8.33$. At $M_\infty = 8.33$, good agreement was obtained with existing experimental and

---

* The manner of this specification implies the flow downstream to be compatible with the computed flow. This is a usual "intake assumption", and is not a practical disadvantage.

numerical results. This provided a reliable check on the basic numerical scheme which was subsequently modified to enable the SUBIB to be solved.

5) For the SUBIB problem, converged results were presented in the Mach number range $1.82 \leq M_\infty \leq 3.0$ for two-dimensional and axisymmetric shapes with $t_H = 0.5$.

6) A study was made of the two-dimensional flow about Inlet A(Fig (4)) in the Mach number range $2 \leq M_\infty \leq 3$ at MFR = 0.6 and at a constant $M_\infty = 2.5$ for the Mass Flow Ratio range of $0.5 \leq MFR \leq 0.9$. An analysis of the bow shock shape and position, pressure and Mach number distribution on the inlet surface and the drag results showed that the numerical method interpreted the physical situation correctly.

7) The conjectured position of the point of intersection between the bow shock and the stagnation streamline was obtained by studying the steady state streamline pattern. This position agreed well with that obtained from the actual MFR. This agreement provided an independent check on the overall consistency and accuracy of the numerical scheme.

5.2. Recommendations for Future Work

Experimental work on inlets given in Gibbings Ref (104) and Petersen Ref (118) and also Ref (116) indicate that practical inlet thickness parameters t_H lie in the range $0.1 \leq t_H \leq 0.3$. Due to current interest in transonic transports, results in the Mach number range $1.1 \leq M_\infty \leq 1.3$ are also desirable. There is a need for further refinement of the present method in order to produce results for these values of M_∞ and t_H.

The effect of smoothing variables in Mesh B needs to be studied. Smoothing variables on the axis of symmetry could reduce the oscillations such as those shown in Fig (36) and possibly extend the range of application of the present method.

The effect of smoothing on the bow shock wave should also be studied The use of an improved version of the MOC for the shock points (see Elliot Ref (41)) is also recommended. Elliot's method is not influenced by the local direction of the flow and uses only one bi-characteristic. Hence if

a stable interpolation scheme can be derived, an improvement in the results for the shock points near the axis of symmetry can be expected. Similarly Butler's method Ref (39) for the subsonic boundary points could also be used. The use of Elliot's and Butler's method would require more computational effort. However it is possible that with improved accuracy at the shock and subsonic boundary points, the rate of convergence could increase hence fewer time steps would be required.

The CFL condition governs the size of time increment ΔT for each step k. Recently some effort has been devoted to deriving transient differencing schemes which are stable for a larger values of ΔT. MacCormack and Paullay Ref (44) introduced a fractional-step or time spliting method wherein the scheme for a multi-dimensional problem is split up into a sequence of one-dimensional operators each of which is integrated for a fraction of ΔT. Since the resulting ΔT is larger the computation is more economical. MacCormack Ref (112), contains a successful application of the time spliting scheme to a shock boundary layer interaction problem. Rizzi and Inouje Ref (113), recently applied this method to compute the supersonic flow about axisymmetric blunt bodies at zero incidence and at an incidence of 30°. Unfortunately the numerical schemes presented in Refs(44), (112) and (113) cannot be adapted without a major change in the computational procedures because the proponents of the time split method use the conservation form of the equations and also use finite differences at the boundary points. The time-split method nevertheless shows promise; Ref (44) reported that the CPU time was a factor of 0.39 that of conventional unsplit methods.

The co-ordinate and derivatives at the node points on the inlet surface were calculated using an analytical expression. A general subroutine needs to be developed which can calculate the co-ordinates and derivatives at any point on an inlet surface represented by tabulated co-ordinates. Since the node points in the physical plane change position at each time step, an accurate and computationally efficient method

(possibly using splines) needs to be developed so that inlet surfaces represented by tabulated data can also be used in the present method.

REFERENCES

1. Williams, L.J., Transonic Transports Study - Summary, NASA-TM-X 62156, (May 1972).

2. Smith, C.L. and Wilcox, D.E., Transonic Transports Study, NASA-TM-X 62159, (May 1972).

3. Pearcey, H.H. and Osborne, J., Some Problems and Features of Transonic Aerodynamics, ICAS Paper No. 70-14, (1970).

4. Ardema, M.D. and Williams, L.J., Transonic Transports Study - Structures and Aerodynamics, NASA-TM-X 62157, (May 1972).

5. Goodmanson, L.T., Transonic Transports, Astronautics and Aeronautics J., Vol 9, No 11, (1971).

6. Jones, R.T., New Design Goals and a New Shape for the SST, Astronautics and Aeronautics J., Vol 10, No 12, (1972).

7. Zonars, D., Dynamic Characteristics of Engine Inlets, (Aircraft/Engine Integration), AGARD-LS-53, (May 1972).

8. Dobson, M.D., The External Drag of Fuselage Side Intake Semi-Circular Configuration both with and without Half Cone Compression Surfaces, RAE TR 72203, (1972).

9. Presley, L.L. and Mossman, E.A., A Study of Several Theoretical Models for Computing the Zero Lift Wave Drag of a Family of Open Nosed Bodies of Revolution in the Mach Number Range 2.0 and 4.0, NACA TN 4368, (1958).

10. Sorensen, V.L., A Computer Program for Calculating Flow Fields in Supersonic Inlets, NASA TND-2897, (1965).

11. Anderson, B.H., Design of Supersonic Inlets by a Computer Program incorporating the Method of Characteristics, NASA TND-4960, (1969).

12. Chinneck, A. and Holder, D.W., Observation of the Flow past Elliptic-nosed Two-Dimensional Cylinders and Bodies of Revo-

12. continued — lution in Supersonic Air Streams, Aeronaut. Q., Vol 4, Pt 4, (1954).

13. Xerikos, J. and Anderson, W.A., — An Experimental Investigation of the Shock Layer surrounding a Sphere in Supersonic Flow, AIAA J., Vol 3, No 3, pp 451-457, (March 1965).

14. Philpott, D.R., — An investigation into the Flow around a Family of Elliptical Nosed Cylinders at zero Incidence at $M_\infty = 2.5$ and $M_\infty = 4$, Aeronaut.Q, pp315 - 326, (November 1972).

15. Hall, M.I. and Rogers, E.W.E., — Wall Interference at Transonic Speeds on a Hemisphere-Cylinder, ARC CP 510, (1959).

16. Traugott, S.C., — Some Features of Supersonic and Hypersonic Flow about Blunted Cones, J.Aero/Space Sci., Vol 29, No 4, (1962).

17. Hunt, B.L., — Waves near the Sonic Line in Non-Homentropic Flow, Aeronaut. Q., (February 1972).

18. Molder, S., — Reflection of Curved Shock Waves, ICAS Paper No 70-11, (1970).

19. Hayes, W.D. and Probstein, R.F., — Hypersonic Flow Theory - Inviscid Flow, Vol 1, Academic Press, (1966).

20. Chernyi, G.G., — Introduction to Hypersonic Flow, Academic Press, (1961).

21. Ferri, A., — Elements of Aerodynamics of Supersonic Flows, Macmillan and Company Ltd.

22. Cole, J.D., — Twenty Years of Transonic Flow,Boeing Scientific Research Labs., D1-82-0878, (July 1969).

23. Yoshihara, H., — Some Recent Developments in Planar Inviscid Transonic Airfoil Theory, AGARD-AG-156,(Feb 1972).

24. Courant, R. and Hilbert, D., — Methods of Mathematical Physics, Vol 2, Interscience Publishers, (1962).

25. Rusanov, V.V., Characteristics of the General Equations of Gas Dynamics, USSR Comp.Math.Math.Phys., Vol 3, No 3, pp 674, (1963).

26. Ferri, A., General Theory of High Speed Aerodynamics, Vol 4, Section G, Princeton University Press,(1954).

27. Fox, L., Numerical Solution to Ordinary and Partial Differential Equations, Pergamon Press,(1962).

28. Von Mises, L., Mathematical Theory of Compressible Flow, Academic Press, (1958).

29. Courant, R., Fredricks, K., & Lewy,H., On the Partial Differential Equations of Mathematical Physics, IBM J.Res. Develop., Vol 11, No 2, (1967).

30. Sauerwein, H., The Calculation of Two and Three Dimensional Inviscid Flows by the Method of Characteristics, Ph.D. Thesis, Massachusetts Institute of Technology, (1964).

31. Sauerwein, H., A General Numerical Method of Characteristics, AIAA Paper No 65-25, (1965).

32. Sauerwein, H., Numerical Calculation of Multi-dimensional and Unsteady Flows by the Method of Characteristics, JNL. COMPUT.PHYS., No 1, pp 406-432, (1967).

33. Chushkin, P.I., Chapter 2, Progress in Aeronautical Science: D.Kuchemann (Ed.), Vol 9,Pergamon Press,(1968).

34. Ransom, V.H., A Second-Order Numerical Method of Characteristics for Three-Dimensional Supersonic Flow, Ph.D. Thesis, Purdue University, (1970).

35. Heie, H. and Leigh, D.C., Numerical Stability of Hyperbolic Equations in Three Independent Variables, AIAA J., Vol 3, No 6, (June 1965).

36. Carriere, P. and Capelier, C., Application of the Method of Characteristics to the Numerical Computation of Steady Compressible Flow, AGARD CP 35, (1968).

37. Bruhn, G. and Haack, W., Ein Charakteristikenverfahren fur Drei-dimensionale Instationare Gasstromungen, Z.Ang. Math.Phys., Vol 9, (1959).

38. Osnaghi, C. and Macchi, E., On the Application of a Time Dependent Technique in Transonic Double Flow Nozzle Solutions, AGARD-CP-91-71, (1971).

39. Butler, D.S., The Numerical Solution of Partial Differential Equations in Three Independent Variables, Proc.Roy.Soc., Series A, No 255, (1960).

40. Richardson, D.J., The Solution of Two-Dimensional Hydrodynamic Equations by the Method of Characteristics, Methods in Computational Physics: B.Alder et al (Eds), Vol 3, Academic Press, (1964).

41. Elliot, L.A., Shock Fronts in Two Dimensional Flow, Proc.Roy. Soc., A267, (1962).

42. Anderson, J.L, Preiser, S. and Rubin, E.L., Conservation Form of the Equations of Hydrodynamics in Curvilinear Co-ordinate Systems, JNL. COMPUT.PHYS., No 2, (1968).

43. MacCormack, R.W., The Effect of Viscosity on Hypervelocity Impact Cratering, AIAA Paper No 69-354,(1969).

44. MacCormack, R.W.and Paullay, A.J., Computational Efficiency achieved by Time Splitting of Finite Difference Operators, AIAA Paper No 72-15, (1972).

45. Emery, A.F., An Evaluation of Several Differencing Methods for Inviscid Flow Problems, JNL.COMPUT.PHYS., Vol 2, No 3, (1968).

46. Eilon,B.,Gottlieb,D. and Zwas, G., Numerical Stabilizers and Computing Time for Second-Order Accurate Schemes, JNL.COMPUT.PHYS., Vol 9, pp 387-397, (1972).

47. Taylor, T.D., Ndefo, E. and Masson, B.S., A Study of Numerical Methods for solving Viscous and Inviscid Flow Problems, Vol 9, pp 99-119, JNL.COMPUT.PHYS., (1972).

48. Holt, M.,(Editor) Proc. Second International Conference on Numerical Fluid Dynamics, Springer-Verlag, Berlin, (1971).

49. Tyler, L.D., Heuristic Analysis of Convective Finite Difference Techniques, see Holt, M., Ref (48).

50. Roache, P.J., An Artificial Viscosity, JNL. COMPUT.PHYS., Vol 10, 169-187, (1972).

51. Burstein, S.Z., Numerical Calculations of Multi-dimensional Shocked Flows, Courant Institute of Mathematical Sciences, New York University, NYO-10, 433, (November 1963).

52. Kentzer, C.P., Discretization of Boundary Conditions on Moving Discontinuities, see Holt, M.,Ref (48).

53. Moretti, G., Importance of Boundary Conditions in the Numerical Treatment of Hyperbolic Equations, Polytechnic Institute of Brooklyn, PIBAL Report No 69-25, (1969).

54. Moretti,G., A Critical Analysis of Numerical Techniques: The Piston-Driven Inviscid Flow, Von Karman Institute for Fluid Dynamics, Lecture Series 26,(1970).

55. Roesner, K., Numerical Integration of Eulers Equations for three dimensional Unsteady Flows, see Holt, M., Ref (48).

56. Murman, E.M., Computation Methods for Inviscid Transonic Flows with Embedded Shock Waves, Numerical Methods in Fluid Dynamics, Von Karman Institute for Fluid Dynamics, Lecture Series 34,(March 1971).

57. Krupp, J.A., The Numerical Calculation of Plane Steady Transonic Flow Past Thin Lifting Airfoils, Ph.D. Thesis, University of Washington,(1971).

58. Wear, R.R., Numerical Computation of Transonic Flow in Nozzles with small throat radii of curvature, Ph.D. Thesis, Iowa State University, (1971).

59. Steger, J.L., and Lomax, H., Numerical Calculation of Transonic Flow about Two-Dimensional Airfoils by Relaxation Procedures, AIAA Paper No 71-569, (1971).

60. Bailey, F.R., Numerical Calculation of Transonic Flow about Slender Bodies of Revolution, NASA TN D-6582, (1971).

61. Dorodnitsyn, A.A., A Contribution to the Solution of Mixed Problems of Transonic Aerodynamics, Advances in Aeronautical Sciences, Vol 2, 832-843, Pergamon, New York, (1959).

62, Belotserkovskii,O.M. and Chushkin, P.I., The Numerical Method of Direct Integrals Relations, USSR Journal of Comp.Math. and Math. Physics, Vol 2, pp 823, (1963).

63. Belotserkovskii,O.M., (Editor) Numerical Methods for solving problems of Mechanics of Continuous Media, NASA TT F-667, (1972).

64. Moretti, G. and Abbett, M., A Time Dependent Computation for Blunt Body Flows, AIAA J., Vol 4, No 12, (1966).

65. Moretti, G., and Bleich, G., Three-Dimensional Flow around Blunt Bodies, AIAA J., Vol 5, (1967).

66. Bohachevsky, I.O. and Rubin, E.L., A Direct Method for Computation of Non-Equilibrium Flows with Detached Shock Waves, AIAA J., Vol 4, No 4, (1966).

67. Bohachevsky,I.O.and Mates, R.E., A Direct Method for Calculation of the Flow about an Axisymmetric Blunt Body at an Angle of Attack, AIAA J., Vol 4, No 5, (1966).

68. Bohachevsky,I.O. and Kostoff, R.N. Hypersonic Flow over Cones with Attached and Detached Shock Waves, AIAA Paper No 71-55,(1971).

69. Albone, C., The Calculation of Axisymmetric Blunt Body Flows with Application to Minimum Drag Forebody Design at Supersonic Speeds, Ph.D. Thesis, The City University, London, (1971).

70. Parker, J.R., A Time Dependent Computation Method for Flow with Discontinuous Curvatures, Ph.D. Thesis, North Carolina University, (1970).

71. Bastianon, R.A. Steady and Unsteady Solution of the Flow Field over Concave Bodies in a Supersonic Free Stream, AIAA Paper No 68-946, (1968).

72. Burstein, S.Z., Finite Difference Calculations for Hydro-Dynamic Flows containing Discontinuities, JNL.COMPUT.PHYS., pp 198-222, (Nov.1966).

73. Lapidus, A., A Detached Shock Calculation by a Second-Order Finite Differences, JNL.COMPUT.PHYS., pp 154-177, (1967).

74. Xerikos, J. and Anderson, W.A., A Time Dependent Approach to the Numerical Solution of the Flow Field about an Axisymmetric Vehicle at Angle of Attack, NASA CR-61982, (June 1968).

75. Godunov, S.K. Zabrodin, A.V. and Prokopov, G.P., A Computational Scheme for Two-Dimensional Non-Stationary Problems of Gas Dynamics and Calculation of the Flow from a Shock Wave approaching a Stationary State, USSR Comp.Math. Math.Phys., pp 1187-1219, (1962).

76. Mason, B.S., Taylor, T.D. and Foster, R.M., Application of Godunov's Method to Blunt Body Calculations, AIAA J., Vol 7, No 4, (1969).

77. Barnwell, R.W., A Time Dependent Method for Calculating Supersonic Blunt-Body Flow Fields with Sharp Corners and Embedded Shock Waves, NASA TN D-6031, (1970).

78. Barnwell, R.W., A Time Dependent Method for Calculating Supersonic Angle of Attack Flow about Axisymmetric Blunt Bodies with Sharp Shoulders and smooth Non-axisymmetric Blunt Bodies, NASA TN D-6283, (1971).

79. Anderson, J.D., Albacete, L.M. and Winkelmann, A.E., On Hypersonic Blunt Body Flow Fields Obtained with a Time-Dependent Technique, U.S. Naval Ordinance Lab., NOLTR 68-129, (1968).

80. Hirose, N., Numerical Calculations of Some Complicated Aerodynamic Problems by a Time Dependent Finite-Difference Method, Inst. of Space and Aeronautical Science, University of Tokyo, ISAS Rept No 475, Vol 37, No 1, (1972).

81. Magnus, R. and Yoshihara, H., Inviscid Transonic Flow over Aerofoils, AIAA Paper No 70-47, (1970).

82. Singleton, R.E., Lax-Wendroff Scheme Applied to the Transonic Aerofoil Problem, AGARD CP 35, (1968).

83. Mackenzie, D. and Moretti, G., Time-Dependent Calculation of the Compressible Flow about Airfoil, AGARD CP 35, (1968).

84. Grossman, B. and Moretti, G., Time-Dependent Computation of Transonic Flows, AIAA Paper No 70-1322, (1970).

85. Laval, P., Method for a Super-critical Flow over an Aerofoil in a Nozzle, ONERA-NT-189, (1972).

86. Lipnitskii, M. and Lifshits, Iu.B., Analysis of Transonic Flows Past Solids of Revolution, PMM, Vol 34, No 3, (1970).

87. Migdal, D. Klein, K. and Moretti, G., Time-Dependent Calculations for Transonic Nozzle Flow, AIAA J., Vol 7, No 2, (1969).

88. Serra, R., The Determination of Internal Gas Flows by a Transient Numerical Technique, Ph.D.Thesis, Renssalaer Polytechnic Institute, (1970).

89. Alzner, E. and Erdos, J., Unsteady Flow through compressor Stages, NASA-CR-127765, (1972).

90. Bucher, R.E., Computer Simulation of High Frequency Combustion Instability and its Suppression, NASA-CR-94304, (1968).

91. Laval, P., A Time-Dependent Calculation Method for Transonic Nozzle Flows, (see Holt, M., Ref(48)).

92. Brown, E.F. and Ozcan, H.M., A Time-Dependent Solution of Mixed Flow through Convergent Nozzles, Paper No 72-680, (1972).

93. Wehofer, S. and Moger, W.C., Transonic Flow in Conical Convergent and Convergent-Divergent Nozzles with Non Uniform Inlet Conditions, AIAA Paper No 70-635, (1970).

94. Merryweather, H., The Calculation of Supersonic and Subsonic Flow in Ducts, Ph.D. Thesis, University of Cambridge, (1969).

95. Sinha, R.,Zakkay, V. and Erdos, J., Flow Field Analysis of Plumes of Two-Dimensional Underexpanded Jet by a Time-Dependent Method, Israel Journal of Technology, Vol 9, No 1-2, pp 151-163, (1971).

96. Bowley, W.W. and Prince J.P., Finite Element Analysis of General Fluid Flow Problem, AIAA Paper No 71-602, (1971).

97. D'Souza, N., Hypersonic Internal Flow over Blunt Leading Edges, Ph.D. Thesis, McGill University, (1971).

98. Bansod, P., A Transient Numerical Method for Computing Low Supersonic Flow about Ducted Bodies with Subsonic Internal Boundaries, RM-Aero 72/5, The City University, London, (June 1972).

99. Garner, J.E., Inlet Flow Field analysis using the Gudunov Differencing Technique, Ph.D.Thesis, University of Tennessee, (1972).

100. Abbett, J.M., Boundary Condition Computational Procedures for Inviscid Supersonic Steady Flow Field Calculations, NASA-CR-114446, (1971).

101. McCracken, D.D. and Dorn, W.S., Numerical Methods and Fortran Programming, Wiley International Edition, (1966).

102. Houghton, E.L. and Brock, A.E., Tables of Compressible Flow of Dry Air, Edward Arnold (Publishers Ltd), (1961).

103. Fairbairn, J., Mass Flow and Pressure Recovery Measurements on a Sharp Lipped Pitot Intake at zero Incidence and a Mach Number of 1.20, Sir W.G. Armstrong Whitworth Aircraft Ltd., Coventry, Report No A.R.L. 58/13, (1958).

104. Gibbings, J.C., Pressure Measurements on Three Nose Air Intakes at Transonic and Supersonic Speeds with an Analysis of their Drag Characterisitcs, R.A.E. Report Aero 2637 (1960).

105. Moretti, G., Three-Dimensional Supersonic Flow Computations, AIAA J., (September 1963).

106. Dash, S.M. and Del Guidice, P.D., Three-Dimensional Nozzle-Exhaust Flow Field Analysis by a Reference Plane Technique, AIAA Paper No 72-704, (1972).

107. Friedrichs, K.O., Mathematical Aspects of Flow Problems of Hyperbolic Type, General Theory of High Speed Aerodynamics, Editor: W.R. Sears, Oxford University Press, Vol VI, (1955).

108. Liepmann, H.W. and Roshko, A., Elements of Gas Dynamics, John Wiley & Son, (1957).

109. Hahn, S.G., Stability Criteria for Difference Schemes, Comm.Pure Appl.Math., Vol 11,pp 243-255, (1958).

110. O'Brien, G.G. Hyman,M.A. and Kaplan, S., A Study of the Numerical Solution of Partial Differential Equations, J.Mathematics and Physics, Vol 29, (1950).

111. Richtmyer, R.D. and Morton, K.W., Difference Methods for Initial Value Problems, Interscience Publishers, Second Edition,(1967).

112. MacCormack, R.W., Numerical Solution of the Interaction of a Shock Wave with a Laminar Boundary Layer, See Holt, M., Ref (48).

113. Rizzi, A.W.and Inouye,M. A Time-Split Finite Volume Technique for Three-Dimensional Blunt Body Flow, AIAA Paper No 73-133, (1973).

114. Shifrin, E.G., On the External Properties of Entropy on a Critical Streamline, J.Appl.Math.Mech.,Vol 31, pp 618-620, (1967).

115. Ladyzhenskii, M.D., On the Question of the Value of Entropy on the Surface of a Body of Revolution at a non-zero Angle of Attack, Prostranstvennye, Giper-zvukovye Techeniia Gaza, Moscow Mashinostroenie, pp 28 - 29, (1968).

116. Bagley, J., (Private Communication), Aerodynamics Division, The Royal Aircraft Establishment, Farnborough, Hants, U.K.,(March 1973).

117. Porter, R.W. and Coakley, J.F., Use of Characterisitcs for Boundaries in Time Dependent Finite Difference Analysis of Multi-dimensional Gas Dynamics, Int.J.Num.Meth. Engrg., Vol 5, No 1, pp 97-102, (1972).

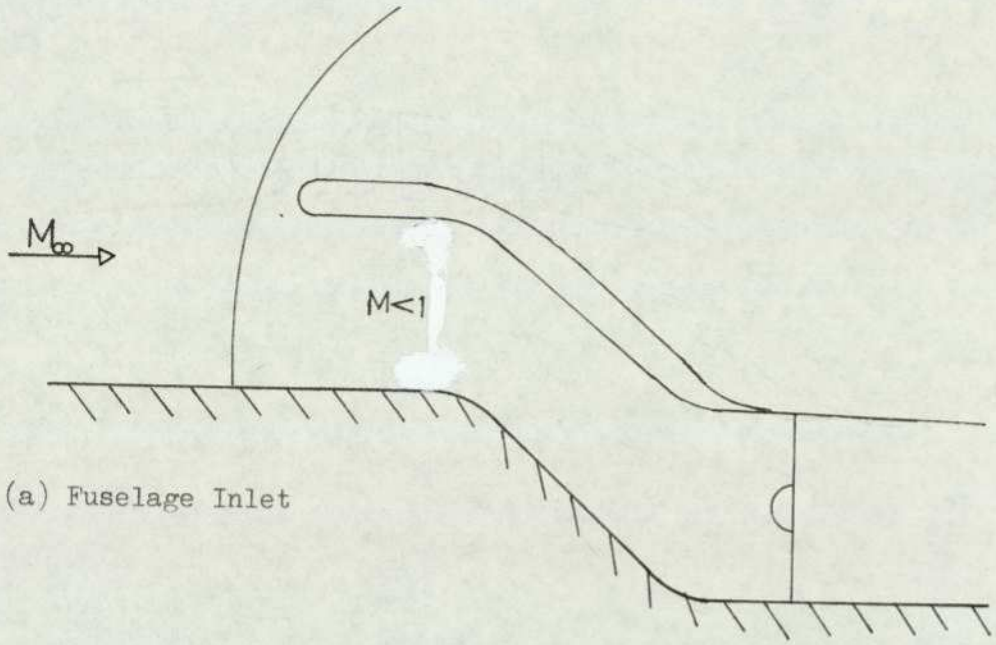
118. Petersen, M.W. and Tamplin, G.C., Open Nose Inlet Additive Drag Tests at Sub-sonic and Transonic Speeds, North American Aviation, Los Angeles Div.,Rept.No NA-64-921, (1964).

119. Mair, W.A. et al, Report on the Definitions Panel on the Definition of the Thrust of a Jet-Engine and the Internal Drag of a Ducted Body, ARC CP190,(1954).

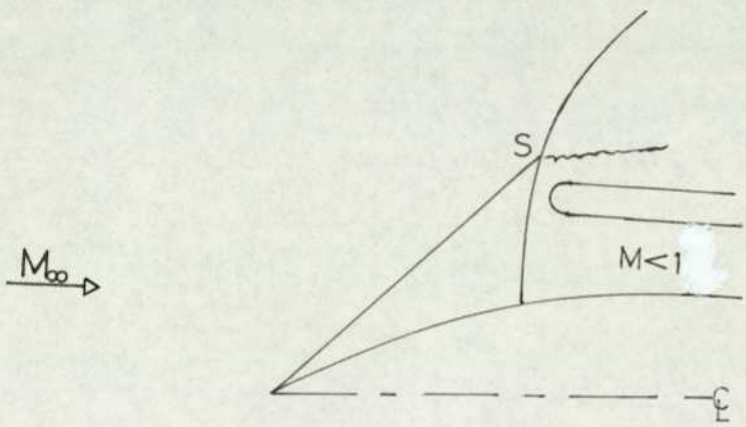
120. Ashley, H. and Landahl, M.T., Aerodynamics of Wings and Bodies, Addison-Wesley Publishing Company, (1965).

F I G U R E S

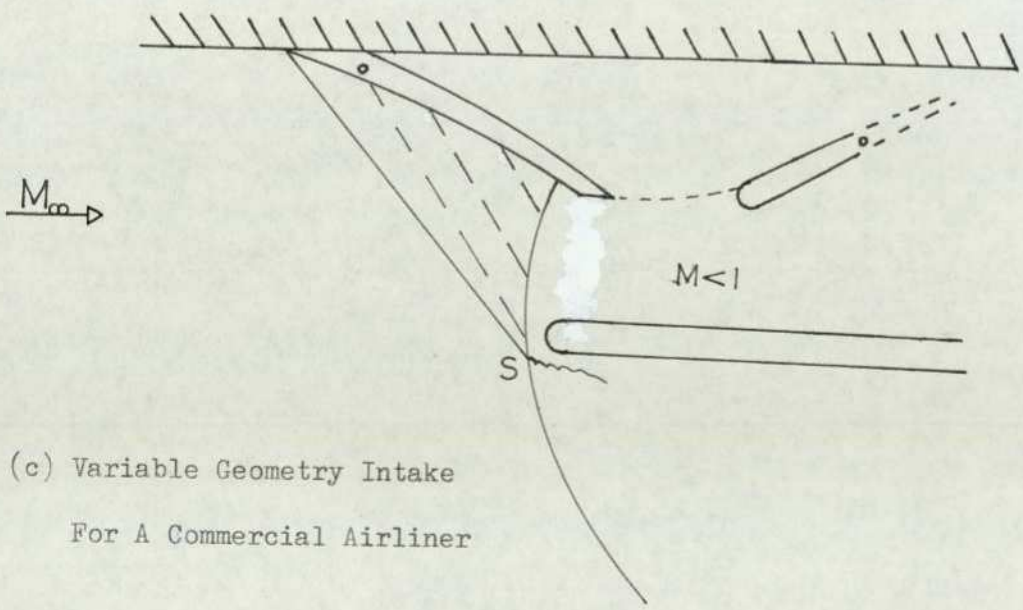
THREE TYPES OF AIRCRAFT AIR-INTAKES



(a) Fuselage Inlet



(b) Centre-body Intake



(c) Variable Geometry Intake

For A Commercial Airliner

FIGURE 1

HIGH BY-PASS RATIO ENGINE

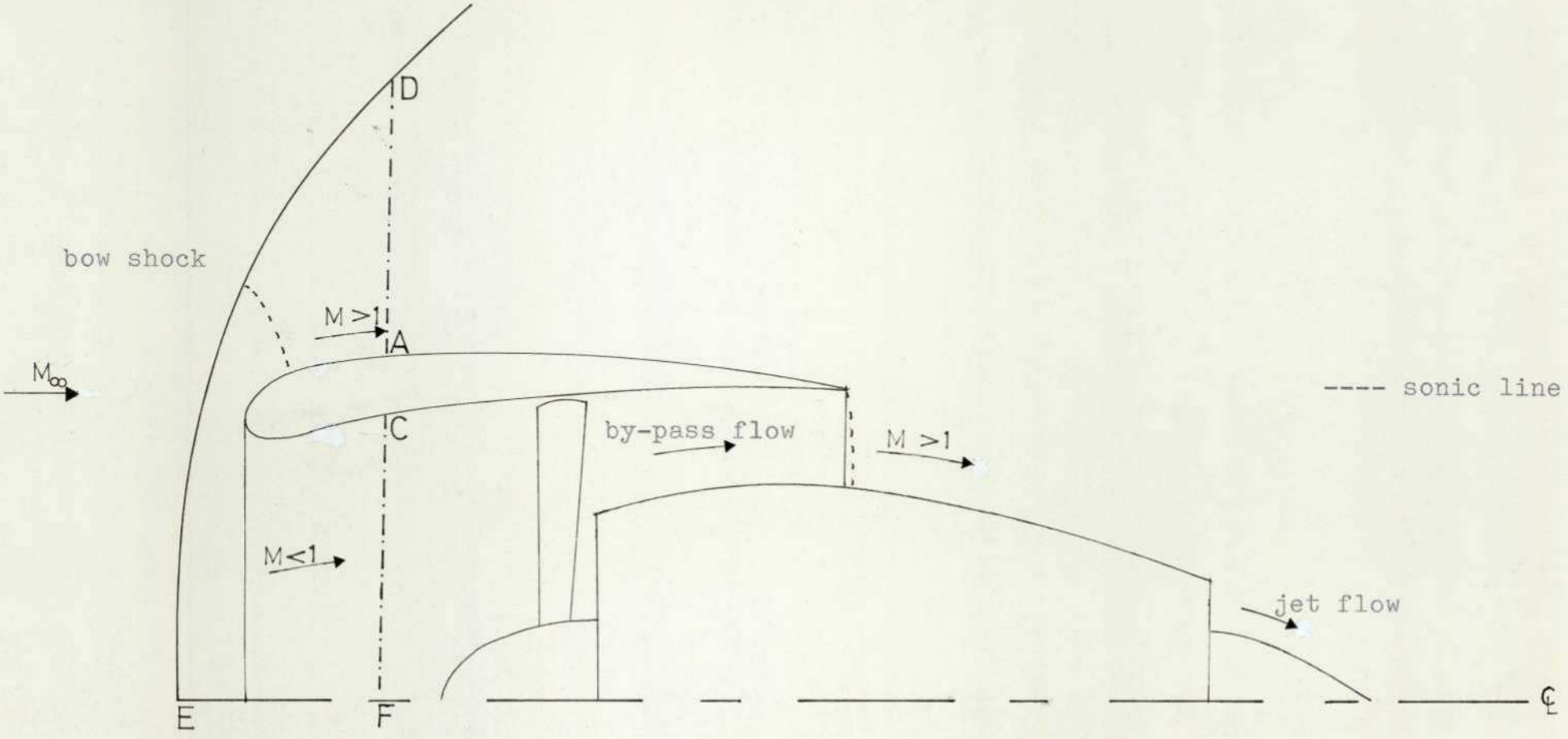
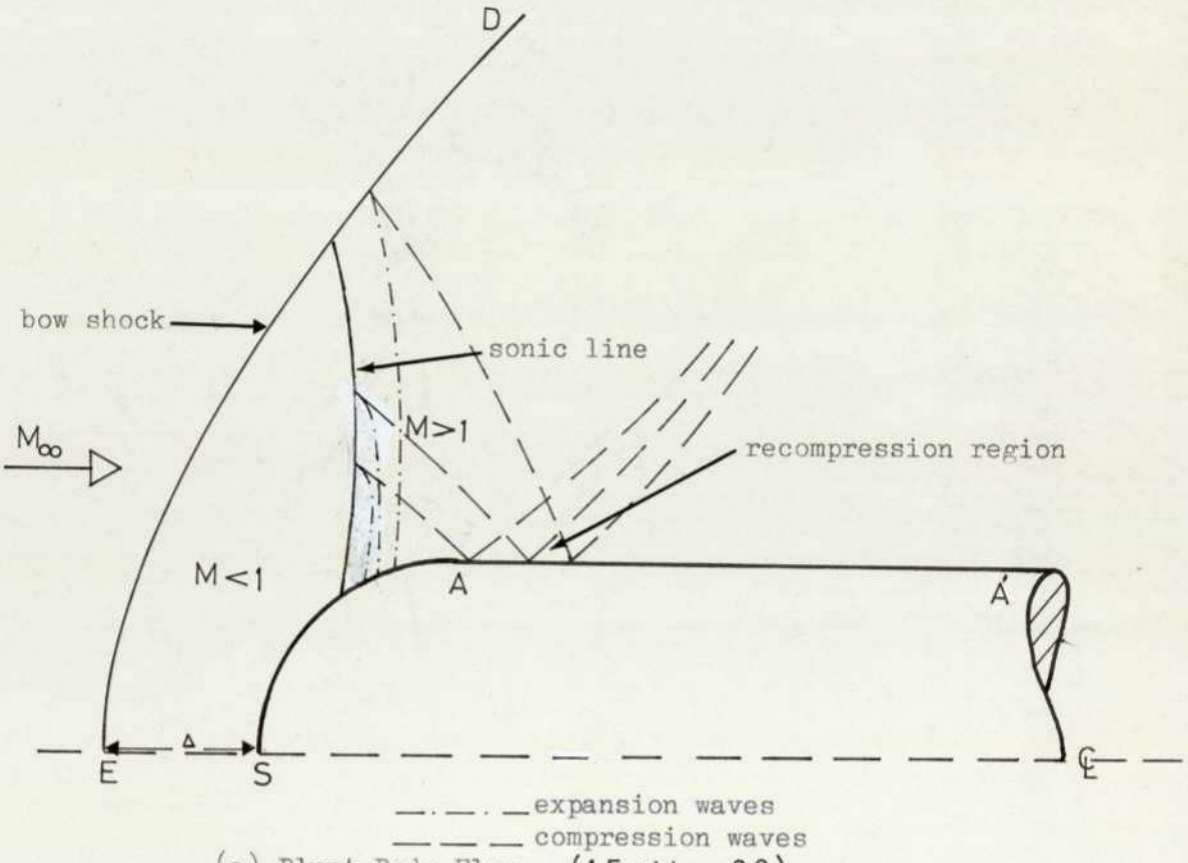
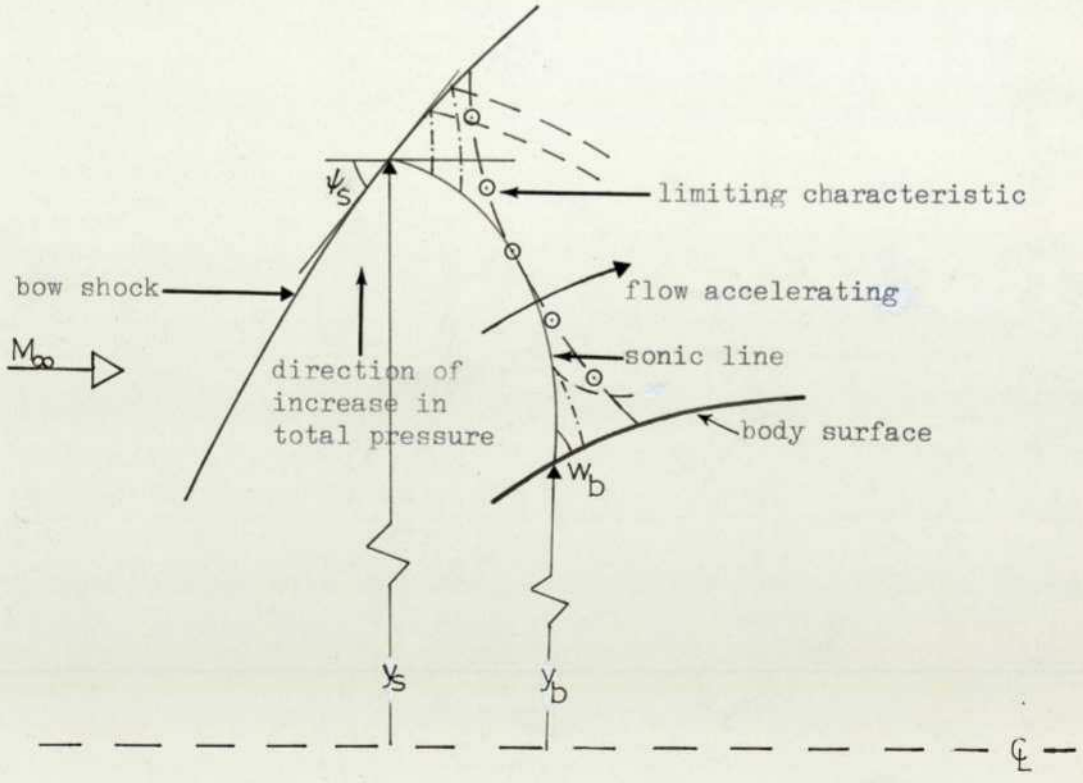


FIGURE 2

THE SUPERSONIC FLOW ABOUT A BLUNT BODY WITH A DETACHED SHOCK WAVE



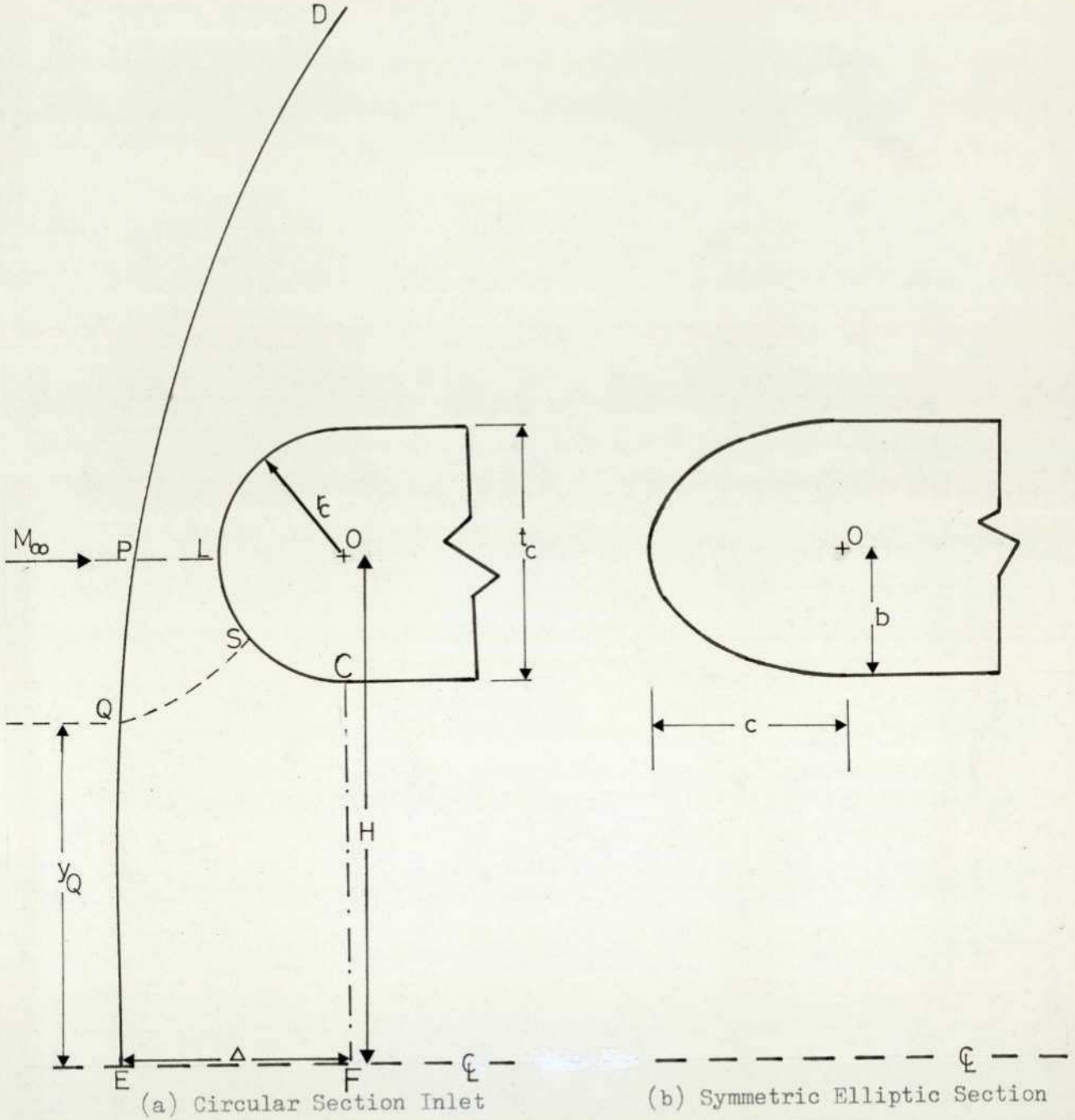
(a) Blunt Body Flow $(1.5 < M_\infty < 3.0)$



(b) Sonic Line and Limiting Characteristic

FIGURE 3

INLET LIP GEOMETRY AND NOTATION



(a) Circular Section Inlet (b) Symmetric Elliptic Section

$$MFR=(y_Q/H)^{1+j}$$

{j=0 for two dimensional flow
j=1 for axisymmetric flow}

CIRCULAR SECTIONS

Inlet Lip Reference	A	B
R_H	0.35	0.25
t_H	0.70	0.50

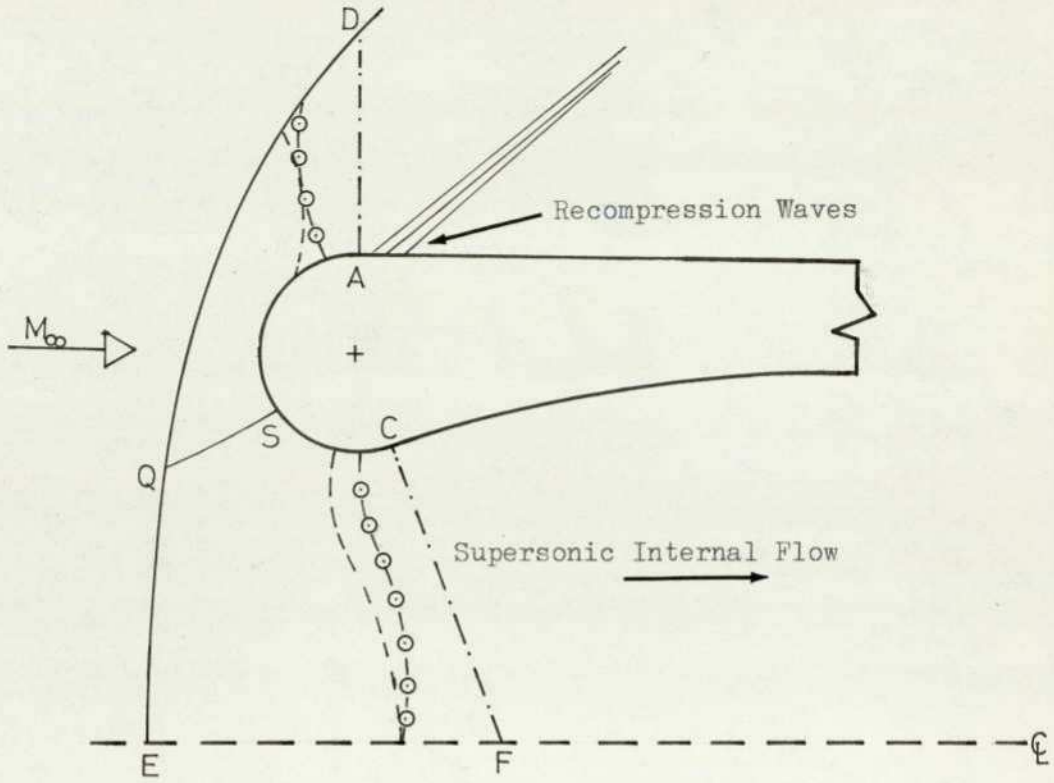
ELLIPTIC SECTION

Inlet Lip Reference	C
b	0.25
t_H	0.50
λ	1.5

where $H=1, R_H=r_c/H$, $t_H=t_c/H$ and $\lambda=c/b$

FIGURE 4

SUPERSONIC FLOW ABOUT BLUNT LIPPED DUCTED BODIES $(1.5 < M_\infty < 3.0)$

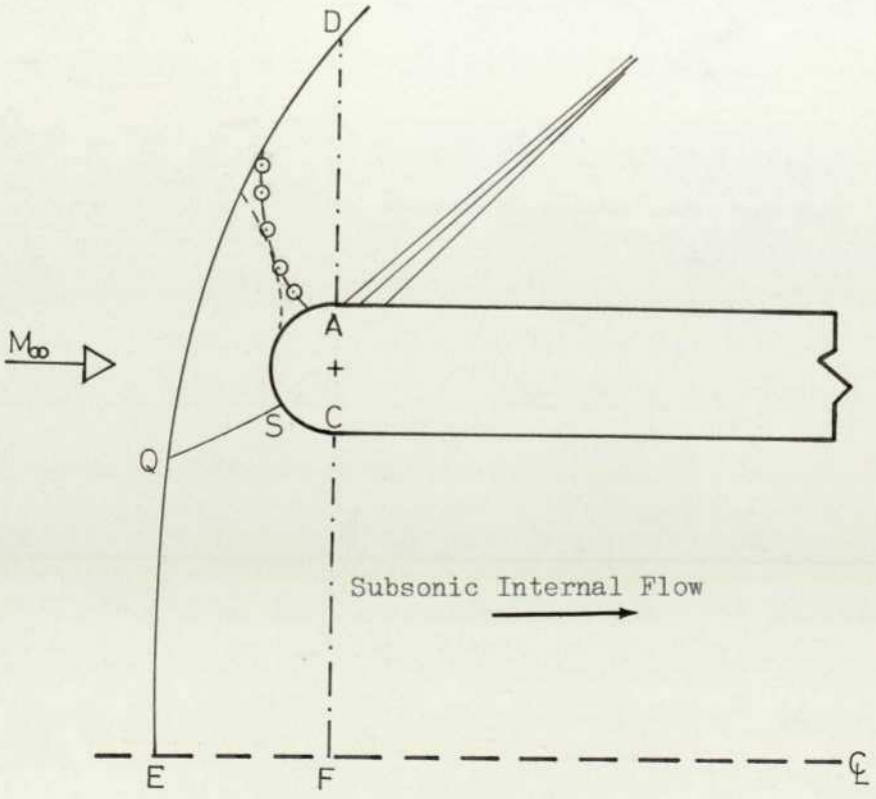


(a) Supersonic Internal Boundary Problem (SUPIB)

--- Sonic Line

—⊙— Limiting Characteristic

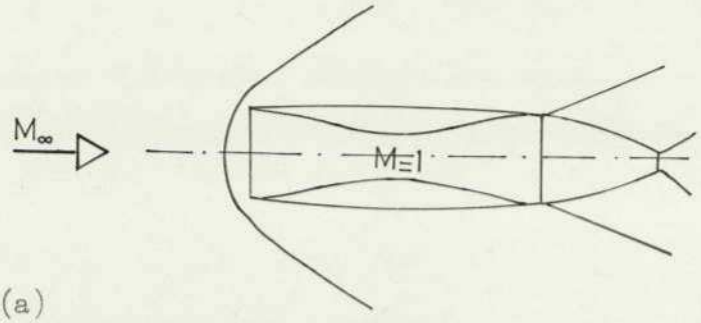
—·— Computational Boundaries



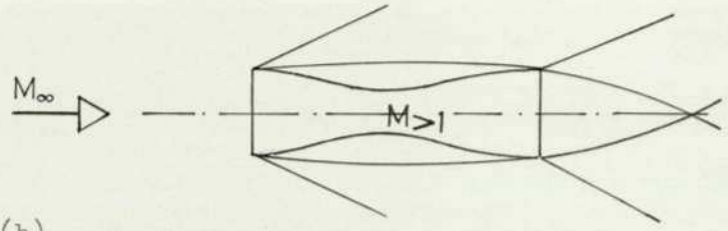
(b) Subsonic Internal Boundary Problem (SUBIB)

FIGURE 5

BOW SHOCK SHAPES FOR THE SUPIB PROBLEM

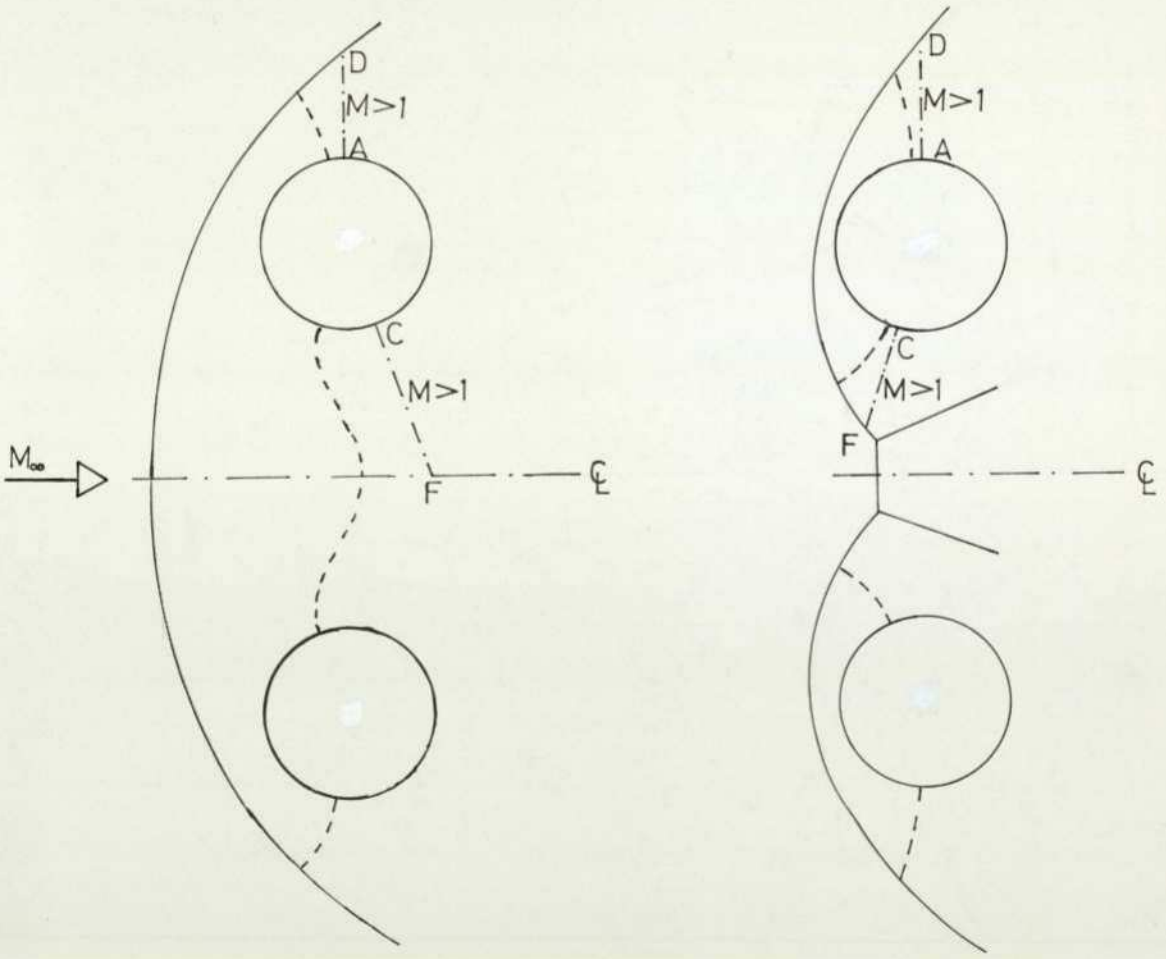


(a)



(b)

(reproduced from Ref(20))



(c)Continuously curved shock

(d)Mach interaction at axis

---- Sonic line

—·—·— Computational boundary

FIGURE 6

A GENERAL SEQUENCE OF COMPUTATION FOR A TRANSIENT NUMERICAL SCHEME

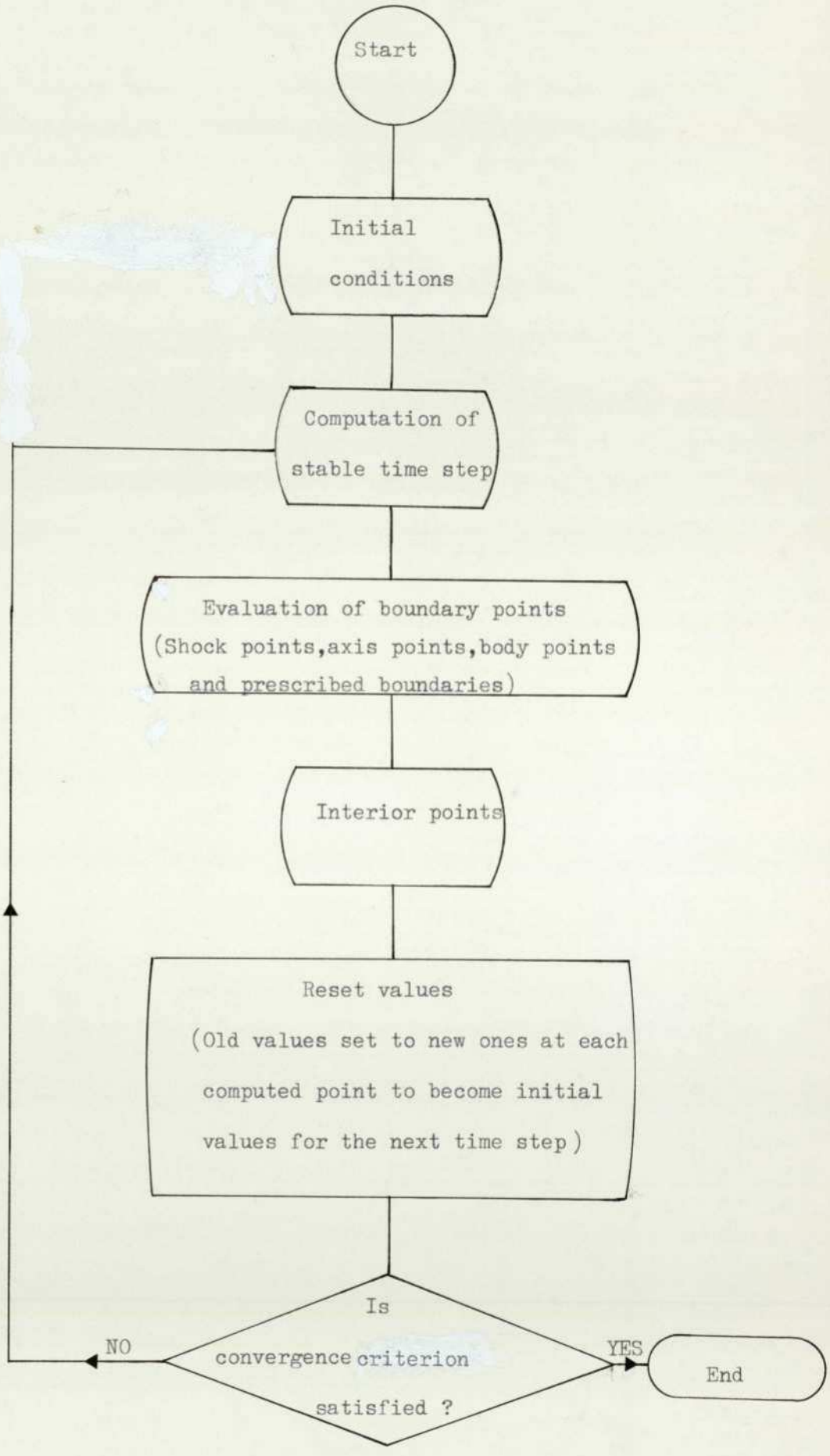
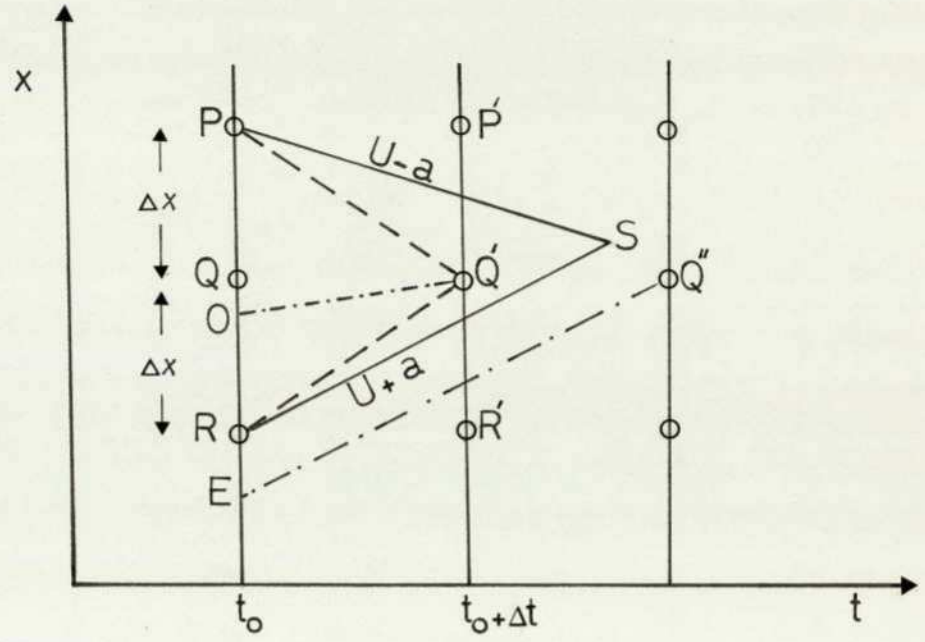
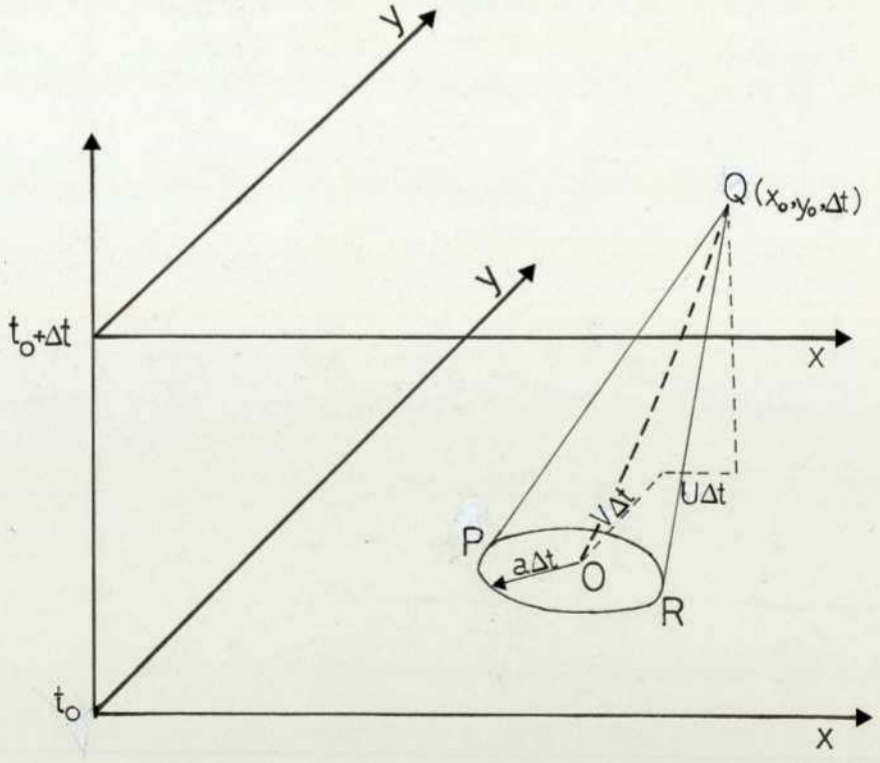


FIGURE 7

THE CFL CONDITION AND THE MACH CONE



(a) The CFL condition for one dimensional unsteady flow



(b) Mach Cone P,Q,R with the equation,

$$(x_o - U\Delta t - x)^2 + (y_o - V\Delta t - y)^2 = (a\Delta t)^2$$

FIGURE 8

THE GEOMETRY OF CHARACTERISTIC SURFACES AND BICHARACTERISTIC CURVES FOR THREE INDEPENDENT VARIABLES

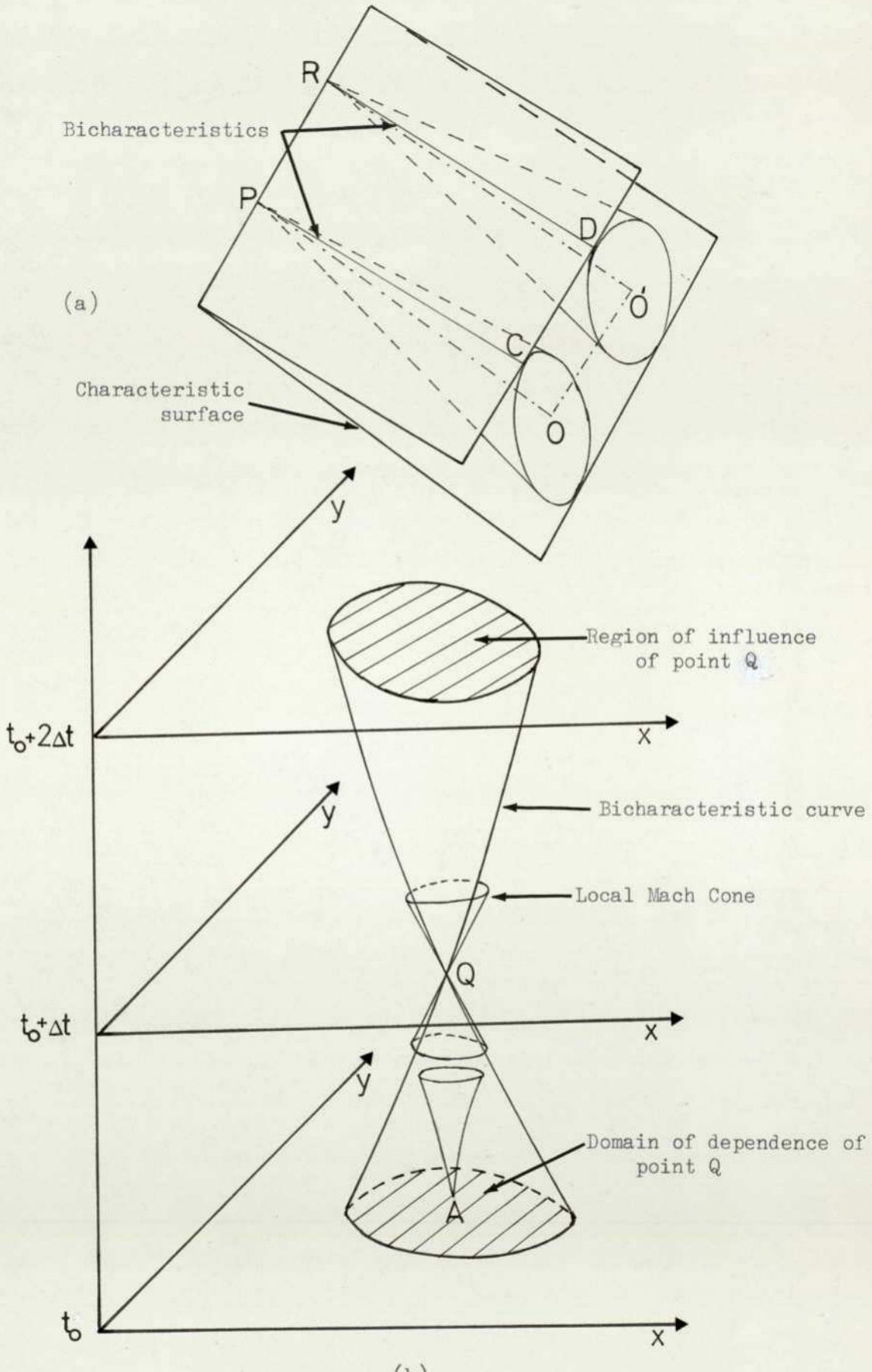
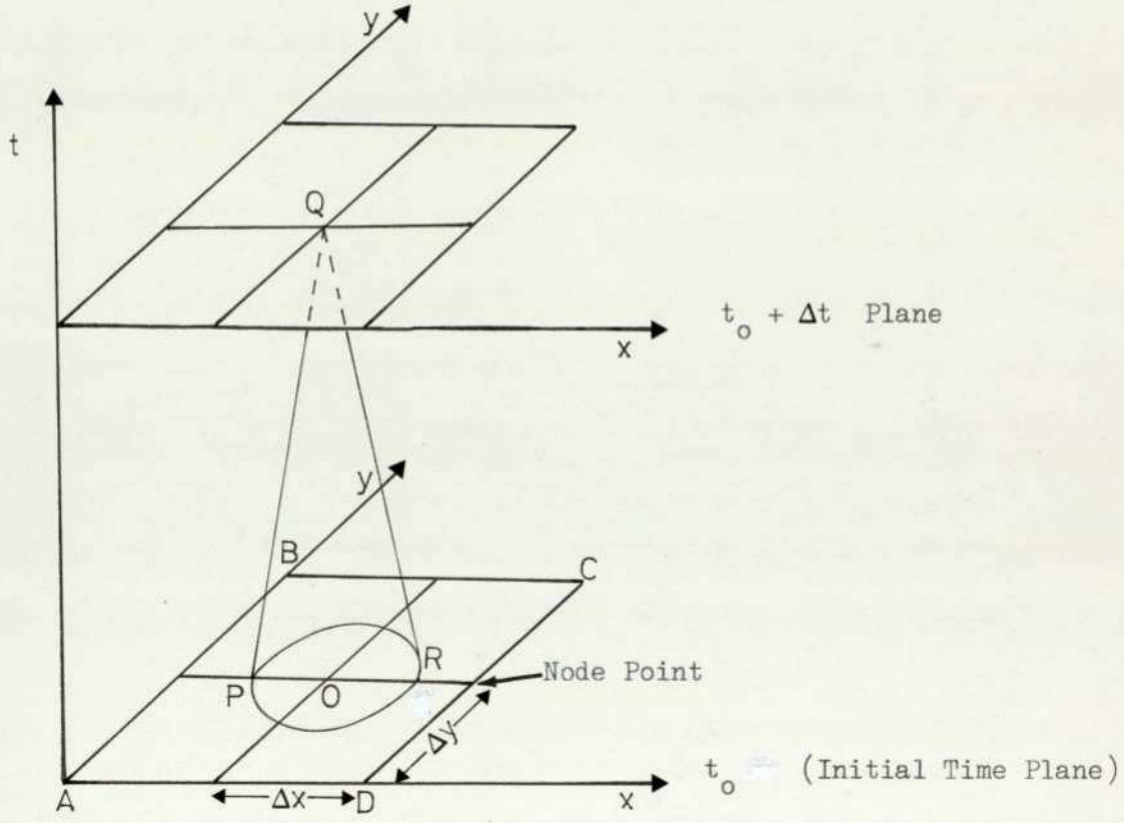
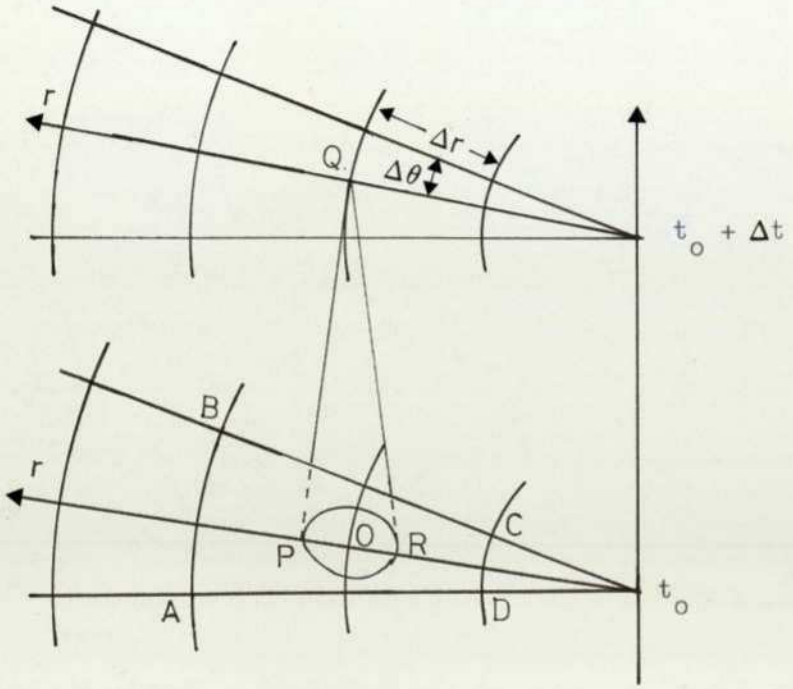


FIGURE 9

THE CFL CONDITION IN CARTESIAN AND POLAR COORDINATES



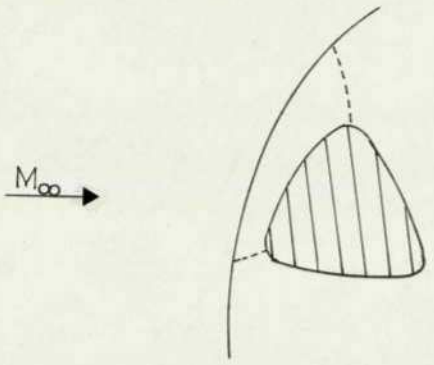
(a) Cartesian Coordinates



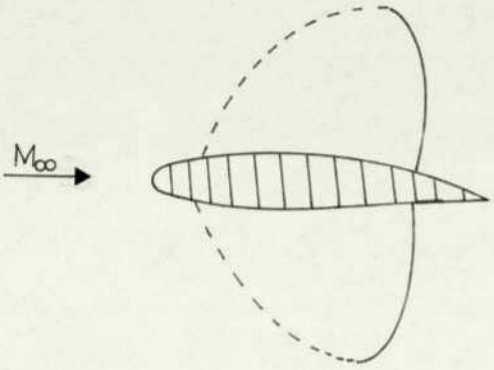
(b) Polar Coordinates

FIGURE 10

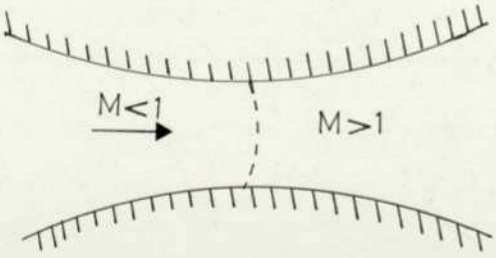
CATEGORIES OF TRANSONIC FLOW PROBLEMS SOLVED USING TRANSIENT FINITE DIFFERENCE METHODS



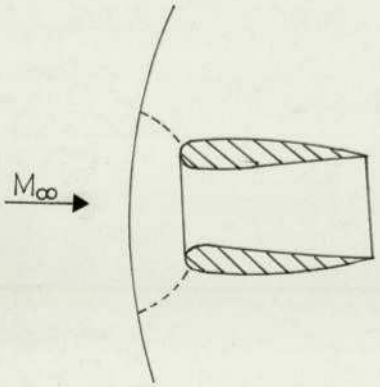
(a) Blunt bodies in supersonic flow



(b) Supercritical flow
(aerofoils and bodies of revolution)



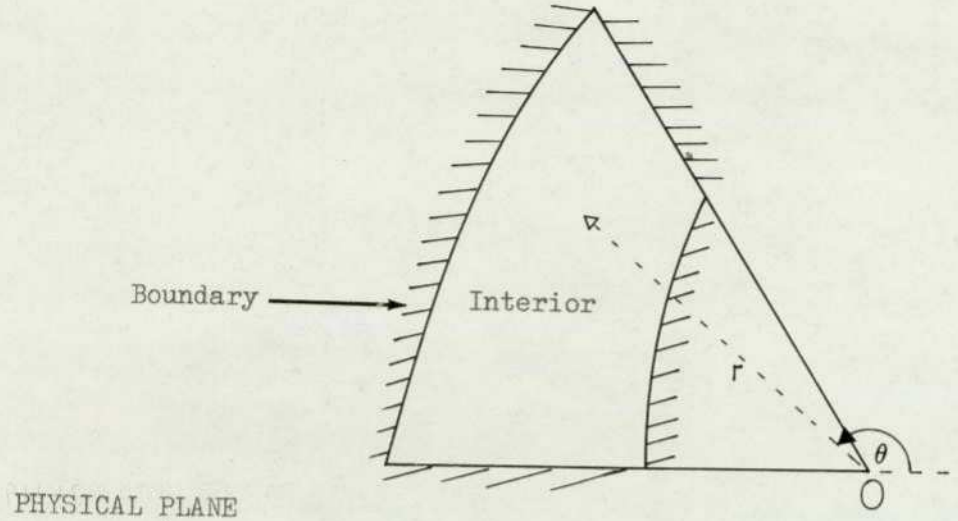
(c) Internal flows
(flows in nozzles, jets and turbine blade passages)



(d) Blunt lipped ducted bodies in supersonic flow
(subsonic and supersonic internal flow)

FIGURE 11

COMPUTATION OF INTERIOR POINTS



PHYSICAL PLANE

TRANSFORMATION EQUATIONS

$$\begin{bmatrix} Y=F(\theta) \\ Z=G(r,\theta) \\ T=t \end{bmatrix}$$

COMPUTATIONAL PLANE

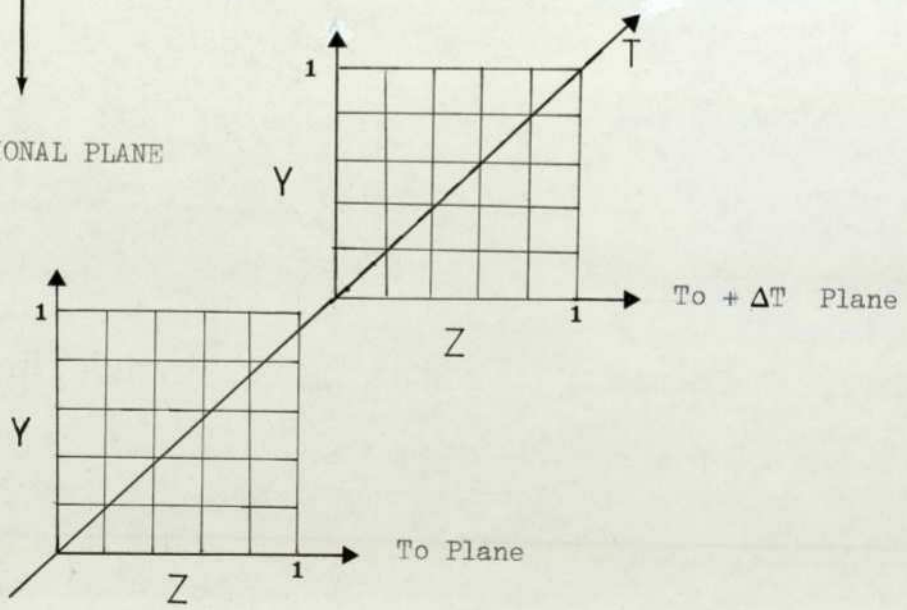
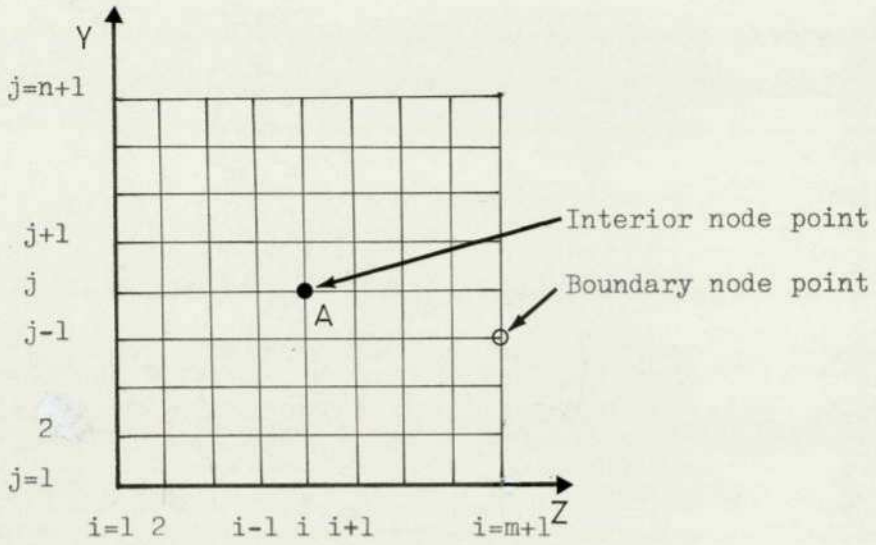


FIGURE 12

BASIC ELEMENTS OF THE FINITE DIFFERENCE SCHEME



COMPUTATIONAL GRID

Central Differences at point $A^k_{i,j}$

$$\left(\frac{\partial g}{\partial Z}\right)^k_{i,j} = (g^k_{i+1,j} - g^k_{i-1,j})/(2\Delta Z)$$

$$\left(\frac{\partial^2 g}{\partial Z^2}\right)^k_{i,j} = (g^k_{i+1,j} + g^k_{i-1,j} - 2g^k_{i,j})/(\Delta Z^2)$$

$$\left(\frac{\partial^2 g}{\partial Y \partial Z}\right)^k_{i,j} = (g^k_{i+1,j+1} - g^k_{i+1,j-1} - g^k_{i-1,j+1} + g^k_{i-1,j-1})/(4\Delta Y \Delta Z)$$

Forward Difference

$$\left(\frac{\partial g}{\partial Z}\right)^k_{i,j} = (g^k_{i+1,j} - g^k_{i,j})/(\Delta Z)$$

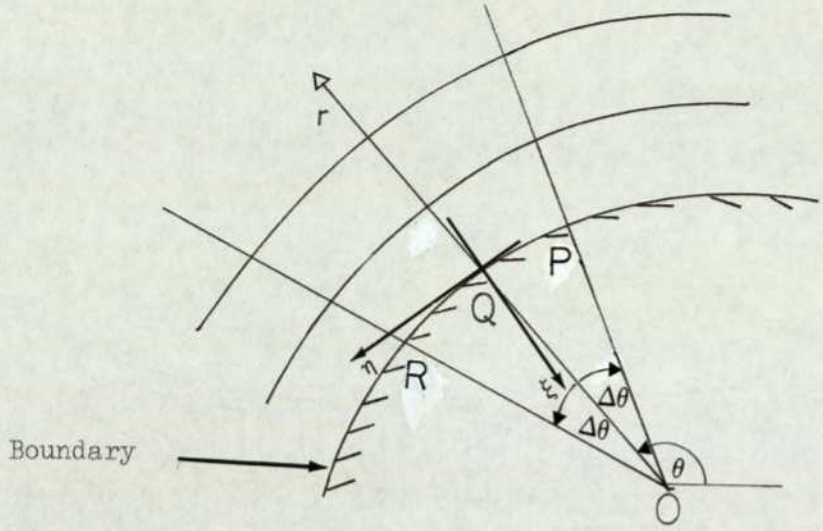
Backward Difference

$$\left(\frac{\partial g}{\partial Z}\right)^k_{i,j} = (g^k_{i,j} - g^k_{i-1,j})/(\Delta Z)$$

Similarly for $\left(\frac{\partial g}{\partial Y}\right)^k_{i,j}$ and $\left(\frac{\partial^2 g}{\partial Y^2}\right)^k_{i,j}$

FIGURE 13

EVALUATION OF BOUNDARY POINTS



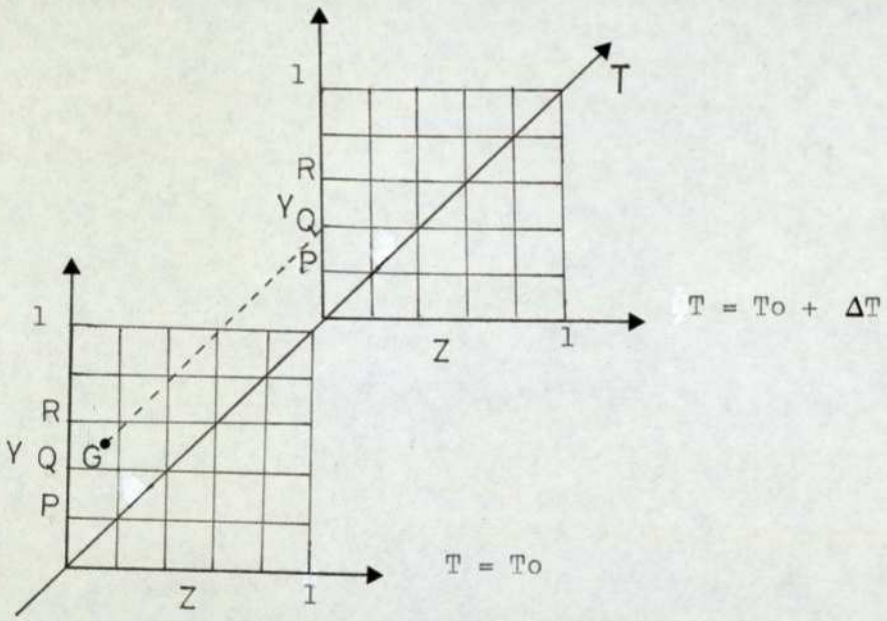
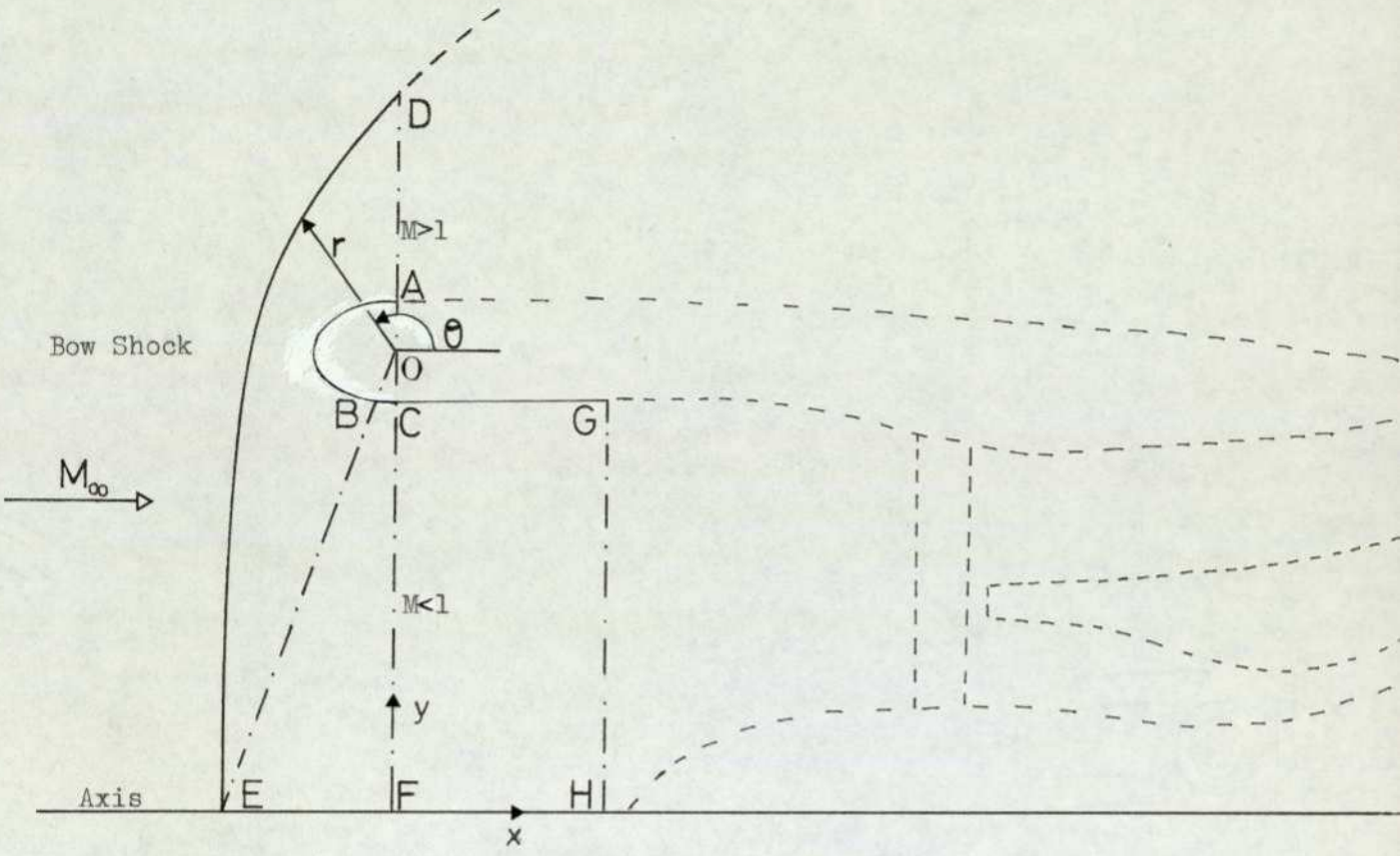


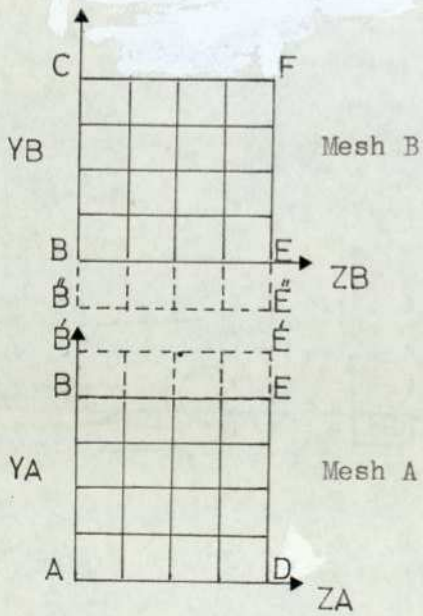
FIGURE 14

SUBSONIC INTERNAL BOUNDARY PROBLEM

PHYSICAL PLANE



COMPUTATIONAL PLANE



TRANSFORMATIONS

$$ZB = \frac{r - BOB}{SHX - BOB}$$

$$YB = \frac{\theta - \theta_B}{\theta_C - \theta_B}$$

$$ZA = \frac{r - BOA}{SH - BOA}$$

$$YA = \frac{\theta - \theta_A}{\theta_B - \theta_A}$$

FIGURE 15

DISTRIBUTION OF NODE POINTS IN THE PHYSICAL PLANE

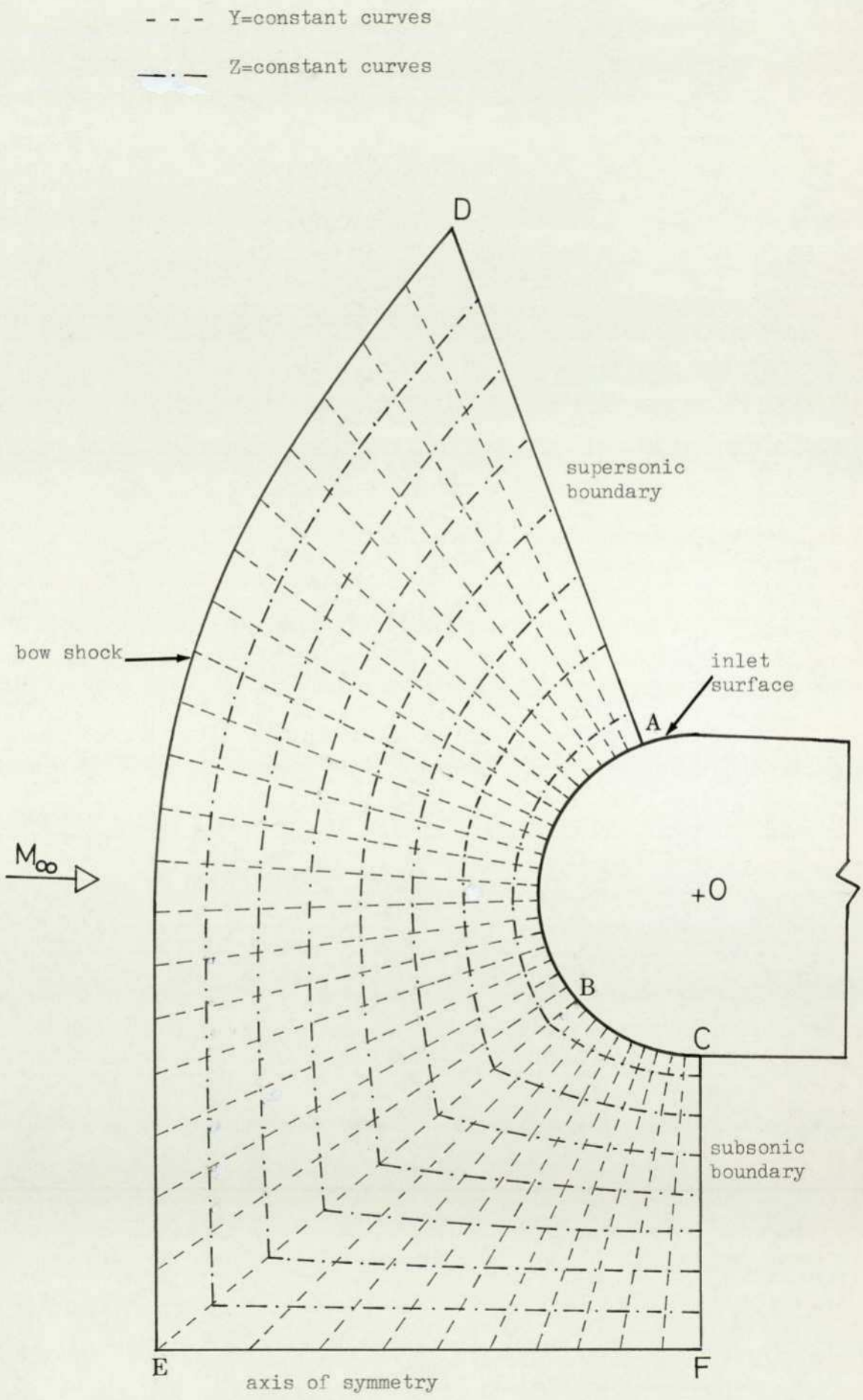


FIGURE 16

ORIENTATION OF LOCAL CO-ORDINATE SYSTEM FOR BOUNDARY POINT EVALUATION

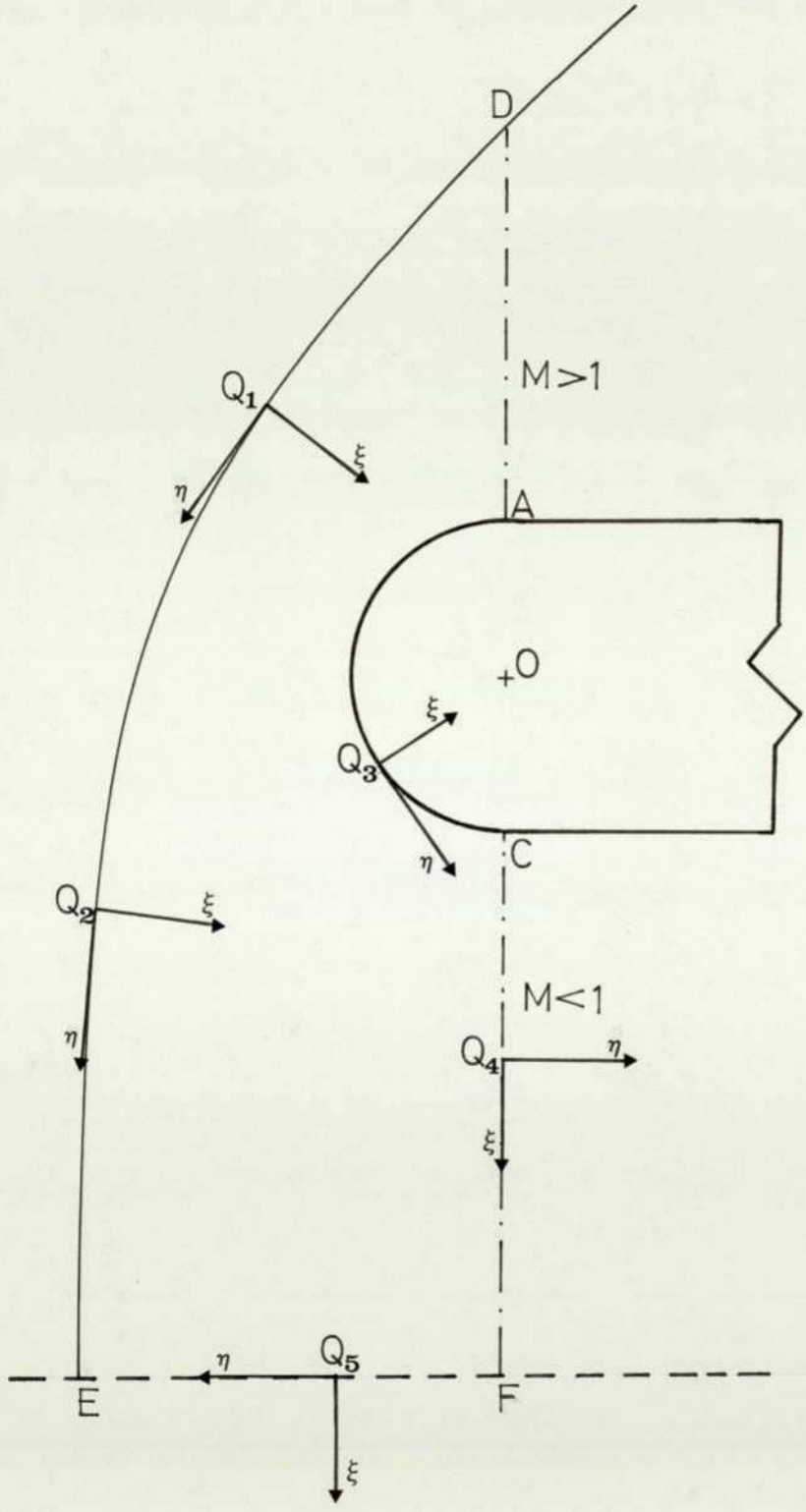
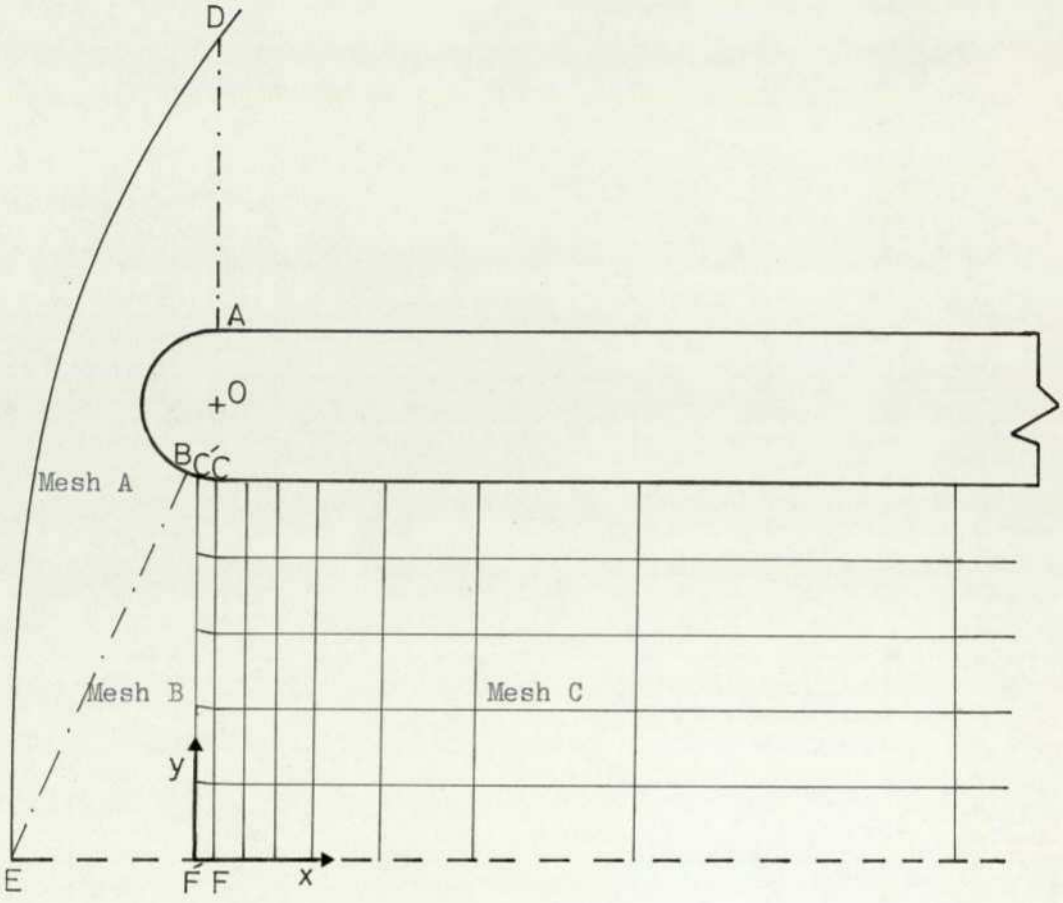
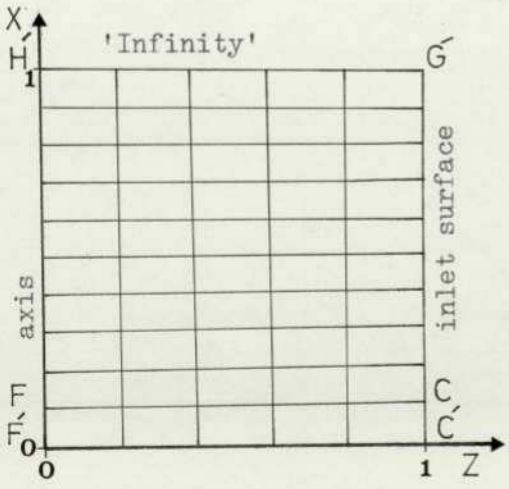


FIGURE 17

SCHEME 1 : CO-ORDINATE STRETCHING METHOD FOR THE SUBSONIC BOUNDARY



(a) Physical Plane



(b) Computational Plane

Transformations

$X = (x)/(x+C)$ or $X = 1 - e^{-xC}$

$Z = (y)/(BOC)$

FIGURE 18

CHECK ON THE INITIAL ESTIMATE OF VARIABLES ON THE SUBSONIC BOUNDARY CF

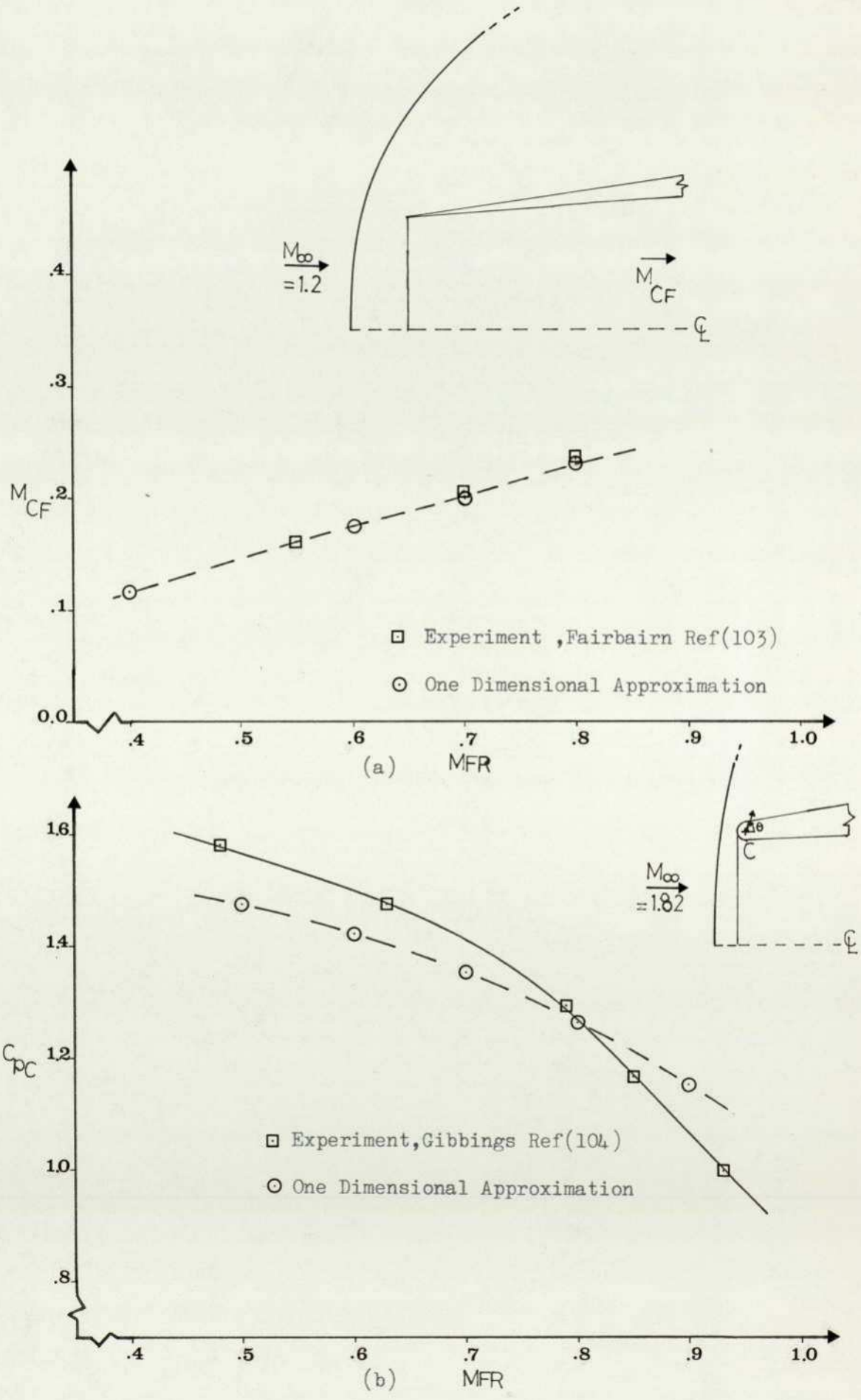


FIGURE 19

AN EXAMPLE OF INITIAL VALUES FOR THE SUBSONIC INTERNAL BOUNDARY PROBLEM

Flow Direction Plot about Inlet A (two-dimensional Flow)

Mesh A 15x20

Mesh B 15x10

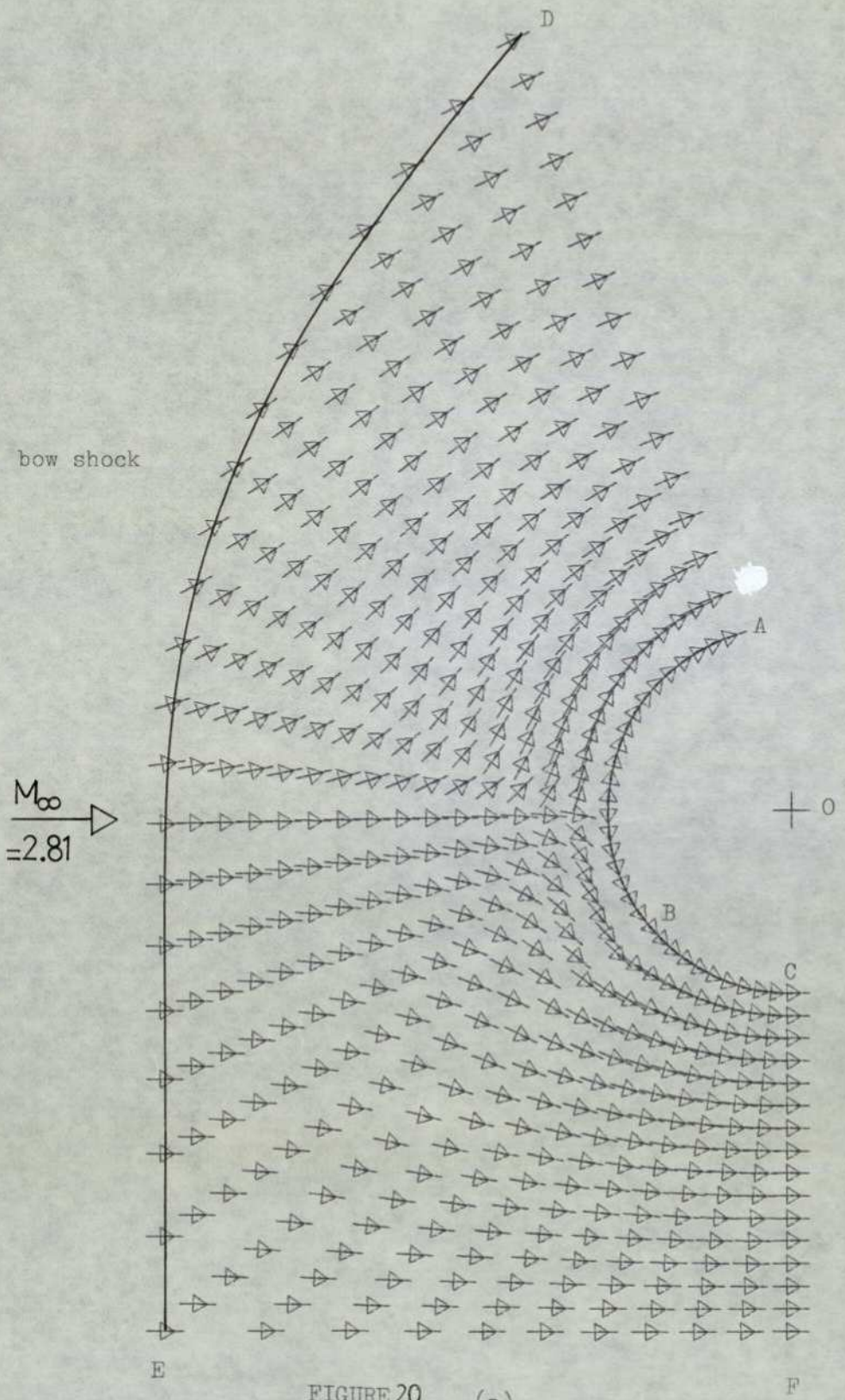
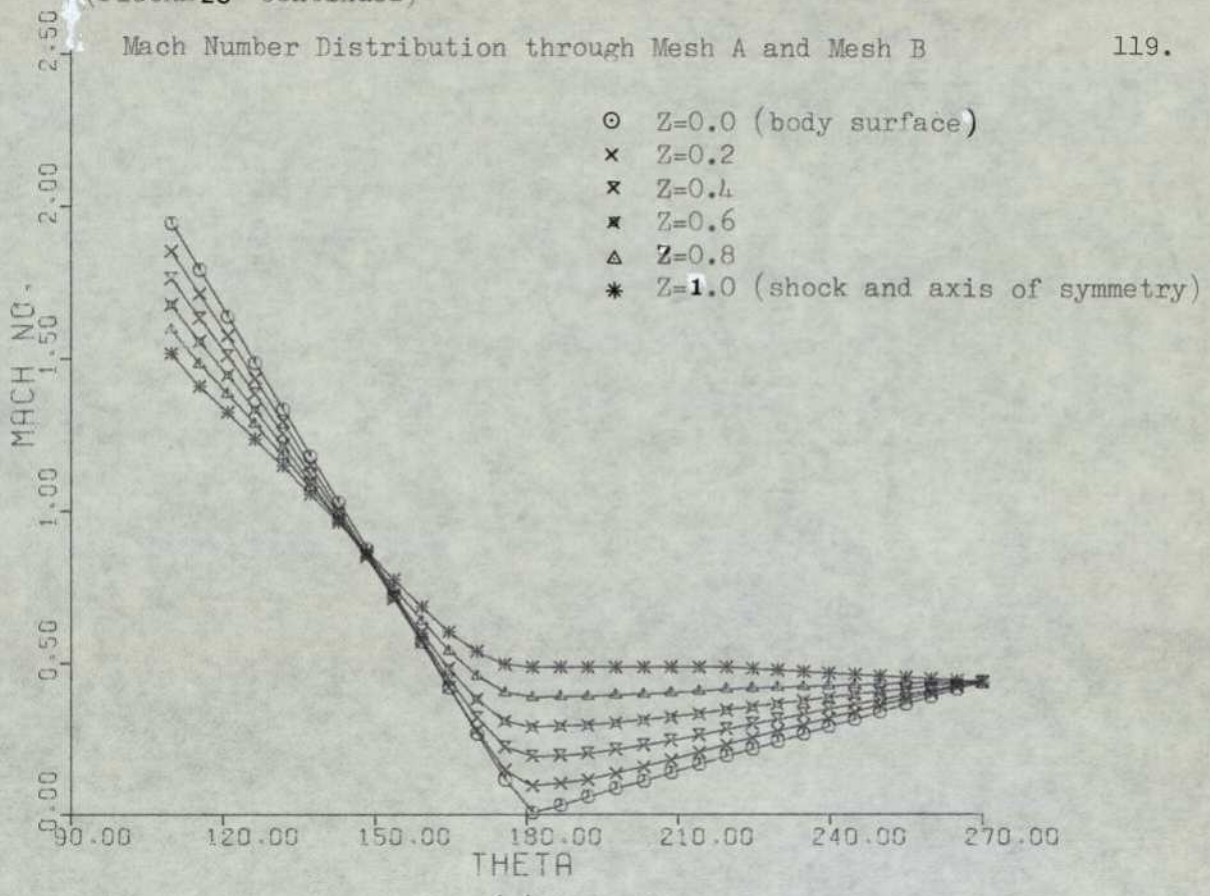


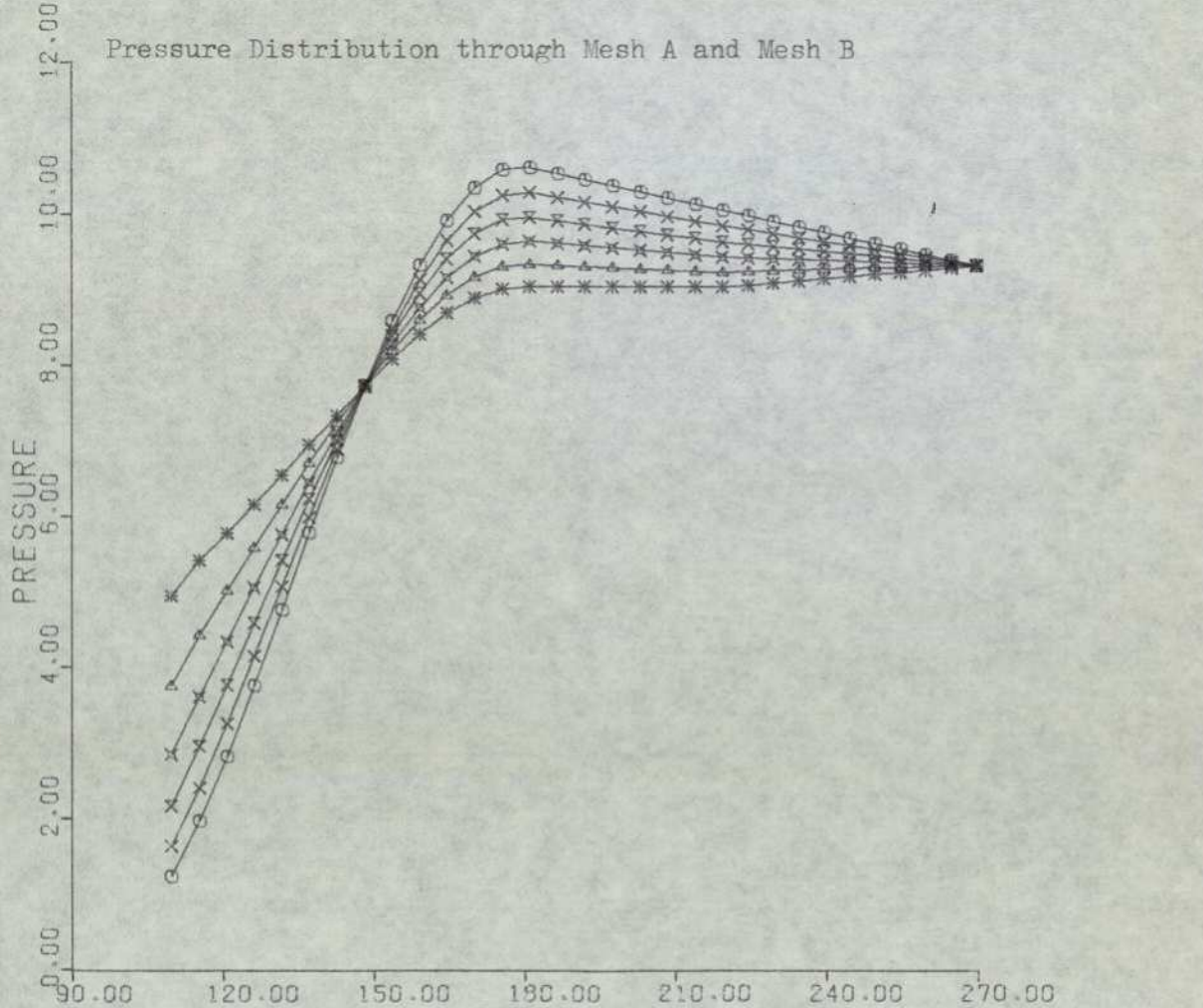
FIGURE 20 (a)

(FIGURE 20 Continued)



(b)

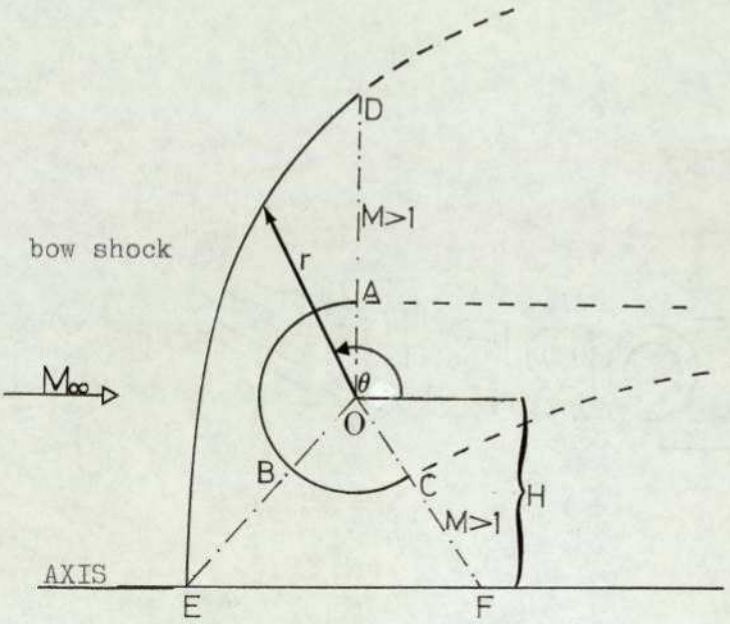
NO OF TIME STEPS= 0. .MACH NO.= 2.810



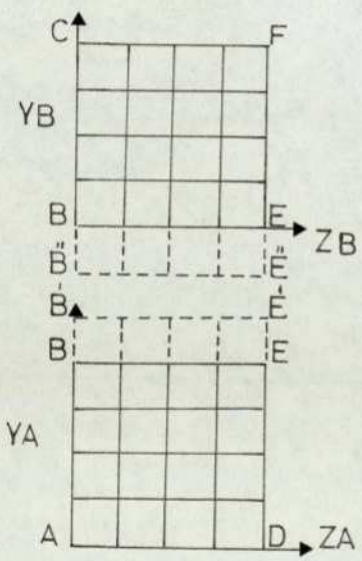
(c)

SUPERSONIC INTERNAL BOUNDARY PROBLEM

PHYSICAL PLANE



COMPUTATIONAL PLANE



Transformations

$$ZB = \frac{r - BOB}{SHX - BOB}$$

$$YB = \frac{\theta - \theta_B}{\theta_C - \theta_B}$$

$$ZA = \frac{r - BOA}{SH - BOA}$$

$$YA = \frac{\theta - \theta_A}{\theta_B - \theta_A}$$

FIGURE 21

FLOW DIRECTION PLOT ABOUT AN INLET WITH A SUPERSONIC INTERNAL BOUNDARY

(Axisymmetric Flow, MFR=0.44)

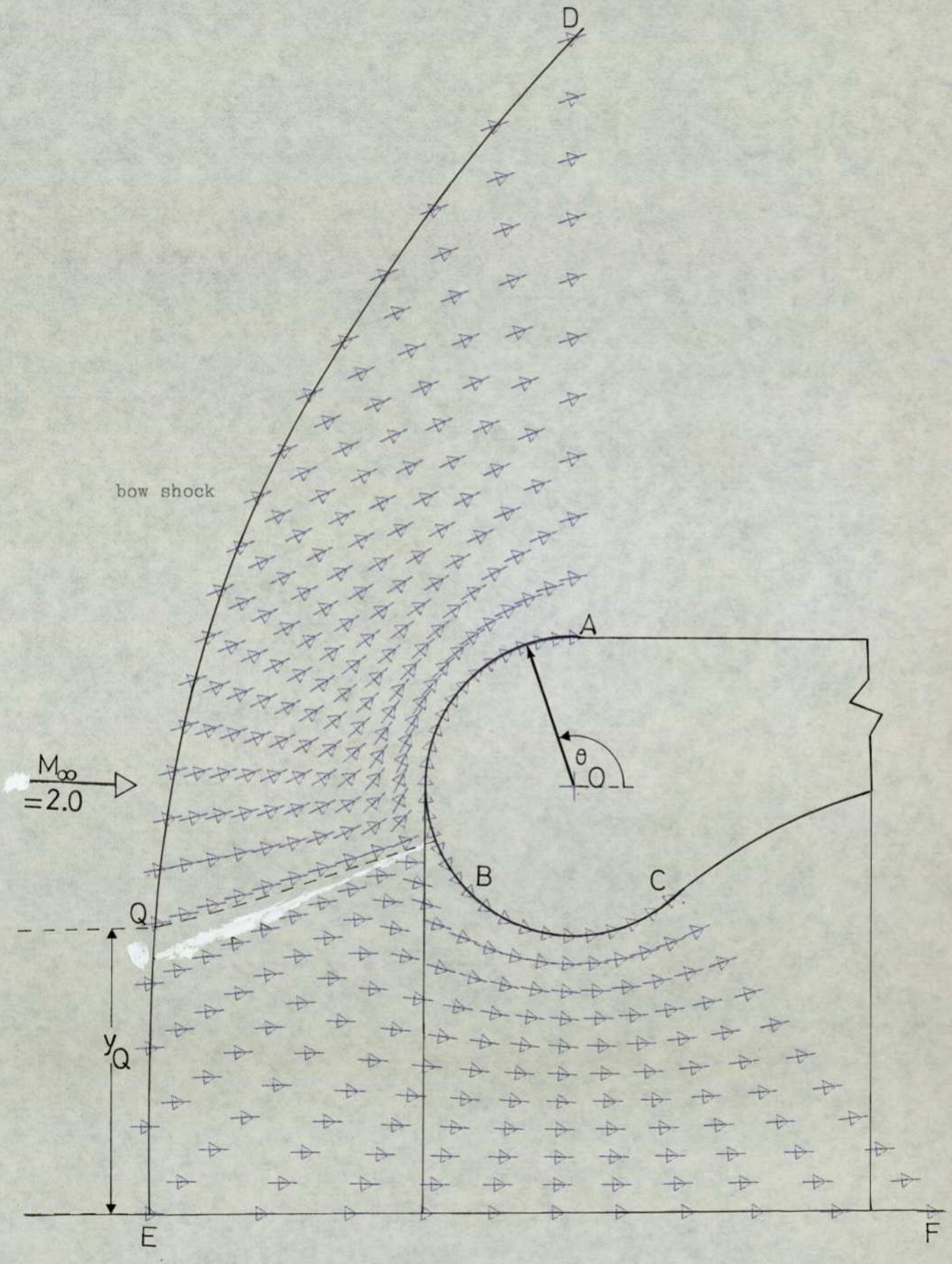


FIGURE 22

MACH NUMBER CONTOURS ABOUT AN INLET WITH A SUPERSONIC INTERNAL BOUNDARY

(R_H=0.35, MFR=0.44, Axisymmetric Flow)

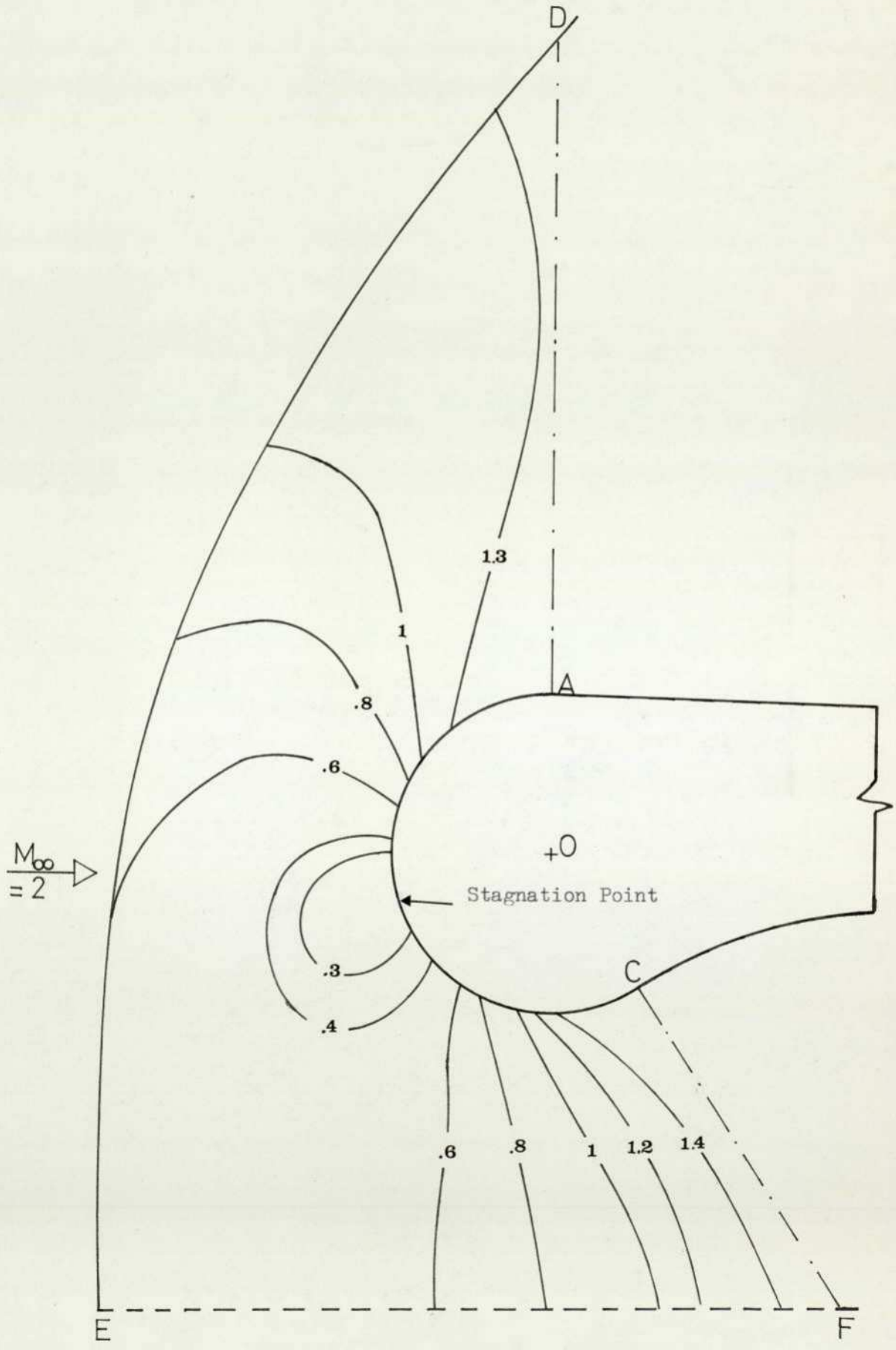


FIGURE 23

MACH NUMBER AND PRESSURE DISTRIBUTION ON THE SURFACE OF INLET A

(M_∞=2.0,MFR=0.44,axisymmetric flow)

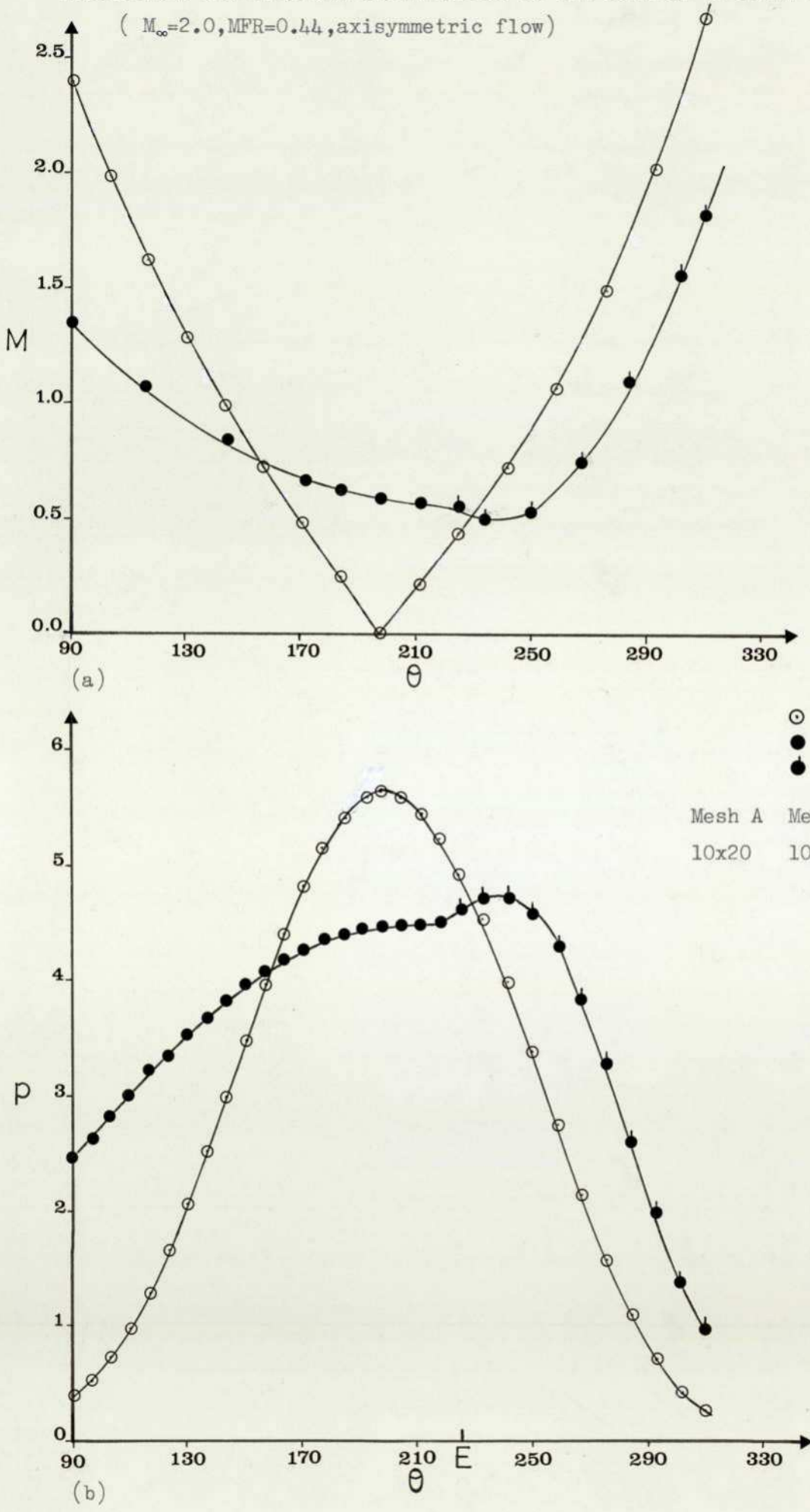


FIGURE 24

ENTROPY DISTRIBUTION CALCULATED USING METHOD 2

(SUPIB problem, Inlet A, M_∞=2.0, axisymmetric flow, MFR=0.44)

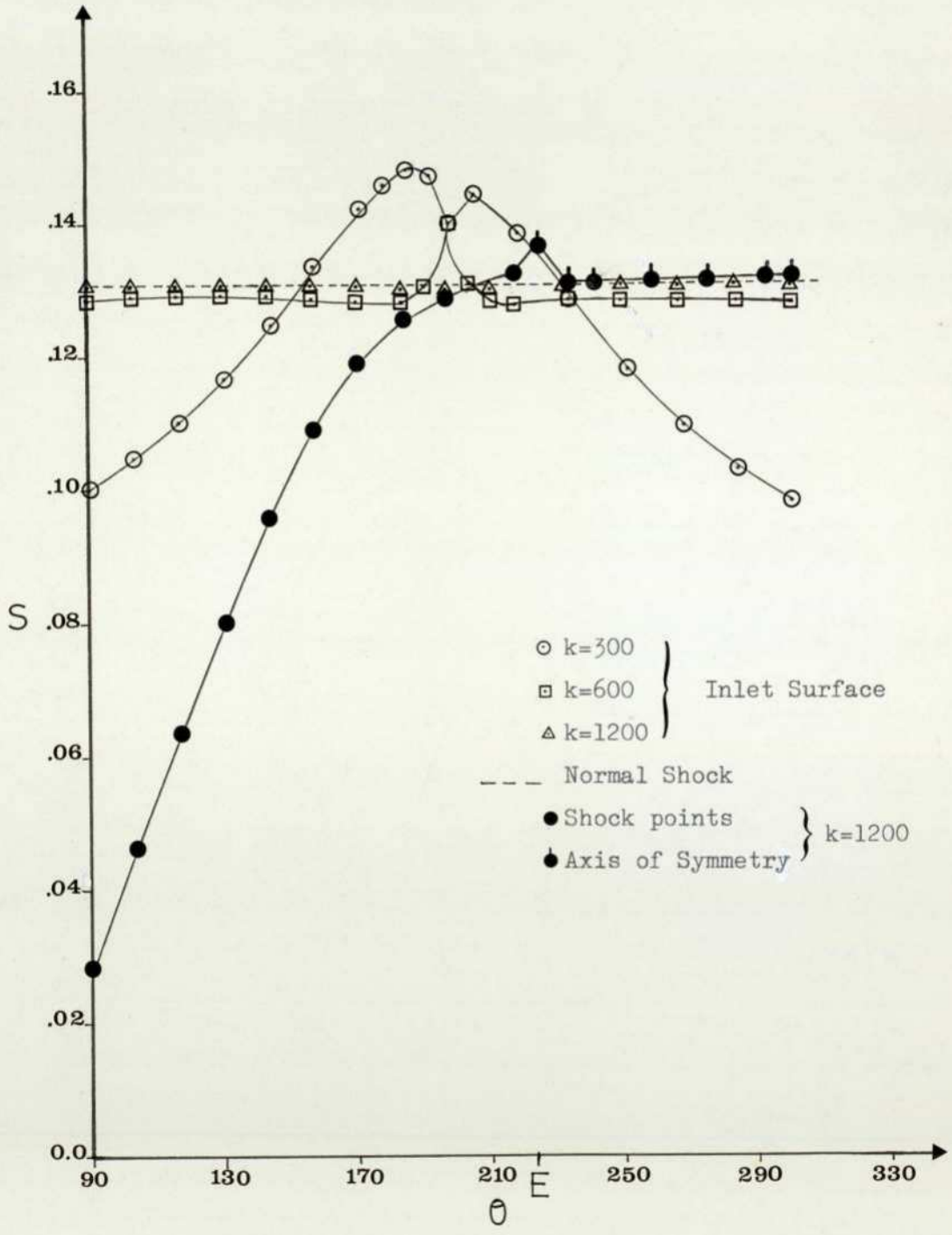


FIGURE 25 (a)

ENTROPY DISTRIBUTION AT Z=0.5 FOR k =600 AND 1200

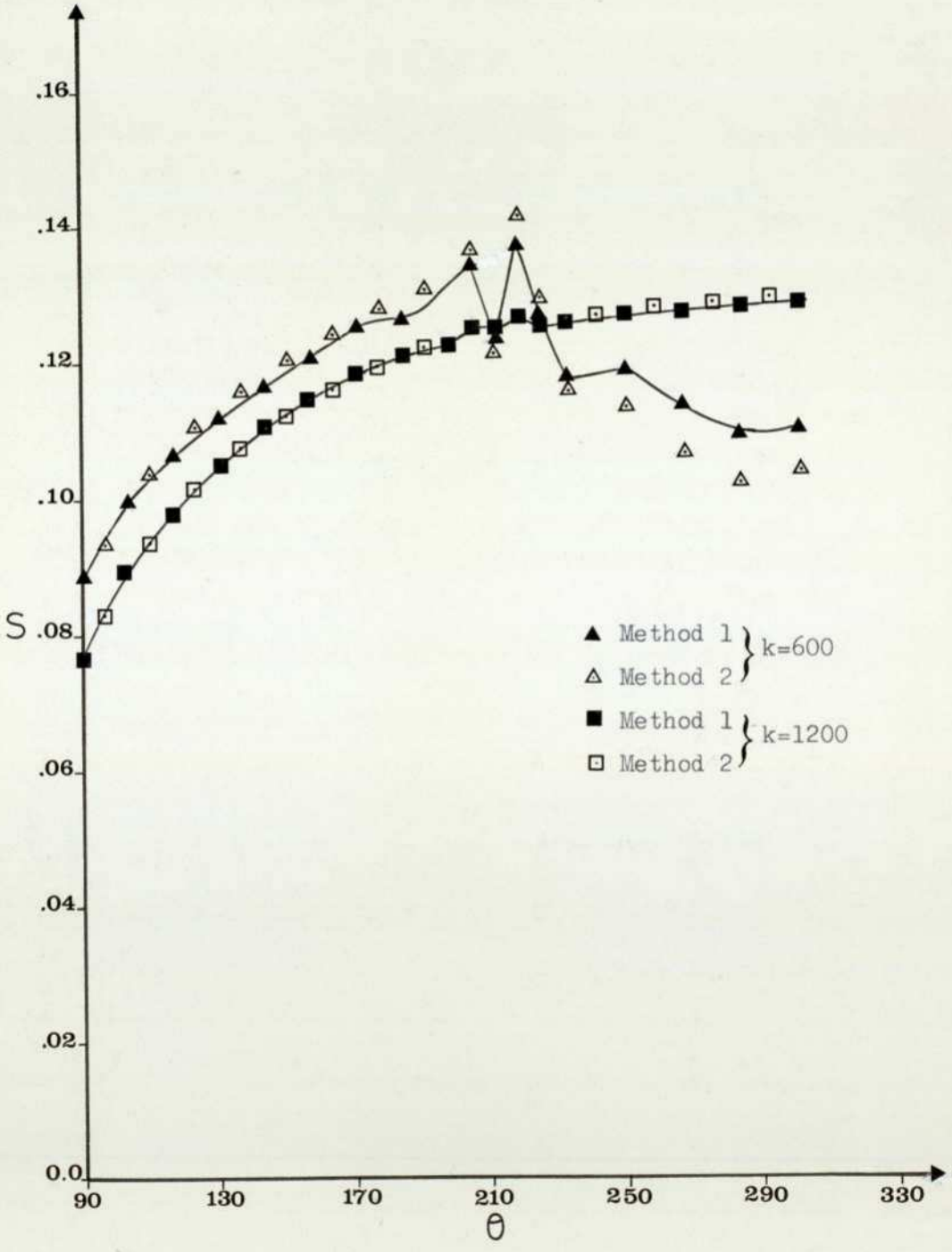


FIGURE 25 (b)

PRESSURE DISTRIBUTION ON A TOROID

(SUPIB problem,axisymmetric flow,MFR=0.36)

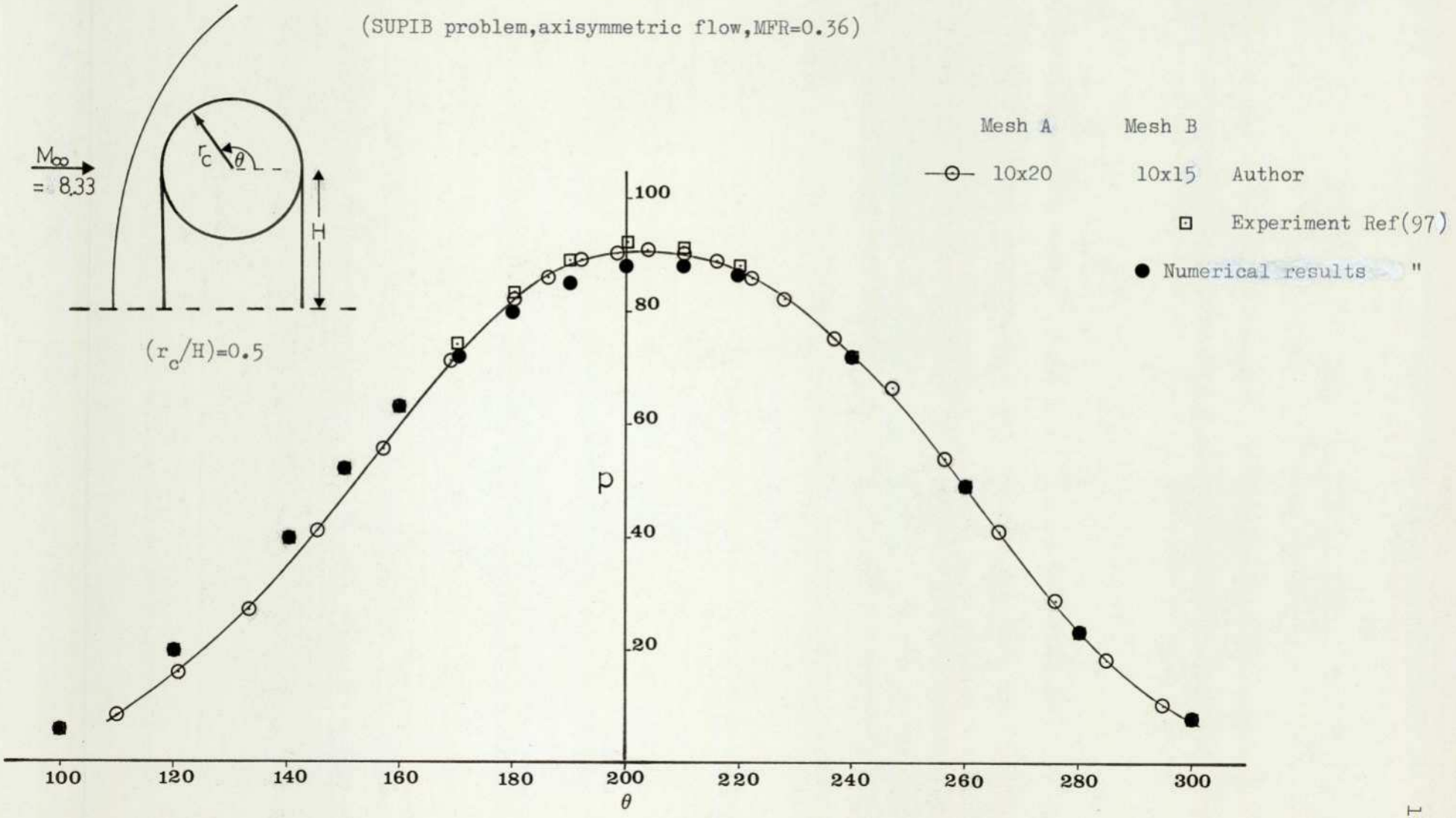


FIGURE 26

COMPARISON OF FLOW DIRECTION PLOTS FOR COARSE AND FINE MESH SIZES

(Inlet B, axisymmetric flow, M_∞=2.81, MFR=0.59)

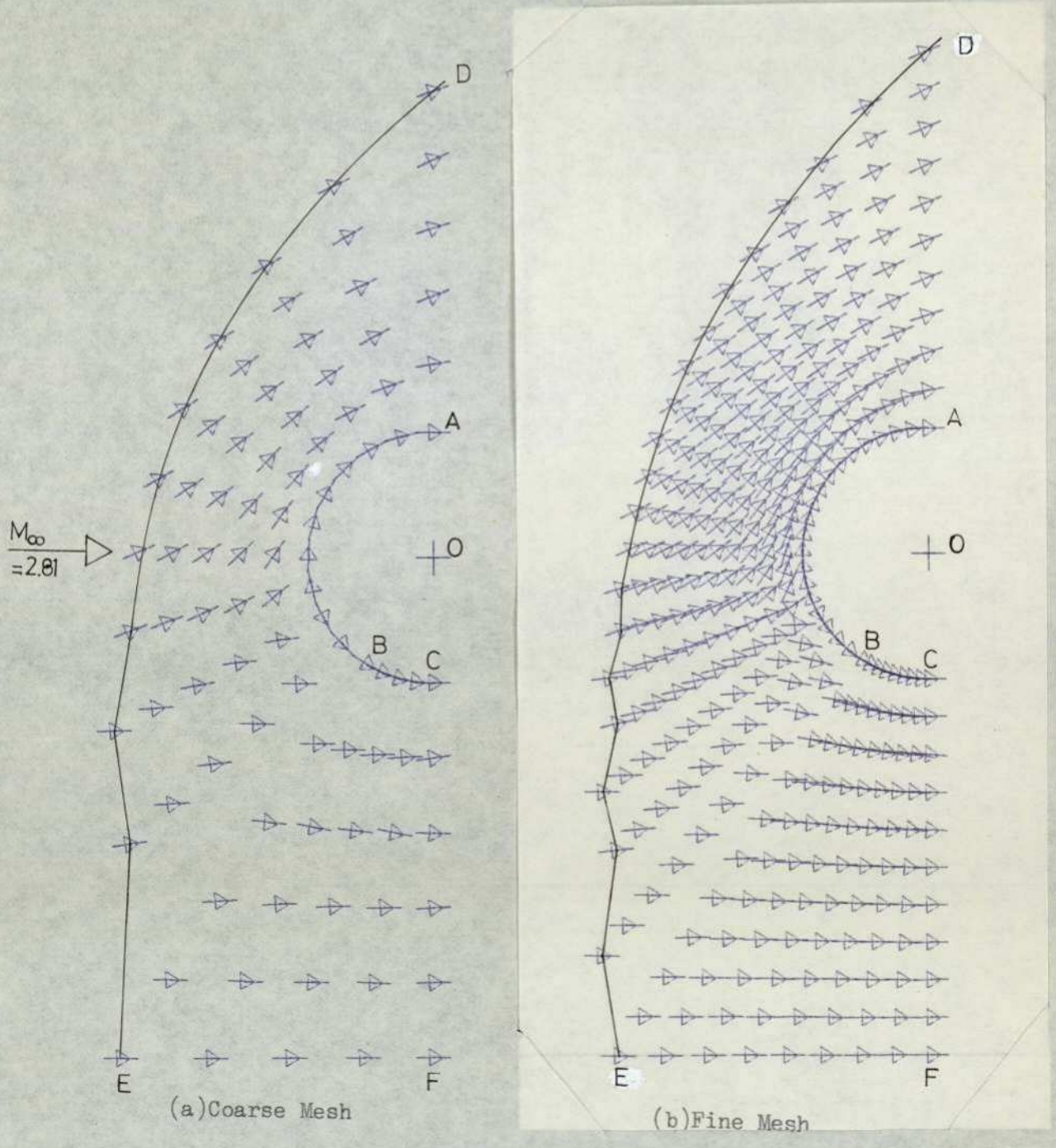


FIGURE 27

PRESSURE AND MACH NUMBER DISTRIBUTION FOR INLET B

(M_∞=2.81,axisymmetric flow,MFR=0.59)

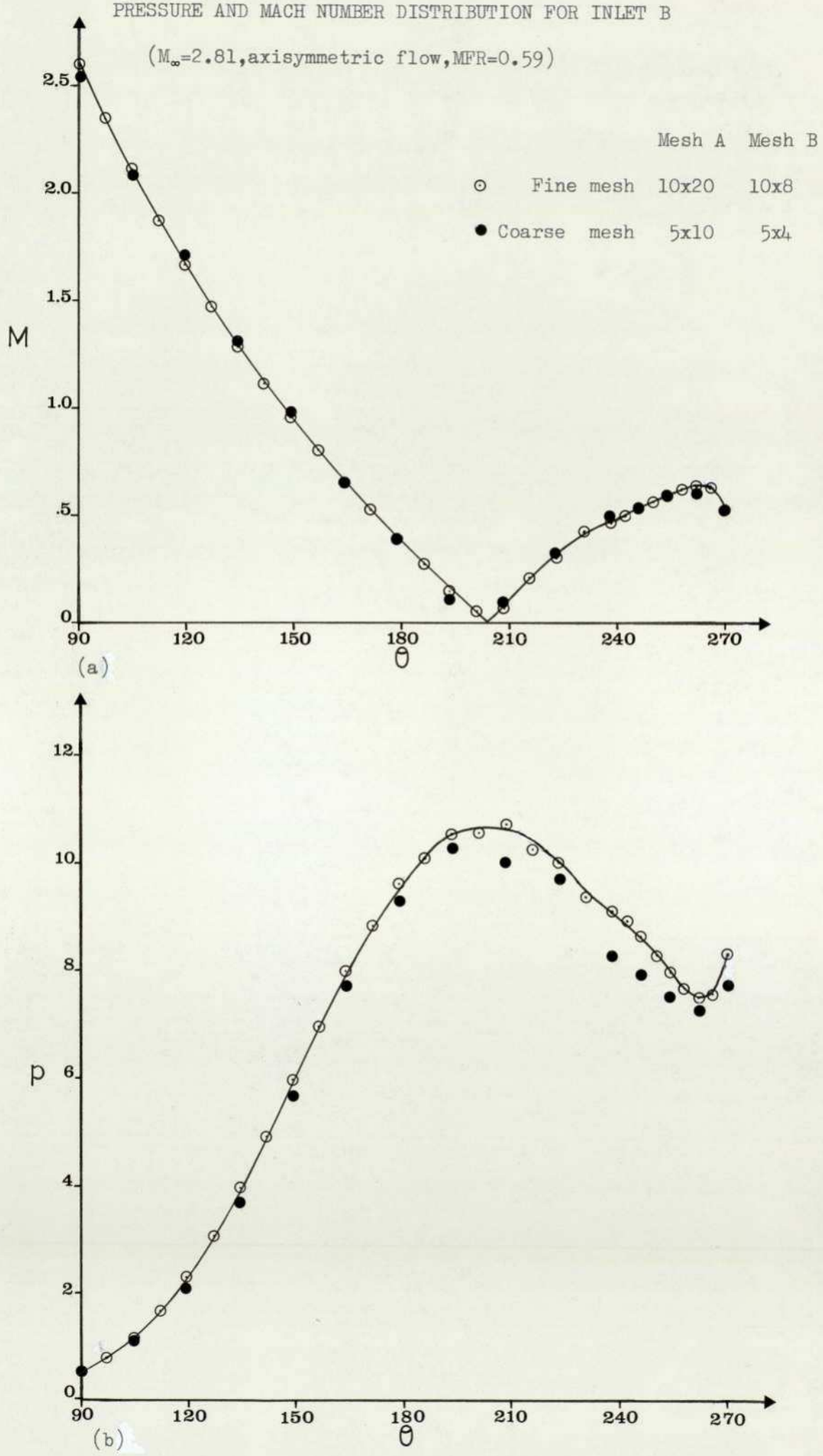
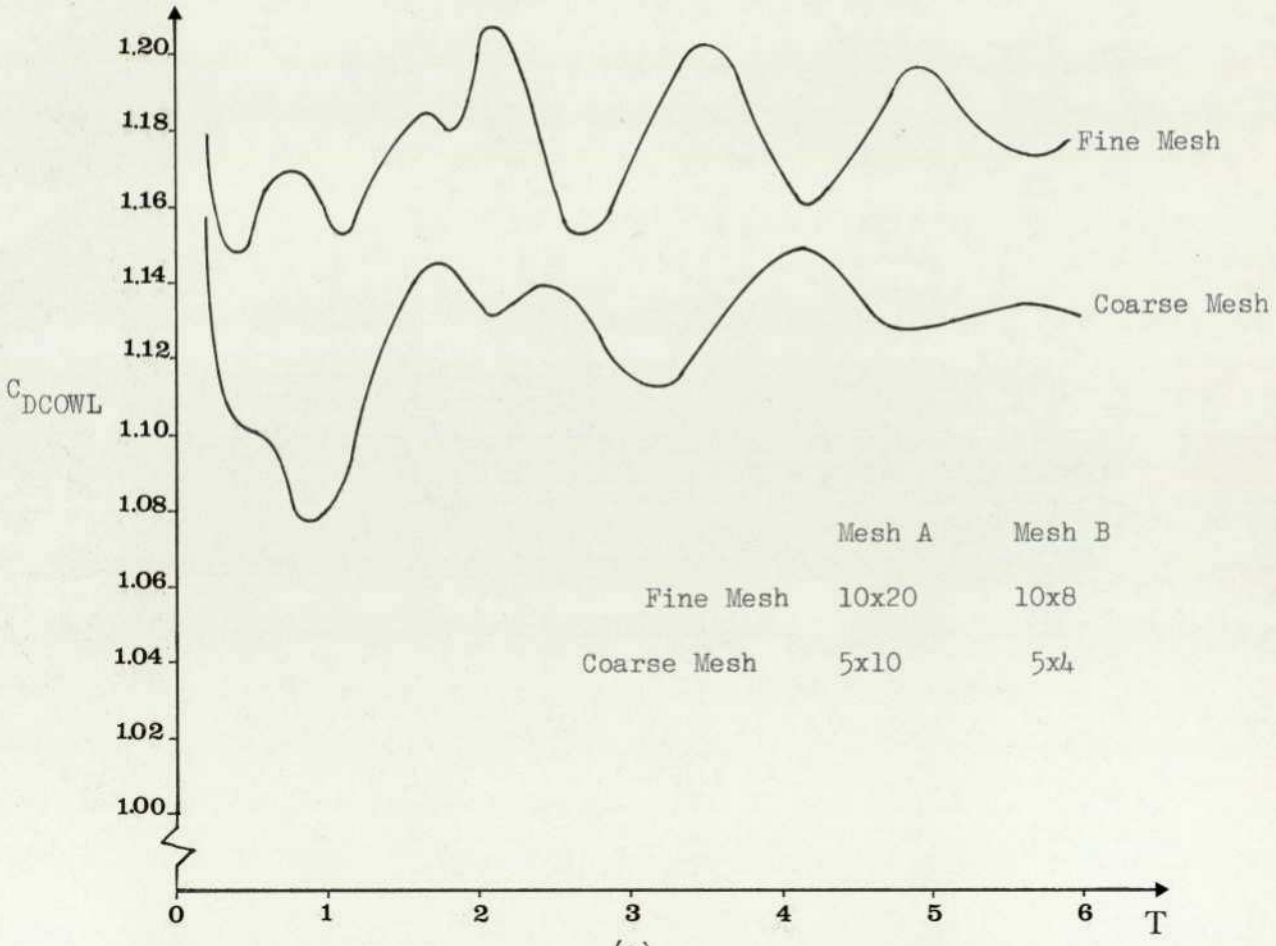


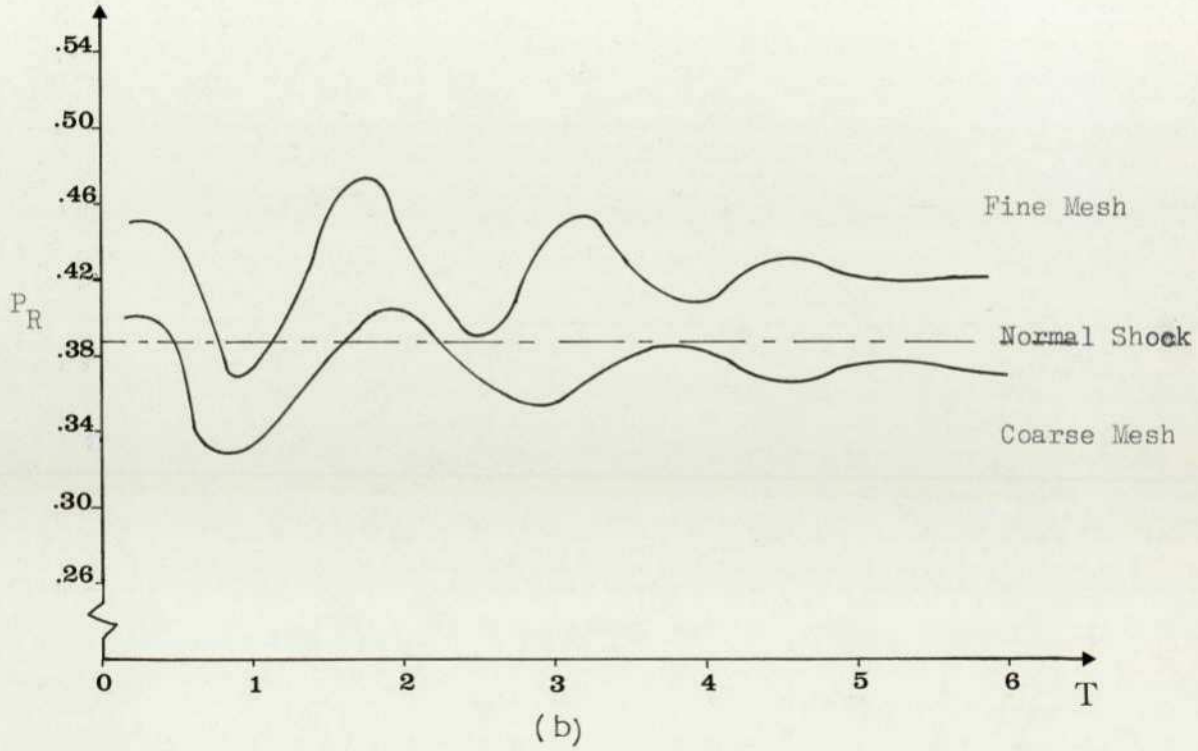
FIGURE 28

A STUDY OF THE TRANSIENT BEHAVIOR OF C_{DCOWL} AND P_R FOR THE SUBIB PROBLEM

(Inlet B, axisymmetric flow, M_∞ =2.81, MFR=0.59)



(a)



(b)

FIGURE 29

THE TRANSIENT BEHAVIOR OF THE SHOCK MOVEMENT CONVERGENCE CRITERION (CONCRIT)

$$CONCRIT = \int_0^1 |W| \Delta T \, dYA$$

where YA is the co-ordinate direction in the computational plane.

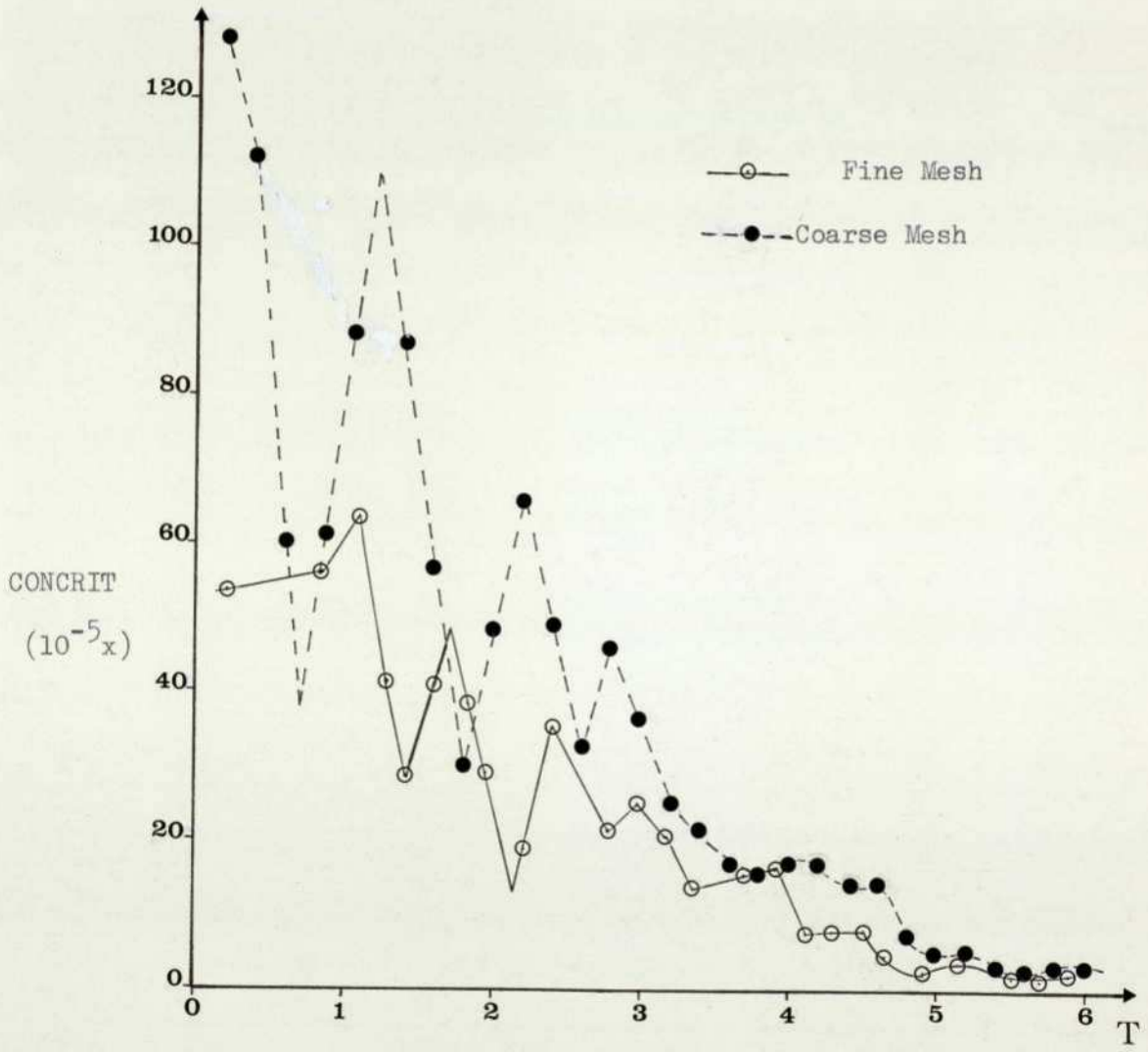
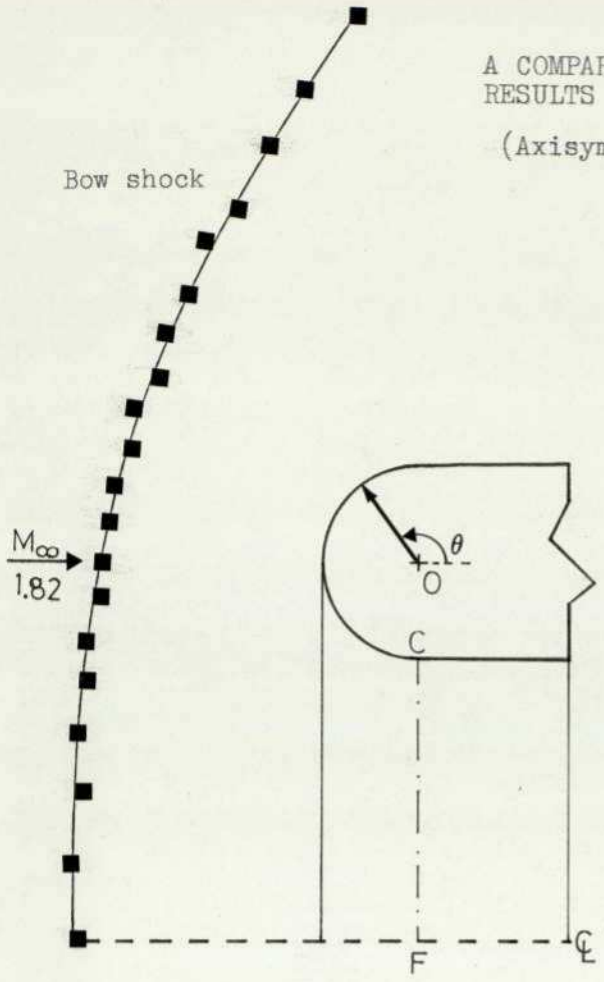


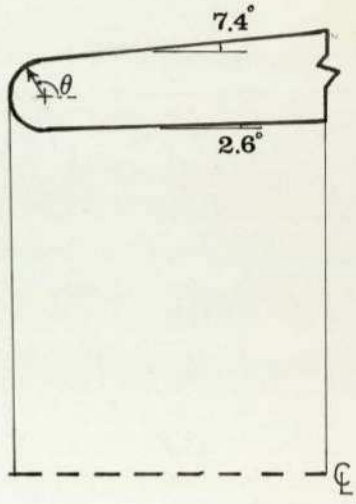
FIGURE 29 (c)

A COMPARISON BETWEEN EXPERIMENTAL AND NUMERICAL RESULTS

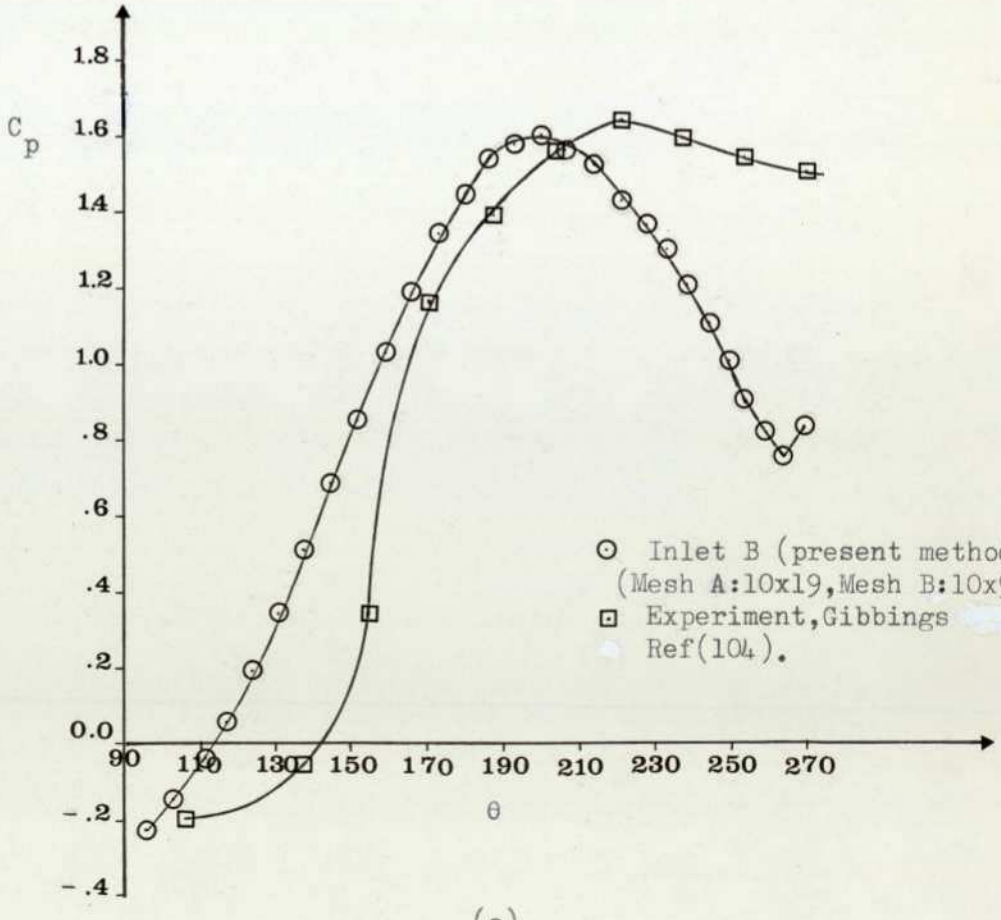
(Axisymmetric flow, $\dot{M}FR=0.58$, $M_\infty = 1.82$)



(a) Inlet B



(b) Inlet used in an experiment by Gibbings Ref(104)



(c)

FIGURE 30

FLOW DIRECTION PLOT ABOUT INLET C WITH A SUBSONIC INTERNAL BOUNDARY

(Axisymmetric Flow, MFR=0.59)

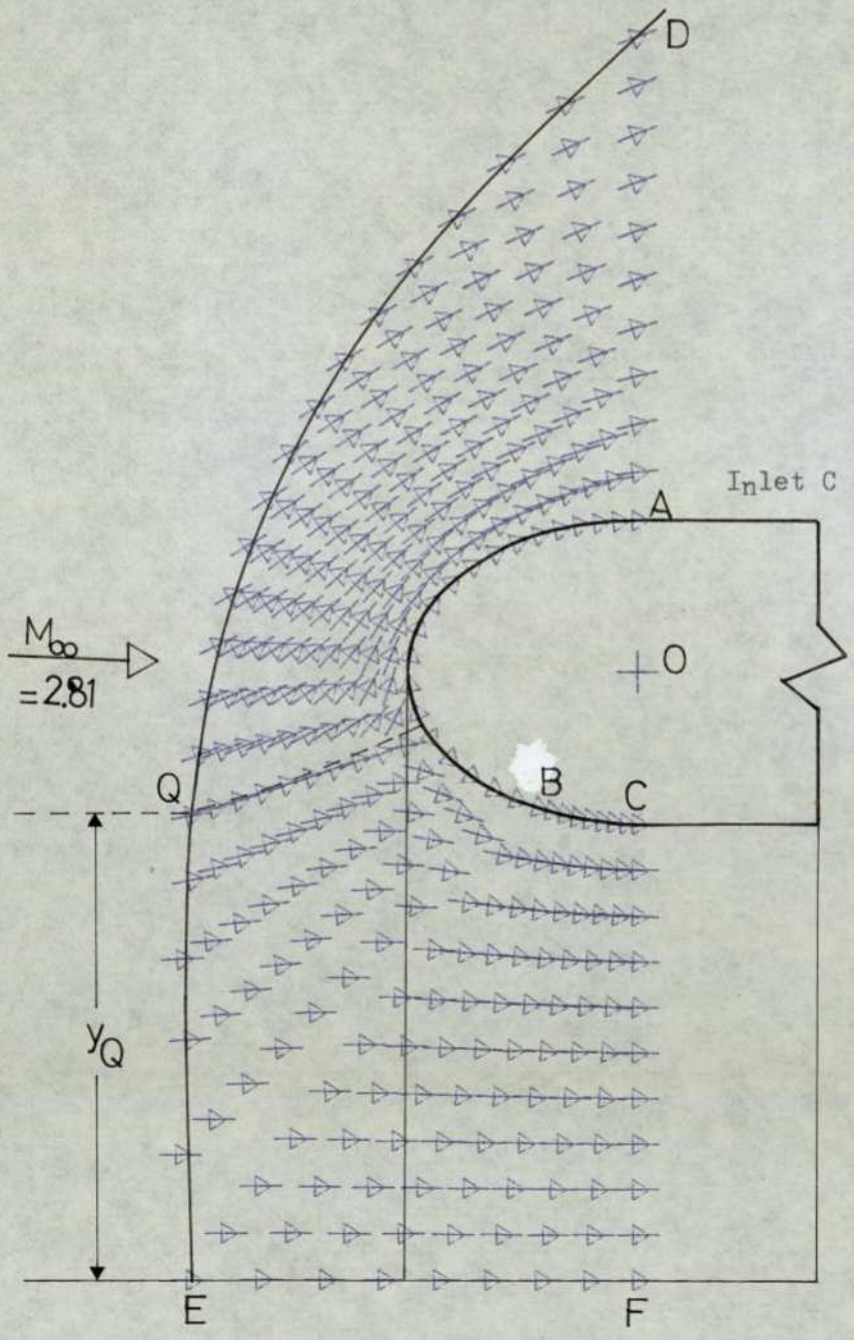


FIGURE 31

MACH NUMBER CONTOURS FOR INLET C

(Axisymmetric Flow, MFR= 0.59)

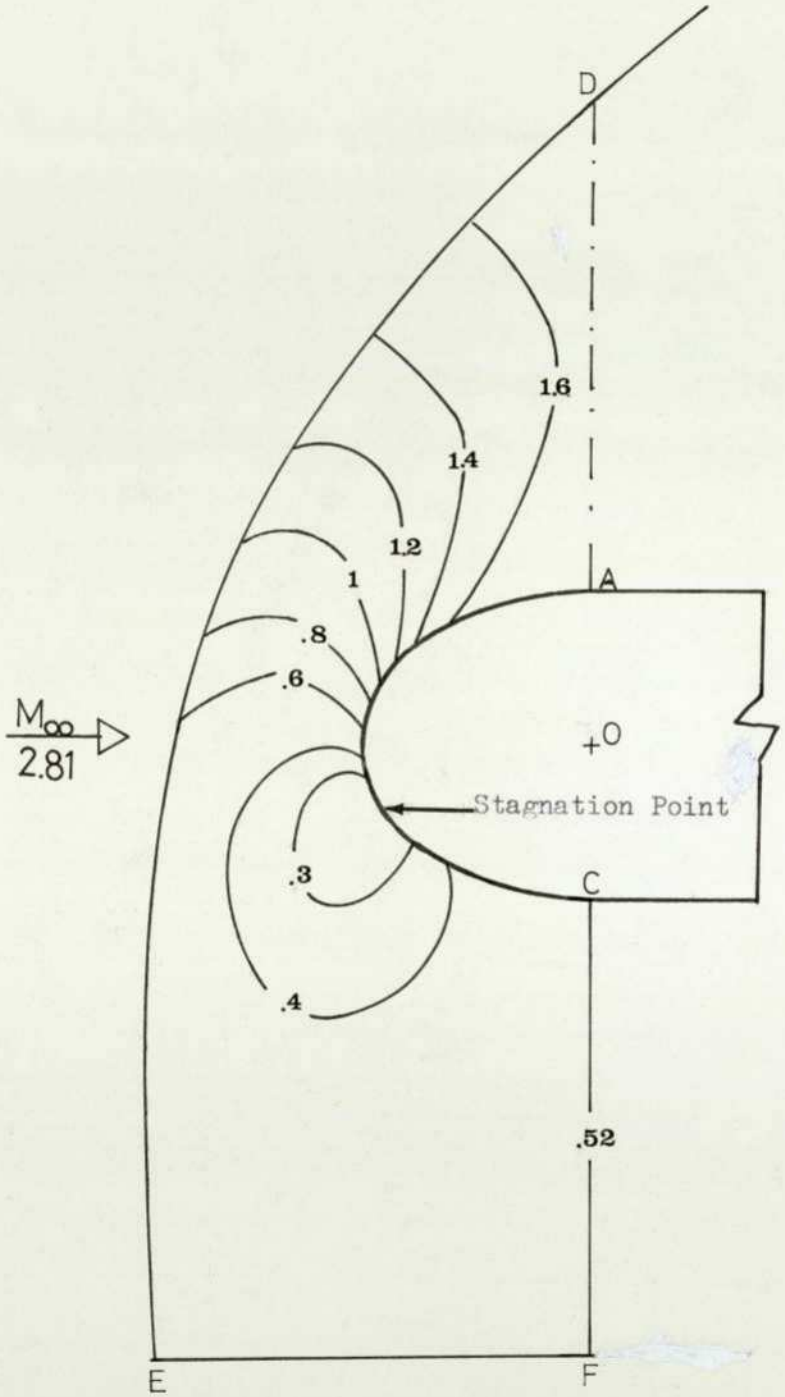
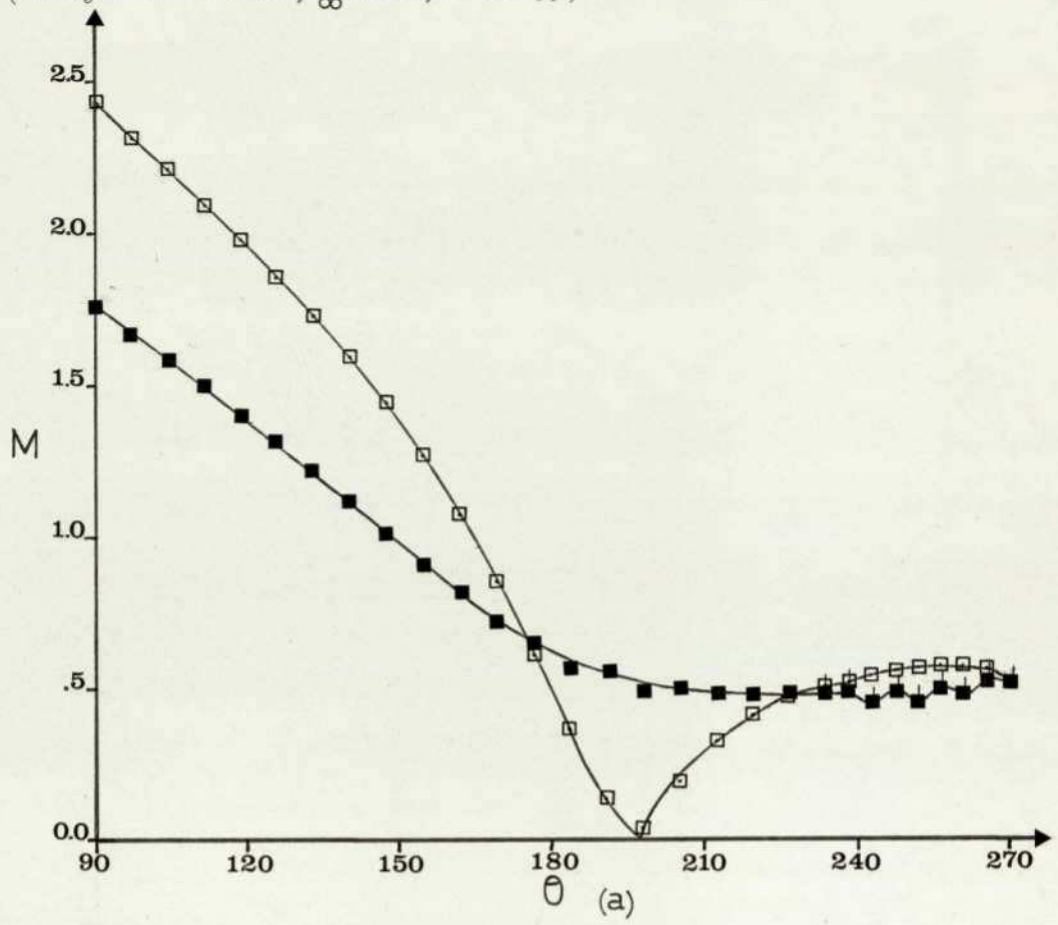


FIGURE 32

PRESSURE AND MACH NUMBER DISTRIBUTION FOR INLET C

(Axisymmetric Flow, M_∞=2.81, MFR=0.59)



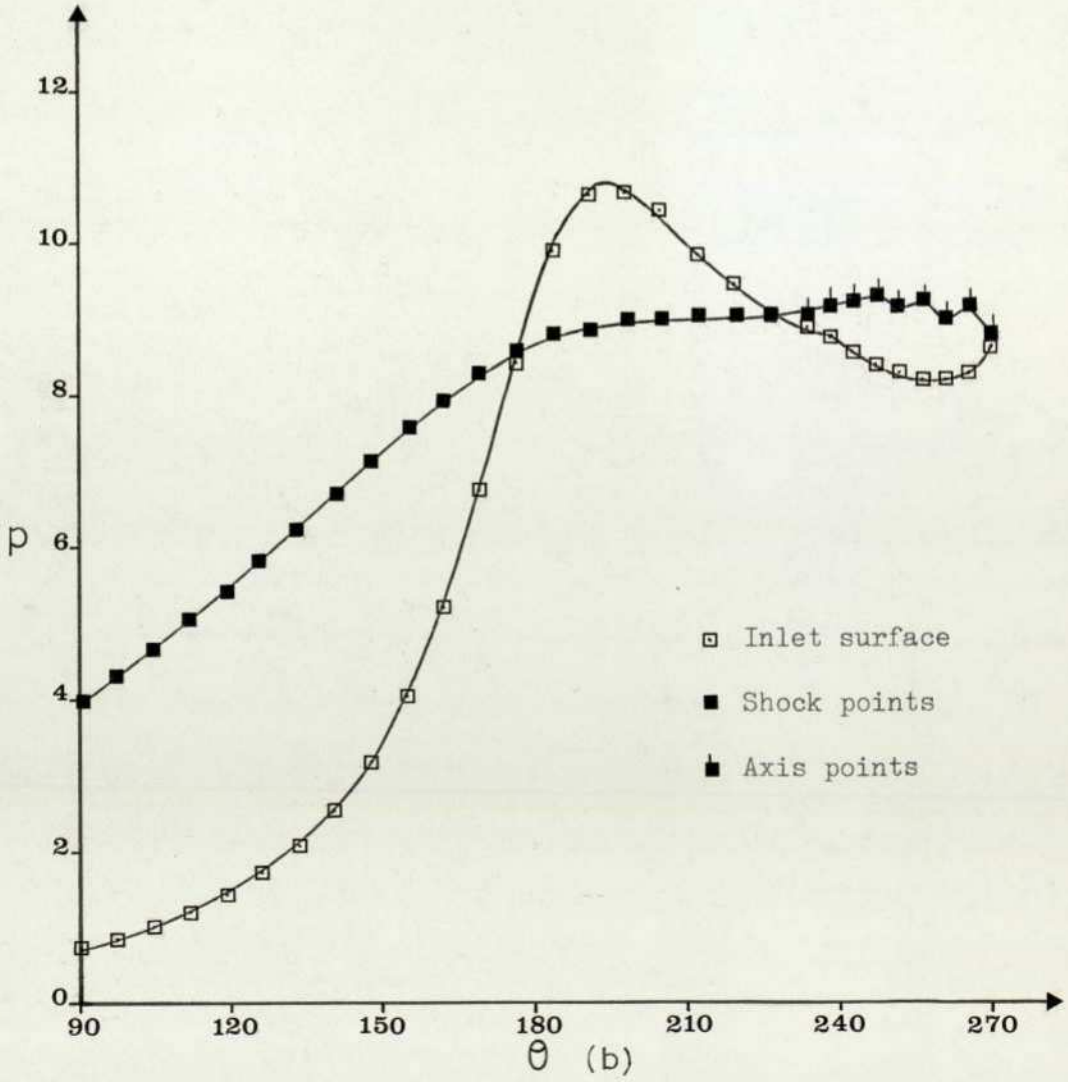


FIGURE 33

FLOW DIRECTION PLOT ABOUT INLET A

(Two-dimensional flow, M_∞=2.81, MFR=0.6)

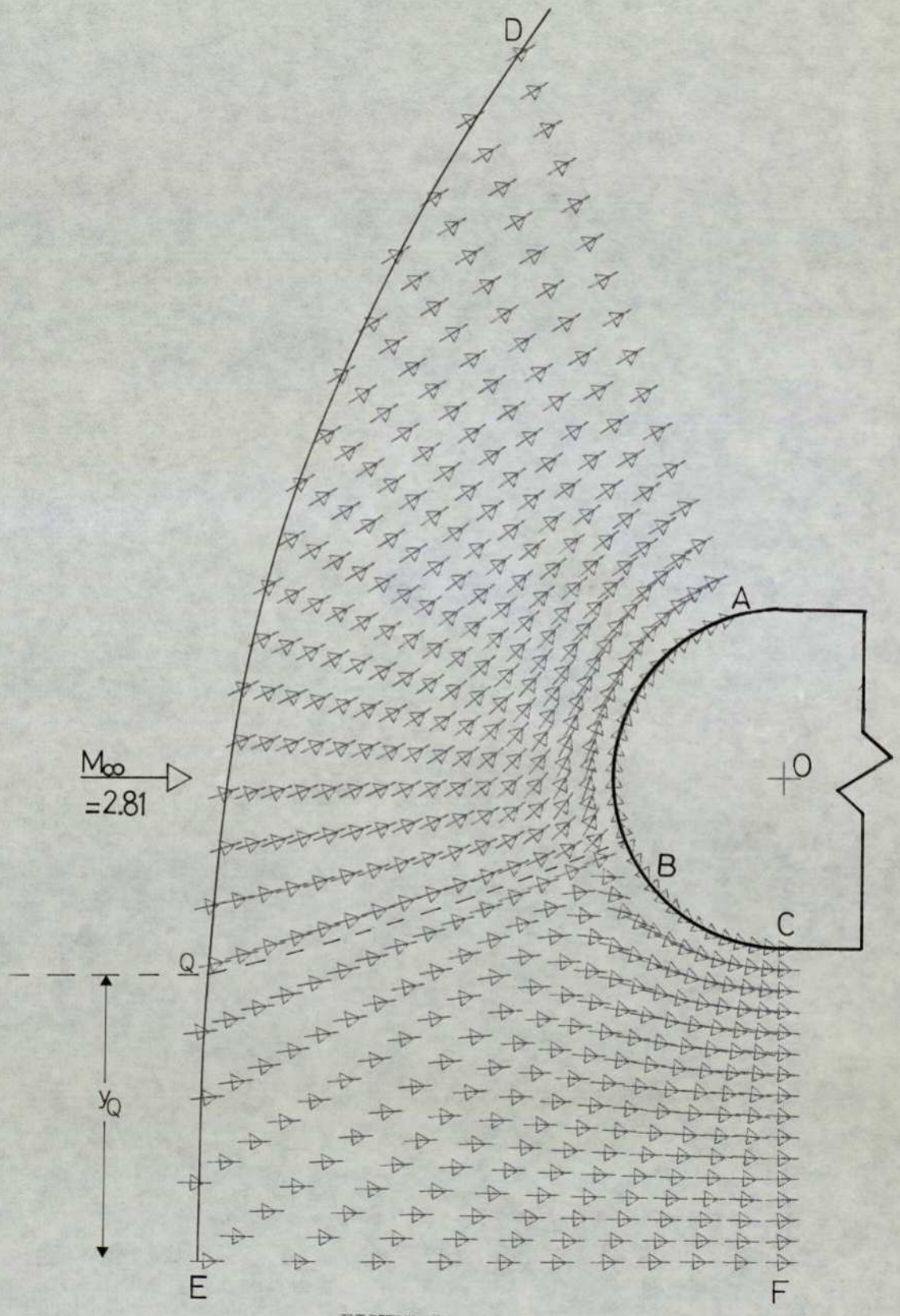
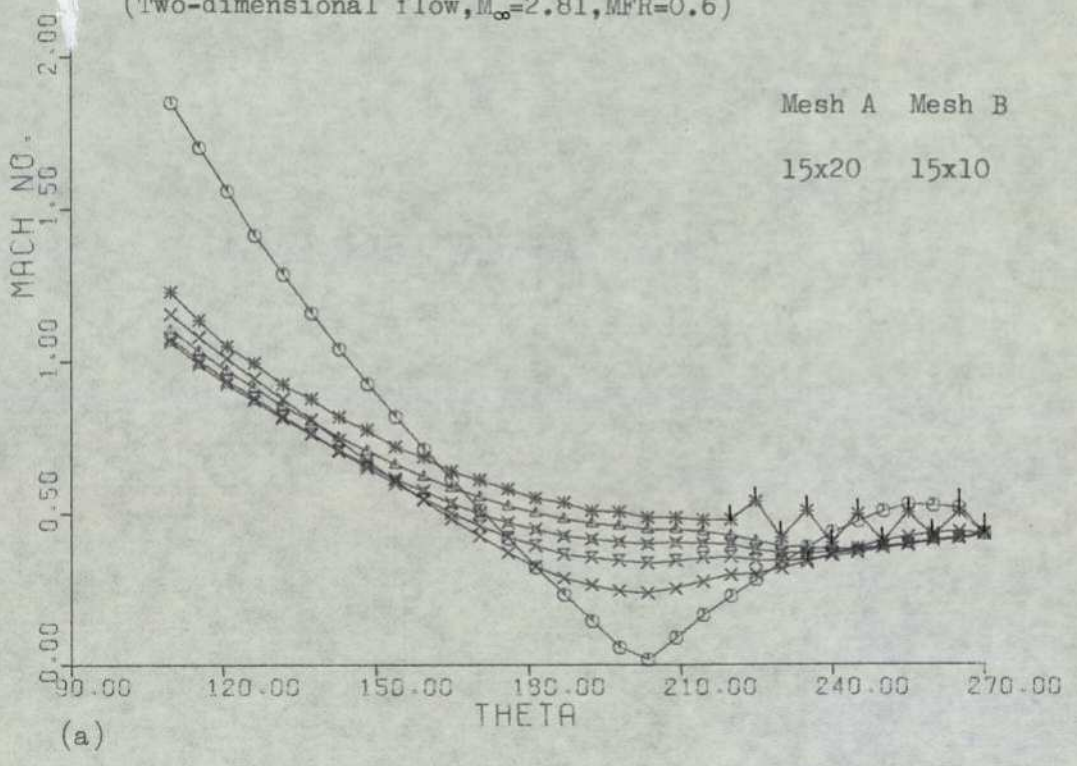


FIGURE 34

MACH NUMBER AND PRESSURE DISTRIBUTION FOR INLET A

(Two-dimensional flow, M_∞=2.81, MFR=0.6)



(a)

NO OF TIME STEPS= 2400. ,MACH NO.= 2.810

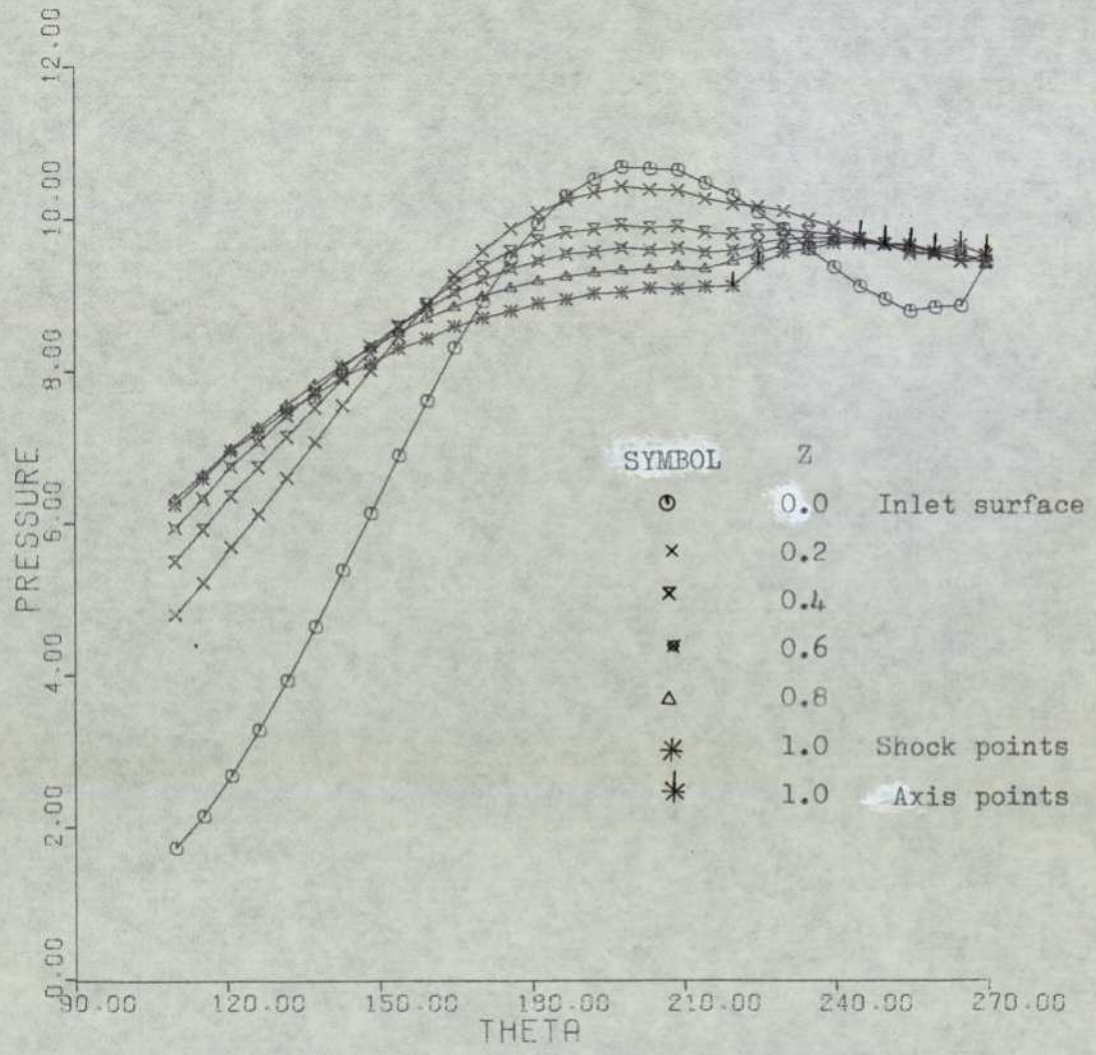
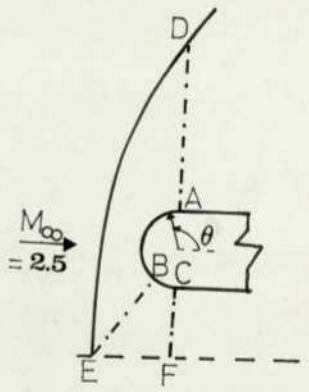


FIGURE 35

MACH NUMBER DISTRIBUTION ON THE AXIS OF SYMMETRY (E-F)

(Inlet A, two-dimensional flow, $M_\infty = 2.5$)



$YB=(\theta-\theta_B)/(\theta_C-\theta_B)$

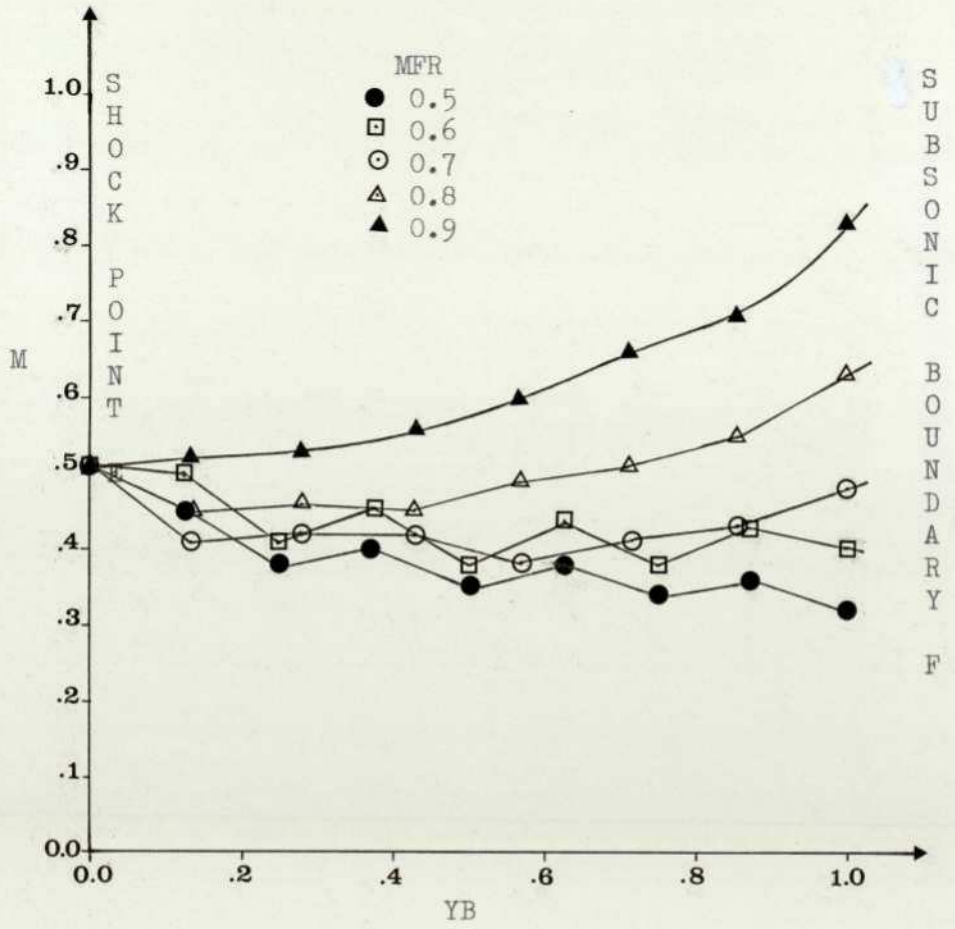


FIGURE 36

VARIATION OF BOW SHOCK POSITION WITH MFR AT M_∞ =2.5

(Two-dimensional flow, Inlet A)

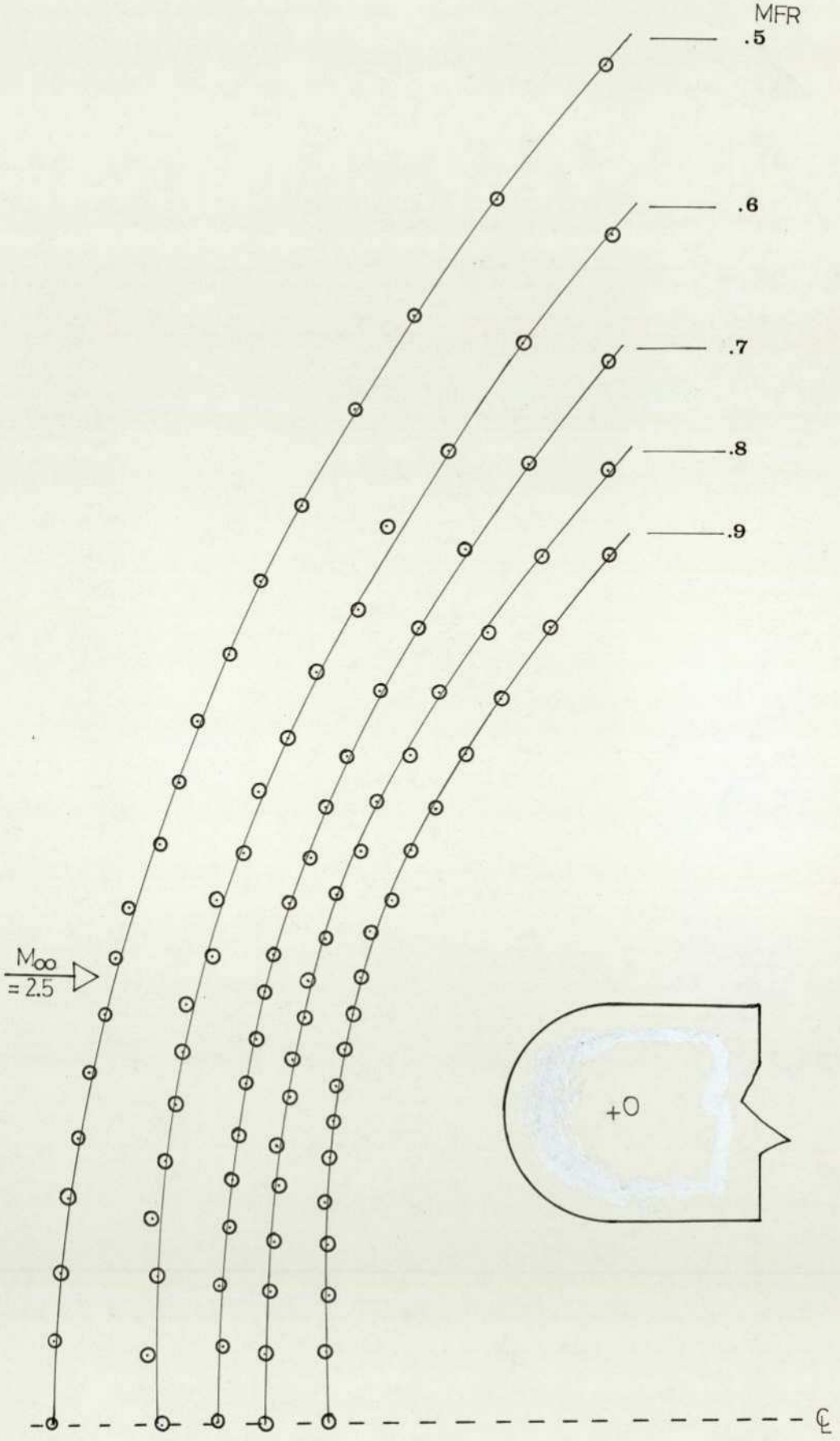


FIGURE 37

VARIATION OF BOW SHOCK POSITION WITH M_∞

AT MFR=0.6

(Two dimensional flow, Inlet A)

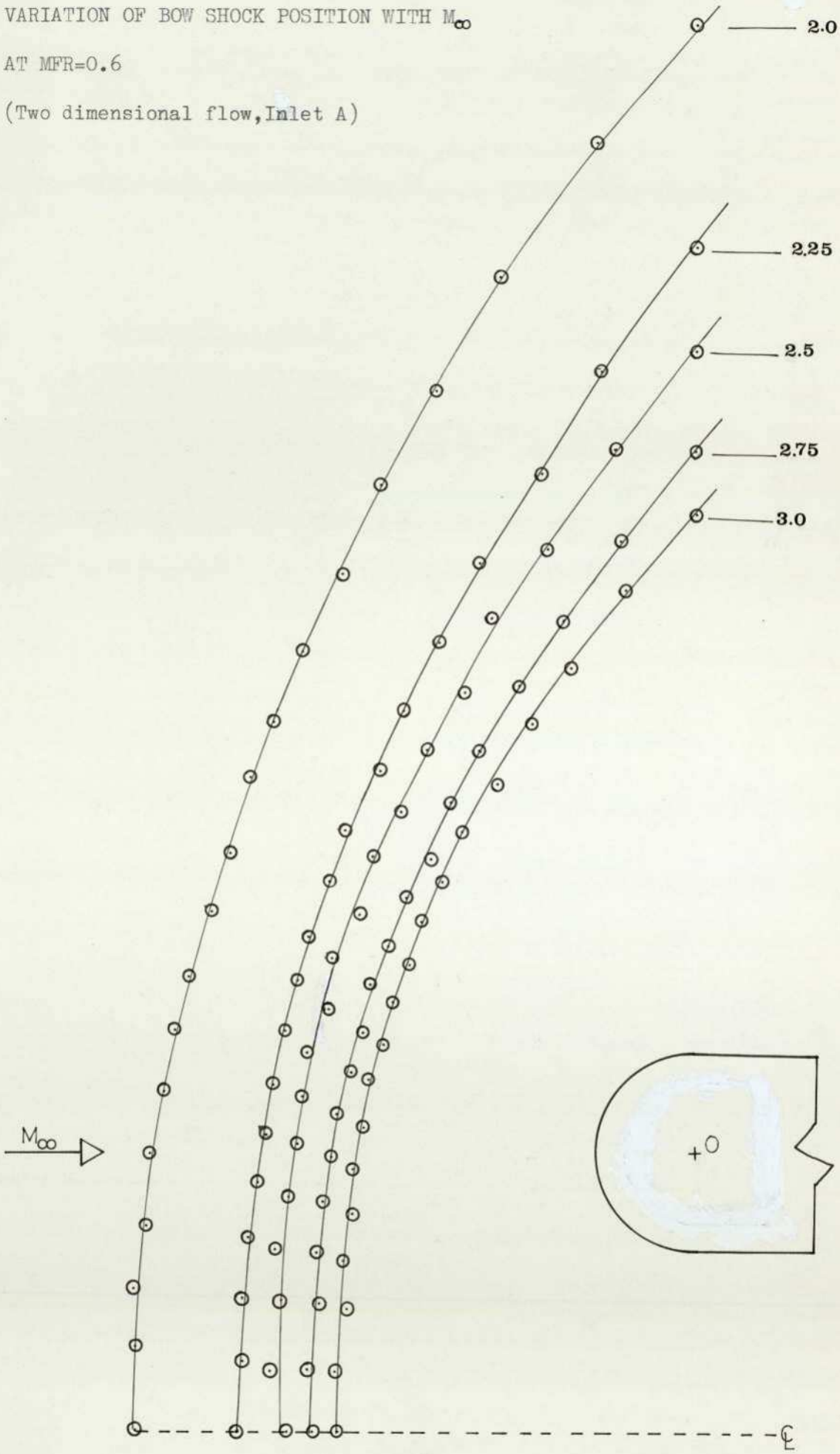


FIGURE 38

VARIATION OF MACH NUMBER (M) AND PRESSURE COEFF. (C_p) FOR DIFFERENT MFR

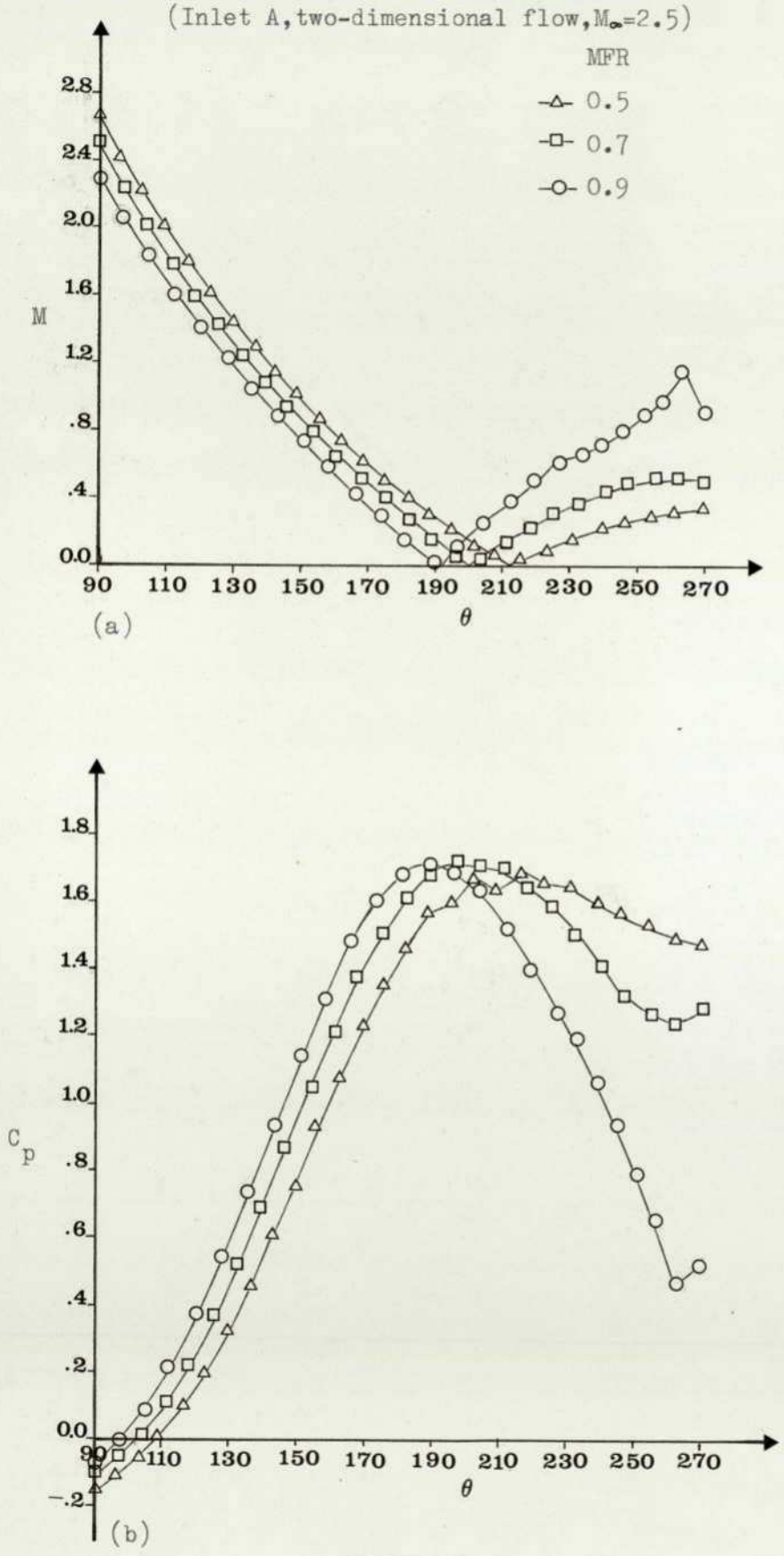


FIGURE 39

VARIATION OF MACH NUMBER (M) AND PRESSURE COEFF. (C_p) FOR MFR=0.6

(Inlet A, two-dimensional flow)

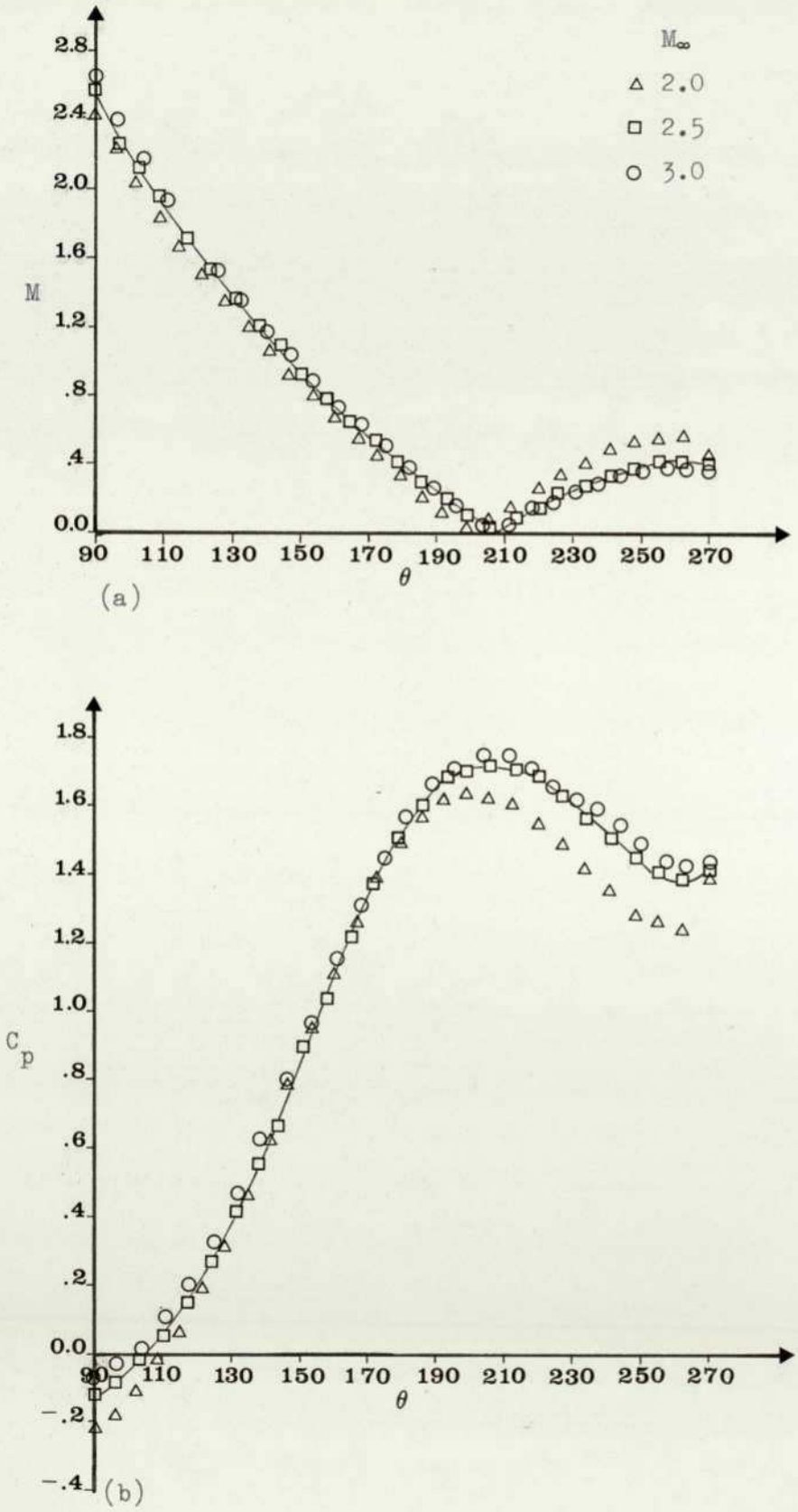


FIGURE 40

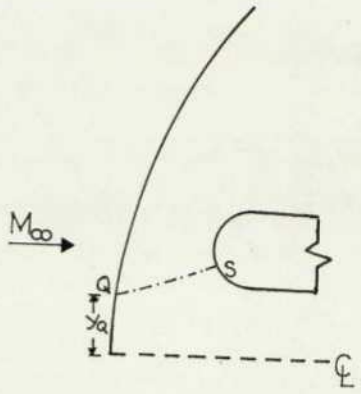
C_{DCOWL}, C_{DEXT} and C_{DADD} for inlet A

(two-dimensional flow)

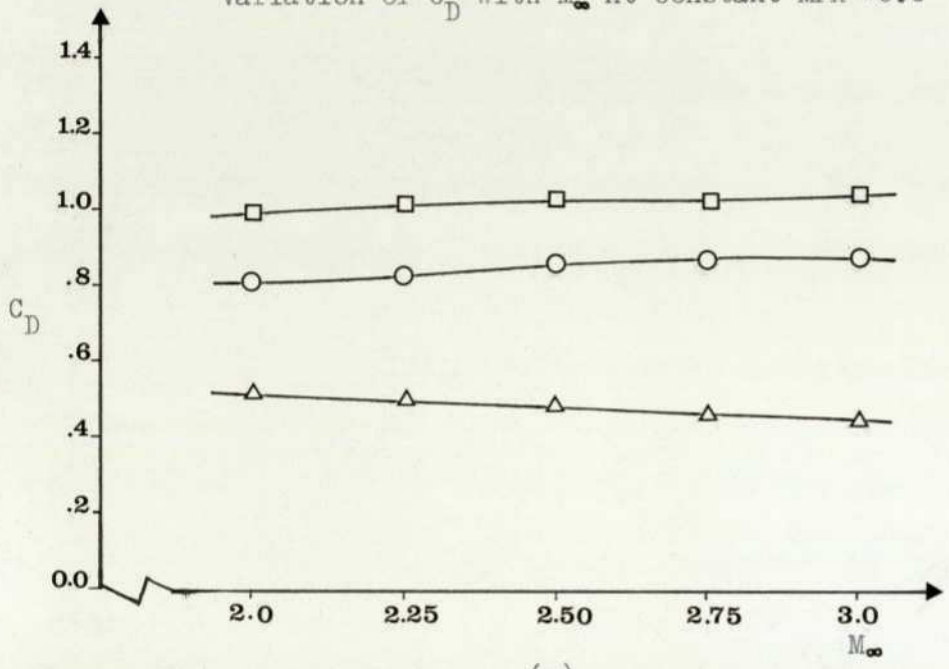
○ C_{DCOWL}

□ C_{DEXT}

△ C_{DADD}

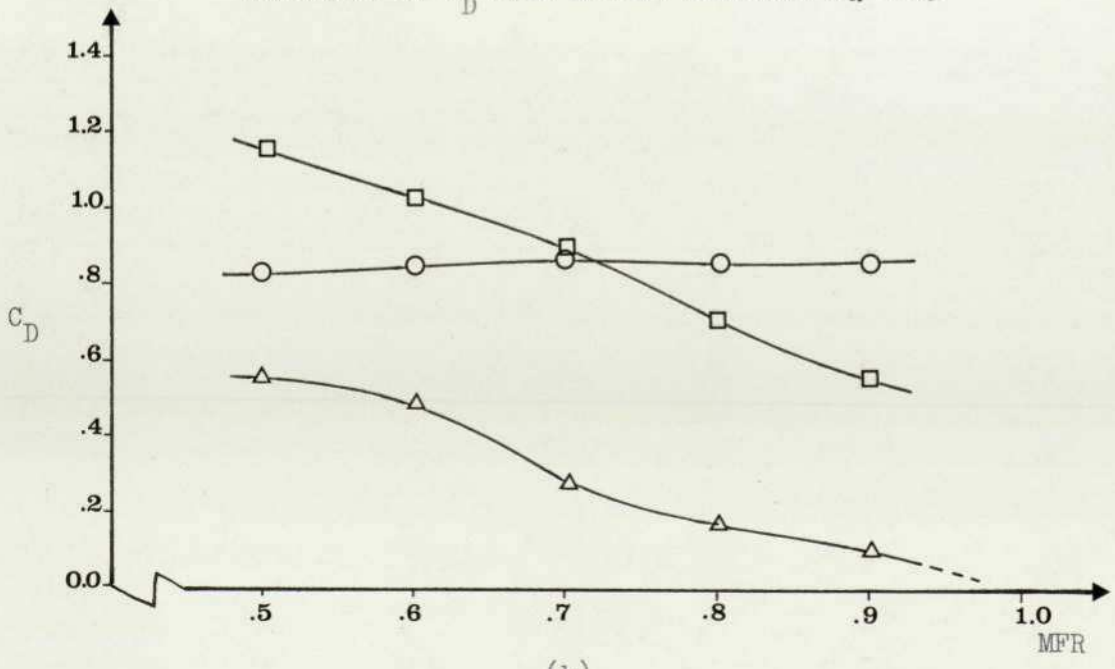


Variation Of C_D With M_∞ At Constant MFR =0.6



(a)

Variation Of C_D With MFR At Constant M_∞ =2.5

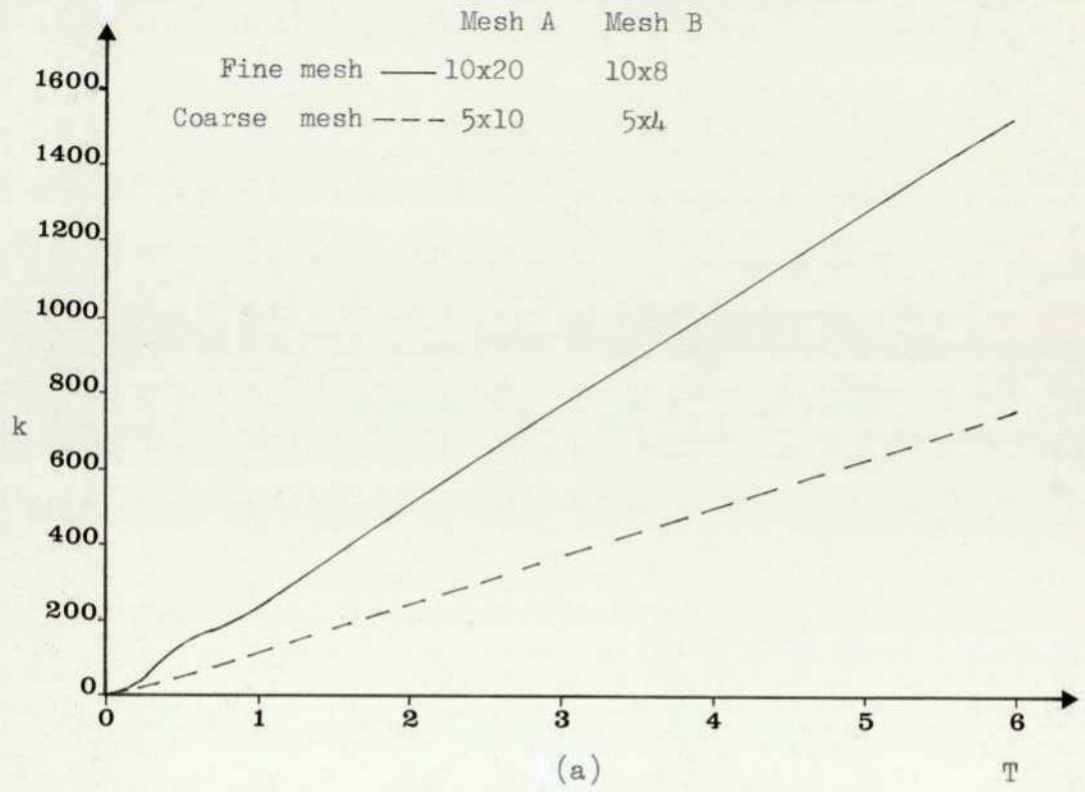


(b)

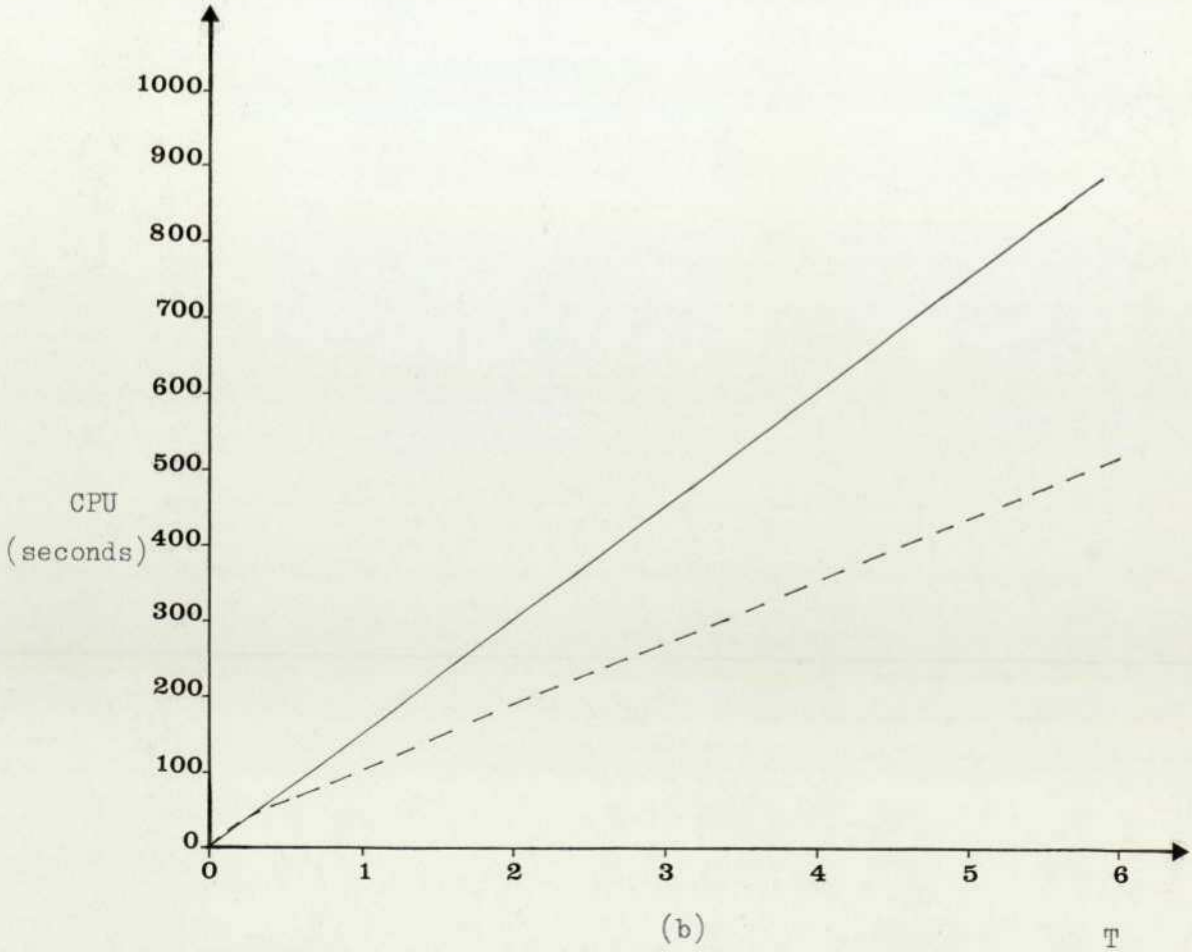
FIGURE 41

VARIATION OF TIME STEP (k) AND CENTRAL PROCESSOR UNIT TIME (CPU) WITH COMPUTATIONAL TIME (T)

(Inlet B, axisymmetric flow, M_∞=2.81, MFR=0.59)



(a)



(b)

FIGURE 42

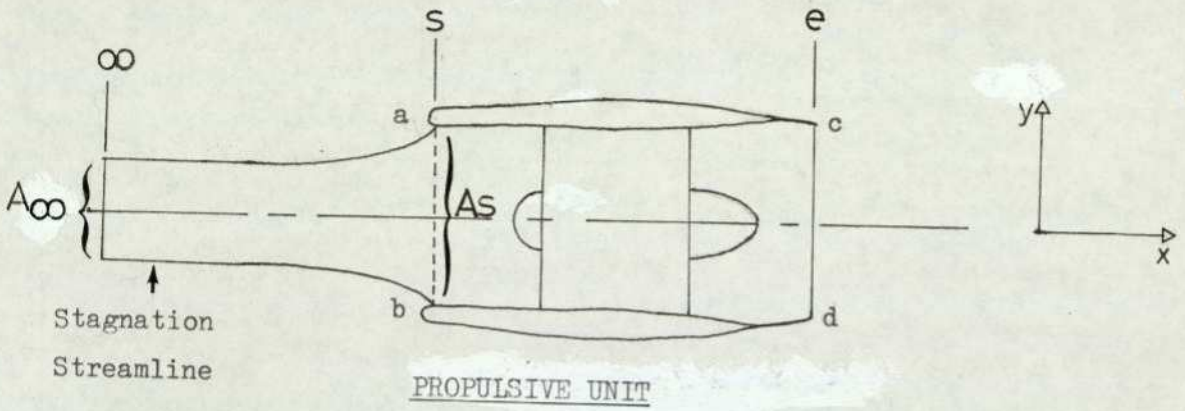
A P P E N D I C E S

APPENDIX (A)

DEFINITIONS AND DERIVATION OF EXPRESSIONS FOR INLET DRAG

ADDITIVE DRAG AND INTERNAL THRUST

*(assuming one-dimensional flow, see Ref(118))



PROPULSIVE UNIT

The internal thrust F_{INT} is defined as, $F_{INT}=\int_s^e (p-p_\infty)dA$, where -(A-1)

dA is the projected frontal area and the integral is taken around all of the internal surfaces of the system, from the stagnation point on the inlet lip to the exit station e. Internal thrust is the force generated within the propulsive system.

The engine manufacturer's definition of net-thrust is :-

$$F_N = \left[(p_e-p_\infty)A_e + \dot{m}_e V_e\right] - \left[(p_\infty - p_\infty)A_\infty + \dot{m}_\infty V_\infty\right] \qquad -(A\text{-}2)^*$$

Equation (A-1) is evaluated by establishing a force-momentum balance on a control-surface comprising of station ∞ (far upstream), the stagnation streamline, the internal surface of the cowl and the exit station e. The forces in the x direction exerted on the fluid within the control volume equals the net change in momentum in the x direction,

$$\left[(p_\infty - p_\infty)A_\infty + \dot{m}_\infty V_\infty\right] + \int_\infty^s (p-p_\infty)dA + \int_s^e (p-p_\infty)dA - \left[(p_e-p_\infty)A_e + \dot{m}_e V_e\right] = 0 \qquad (A\text{-}3)^*$$

$$F_{INT} = F_N - \int_\infty^s (p-p_\infty)dA = F_N - D_{ADD} \qquad -(A\text{-}4)$$

Additive drag D_{ADD} can be evaluated by applying the momentum theorem to the control volume containing the stagnation streamline up to station s.

$$D_{ADD} = (p_s-p_\infty)A_s + \dot{m}_\infty V_s - \dot{m}_\infty V_\infty \qquad -(A\text{-}5)^*$$

Additive drag in concept is the external force on the entering streamtube which causes the total axial change in momentum between freestream and the station at which the stagnation streamlines intercept the cowl lip.

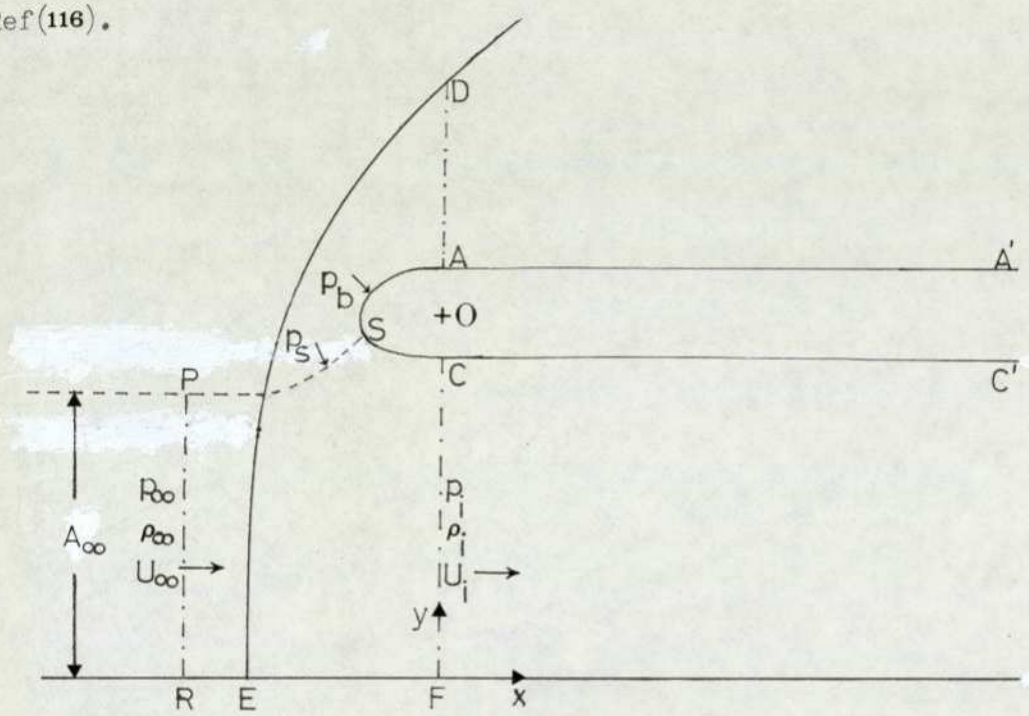
Derivation of Expressions for External Drag and Additive Drag of a Ducted Two-Dimensional or Axisymmetrical Body

The drag of a ducted body such as an aircraft Pitot intake is resolved into two components :-

(a) The drag associated with the external flow, and

(b) The drag or internal thrust F_{INT} associated with the internal flow.

This division is a matter of convenience and stems traditionally from a division of responsibility between aerodynamicists and engine designers, Ref(116).



A-S-C represents the inlet lip.A-A' and C-C'are parallel to the axis of symmetry.P-S is the stagnation streamline and D-E is the bow shock wave. As the computed region is terminated at the internal boundary C-F,F_{INT} as defined in (A-4) cannot be evaluated.However the external drag and the additive drag can be evaluated.

The External Drag is defined as

$$D_{EXT}=\int_P^S (2\pi y)^j (p_s-p_\infty)dy + \int_S^A (2\pi y)^j (p_b-p_\infty)dy \qquad -(A\text{-}6)$$

where j=0 for two-dimensional flow and j=1 for axisymmetric flow.p_s is the local pressure acting at any point on the stagnation streamline and

p_b is the pressure acting at any point on the inlet surface. The first integral in (A-6) is defined as the Additive drag D_{ADD} and is evaluated by applying the momentum theorem to control volume P-S-C-F-R.

The net change of momentum in this control volume is given by

$$\int_F^C (\rho_i U_i) U_i (2\pi y)^j dy - \int_R^P (\rho_\infty U_\infty) U_\infty (2\pi y)^j dy \quad \text{in the x direction.}$$

This change in momentum is equal to the forces acting on the boundaries of the control volume resolved in the x direction.

$$\int_R^P (p_\infty - p_\infty)(2\pi y)^j dy + \int_P^S (p_s - p_\infty)(2\pi y)^j dy - \int_C^S (p_b - p_\infty)(2\pi y)^j dy - \int_F^C (p_i - p_\infty)(2\pi y)^j dy$$

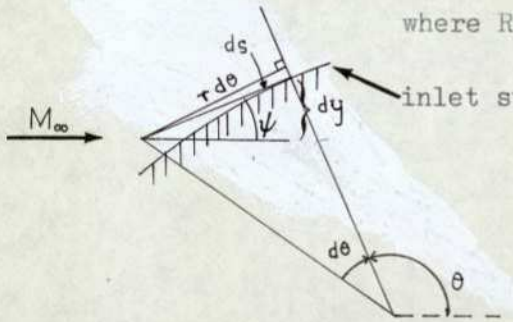
Hence D_{ADD} is given by,

$$\int_P^S (p_s - p_\infty)(2\pi y)^j dy = \int_C^S (p_b - p_\infty)(2\pi y)^j dy + \int_F^C (p_i - p_\infty)(2\pi y)^j dy - \int_{R_2}^P (\rho_\infty U_\infty^2)(2\pi y)^j dy + \int_F^C (\rho_i U_i^2)(2\pi y)^j dy \qquad -(A\text{-}7)$$

Dividing (A-7) by $\frac{1}{2}\gamma p_\infty M_\infty^2 A_H$ the additive drag coefficient is obtained. (A_H is the reference area based on the highlight length H which is set equal to unity; $A_H = \pi H^2 = \pi$ when j=1 and $A_H = 1$ when j=0)

$$C_{DADD} = \int_C^S C_{pb}(2y)^j dy + \int_F^C C_{pi}(2y)^j dy - 2(MFR)(MFR)^j + (2/\gamma M_\infty^2)\int_F^C e^R v_i^2 (2y)^j dy \qquad -(A\text{-}8)$$

where $R = \log_e\left(\frac{p_i}{p_\infty}\right)$



$ds = rd\theta / \sin(\theta - \psi)$

$|dy| = |ds \sin\psi|$

$+dy = -r\sin\psi d\theta / \sin(\theta - \psi)$

where ψ is the angle the local surface element makes with the freestream direction

$$C_{DADD} = \int_{\theta_S}^{\theta_C} C_{pb} \frac{(2y)^j r \sin\psi d\theta}{\sin(\theta - \psi)} + \int_F^C C_{pi}(2y)^j dy - 2MFR(MFR)^j + (2/\gamma M^2)\int_F^C e^R v_i^2 (2y)^j dy \qquad -(A\text{-}9)$$

$$C_{DEXT} = \int_S^A C_{pb}(2y)^j dy + C_{DADD} \qquad -(A\text{-}10)$$

$$\text{or } C_{DEXT} = \int_{\theta_A}^{\theta_S} C_{pb} \frac{(2y)^j r \sin\psi d\theta}{\sin(\theta - \psi)} + C_{DADD} \qquad -(A\text{-}11)$$

The cowl drag coeffient is defined as $C_{DCOWL} = \int_{\theta_A}^{\theta_C} C_{pb} \frac{(2y)^j r \sin\psi d\theta}{\sin(\theta - \psi)}$ $\qquad -(A\text{-}12)$

Most British technical literature concerned with the aerodynamics of air-intakes use the term Pre-Entry Drag Coeffient λ^{ci} which is defined in Ref(119) for sharp lipped intakes and by Gibbings Ref(104) for blunt lipped intakes

as follows :-

$$C_{DPRE} = \int_P^S C_{ps}(2y)^j dy + \int_S^C C_{pb}(2y)^j dy \qquad -(A\text{-}13)$$

$$C'_{DCOWL} = \int_S^A C_{pb}(2y)^j dy - \int_S^C C_{pb}(2y)^j dy \qquad -(A\text{-}14)$$

$$C_{DEXT} = C_{DPRE} + C_{DCOWL} = \int_P^S C_{ps}(2y)^j dy + \int_S^A C_{pb}(2y)^j dy \qquad -(A\text{-}15)$$

Although C_{DPRE} differs from C_{DADD} which is used more extensively in North American technical literature, comparing equation (A-6) and (A-15), there is no difference regarding the definition of External Drag.

APPENDIX B

Some Mathematical Aspects of the Numerical Solution of Hyperbolic Equations

The unsteady equations of motion (which are hyperbolic throughout the region of interest), pose an initial value problem. The mathematical nature of the phenomenon represented by the equations of motion is such that starting from an arbitrary set of initial conditions at time t_o, a solution is expected to exist at some time $t_o + \Delta t$ for the given fixed boundary conditions. Friedrichs Ref (107) pointed out that the problems facing numerical analysts are the determination of the existence, uniqueness and stability of the solution. If the equations of motion correctly describe the physical situation and also avoid or treat discontinuities (should they develope within the region of interest), then solutions are expected to exist if they are observed experimentally for the same boundary conditions. The uniqueness of the solution can be checked by varying the arbitary initial conditions and comparing the final results for the same boundary conditions. However if two or more solutions are possible for the same fixed boundary conditions (for example M_∞ and body shape), as is the case for the SUPIB problem described in chapter 1 with reference to Figs(6)(c) and (d), then the numerical solution may be dependent on initial conditions but would still converge to one of the possible solutions. D'Souza Ref (97) developed two computer programs, one for case (c) the continuous curved shock and case(d) for Mach interaction at the Axis. He was able to demonstrate that both solutions could be obtained for the same freestream conditions and body shape.

Convergence occurs when the solution of the difference equations approaches the exact solution of the differential equations as the mesh sizes ΔZ and ΔY are reduced.

Instability is defined by Friedrichs Ref (107) as the situation that occurs when the numerical solution is not continuously dependent on the initial data. In practice, instability manifests itself in the form of large unbounded oscillations which grow in amplitude with each time step.

These oscillations usually occurred at the boundaries where the dependent variables were found to be orders of magnitude larger than expected. The computation was terminated either by an overflow condition on the digital computer or stopped by an error check incorporated into the computer program.

Truncated Error

The accuracy of the difference scheme is determined by the truncation error which can the evaluated for the Moretti scheme using a linear one-dimensional equation of the form:

$$\frac{\partial q}{\partial T} = -\frac{\partial q}{\partial Z} \qquad \text{- (B-1)}$$

As shown in chapter 2 section (2.1.3.1), the Moretti difference scheme gives

$$q_i^{k+1} = q_i^k - \frac{(q_{i+1}^k - q_{i-1}^k)}{2\,\Delta Z}(\Delta T) + \frac{(q_{i+1}^k + q_{i-1}^k - 2q_i^k)}{2(\Delta Z)^2}(\Delta T)^2 \qquad \text{- (B-2)}$$

Using a Taylor series expansion, q_i^{k+1} and $q_{i\pm1}^k$ can be replaced by

$$q_i^{k+1} = q_i^k + \left(\frac{\partial q}{\partial T}\right)_i^k \Delta T + \frac{1}{2}\left(\frac{\partial^2 q}{\partial T^2}\right)_i^k \Delta T^2 + \frac{1}{6}\left(\frac{\partial^3 q}{\partial T^3}\right)_i^k \Delta T^3 + - - - -$$

and

$$q_{i\pm1}^k = q_i^k \pm \left(\frac{\partial q}{\partial Z}\right)_i^k \Delta Z + \frac{1}{2}\left(\frac{\partial^2 q}{\partial Z^2}\right)_i^k \Delta Z^2 \pm \frac{1}{6}\left(\frac{\partial^3 q}{\partial Z^3}\right)_i^k \Delta Z^3 + - - -$$

The equivalent differential equation actually solved by the Moretti difference scheme can then be expressed as,

$$\frac{\partial q}{\partial T} = -\frac{\partial q}{\partial Z} - \frac{1}{6}\left\{\frac{\partial^3 q}{\partial T^3}\Delta T^2 + \frac{\partial^3 q}{\partial Z^3}\Delta Z^2\right\} + \text{higher order terms} \qquad \text{- (B-3)}$$

Comparing (B-1) with (B-3) the leading term of the truncation error is $-\frac{1}{6}\left\{\frac{\partial^3 q}{\partial T^3}\Delta T^2 + \frac{\partial^3 q}{\partial Z^3}\Delta Z^2\right\}$ and hence since (B-3) is a first order equation, the Moretti scheme is second order accurate. The equivalent differential equation approaches the exact differential equation as ΔZ and ΔT tend to zero.

Artificial Viscosity

For continuum flow problems at high Reynolds numbers, shock wave thicknesses are of the order of a few molecular mean free paths, (see for example, Ferri Ref (21), page 61). Under these conditions it is justifiable to treat the shock wave as a sharp mathematical discontinuity (as in the

case for the bow shock in the present problem) across which the Rankine-Hugoniot relations hold. In practice, these sharp discontinuities do not occur in nature because of the dissipative mechanism of viscosity and heat transfer which caters for a heat loss over a finite but small region across which the flow variables change smoothly from upstream to downstream conditions. The entropy rise has been shown by Liepmann and Roshko Ref(108) to be given by,

$$S_2 - S_1 = \int_1^2 \frac{\bar{\mu}}{T}\left(\frac{du}{dx}\right)^2 dx + \int_1^2 \frac{K}{T^2}\left(\frac{dT}{dx}\right)^2 dx \qquad \text{- (B-4)}$$

where $\bar{\mu}$ is the compressive coefficient of viscosity; K is the coefficient of heat conduction and T is the temperature. 1 and 2 denote the upstream and downstream conditions in the direction x for the shock wave.

Liepmann and Roshko show by a simplified analysis that the shock thickness is proportional to $\bar{\mu}$. Most difference schemes introduce implicity the effect of viscosity through their truncation errors (see Roache Ref (50)) as indicated above for the Moretti scheme, equation (B-3). The effect of these viscous-like terms which are analogous to the temperature and velocity gradients in (B-4) and also similar to the viscous terms in the Navier-Stokes equations, is to smear the shock waves through several grid points. When this occurs the numerical scheme is said to possess artificial viscosity.

When artificial viscosity is used as a device for calculating flows with shock waves, the conservative form of the equations of motion (chapter 2, equations (8)(a) to (d)) must be used. This insures that the Rankine-Hugoniot conditions are satisfied in the region of the smeared shock. Bohachevsky and Mates Ref (67) used an artificial viscosity technique for the bow wave in their solution of the supersonic blunt body problem. The bow wave was smeared through at least 10 mesh widths. This shock geometry is unrealistic. Moreover the approach assumes the existence of continuum flow yet produces results akin to those observed for non-continuum low density hypersonic flows, where the molecular mean free path approaches a characteristic length scale; for example the inlet lip radius in this problem.

However, by using a reasonably fine mesh and thus confining the embedded shocks to small regions in the physical plane, Barnwell Ref (77) and Serra Ref (88) achieved good agreement with experimental results for continuum flow problems.

The von Neumann Stability Condition

If n is the number of space variables in the initial time plane t_o, simplicial schemes are defined as those which do not use more than n + 1 points in the initial time plane to calculate new values in the $t_o + \Delta t$ plane. Hahn Ref (109) showed that for a simplicial scheme the CFL condition is sufficient as well as necessary for convergence. Although the schemes for the interior and boundary points for the present problem are non-simplicial it was found in practice that the size of the time step governed by the CFL condition (Equation (37) chapter 3) was small enough to insure stability. However during the preliminary development of the boundary point schemes, certain instabilities were observed at the stagnation point which were thought to be related to the von Neumann stability condition. The von Neumann condition was described by O'Brien Ref (110) and can be demonstrated on the equations for unsteady one-dimensional isentropic flow.

$$\frac{\partial R}{\partial t} + U\frac{\partial R}{\partial x} + \frac{\partial U}{\partial x} = 0 \qquad \text{(a)} \quad - \tag{B-5}$$

$$\frac{\partial U}{\partial t} + a^2\frac{\partial R}{\partial x} + U\frac{\partial U}{\partial x} = 0 \qquad \text{(b)} \quad -$$

which can be expressed in matrix form as

$$\begin{bmatrix} \frac{\partial R}{\partial t} \\ \frac{\partial U}{\partial x} \end{bmatrix} + \underbrace{\begin{bmatrix} U & 1 \\ a^2 & U \end{bmatrix}}_{A} \begin{bmatrix} \frac{\partial R}{\partial x} \\ \frac{\partial U}{\partial x} \end{bmatrix} = 0 \qquad - \text{(B-6)}$$

or

$$\frac{\partial w}{\partial t} + A\frac{\partial w}{\partial x} = 0 \qquad - \text{(B-7)}$$

where w is a column vector with components R and U. A is the Matrix which represents the coefficients of the spatial deriviatives. The von Neumann analysis applies only to linear equations. The above equations can be conveniently linearised by considering A to be a Matrix of constant coefficients. Applying the Moretti scheme (equation (B-2)) to equation (B-7) gives,

$$\omega_j^{k+1} = \omega_j^k - \frac{A}{2}\left(\omega_{j+1}^k - \omega_{j-1}^k\right)\left(\frac{\Delta t}{\Delta x}\right) + \left(\omega_{j+1}^k + \omega_{j-1}^k - 2\omega_j^k\right)\left(\frac{A\Delta T}{\Delta x}\right)^2 \frac{1}{2} \quad -(B\text{-}8)$$

Since equation (B-8) represents the approximate solution of a linear equation, the errors generated by it can be represented by a Fourier series of the form,

$$W_j^k = \sum_{t=0}^{t_o} \sum_{j=1}^{N} W_o e^{i\left(\frac{j2\pi\,\Delta x}{\ell}\right)} e^{\alpha t} \quad -(B\text{-}9)$$

where N is the total number of nodes, $i = \sqrt{-1}$, ℓ is the wave length of the error and α is a complex constant. Since only linear equations are involved, the separate solutions will be additive so in order to determine whether the errors amplify from time step k to k + 1, it is sufficient to consider one node point, jo.

$$W_{j_o}^k = W_o\, e^{\alpha t}\, e^{j_o(\beta)i} \quad -(B\text{-}10)$$

where $\beta = \frac{2\pi\,\Delta x}{\ell}$. By replacing w_j^k by the W_{jo}^k the following is obtained:-

$$W_{j_o}^{k+1} = W_{j_o}^k - \frac{A W_o e^{\alpha t}}{2}\left(e^{(j_o+1)\beta i} - e^{(j_o-1)\beta i}\right)\left(\frac{\Delta t}{\Delta x}\right) + \frac{W_o e^{\alpha t} A^2}{2}\left(e^{(j_o+1)\beta i} + e^{(j_o-1)\beta i} - 2e^{j_o\beta i}\right)\left(\frac{\Delta T}{\Delta x}\right)^2$$

$$W_{j_o}^{k+1} = G\, W_{j_o}^k \quad -(B\text{-}11)$$

where $G = I - \frac{A\Delta t\, i}{\Delta x}\sin\beta + (\cos\beta - 1)\left(\frac{A\Delta t}{\Delta x}\right)^2$

I is an identity matrix and G is defined as the Amplification matrix. The eigen values of G can be represented by

$$h = 1 - \frac{\lambda\Delta t}{\Delta x} i \sin\beta + (\cos\beta - 1)\left(\frac{\lambda\Delta t}{\Delta x}\right)^2 \quad -(B\text{-}12)$$

where $\lambda = U \pm a$ are the eigen values of matrix A of equation (B-6).

The von Neumann condition states that the scheme is stable if the eigen values of Amplification matrix G are less than unity in absolute value. As β varies from 0 to 2π, h traces out an ellipse in the complex plane. This ellipse lies inside the unit circle if

$$\frac{|\lambda|\,\Delta t}{\Delta x} < 1$$

or

$$\Delta t < \frac{\Delta x}{(|U| + a)} \quad -(B\text{-}13)$$

This condition is identical (in this one dimensional case) to the CFL condition. It is also interesting to note that Richtmyer and Morton Ref(111)

arrived at the same result for the two step Lax-Wendroff scheme (similar to that described in section (2.1.3.2) of chapter 2) applied to equation (B-7).

Interpolation Procedure for the MOC at the Boundary Points

In chapter 3 section (3.2) which dealt with the treatment of Boundary Points, the MOC for evaluating the boundary points was shown.

For the inlet surface points, this scheme involved the integration of a compatibility equation along a characteristic curve which originated in the $T_o + \Delta T$ plane and intersected the initial time plane T_o. The compatibility equation is given by

$$\frac{dP}{dT} + \frac{a}{\gamma}\frac{dU}{dT} = -\left(\gamma\frac{\partial V}{\partial \eta} + V\frac{\partial P}{\partial \eta} + \frac{V\gamma}{a}\frac{\partial U}{\partial \eta} + j\frac{\gamma V_c}{y}\right) = (RHS)_{T_o}$$

If the right hand side is independent of T, integrating the above with respect to T gives

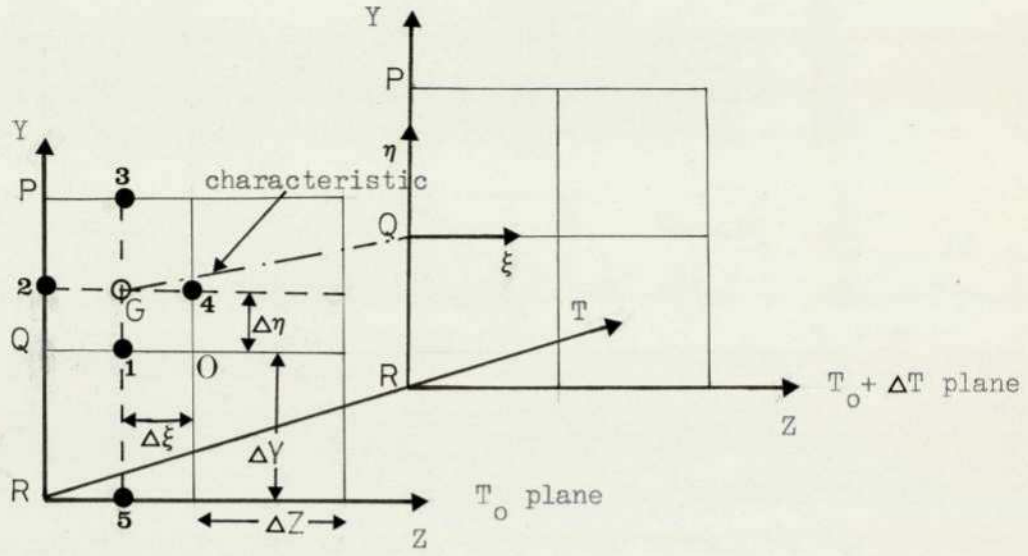
$$P(T_o + \Delta T) = \frac{a(T_o)}{\gamma} U(T_o) + (RHS)_{T_o}\Delta T \qquad \text{- (B-14)}$$

$U(T_o + \Delta T) = 0$ on the surface of the body as it is the normal component of velocity. The problem then reduces to evaluating the quantities with suffix (T_o) in the initial time plane by an interpolation procedure.

Fig (A) shows the initial time plane T_o and the new time plane $T_o + \Delta T$. PQR is a segment of the inlet surface with the origin of the ξ, η co-ordinates in the $T_o + \Delta T$ plane. To simplify the presentation without any loss of generality, it is assumed that the computational co-ordinate directions (Z, Y) are parallel to the (ξ, η) system. Hence $\frac{\partial g}{\partial \eta} = \frac{\partial g}{\partial Y}$ where g represents U, V or P. The U + a characterisitic intersects the T_o plane at point G. Initially a second order Taylor series expansion was used to calculate the required variables on the right hand side of equation (B-14). The deriv atives with suffix 0 in (B-15), Fig (A), were evaluated using central differences about point 0 which involved nine node points including point 0.

Using the second order Taylor series method, an attempt was made to compute the flow about a toroid at $M_\infty = 8.33$ (a SUPIB problem) so as to

COMPARISON OF INTERPOLATION PROCEDURES FOR THE EVALUATION OF BOUNDARY POINTS USING THE METHOD OF CHARACTERISTICS



Second Order Taylor Series Method

$$g_G = g_0 + \left(\frac{\partial g}{\partial \eta}\right)_0 \Delta\eta + \left(\frac{\partial g}{\partial \xi}\right)_0 \Delta\xi + \frac{1}{2}\left\{\left(\frac{\partial^2 g}{\partial \eta^2}\right)_0 (\Delta\eta)^2 + \left(\frac{\partial^2 g}{\partial \xi^2}\right)_0 (\Delta\xi)^2\right\} + \left(\frac{\partial^2 g}{\partial \xi \partial \eta}\right)_0 \Delta\xi\Delta\eta \quad \text{(a)}$$

$$\left(\frac{\partial g}{\partial \eta}\right)_G = \left(\frac{\partial g}{\partial \eta}\right)_0 + \left(\frac{\partial^2 g}{\partial \eta^2}\right)_0 \Delta\eta + \left(\frac{\partial^2 g}{\partial \eta \partial \xi}\right)_0 \Delta\xi \quad \text{(b)} \qquad \text{(B-15)}$$

where g represents U,V or P and suffixes G and O refer to points G and O respectively.

Linear Interpolation

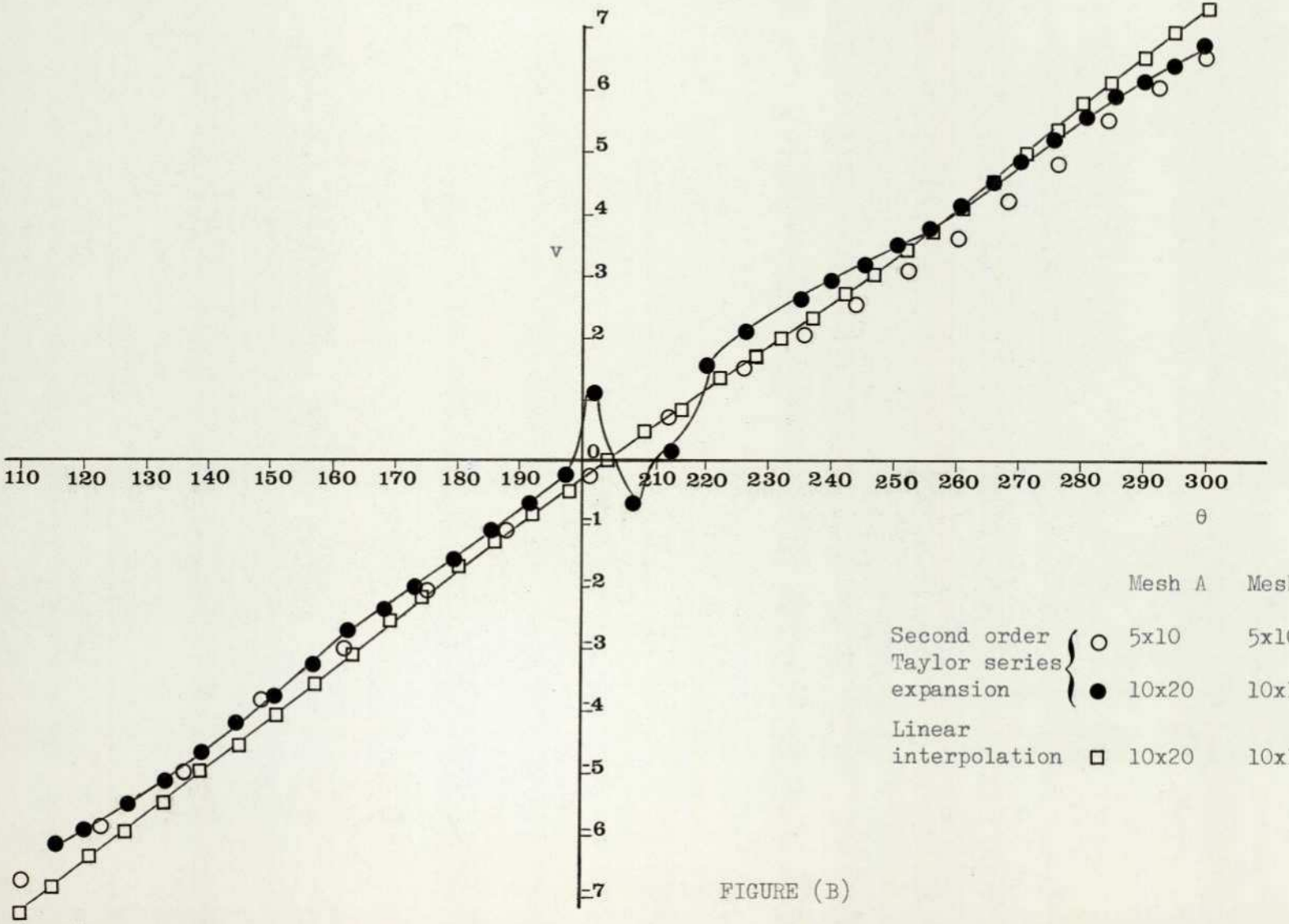
$$g_G = g_4 + \frac{(g_2 - g_4)}{\Delta Z}(\Delta\xi) \quad \text{(a)}$$

$$\left(\frac{\partial g}{\partial \eta}\right)_G = \frac{g_3 - g_5}{2\Delta Y} + \frac{(g_3 + g_5 - 2g_1)}{\Delta Y^2}(\Delta\eta) \quad \text{(b)} \qquad \text{(B-16)}$$

FIGURE (A)

COMPARISON OF RESULTS USING DIFFERENT INTERPOLATION PROCEDURES

(Velocity (v) distribution on the inlet surface, M_∞=8.33, axisymmetric flow about a toroid with R_H=0.5)



		Mesh A	Mesh B	k
Second order Taylor series expansion	○	5x10	5x10	900
	●	10x20	10x15	300
Linear interpolation	□	10x20	10x15	800

FIGURE (B)

enable a comparison to be made with existing results. Fig (B) shows a plot of non-dimensionalized velocity v on the toroid surface against θ. Converged results were obtained for a coarse mesh. However when the computation was repeated with a fine mesh, the second order interpolation results were unstable in the region of the stagnation point. Results for $k = 300$ show the instability developing in the vicinity of the stagnation point. The time step size was governed by the CFL condition (equation (37) chapter 3), which was not violated by this interpolation scheme. Reducing the size of ΔT only served to delay the incidence of instability. Hence it was concluded that this instability resulted due to a violation of the Von Neumann condition. A von Neumann analysis (such as demonstrated by Ransom Ref (35))was not attempted for this problem, instead a stable scheme was developed using a heuristic approach. This scheme involved the use of linear interpolation and is given by equations (B-16) (a) and (b) Fig (A). At points 1 to 5, quantities g_i ($i = 1, 2 \ldots 5$) were calculated from adjacent node points using linear interpolation. A method equivalent to Lagrange interpolation was used to evaluate the derivatives $\left(\frac{\partial q}{\partial \eta}\right)_G$ using points 1, 3 and 5.

When equations (B-16)(a) and (b) were used to evaluate the right hand side of equation (B-14), a stable scheme resulted for both coarse and fine mesh sizes. The fine mesh results are presented in Fig (B). The corresponding pressure distribution is given in Fig (26) and shows good agreement with experiment.

Heie and Leigh Ref (35), conducted numerical experiments on the solution of linear hyperbolic equations for three independent variables, using the MOC. Their findings support the author's own experience in this field. They showed that non-simplicial networks which satisfy the CFL condition, should be further analysed using the von Neumann condition. The serious limitation of the von Neumann condition is the need to linearize the equations before the analysis is performed. However the literature has several examples of successful application of the von Neumann condition

(Barnwell Ref(77) and Ransom Ref (34)) where the instabilities in the full non-linear problem were avoided by studying the amplification of errors for the linearized case.

APPENDIX C

Derivation of the Characteristic and Compatibility Equations for Two and Three Independent Variables

When the partial differential equations governing gas-dynamic problems are hyperbolic, disturbances propagate along Characteristic Lines or Characteristic Surfaces for two and three independent variable problems respectively. Fig (8a) shows the characteristic lines PS and RS for one dimensional unsteady flow. PR is an initial line with PS and RS being two prefered directions along which the disturbances propagate. An analogous situation arises with three independent variables. In Fig (9a) disturbances propagate along Characteristic Surfaces P-C-D-R which envelope the Characteristic Conoids passing through the points P and R. The locus of points of tangency between the conoids and the characteristic surfaces are known as Bi-characteristics. The geometry of the characteristic Cones is determined by the local properties at any point such as Q and is illustrated in greater detail in Fig (8b). The generators of these cones are tangential to the characteristic conoid at Q Fig (9b). The Particle Path is just one of an infinite number which make up the stream surface, P-R-O-O'. Similarly there are an infinite number of characteristic surfaces which can be drawn through points P or R and consequently there are an infinite number of bi-characteristic curves.

Algebraic expressions can be derived which describe the geometry of the characteristic lines and surfaces and the corresponding differential equations which hold along them called compatibility equations.

We now proceed to derive expressions for the characteristic equations and compatibility equations. The approach followed here is given in Sauerwein Ref (31) and Richardson Ref (40).

The gas dynamic equations for compressible, inviscid and adiabatic flow comprise a set of quasi-linear (i.e. the derivatives occurringare of first degree) first order partial differential equations of the form,

$$A_{ijk} \frac{\partial u_k}{\partial x_i} + B_j = 0 \qquad \text{- (C-1)}$$

using cartesian tensor notation where A_{ijk} and B_j are functions of u_k the dependent variables and x_i are the independent variables.

The above equations are transformed to a new set of co-ordinates α_m to give

$$A_{ijk} \frac{\partial u_k}{\partial \alpha_m} \frac{\partial \alpha_m}{\partial x_i} + B_j = 0 \qquad \text{- (C-2)}$$

Consider a surface α_1 = constant on which u_k and all $\frac{\partial u_k}{\partial \alpha_m}$ are given except $\frac{\partial u_k}{\partial \alpha_1}$. $\frac{\partial u_k}{\partial \alpha_1}$ can be determined from (C-2) if and only if

$$\left| A_{ijk} \frac{\partial \alpha_1}{\partial x_i} \right| \neq 0 \qquad \text{- (C-3)}$$

On surfaces which this is not true are by definition characteristic surfaces (i.e. surfaces across which derivatives of the dependent variables are discontinuous)

This condition is expressed as

$$\left| A_{ijk} \frac{\partial \alpha_1}{\partial x_i} \right| = 0 \qquad \text{- (C-4)}$$

Characteristic Equations and Compatibility Equations for one dimensional unsteady Flow

Consider the equations of motion in axisymmetric cylindrical co-ordinates.

Continuity Equation

$$\frac{\partial R}{\partial t} + U\frac{\partial R}{\partial x} + V\frac{\partial R}{\partial y} + \frac{\partial U}{\partial x} + \frac{\partial V}{\partial y} + j\frac{V}{y} = 0 \qquad \text{- (C-5)}$$

Momentum Equations

$$\frac{\partial U}{\partial t} + U\frac{\partial U}{\partial x} + V\frac{\partial U}{\partial y} + \frac{a^2}{\gamma}\frac{\partial P}{\partial x} = 0 \qquad \text{- (C-6)}$$

$$\frac{\partial V}{\partial t} + U\frac{\partial V}{\partial x} + V\frac{\partial V}{\partial y} + \frac{a^2}{\gamma}\frac{\partial P}{\partial y} = 0 \qquad \text{- (C-7)}$$

Conservation of Entropy along a Particle Path

$$\frac{\partial S}{\partial t} + U\frac{\partial S}{\partial x} + V\frac{\partial S}{\partial y} = 0 \qquad \text{(a)} \qquad \text{- (C-8)}$$

$$S = P - \gamma R \qquad \text{(b)}$$

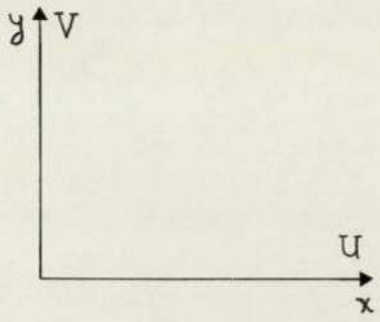
Combining (C-8) (a) & (b) gives,

$$\frac{\partial P}{\partial t} + U\frac{\partial P}{\partial x} + V\frac{\partial P}{\partial y} = \gamma\left[\frac{\partial R}{\partial t} + U\frac{\partial R}{\partial x} + V\frac{\partial R}{\partial y}\right]$$

hence the continuity equation becomes

$$\frac{\partial P}{\partial t} + U\frac{\partial P}{\partial x} + V\frac{\partial P}{\partial y} + \gamma\left(\frac{\partial U}{\partial x} + \frac{\partial V}{\partial y} + j\frac{V}{y}\right) = 0 \qquad \text{- (C-9)}$$

Thus having eliminated the density function R, (C-9), (C-6) and (C-7) derivatives of the comprise a set of partial differential equations with three dependent variables P, U and V and three independent variables x, y and t.



Using Moretti's approximation Ref (105) assume that the cross derivatives, that is deriviatives with respect to y are independent of time t hence the above equations are one-dimensionalized as follows:-

$$\left.\begin{aligned}
&\frac{\partial P}{\partial t} + U\frac{\partial P}{\partial x} + \gamma\frac{\partial U}{\partial x} = -\left(\gamma\frac{\partial V}{\partial y} + j\frac{\gamma V}{y} + V\frac{\partial P}{\partial y}\right) = b_1\\
&\frac{\partial U}{\partial t} + U\frac{\partial U}{\partial x} + \frac{a^2}{\gamma}\frac{\partial P}{\partial x} = -\left(V\frac{\partial U}{\partial y}\right) = b_2\\
&\frac{\partial V}{\partial t} + U\frac{\partial V}{\partial x} = -\left(V\frac{\partial V}{\partial y} + \frac{a^2}{\gamma}\frac{\partial P}{\partial y}\right) = b_3
\end{aligned}\right\} \quad - (C\text{-}10)$$

Consider a transformation to the following co-ordinate system $\alpha = \alpha(x,t)$

$$\frac{\partial P}{\partial \alpha}\frac{\partial \alpha}{\partial t} + U\frac{\partial P}{\partial \alpha}\frac{\partial \alpha}{\partial x} + \gamma\frac{\partial U}{\partial \alpha}\frac{\partial \alpha}{\partial x} = b_1 \quad - (C\text{-}11)$$

$$\frac{\partial U}{\partial \alpha}\frac{\partial \alpha}{\partial t} + U\frac{\partial U}{\partial \alpha}\frac{\partial \alpha}{\partial x} + \frac{a^2}{\gamma}\frac{\partial P}{\partial \alpha}\frac{\partial \alpha}{\partial x} = b_2 \quad - (C\text{-}12)$$

$$\frac{\partial V}{\partial \alpha}\frac{\partial \alpha}{\partial t} + U\frac{\partial V}{\partial \alpha}\frac{\partial \alpha}{\partial x} = b_3 \quad - (C\text{-}13)$$

$$\begin{bmatrix}
\left(\frac{\partial \alpha}{\partial t} + U\frac{\partial \alpha}{\partial x}\right) & \gamma\left(\frac{\partial \alpha}{\partial x}\right) & - \\
\frac{a^2}{\gamma}\left(\frac{\partial \alpha}{\partial x}\right) & \left(\frac{\partial \alpha}{\partial t} + U\frac{\partial \alpha}{\partial x}\right) & - \\
- & - & \left(\frac{\partial \alpha}{\partial t} + U\frac{\partial \alpha}{\partial x}\right)
\end{bmatrix}
\begin{bmatrix}
\frac{\partial P}{\partial \alpha} \\ \frac{\partial U}{\partial \alpha} \\ \frac{\partial V}{\partial \alpha}
\end{bmatrix} =
\begin{bmatrix}
b_1 \\ b_2 \\ b_3
\end{bmatrix}$$

hence from equation (C-4) the characteristic equation is given by

$$\begin{vmatrix}
\frac{\partial \alpha_1}{\partial t} + U\frac{\partial \alpha_1}{\partial x} & \gamma\frac{\partial \alpha_1}{\partial x} & - \\
\frac{a^2}{\gamma}\frac{\partial \alpha_1}{\partial x} & \frac{\partial \alpha_1}{\partial t} + U\frac{\partial \alpha_1}{\partial x} & - \\
- & - & \frac{\partial \alpha_1}{\partial t} + U\frac{\partial \alpha_1}{\partial x}
\end{vmatrix} = 0$$

$$\left(\frac{\partial \alpha_1}{\partial t} + U\frac{\partial \alpha_1}{\partial x}\right)\left[\left(\frac{\partial \alpha_1}{\partial t} + U\frac{\partial \alpha_1}{\partial x}\right)^2 - a^2\left(\frac{\partial \alpha_1}{\partial x}\right)^2\right] = 0$$

The characteristic curves are given by

$$\left(\frac{\partial \alpha_1}{\partial t} + U\frac{\partial \alpha_1}{\partial x}\right) = 0 \qquad \text{- (C-14a)}$$

$$\left[\left(\frac{\partial \alpha_1}{\partial t} + U\frac{\partial \alpha_1}{\partial x}\right)^2 - a^2\left(\frac{\partial \alpha_1}{\partial x}\right)^2\right] = 0 \qquad \text{- (C-14b)}$$

If $\alpha_1 = \alpha_1 (x, t)$

$$\frac{\partial \alpha_1}{\partial t} dt + \frac{\partial \alpha_1}{\partial x} dx = d\alpha_1 = 0$$

$$\therefore \frac{dx}{dt} = -\left(\frac{\partial \alpha_1}{\partial t}\right)\Big/\left(\frac{\partial \alpha_1}{\partial x}\right) \qquad \text{- (C-15c)}$$

from (C-14a) and (C-14b) respectively,

$$\frac{dx}{dt} = U \qquad \text{- (C-15)}$$

and $$\frac{dx}{dt} = U \pm a \qquad \text{- (C-16)}$$

(C-15) is interpreted as the particle path while (C-16) represents the two wave fronts, Fig (8a). The variation of any dependent variable g along the characteristic lines in the x - t plane is given by

$$\frac{dg}{d\tau} = \frac{\partial g}{\partial t}\frac{dt}{d\tau} + \frac{\partial g}{\partial x}\frac{dx}{d\tau}$$

if $T = t$

$$\frac{dg}{d\tau} = \frac{\partial g}{\partial t} + \frac{\partial g}{\partial x}\frac{dx}{dt}$$

hence $$\frac{dU}{d\tau} = \frac{\partial U}{\partial t} + \frac{\partial U}{\partial x}\frac{dx}{dt}$$

and $$\frac{dP}{d\tau} = \frac{\partial P}{\partial t} + \frac{\partial P}{\partial x}\frac{dx}{dt}$$

hence from (C-10) for the characteristic corresponding to $\frac{dx}{dt} = U + a$ the first two equations are rewritten as

$$\frac{\partial u}{\partial t} + (U+a)\frac{\partial u}{\partial x} + \frac{a^2}{\gamma}\frac{\partial P}{\partial x} - a\frac{\partial U}{\partial x} = b_2$$

hence $$\frac{dU}{d\tau} + \frac{a^2}{\gamma}\frac{\partial P}{\partial x} - a\frac{\partial u}{\partial x} = b_2 \qquad \text{- (C-16a)}$$

$$\frac{\partial P}{\partial t} + (U+a)\frac{\partial P}{\partial x} - \gamma\frac{\partial U}{\partial x} - a\frac{\partial P}{\partial x} = b_1$$

hence $$\frac{dP}{d\tau} + \gamma\frac{\partial u}{\partial x} - a\frac{\partial P}{\partial x} = b_1 \qquad \text{- (C-16b)}$$

to eliminate the x derivatives in (C-16a) and (C-16b) multiply (C-16a) by $\frac{\gamma}{a}$ and add the resulting equation to (C-16b)

$$\frac{dP}{d\tau} + \frac{\gamma}{a}\frac{dU}{d\tau} = -\left(\frac{V\gamma}{a}\frac{\partial U}{\partial y} + \gamma\frac{\partial V}{\partial y} + V\frac{\partial P}{\partial y} + j\frac{\gamma V}{y}\right) \qquad \text{- (C-17)}$$

similarly for the U - a characteristic

$$\frac{dP}{d\tau} - \frac{\gamma}{a}\frac{dU}{d\tau} = -\left(-\frac{V\gamma}{a}\frac{\partial U}{\partial y} + \gamma\frac{\partial V}{\partial y} + V\frac{\partial P}{\partial y} + j\frac{\gamma V}{y}\right) \qquad \text{- (C-18)}$$

Similarly if g = S, from equation (C-8)

$$\frac{dS}{d\tau} = \frac{\partial S}{\partial t} + U\frac{\partial S}{\partial x} = -V\frac{\partial S}{\partial y} \qquad \text{- (C-19)}$$

which holds along particle path $\frac{dx}{dt} = U$.

Derivation of Characteristic Equations and compatibility equations for three independent variables

The derivations of the relevant expressions follow a similar pattern as outlined above for the two independent variable cases. Again the equations of motion (C-5) to (C-9) are transformed to a co-ordinate system of the type $\alpha = \alpha(x, y, t)$ and (C-6), (C-7) and (C-9) can be expressed as follows:-

$$\frac{\partial U}{\partial \alpha}\left\{\frac{\partial \alpha}{\partial t} + U\frac{\partial \alpha}{\partial x} + V\frac{\partial \alpha}{\partial y}\right\} + \frac{\partial P}{\partial \alpha}\frac{a^2}{\gamma}\frac{\partial \alpha}{\partial y} = 0$$

$$\frac{\partial V}{\partial \alpha}\left\{\frac{\partial \alpha}{\partial t} + U\frac{\partial \alpha}{\partial x} + V\frac{\partial \alpha}{\partial y}\right\} + \frac{\partial P}{\partial \alpha}\left\{\frac{a^2}{\gamma}\frac{\partial \alpha}{\partial y}\right\} = 0$$

$$\frac{\partial U}{\partial \alpha}\left\{\gamma\frac{\partial \alpha}{\partial x}\right\} + \frac{\partial V}{\partial \alpha}\left\{\gamma\frac{\partial \alpha}{\partial y}\right\} + \frac{\partial P}{\partial \alpha}\left\{\frac{\partial \alpha}{\partial t} + U\frac{\partial \alpha}{\partial x} + V\frac{\partial \alpha}{\partial y}\right\} = -\gamma V_y$$

or in matrix form as,

$$\begin{bmatrix} \left(\frac{\partial \alpha}{\partial t} + U\frac{\partial \alpha}{\partial x} + V\frac{\partial \alpha}{\partial y}\right) & 0 & \frac{a^2}{\gamma}\frac{\partial \alpha}{\partial x} \\ 0 & \left(\frac{\partial \alpha}{\partial t} + U\frac{\partial \alpha}{\partial x} + V\frac{\partial \alpha}{\partial y}\right) & \frac{a^2}{\gamma}\frac{\partial \alpha}{\partial y} \\ \gamma\frac{\partial \alpha}{\partial x} & \gamma\frac{\partial \alpha}{\partial y} & \left(\frac{\partial \alpha}{\partial t} + U\frac{\partial \alpha}{\partial x} + V\frac{\partial \alpha}{\partial y}\right) \end{bmatrix} \begin{bmatrix} \frac{\partial U}{\partial \alpha} \\ \frac{\partial V}{\partial \alpha} \\ \frac{\partial P}{\partial \alpha} \end{bmatrix} = \begin{bmatrix} 0 \\ 0 \\ -\gamma V_y j \end{bmatrix} \qquad \text{- (C-20)}$$

If a characteristic surface α_1 exists such that $\frac{\partial U}{\partial \alpha_1}$, $\frac{\partial V}{\partial \alpha_1}$, $\frac{\partial P}{\partial \alpha_1}$ are indeterminate on α_1 this implies that the determinant of the coefficient matrix of (C-20) is zero for $\alpha_1 = \alpha_1(x, y, t)$

i.e.

$$\left(\frac{D\alpha_1}{Dt}\right)\left[\left(\frac{D\alpha_1}{Dt}\right)^2 - a^2\left\{\left(\frac{\partial \alpha_1}{\partial y}\right)^2 + \left(\frac{\partial \alpha_1}{\partial x}\right)^2\right\}\right] = 0 \qquad \text{- (C-21)}$$

The first condition is given by $\frac{D\alpha_1}{Dt} = 0$

or $$\frac{\partial \alpha_1}{\partial t} + U\frac{\partial \alpha_1}{\partial x} + V\frac{\partial \alpha_1}{\partial y} = 0 \qquad \text{- (C-22)}$$

which is the dot product of velocity vector $\underline{Q} = U\underline{i} + V\underline{j} + \underline{K}$ (where $\underline{i}$ $\underline{j}$ and $\underline{K}$ are unit vectors along the x, y and t axis respectively) with vector $\nabla\alpha_1$.

$$\nabla\alpha_1 = \frac{\partial \alpha_1}{\partial x}\underline{i} + \frac{\partial \alpha_1}{\partial y}\underline{j} + \frac{\partial \alpha_1}{\partial t}\underline{K}$$

$\nabla\alpha_1$ is normal to the characterisitic surface and $\underline{Q}$ is tangential to the particle paths. Hence these characteristic surfaces are made up of particle paths and

are called stream surfaces. These stream surfaces are generated by particle paths given by $\frac{dx}{dt} = U$ and $\frac{dy}{dt} = V$.

From (C-21) the second condition is,

$$\left(\frac{\partial \alpha_1}{\partial t} + U \frac{\partial \alpha_1}{\partial x} + V \frac{\partial \alpha_1}{\partial y} \right)^2 - a^2 \left[\left(\frac{\partial \alpha_1}{\partial x} \right)^2 + \left(\frac{\partial \alpha_1}{\partial y} \right)^2 \right] = 0 \quad \text{- (C-23)}$$

This equation represents the characteristic cone at point Q in Fig (8b) with the equation

$$(dx - Udt)^2 + (dy - Vdt)^2 = (a\,dt)^2 \quad \text{- (C-24)}$$

As remarked earlier this characterisitc cone is tangential to the conoid passing through point Q. This conoid shown in Fig (9b) is a surface in (x, y, t) space may be defined by giving the co-ordinates of every point on this surface in terms of two parameters ϕ and T ($\equiv t$). Each characteristic surface through point Q touches the conoid along a bi-characteristic curve, ϕ is constant along any bi-characteristic and may take any value in the range $0 \leq \phi \leq 2\pi$.

Equation (C-24) can be satisfied by

$$\begin{aligned} dx &= (U + a\cos\bar{\theta})\,dT \\ dy &= (V + a\sin\bar{\theta})\,dT \end{aligned} \quad \text{- (C-25)}$$

where $\bar{\theta}$ is a parametric angle.

Butler Ref (39) and later Richardson Ref (40) showed that if $\bar{\theta}$ is set equal to ϕ (for any bi-characteristic 'i') at point Q in the $T_o + \Delta T$, $\bar{\theta}$ is subsequently defined as

$$\tan(\bar{\theta}_i) = -\left(\frac{\partial x}{\partial \phi} \Big/ \frac{\partial y}{\partial \phi} \right)_i \quad \text{- (C-26)}$$

$\bar{\theta}$ is given by

$$\bar{\theta}_i = \phi_i + \Delta T\, D_i \quad \text{- (C-27a)}$$

where

$$D_i = \left[-\sin\phi_i \left(\frac{\partial a}{\partial x} \right)_i + \cos\phi_i \left(\frac{\partial a}{\partial y} \right)_i + \cos^2\phi_i \left(\frac{\partial U}{\partial y} \right)_i \right.$$

$$\left. - \sin\phi_i \cos\phi_i \left(\frac{\partial U}{\partial x} - \frac{\partial V}{\partial y} \right)_i - \sin^2\phi_i \left(\frac{\partial V}{\partial x} \right)_i \right] \quad \text{- (C-27b)}$$

Consequently along any bi-characteristic ϕ_i the co-ordinates of the points of intersection of the bi-characteristic curve with the initial time plane T_o are given by the following relations:-

$$x_i = x_N - \frac{1}{2}\Delta T \left(U_N + a_N \cos\phi_i + U_i + a_i \cos\bar{\theta}_i \right) + O(\Delta T)^3 \quad \text{- (C-27c)}$$

$$y_i = y_N - \frac{1}{2}\Delta T\left(V_N + a_N \sin\phi_i + V_i + a_i \cos\bar{\theta}_i\right) + O(\Delta T)^3 \quad \text{- (C-27d)}$$

quantities with the subscript N are those in the $T_o + \Delta T$ plane and with subscript i are those evaluated at the intersection of the bi-characteristic ϕ_i with the T_o plane.

The compatibility equations holding along any general bi-characteristic are derived in similar fashion to those in the two independent variable case. Along a bi-characteristic for any arbitrary function g the following relations hold,

$$\frac{\partial g}{\partial T} = \frac{\partial g}{\partial x}\frac{\partial x}{\partial T} + \frac{\partial g}{\partial y}\frac{\partial y}{\partial T} + \frac{\partial g}{\partial t}\frac{\partial t}{\partial T} \quad \text{- (C-28)}$$

as $\frac{dx}{dt} = U + a\cos\bar{\theta}$, $\frac{dy}{dt} = V + a\sin\bar{\theta}$ and $t = T$

$$\frac{\partial g}{\partial T} = \frac{\partial g}{\partial t} + \frac{\partial g}{\partial x}(U + a\cos\bar{\theta}) + \frac{\partial f}{\partial y}(V + a\sin\bar{\theta})$$

from (C-6), (C-7), (C-9) and (C-28) the following can be derived

$$\frac{\partial U}{\partial T} + (U + a\cos\bar{\theta})\frac{\partial U}{\partial x} + (V + a\sin\bar{\theta})\frac{\partial U}{\partial y} + \frac{a^2}{\gamma}\frac{\partial P}{\partial x} - \left(a\cos\bar{\theta}\frac{\partial U}{\partial x} + a\sin\bar{\theta}\frac{\partial U}{\partial y}\right) = 0$$

or

$$\frac{\partial U}{\partial T} + \frac{a^2}{\gamma}\frac{\partial P}{\partial x} - \left(a\cos\bar{\theta}\frac{\partial U}{\partial x} + a\sin\bar{\theta}\frac{\partial U}{\partial y}\right) = 0 \quad \text{- (C-29)}$$

$$\frac{\partial V}{\partial T} + \frac{a^2}{\gamma}\frac{\partial P}{\partial x} - \left(a\cos\bar{\theta}\frac{\partial V}{\partial x} + a\sin\bar{\theta}\frac{\partial V}{\partial y}\right) = 0 \quad \text{- (C-30)}$$

$$\frac{\partial P}{\partial T} + \gamma\left(\frac{\partial U}{\partial x} + \frac{\partial V}{\partial y} + j\frac{V}{y}\right) - \left(a\cos\bar{\theta}\frac{\partial P}{\partial x} + a\sin\bar{\theta}\frac{\partial P}{\partial y}\right) = 0 \quad \text{- (C-31)}$$

A linear combination of (C-29), (C-30) and (C-31) such as (C-29) x $\frac{\gamma}{a}\cos\bar{\theta}$ + (C-30) x $\frac{\gamma}{a}\sin\bar{\theta}$ gives the required compatibility equation

$$\frac{\partial P}{\partial T} + \frac{\gamma}{a}\cos\bar{\theta}_i\frac{\partial U}{\partial T} + \frac{\gamma}{a}\sin\bar{\theta}_i\frac{\partial V}{\partial T} = -\gamma\left\{\frac{\partial U}{\partial x}\sin^2\bar{\theta} + \frac{\partial V}{\partial y}\cos^2\bar{\theta} - \sin\bar{\theta}\cos\bar{\theta}\left(\frac{\partial U}{\partial x} + \frac{\partial V}{\partial y}\right) + j\frac{V}{y}\right\}_i$$

- (C-32)

This expression holds along any bi-characterisitc ϕ_i = constant with $\bar{\theta}_i$ determined by equation (C-27a).

APPENDIX D

The Computer Program

Data on Punched Cards

The data required to start the numerical computations are read-in on three data cards. The first card consists of integer variables only and the second and third consist of real variables.

First Card

M Number of mesh lengths in the Z direction of the computational plane for both Mesh A and Mesh B

NA Number of mesh lengths in the Y direction of Mesh A

NB Number of mesh lengths in the Y direction of Mesh B

JK Frequency of output of boundary point results, CPU, C_D, P_R and CONCRIT results.

KJ Frequency of output of all node points for Mesh A and B.

MP Frequency of output of results on magnetic tape.

IJKMAX Total number of iterations permissible at boundary points

K Number of time steps k

KRUN Total number of time steps, K_{RUN}

MAGR Set equal to unity if the program reads data from magnetic tape

MAGW Set equal to unity if output on magnetic tape is required

MAXSY Set equal to unity of the flow field is axisymmetric

NRUN Run number

Second Card

THETAA θ_A

THETAC θ_C (270.0°)

DELTA Initial estimate of shock detachment distance measured from the origin O

RVERT Initial estimate of the radial position of the shock point at $\theta = 90^\circ$

XMACH M_∞

G γ (ratio of specific heats)

EPS1 Convergence criterion at shock points

EPS2 Convergence criterion at body and axis of symmetry points

EPS3 Convergence criterion for the subsonic internal boundary points

Third Card

XMAI Initial estimate of Mach number at point A on the body surface (at the supersonic external boundary)

AMFR Mass Flow Ratio (MFR)

AELPS Semi-major axis of the elliptic Inlet section

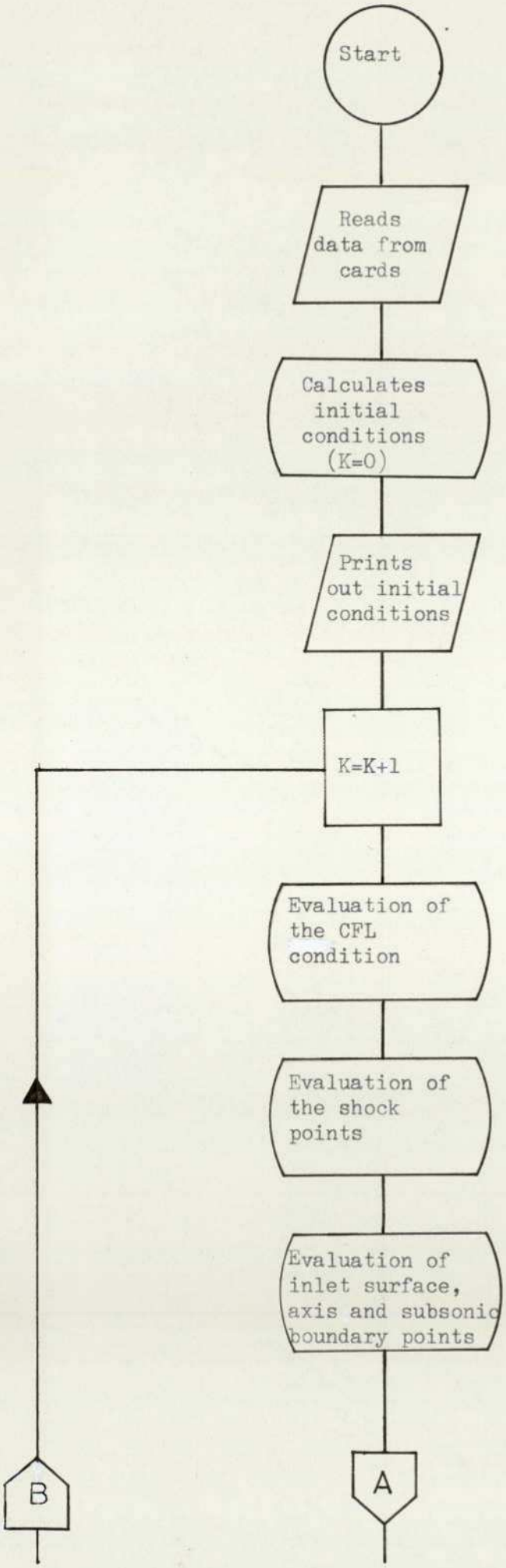
BELPSU Semi-minor axis of the elliptic section from $\theta = 90^\circ$ to $\theta = 180^\circ$

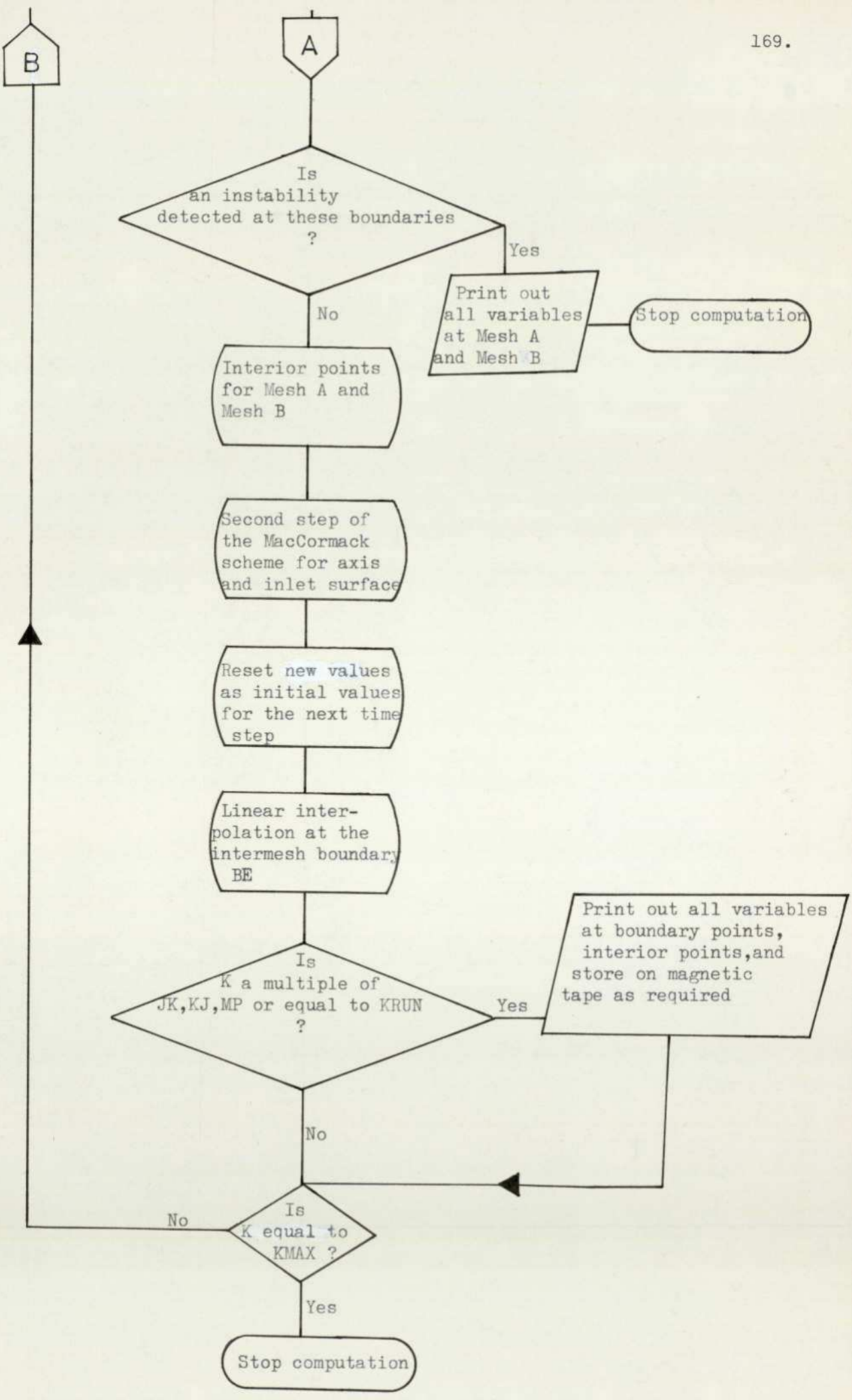
BELPSL Semi-minor axis of the elliptic section from $\theta = 180^\circ$ to $\theta = 270^\circ$.

The flow diagram overleaf shows the sequence of numerical computations. The computation begins after the data cards described above are read. The Initial conditions are created and printed out. The computation then enters the main computational loop of the program wherein the CFL condition, the boundary points and the interior points are evaluated for each time step. This sequence is repeated for each time step until K = KRUN and is only interupted when K is a multiple of JK, KJ or MP at which stage results are listed and stored on magnetic tape if required. The computation is terminated if an instability is detected at the boundary points.

A user who is initially unfamiliar with the running of this computer program may find Table 2 which was presented in chapter 4 useful for selecting values of KRUN and node density (MxNA, MxNB). Corresponding CPU seconds are also given for the CDC 6600 and CDC 7600 computers.

The computer program presented in this Appendix starts the calculations after reading data on punched cards. A simple modification of this program would enable the program to read generated results from magnetic tape and continue the calculation. This modification would involve the inclusion of READ (3) statements at the beginning of the program similar to the WRITE (3) statements which occur when results are written to magnetic tape.


Start
Reads data from cards
Calculates initial conditions (K=0)
Prints out initial conditions
K=K+1
Evaluation of the CFL condition
Evaluation of the shock points
Evaluation of inlet surface, axis and subsonic boundary points
A
B


B
A
Is an instability detected at these boundaries ?
Yes
Print out all variables at Mesh A and Mesh B
Stop computation
No
Interior points for Mesh A and Mesh B
Second step of the MacCormack scheme for axis and inlet surface
Reset new values as initial values for the next time step
Linear interpolation at the intermesh boundary BE
Is K a multiple of JK,KJ,MP or equal to KRUN ?
Yes
Print out all variables at boundary points, interior points,and store on magnetic tape as required
No
Is K equal to KMAX ?
No
Yes
Stop computation

A List of Main Identifiers (Other than those defined for the Data Cards)

Integer Identifiers

(identifiers ending with A and B usually imply Mesh A and B respectively)

I node position in the radial direction

IA node position in the ZA direction (Mesh A, Fig (15))

IB node position in the ZB direction (Mesh B, Fig (15))

IJK number of interations at a boundary point

J node position in the angular sense

JA node position in the YA direction (Mesh A, Fig (15))

JB node position in the YB direction (Mesh B, Fig (15))

JMAX total number of nodes in the Y direction for both Mesh A and Mesh B not including the extra mesh points

JSTAG angular node point on the inlet surface nearest the stagnation point.

KMAX total number of time steps. KMAX = KRUN if K = 0 when the computation begins

One Dimensional Arrays

BOA(JA)	BOA
BOB(JB)	BOB
BOYA(JA)	$\frac{\partial BOA}{\partial \theta}$
BOYB(JB)	$\frac{\partial BOB}{\partial \theta}$
BOYYA(JA)	$\frac{\partial^2 BOA}{\partial \theta^2}$
BOYYB(JB)	$\frac{\partial^2 BOB}{\partial \theta^2}$
CP(J)	C_p
DA(JA)	D
DB(JB)	D
W(JA)	$W(T_o)$
WNT(JA	$W(To + \Delta T)$
XCOT(JA)	$\text{Cot}(\alpha)$, where α is the angle between the tangent at the shock wave and the radial co-ordinate direction.

Two Dimensional Arrays (Real)

PA(IA,JA)	P (T_o)
PB (IB, JB)	P (T_o)
PNA (IA, JA)	P ($T_o + \Delta T$)
PNB(IB,JB)	P ($T_o + \Delta T$)
RA(IA,JA)	R(T_o)
RB (IB,JB)	R(T_o)
RNA (IA,JB)	R($T_o + \Delta T$)
RNB(IB,JB)	R($T_o + \Delta T$)
SA (IA,JA)	S (T_o)
SB(IB,JB)	S (T_o)
SNA (IA,JA)	S($T_o + \Delta T$)
SNB (IB,JB)	S($T_o + \Delta T$)
UA(IA,JA)	u(T_o)
UB (IB,JB)	u(T_o)
UNA (IA,JA)	u($T_o + \Delta T$)
UNB (IB,JA)	u($T_o + \Delta T$)
VA(IA,JA)	v(T_o)
VB (IB,JB)	v(T_o)
VNA(IA,JA)	v($T_o + \Delta T$)
VNB(IB,JB)	v($T_o + \Delta T$)

Real Identifiers

ACCT	Accumulative computational time,
ACTMFR	Actual mass flow ratio, ACTMFR = AMFR for two dimensional flow
BIGVN	Tangential component of velocity on the axis of symmetry surface at ($T_o + \Delta T$)
CDADD	C_{DADD}
CDCOWL	C_{DCOWL}
CDEXT	C_{DEXT}
CONCRIT	Convergence criterion defined in Fig (29)(c)

CPU Central Processor Unit time (seconds)

DELT ΔT

DELYA YA

DELYB YB

DELZA ZA

DELZB ZB

DTHA $\Delta\theta_A$ (angular mesh size for Mesh A)

DTHB $\Delta\theta_B$ (angular mesh size for Mesh B)

ETA η co-ordinate of the point of intersection of the characteristic with the T_o plane

ENTBOD Entropy rise through a normal shock wave

PBSUB P at the subsonic boundary C-F

PPYE $(180/\pi)$

PYE π

PRA P_R

PTA $\frac{\partial P}{\partial T}$

PTB $\frac{\partial P}{\partial T}$

RAL Ratio of the static pressure to total pressure across a normal shock

RBSUB ρ at the subsonic boundary C-F

RTA $\frac{\partial R}{\partial T}$

RTB $\frac{\partial R}{\partial T}$

RHX right hand side of the compatibility equation occurring in the unsteady MOC approach for the boundary points.

RHS1 (RHX) x (ΔT) for the U + a characteristic (subsonic boundary)

RHS2 (RHX) x (ΔT) for the U - a characteristic (subsonic boundary)

RTHAOB $(\Delta\theta_A/\Delta\theta_B)$

RTTA $\frac{\partial^2 R}{\partial T^2}$

RTTB $\frac{\partial^2 R}{\partial T^2}$

SIGA $\theta_B - \theta_A$

SIGB $\theta_C - \theta_B$

STA $\frac{\partial S}{\partial T}$

STB $\frac{\partial S}{\partial T}$

STTA $\frac{\partial^2 S}{\partial T^2}$

STTB $\frac{\partial^2 S}{\partial T^2}$

THBT $\left(\frac{\partial \theta_B}{\partial T}\right)_{T_o}$

THETAB $\theta_B(T_o)$

THETABN $\theta_B(T_o + \Delta T)$

THBTN $\left(\frac{\partial \theta_B}{\partial T}\right)_{(T_o + \Delta T)}$

UTA $\frac{\partial u}{\partial T}$

UTB $\frac{\partial u}{\partial T}$

UTTA $\frac{\partial^2 u}{\partial T^2}$

UTTB $\frac{\partial^2 u}{\partial T^2}$

UBSUB u at the subsonic boundary C-F

VBSUB v at the subsonic boundary C-F

VTA $\frac{\partial v}{\partial T}$

VTB $\frac{\partial v}{\partial T}$

VTTA $\frac{\partial^2 v}{\partial T^2}$

VTTB $\frac{\partial^2 v}{\partial T^2}$

X abssissa relative to origin defined in Fig (15)

XI ξ co-ordinate of the point of intersection of the characteristic with T_o plane.

Subroutines

SUBROUTINE WRTBOD

This subroutine prints out information about the inlet surface in terms of

θ, BOA, $\frac{\partial BOA}{\partial \theta}$ $\frac{\partial^2 BOA}{\partial \theta^2}$ and X (similarly for Mesh B) at each node point on the inlet surface.

SUBROUTINE DERIV

The main program is provided with derivatives of the form $\frac{\partial g}{\partial Y}$, $\frac{\partial^2 g}{\partial Y^2}$ etc. which are evaluated using central differences about any interior point (i, j) (see Fig (13))

SUBROUTINE SIMP

Simpson's Rule is used to evaluate areas under curves whose co-ordinates are known in equal or unequal increments. This subroutine was used to calculate the drag coefficients, P_R and CONCRIT.

SUBROUTINE BODYA and SUBROUTINE BODYB

The required information about the inlet surface in the form of BOA, $\frac{\partial BOA}{\partial \theta}$ and $\frac{\partial^2 BOA}{\partial \theta^2}$ are calculated for Mesh A and Mesh B at each time step. The inlet section can be made up of elliptically shaped quadrants of equal or unequal semi-minor axes.

SUBROUTINE SECOND

A library subroutine which calculates the CPU seconds used.

THE COMPUTER PROGRAM (On Microfiche, 40 pages)



```
C     A COMPUTER PROGRAM FOR COMPUTING THE TRANSONIC FLOW ABOUT BLUNT
C     LIPPED DUCTED BODIES WITH SUBSONIC INTERNAL BOUNDARIES.
C     THE COMPUTER PROGRAM WAS WRITTEN IN FORTRAN AND WAS RUN ON THE
C     CDC 6600 AND CDC 7600 DIGITAL COMPUTERS AT THE UNIVERSITY OF
C     LONDON COMPUTER CENTRE,GUILDFORD STREET,LONDON W.C.1.
C
      PROGRAM SUBNRY2(INPUT,OUTPUT,TAPE1=INPUT,TAPE2=OUTPUT,DATAA,
     1TAPE3=DATAA)
      COMMON    UA(16,27),VA(16,27),RA(16,27),PA(16,27),SH(27),SHY(27),
     1XCOT(27),UB(16,27),VB(16,27),RB(16,27),PB(16,27),SA(16,27),
     2SB(16,27),W(27),ZA(16),ZB(16),DA(27),SHXY(27),SHXYY(27),SHYY(27),
     3A1(2),DIF3(2),YW(27),DB(27),ADT(16,27),SH1(27),SHX(27),XCOT1(27),
     4W1(2),ZW1(2),ZDIF(2),PNA(16,27),RNA(16,27),UNA(16,27),DIF2(2),
     5VNA(16,27),SNA(16,27),WNT(27),UNB(16,27),VNB(16,27),RNB(16,27),
     6SNB(16,27),PNB(16,27),AS(2),DIFS(2),SMFR(16),DMFR(16)
     7,CP(60),T(60),DRAG(60),AJX(16),PRY(16)
     8,XVA(27),XVB(27),XVAX(27),DXVDTA(27),DXVDTB(27),DXVDTAX(27)
     9,VMSS(27)
      COMMON/AAA/BOA(27),BOYA(27),BOYYA(27),YA(27),NNA,XNA,DTHA,SBOA(27)
     1,CBOA(27),NNA1,NA
      COMMON/BBB/BOB(27),BOYB(27),BOYYB(27),YB(27),NNB,XNB,DTHB,SBOB(27)
     1,CBOB(27),NB
      COMMON/TTT/THETAA,THETAB,THETAC
      COMMON/ELLIPSE/AELPS,BELPSU,BELPSL
      COMMON/INTG/K
      REAL MBODY,MAXIS1,MAXIS
      COT(X)=1.0/TAN(X)
      PYE=3.14159265
      PPYE=57.29577957
C
C     READS DATA FROM PUNCHED CARDS.
      READ(1,7010)M,NA,NB,JK,KJ,MP,IJKMAX,K,KRUN,MAGR,MAGW,MAXSY,NRUN
 7010 FORMAT(13I5)
      READ(1,2)THETAA,THETAC,DELTA,RVERT,XMACH,G,EPS1,EPS2,EPS3
    2 FORMAT(6F6.2,3F9.6)
      READ(1,7)XMAI,AMFR,AELPS,BELPSU,BELPSL
    7 FORMAT(5F10.6)
      ACCT=0.0
      THBT=0.0
      KMAX=K+KRUN
      THETAB=3.14159265+ATAN(1.0/DELTA)
      THETAB=THETAB*PPYE
      WRITE(2,557) NRUN
  557 FORMAT(/,5X,11HRUN NUMBER=,I5)
      WRITE(2,102)
  102 FORMAT(//,1X,6HTHETAA,4X,6HTHETAB,4X,6HTHETAC,4X,5HDELTA,5X,
     15HRVERT,5X,5HXMACH,7X,1HG,9X,4HEPS1,9X,4HEPS2,9X,4HEPS3)
      WRITE(2,103)THETAA,THETAB,THETAC,DELTA,RVERT,XMACH,G,EPS1,EPS2
     1,EPS3
  103 FORMAT(1X,F6.2,4X,F6.2,4X,F6.2,4X,F6.2,4X,F6.2,4X,F6.2,4X,F6.2,4X,
     1,F9.6,4X,F9.6,4X,F9.6)
  106 FORMAT(/,4X,2HMP,3X,5HMAXSY,4X,4HACCT,6X,5HPBSUB,5X,4HAMFR,/,
     11X,2I5,1X,3F11.6)
      THETAA=THETAA/PPYE
      THETAB=THETAB/PPYE
      THETAC=THETAC/PPYE
      WRITE(2,100)
  100 FORMAT(/,/,5X,1HM,10X,2HNA,10X,2HNB,10X,2HJK,10X,2HKJ,
     112X,6HIJKMAX,10X,1HK,10X,4HKRUN,10X,4HMAGR,10X,4HMAGW)
      WRITE(2,101)M,NA,NB,JK,KJ,IJKMAX,K,KRUN,MAGR,MAGW
```

```
  101 FORMAT(1X,I5,8X,I5,8X,I5,8X,I5,8X,I5,8X,I5,8X,I5,8X,I5,8X,I5,8X,I5
     1)
C
      NNB=NB+2
       NB1=NB+1
      MM=M+1
      NNA=NA+1
      NNA1=NA+2
      XM=M
      XNA=NA
      XNB=NB
      DELYA=1.0/XNA
      DELZA=1.0/XM
      DELYB=1.0/XNB
      DELZB=1.0/XM
      DO 3 IA=1,MM
      XIA=IA-1
      ZA(IA)=DELZA*XIA
      ZB(IA)=ZA(IA)
    3 CONTINUE
      DO 4 JA=1,NNA
      XJA=JA-1
      YA(JA)=DELYA*XJA
    4 CONTINUE
      DO 5 JB=2,NNB
      XJB=JB-2
      YB(JB)=DELYB*XJB
    5 CONTINUE
      DZ2A=2.0*DELZA
      DZSQA=DELZA*DELZA
      DY2A=2.0*DELYA
      DYSQA=DELYA*DELYA
      DZ2B=2.0*DELZB
      DYDZA=4.0*DELYA*DELZA
      DZSQB=DELZB*DELZB
      DY2B=2.0*DELYB
      DYSQB=DELYB*DELYB
      DYDZB=4.0*DELYB*DELZB
      GG=SQRT(G)
      VINF=XMACH*GG
      GP1=G+1.0
      GM1=G-1.0
      ER=(GP1*XMACH*XMACH)/(2.0+GM1*XMACH*XMACH)
      EP=((2.0*G*XMACH*XMACH)/GP1)-(GM1/GP1)
      ENTBOD=ALOG(EP)-G*ALOG(ER)
      CALL BODYA
      CALL BODYB
C     INITIAL VALUES FOR MESH A
      ASMP=ASIN(1.0/XMACH)
      ASMP=TAN(ASMP)
      A=((RVERT/ASMP)**2-(DELTA**2))/(2.0*DELTA)
      DO 190 JA=1,NNA
      THETA1=(THETAB-THETAA)*YA(JA)+THETAA
      IF(THETA1.GT.3.14159269) GO TO 195
      HA=(COS(THETA1))*COS(THETA1)-(SIN(THETA1)/ASMP)*(SIN(THETA1)
     1/ASMP)
       HB=COS(THETA1)*(A+DELTA)
      HC=DELTA*DELTA+2.0*A*DELTA
      SH(JA)=-(HB+SQRT(HB*HB-HA*HC))/HA
      GO TO 196
```

```
  195 SH(JA)=DELTA/COS(THETA1-3.14159265)
  196 DA(JA)=SH(JA)-BOA(JA)
  190 CONTINUE
      DO 187 JA=2,NA
      SHYY(JA)=(SH(JA+1)+SH(JA-1)-2.0*SH(JA))/(DTHA*DTHA)
  187 SHY(JA)=(SH(JA+1)-SH(JA-1))/(2.0*DTHA)
      SHYY(1)=2.0*SHYY(2)-SHYY(3)
      SHY(1)=2.0*SHY(2)-SHY(3)
      SHYY(NNA)=2.0*SHYY(NA)-SHYY(NA-1)
      SHY(NNA)=2.0*SHY(NA)-SHY(NA-1)
      WRITE(2,38)
   38 FORMAT(1H1,1X,22HINITIAL SHOCK POSITION)
      WRITE(2,2045)
 2045 FORMAT(//,1X,2HJA,8X,5HTHETA,8X,6HSH(JA),8X,4HSPSI)
      DO 6 JA=1,NNA
      THETA1=THETAA+YA(JA)*(THETAB-THETAA)
      Y1A=3.14159265-THETA1
      IF(THETA1.GT.3.14159265) GO TO 150
      XCOT(JA)=SHY(JA)/SH(JA)
      ASI=1.0/SQRT(1.0+XCOT(JA)*XCOT(JA))
      ACI=XCOT(JA)*ASI
      SPSI=ASI*COS(Y1A)-ACI*SIN(Y1A)
      CPSI=ACI*COS(Y1A)+ASI*SIN(Y1A)
      GO TO 151
  150 SPSI=1.0
      CPSI=0.0
      ACI=COS(3.14159265*1.5-THETA1)
      ASI=SIN(3.14159265*1.5-THETA1)
  151 CONTINUE
      VSIN=VINF*SPSI
      VSIN1=VSIN*VSIN
      BU=(GM1*VSIN1+2.0*G)/(GP1*VSIN)
      BV=-VINF*CPSI
      UA(MM,JA)=BV*ACI-BU*ASI
      VA(MM,JA)=BV*ASI+BU*ACI
      RRR=VSIN/BU
      RA(MM,JA)=ALOG(RRR)
      PPP=(GM1-GP1*RRR)/(GM1*RRR-GP1)
      W(JA)=0.0
      PA(MM,JA)=ALOG(PPP)
      THETA1=THETA1*PPYE
      WRITE(2,2050)JA,THETA1,SH(JA),SPSI
 2050 FORMAT(1X,I3,5X,F11.6,3X,F11.6,3X,F11.6)
    6 CONTINUE
      RALEX=1.0/GM1
      RALEX2=G*RALEX
      RAL=(GP1*XMACH*XMACH/2.0)**RALEX2
      RAL=RAL/(((2.0*G*XMACH*XMACH-GM1)/GP1)**RALEX)
      AXM=(2.0+GM1*XMACH*XMACH)/(G*XMACH*XMACH*2.0-GM1)
      AXM=SQRT(AXM)
C     ONE DIMENSIONAL ANALYSIS APPLIED TO ESTIMATE PBSUB AND INITIAL
C     VALUES FOR MACH NUMBER,DENSITY AND VELOCITY ON SUBSONIC BOUNDARY
      ASOA1=(((1.0+0.5*GM1*(AXM**2))/(GP1*0.5))**(GP1/(GM1*2.0)))
     1/AXM
      ASOA=1.0/ASOA1
      ASOAN=(ASOA*AMFR)/(1.0-BOB(NNB))
      ME=1
      A1(ME)=AXM
      IJK=0
  140 IJK=IJK+1
```

```
      ASOA1=(((1.0+0.5*GM1*(A1(ME)**2))/(GP1*0.5))**(GP1/(GM1*2.0)))
     1/A1(ME)
      ASOA=1.0/ASOA1
      DIF3(ME)=(ASOA-ASOAN)
      IF(ABS(DIF3(ME)/ASOAN).LT.0.0001.OR.IJK.GT.30) GO TO 145
      GO TO(141,142)ME
  141 A1(2)=(A1(1)+0.05)
      ME=2
      GO TO 140
  142 ABAR=A1(1)-DIF3(1)*(A1(2)-A1(1))/(DIF3(2)-DIF3(1))
      A1(1)=A1(2)
      DIF3(1)=DIF3(2)
      A1(2)=ABAR
      GO TO 140
  145 XMFI=A1(ME)
      PBSUB=RAL/((1.0+0.5*GM1*(XMFI**2))**RALEX2)
      RBSUB=(ALOG(PBSUB)-ENTBOD)/G
      RBSUB=EXP(RBSUB)
      VBSUB=(GG*XMACH*AMFR)/(RBSUB*((1.0-BOB(NNB))**(MAXSY+1)))
      WRITE(2,106)MP,MAXSY,ACCT,PBSUB,AMFR
      DO 9 IB=1,MM
      PB(IB,NNB)=ALOG(PBSUB)
      SB(IB,NNB)=ENTBOD
      RB(IB,NNB)=(PB(IB,NNB)-SB(IB,NNB))/G
      UB(IB,NNB)=0.0
      VB(IB,NNB)=VBSUB
    9 CONTINUE
      XMFI=SQRT(VBSUB/(G*PBSUB/RBSUB))
      COEFFA=XMAI/(0.5*3.14159265)
      COEFFB=XMFI/(0.5*3.14159265)
      DO 125 JA=1,NNA
      THETA1=THETAA+YA(JA)*(THETAB-THETAA)
      PA(1,JA)=RAL*(SBOA(JA)*COS(THETA1)-CBOA(JA)*SIN(THETA1))
     1*(SBOA(JA)*COS(THETA1)-CBOA(JA)*SIN(THETA1))
      IF(THETA1.GT.PYE)PA(1,JA)=RAL+(PBSUB-RAL)*((THETA1-PYE)/
     1(0.5*PYE))
  125 CONTINUE
      ANGNL=(110.0/PPYE)
      IF(THETAA.GT.ANGNL.OR.THETAA.EQ.ANGNL) GO TO 110
      JA=1
  130 THETA1=THETAA+(THETAB-THETAA)*YA(JA)
      IF(THETA1.GT.ANGNL.OR.THETA1.EQ.ANGNL) GO TO 115
      JA=JA+1
      GO TO 130
  115 CONTINUE
      JAX=JA
      THETANL=THETAA+YA(JAX)*(THETAB-THETAA)
      PANL=PA(1,JAX)
  120 JA=JA-1
      THETA1=THETAA+(THETAB-THETAA)*YA(JA)
      PA(1,JA)=PANL/EXP(THETANL-THETA1)
      IF(JA.NE.1) GO TO 120
  110 CONTINUE
      WRITE(2,10)
   10 FORMAT(/,1X,59HINITIAL DISTRIBUTION OF MACH NUMBER ON THE AXIS OF
     1SYMMETRY,/,1X,29HAND INLET SURFACE NODE POINTS)
      WRITE(2,40)
   40 FORMAT(///,1X,2HJA,8X,5HTHETA,8X,6HMBODYA)
      DO 8 JA=1,NNA
      THETA1=THETAA+(THETAB-THETAA)*YA(JA)
```

```
      IF(THETA1.GT.3.14159265) GO TO 37
      MBODY=COEFFA*(3.14159265-THETA1)
      GO TO 39
   37 MBODY=COEFFB*(THETA1-3.14159265)
   39 CONTINUE
      PA(1,JA)=ALOG(PA(1,JA))
      RA(1,JA)=(PA(1,JA)-ENTBOD)/G
       QBOD=(GG*SQRT(EXP(PA(1,JA)-RA(1,JA))))*MBODY
      IF(THETA1.GT.3.14159265) GO TO 12
      UA(1,JA)=-QBOD*CBOA(JA)
      VA(1,JA)=-QBOD*SBOA(JA)
      GO TO 13
   12 UA(1,JA)=QBOD*CBOA(JA)
      VA(1,JA)=QBOD*SBOA(JA)
   13 CONTINUE
      THETA1=THETA1*PPYE
      WRITE(2,2055)JA,THETA1,MBODY
 2055 FORMAT(/,1X,I3,5X,F11.6,3X,F11.6)
    8 CONTINUE
      DO 14 JA=1,NNA
      DO 15 IA=2,M
      XIA=IA-1
      UA(IA,JA)=UA(1,JA)+(XIA/XM)*(UA(MM,JA)-UA(1,JA))
      VA(IA,JA)=VA(1,JA)+(XIA/XM)*(VA(MM,JA)-VA(1,JA))
      RA(IA,JA)=RA(1,JA)+(XIA/XM)*(RA(MM,JA)-RA(1,JA))
      PA(IA,JA)=PA(1,JA)+(XIA/XM)*(PA(MM,JA)-PA(1,JA))
   15 CONTINUE
   14 CONTINUE
      DO 16 JA=1,NNA
      DO 17 IA=1,MM
      SA(IA,JA)=PA(IA,JA)-G*RA(IA,JA)
      SA(1,JA)=ENTBOD
   17 CONTINUE
   16 CONTINUE
C     INITIAL VALUES FOR MESH B
C     INITIAL VALUES ALONG AXIS
      WRITE(2,41)
   41 FORMAT(///,1X,2HJB,8X,5HTHETA,8X,5HMAXIS,8X,7HSHX(JB))
      DO 19 JB=2,NNB
      THETA2=THETAB+YB(JB)*(THETAC-THETAB)
      SHX(JB)=-(1.0/SIN(THETA2))
      TT=THETA2-THETAB
      AXISM=((XMFI-AXM)/(3.14159265*1.5-THETAB))*TT+AXM
      USON=GG*SQRT(EP/ER)
      UAXIS=USON*AXISM
      UB(MM,JB)=UAXIS*COS(THETA2)
      VB(MM,JB)=-UAXIS*SIN(THETA2)
      PEX=G/GM1
      PB(MM,JB)=RAL/((1.0+GM1*AXISM*AXISM/2.0)**PEX)
      PB(MM,JB)=ALOG(PB(MM,JB))
      RB(MM,JB)=(PB(MM,JB)-ENTBOD)/G
      THETA2=THETA2*PPYE
      WRITE(2,2060)JB,THETA2,AXISM,SHX(JB)
 2060 FORMAT(1X,I3,5X,F11.6,3X,F11.6,3X,F11.6)
   19 CONTINUE
      DO 20 JB=2,NNB
      THETA2=THETAB+YB(JB)*(THETAC-THETAB)
      PB(1,JB)=RAL+(PBSUB-RAL)*((THETA2-PYE)/(0.5*PYE))
   20 CONTINUE
      WRITE(2,42)
```

```
   42 FORMAT(///,1X,2HJB,8X,5HTHETA,8X,6HMBODYB)
      DO 22 JB=2,NNB
      THETA2=YB(JB)*(THETAC-THETAB)+THETAB
      MBODY=COEFFB*(THETA2-3.14159265)
      PB(1,JB)=ALOG(PB(1,JB))
      RB(1,JB)=(PB(1,JB)-ENTBOD)/G
      QBOD=(GG*SQRT(EXP(PB(1,JB)-RB(1,JB))))*MBODY
      UB(1,JB)=QBOD*CBOB(JB)
      VB(1,JB)=QBOD*SBOB(JB)
      THETA2=((THETAC-THETAB)*YB(JB)+THETAB)*PPYE
      WRITE(2,2065)JB,THETA2,MBODY
 2065 FORMAT(/,1X,I3,5X,F11.6,3X,F11.6)
   22 CONTINUE
      DO 24 JB=2,NB1
      DO 23 IB=2,M
      XIB=IB-1
      UB(IB,JB)=UB(1,JB)+(XIB/XM)*(UB(MM,JB)-UB(1,JB))
      VB(IB,JB)=VB(1,JB)+(XIB/XM)*(VB(MM,JB)-VB(1,JB))
      RB(IB,JB)=RB(1,JB)+(XIB/XM)*(RB(MM,JB)-RB(1,JB))
      PB(IB,JB)=PB(1,JB)+(XIB/XM)*(PB(MM,JB)-PB(1,JB))
   23 CONTINUE
   24 CONTINUE
      DO 26 JB=2,NNB
      DO 25 IB=1,MM
      SB(IB,JB)=PB(IB,JB)-G*RB(IB,JB)
      SB(1,JB)=ENTBOD
      SB(MM,JB)=ENTBOD
   25 CONTINUE
      THETA2=THETAB+(THETAC-THETAB)*YB(JB)
      TS=(3.14159265*1.5-THETA2)
      SHX(JB)=1.0/COS(TS)
      DB(JB)=SHX(JB)-BOB(JB)
   26 CONTINUE
      DO 51 JB=3,NB
      SHXY(JB)=(SHX(JB+1)-SHX(JB-1))/(DTHB*2.0)
      SHXYY(JB)=(SHX(JB+1)+SHX(JB-1)-2.0*SHX(JB))/(DTHB*DTHB)
   51 CONTINUE
      SHXY(NNB)=2.0*SHXY(NB)-SHXY(NB-1)
      SHXYY(NNB)=2.0*SHXYY(NB)-SHXYY(NB-1)
      SHXY(2)=SHXY(3)*2.0-SHXY(4)
      SHXYY(2)=2.0*SHXYY(3)-SHXYY(4)
      SHX(2)=SH(NNA)
      DB(2)=SHX(2)-BOB(2)
      DA(NNA)=DB(2)
      DO 3036 I=1,MM
      UA(I,NNA1)=UB(I,3)
         VA(I,NNA1)=VB(I,3)
         RA(I,NNA1)=RB(I,3)
         PA(I,NNA1)=PB(I,3)
      SA(I,NNA1)=PA(I,NNA1)-G*RA(I,NNA1)
      UB(I,1)=UA(I,NA)
      VB(I,1)=VA(I,NA)
      RB(I,1)=RA(I,NA)
      PB(I,1)=PA(I,NA)
      SB(I,1)=PB(I,1) -G*RB(I,1)
 3036 CONTINUE
      DO 29 JA=1,NNA
      DO 28 IA=1,MM
      PA(IA,JA)=EXP(PA(IA,JA))
      RA(IA,JA)=EXP(RA(IA,JA))
```

```
   28 CONTINUE
   29 CONTINUE
      DO 34 JB=2,NNB
      DO 33 IB=1,MM
      PB(IB,JB)=EXP(PB(IB,JB))
      RB(IB,JB)=EXP(RB(IB,JB))
   33 CONTINUE
   34 CONTINUE
      CALL WRTBOD
      WRITE(2,27)
   27 FORMAT(1H1,25HINITIAL VALUES FOR MESH A)
      WRITE(2,30)
   30 FORMAT(6X,2HUA,13X,2HVA,13X,2HRA,13X,2HPA,13X,2HSA)
      WRITE(2,31)((UA(IA,JA),VA(IA,JA),RA(IA,JA),PA(IA,JA),SA(IA,JA),IA=
     11,MM),JA=1,NNA)
   31 FORMAT(5E15.7)
      WRITE(2,32)
   32 FORMAT(1H1,25HINITIAL VALUES FOR MESH B)
      WRITE(2,35)
   35 FORMAT(6X,2HUB,13X,2HVB,13X,2HRB,13X,2HPB,13X,2HSB)
      WRITE(2,36)((UB(IB,JB),VB(IB,JB),RB(IB,JB),PB(IB,JB),SB(IB,JB),
     1IB=1,MM),JB=2,NNB)
   36 FORMAT(5E15.7)
      DO 2029 JA=1,NNA
      DO 2028 IA=1,MM
      PA(IA,JA)=ALOG(PA(IA,JA))
      RA(IA,JA)=ALOG(RA(IA,JA))
 2028 CONTINUE
 2029 CONTINUE
      DO 2034 JB=2,NNB
      DO 2033 IB=1,MM
      PB(IB,JB)=ALOG(PB(IB,JB))
      RB(IB,JB)=ALOG(RB(IB,JB))
 2033 CONTINUE
 2034 CONTINUE
C
C     EVALUATION OF THE C.F.L. CONDITION
C
   45 K=K+1
      DO 630 JB=2,NNB
      SHX(JB)=-(1.0/SIN(THETAB+YB(JB)*(THETAC-THETAB)))
      DB(JB)=SHX(JB)-BOB(JB)
  630 CONTINUE
      DO 631 JA=1,NNA
      DA(JA)=SH(JA)-BOA(JA)
  631 CONTINUE
      DO 9005 JA=1,NNA
      ARM1=DA(JA)/XM
      DO 9000 IA=1,MM
      RLA=ZA(IA)*DA(JA)+BOA(JA)
      ARM2=RLA*DTHA
      ARM=AMIN1(ARM1,ARM2)
      YAQ=SQRT(UA(IA,JA)*UA(IA,JA)+VA(IA,JA)*VA(IA,JA))
      YAA=GG*EXP(0.5*(PA(IA,JA)-RA(IA,JA)))
      ADT(IA,JA)=ARM/(1.5*(YAQ+YAA))
 9000 CONTINUE
 9005 CONTINUE
      CFLA=ADT(2,2)
      DO 9010 JA=1,NNA
      DO 9015 IA=1,MM
```

```
      IF(ADT(IA,JA).LT.CFLA) CFLA=ADT(IA,JA)
 9015 CONTINUE
 9010 CONTINUE
      DO 9205 JB=2,NNB
      ARM1=DB(JB)/XM
      DO 9200 IB=1,MM
      RLB=ZB(IB)*DB(JB)+BOB(JB)
      ARM2=RLB*DTHB
      ARM=AMIN1(ARM1,ARM2)
      YAQ=SQRT(UB(IB,JB)*UB(IB,JB)+VB(IB,JB)*VB(IB,JB))
      YAA=GG*EXP(0.5*(PB(IB,JB)-RB(IB,JB)))
      ADT(IB,JB)=ARM/(1.5*(YAQ+YAA))
 9200 CONTINUE
 9205 CONTINUE
      CFLB=ADT(2,3)
      DO 9215 JB=2,NNB
      DO 9210 IB=1,MM
      IF(ADT(IB,JB).LT.CFLB) CFLB=ADT(IB,JB)
 9210 CONTINUE
 9215 CONTINUE
      DELT=AMIN1(CFLA,CFLB)
      ACCT=ACCT+DELT
      DO 50 JA=1,NA
      SH1(JA)=SH(JA)+W(JA)*DELT
   50 CONTINUE
C     COMPUTATION OF AXIAL POSITION OF SHOCK POINT (E)
      XSIN1=SQRT(SH(NNA)*SH(NNA)-1.0)/SH(NNA)
      XCOS1=1.0/SH(NNA)
      SSPN=XCOS1
      DIST=W(NNA)*XSIN1*DELT
      SH1(NNA)=SQRT(DIST*DIST+SH(NNA)*SH(NNA)
     1+2.0*SH(NNA)*DIST*XSIN1)
      DELTAB=-ASIN(DIST*SSPN/SH1(NNA))
       THETABN=THETAB+DELTAB
      SIGA=THETAB-THETAA
      THBTN=(THETABN-THETAB)/DELT
      THBTT=(THBTN-THBT)/DELT
      SIGTA=THBT
      SIGTTA=THBTT
      DO 52 JA=2,NA
      XCOT1(JA)=(SH1(JA+1)-SH1(JA-1))/(2.0*DTHA*SH1(JA))
      SHY(JA)=(SH(JA+1)-SH(JA-1))/(2.0*DTHA)
      SHYY(JA)=(SH(JA+1)+SH(JA-1)-2.0*SH(JA))/(DTHA*DTHA)
      YW(JA)=(W(JA+1)-W(JA-1))/DY2A
   52 CONTINUE
      DO 95 JB=2,NNB
      THETA2=THETAB+YB(JB)*(THETAC-THETAB)
      SHXY(JB)=COS(THETA2)/(SIN(THETA2)*SIN(THETA2))
      SHXYY(JB)=-(COS(THETA2)*COS(THETA2)+1.0)
     1/(SIN(THETA2)*SIN(THETA2)*SIN(THETA2))
   95 CONTINUE
      SHY(1)=2.0*SHY(2)-SHY(3)
      SHYY(1)=2.0*SHYY(2)-SHYY(3)
      SHY(NNA)=2.0*SHY(NA)-SHY(NA-1)
      SHYY(NNA)=2.0*SHYY(NA)-SHYY(NA-1)
      YW(NNA)=2.0*YW(NA)-YW(NA-1)
      XCOT1(1)=2.0*XCOT1(2)-XCOT1(3)
      XCOT1(NNA)=COT(3.14159265*1.5-THETABN)
C
C
```

```
C       EVALUATION OF SHOCK POINTS FOR MESH A
C
        DO 76 JA=2,NA
        SL=SH1(JA)
        ME=1
        XSIN1=1.0/SQRT(1.0+XCOT1(JA)*XCOT1(JA))
        XCOS1=XCOT1(JA)*XSIN1
        THETA1=THETAA+YA(JA)*(THETAB-THETAA)
        THN1=THETAA+YA(JA)*(THETABN-THETAA)
        SPSI=-(XSIN1*COS(THN1)+XCOS1*SIN(THN1))
        CPSI=SIN(THN1)*XSIN1-COS(THN1)*XCOS1
        W1(ME)=W(JA)
        IJK=0
   54   IJK=IJK+1
   55   WS=W1(ME)*XSIN1
        VX=VINF*SPSI+WS
        VXX=VX*VX
        AU=(GM1*VXX+2.0*G)/(GP1*VX)-WS
        AR=VX/(AU+WS)
        AP=(GM1-GP1*AR)/(GM1*AR-GP1)
        AV=-VINF*CPSI
        AA=GG*SQRT(AP/AR)
        XI=(AA-AU)*DELT
        IF(XI.GT.0.0) GO TO 64
        IF(ME.EQ.1) GO TO 57
        MEE=1
        ZW1(1)=W1(1)
        IJZ=0
   58   IJZ=IJZ+1
        WS=ZW1(MEE)*XSIN1
        VX=VINF*SPSI+WS
        VXX=VX*VX
        AU=(GM1*VXX+2.0*G)/(GP1*VX)-WS
        AR=VX/(AU+WS)
        AP=(GM1-GP1*AR)/(GM1*AR-GP1)
        AV=-VINF*CPSI
        AA=GG*SQRT(AP/AR)
        XI=(AA-AU)*DELT
        ZDIF(MEE)=XI
        IF(ABS(ZDIF(MEE)).LT.0.000001.OR.IJZ.GT.20) GO TO 61
        GO TO (59,60),MEE
   59   MEE=2
        ZW1(2)=W1(2)
        GO TO 58
   60   W1BZ=ZW1(1)-ZDIF(1)*(ZW1(2)-ZW1(1))/(ZDIF(2)-ZDIF(1))
        ZW1(1)=ZW1(2)
        ZDIF(1)=ZDIF(2)
        ZW1(2)=W1BZ
        GO TO 58
   61   CONTINUE
        XI=ABS(XI)
        W1(2)=ZW1(MEE)
        MEE=-1
        GO TO 64
   57   W1(1)=W1(1)+0.00001*2.0**IJK
        GO TO 54
   64   ETA=-AV*DELT
        RSTAR=SQRT(SL*SL+XI*XI+ETA*ETA-2.0*SL*(ETA*XCOS1+XI*XSIN1))
        DTHEST=ATAN((XI*XCOS1-ETA*XSIN1)/(SL-(ETA*XCOS1+XI*XSIN1)))
        DELYS=DTHEST/(THETAB-THETAA)
```

```
      BOST=BOA(JA)+ ((BOA(JA+1)-BOA(JA-1))*DELYS)/DY2A +  ((BOA(JA+1)+
     1BOA(JA-1)-2.0*BOA(JA))*0.5*DELYS*DELYS)/DYSQA
      BOYST=BOYA(JA)+(BOYA(JA+1)-BOYA(JA-1))*DELYS/DY2A +(BOYA(JA+1)
     1+BOYA(JA-1)-2.0*BOYA(JA))*0.5*DELYS*DELYS/DYSQA
      DELYS=DELYS/DELYA
      FAC=1.0
      L=JA+1
      IF(DELYS.LT.0.0) FAC=-1.0
      IF(DELYS.LT.0.0) L=JA-1
      DELYS=ABS(DELYS)
      SHST=SH(JA)+(SH(L)-SH(JA))*DELYS
      SHYST=SHY(JA)+(SHY(L)-SHY(JA))*DELYS
      DAST=SHST-BOST
      ZAST=(RSTAR-BOST)/(SHST-BOST)
      DELZS=ZAST-ZA(M)
      DELZS=(1.0-ZAST)/DELZA
      U1=UA(MM,JA)+(UA(MM,L)-UA(MM,JA))*DELYS
      V1=VA(MM,JA)+(VA(MM,L)-VA(MM,JA))*DELYS
      R1=RA(MM,JA)+(RA(MM,L)-RA(MM,JA))*DELYS
      P1=PA(MM,JA)+(PA(MM,L)-PA(MM,JA))*DELYS
      U3=UA(M,JA)+(UA(M,L)-UA(M,JA))*DELYS
      V3=VA(M,JA)+(VA(M,L)-VA(M,JA))*DELYS
      R3=RA(M,JA)+(RA(M,L)-RA(M,JA))*DELYS
      P3=PA(M,JA)+(PA(M,L)-PA(M,JA))*DELYS
       U2=UA(MM,L)+(UA(M,L)-UA(MM,L))*DELZS
      V2=VA(MM,L)+(VA(M,L)-VA(MM,L))*DELZS
      R2=RA(MM,L)+(RA(M,L)-RA(MM,L))*DELZS
      P2=PA(MM,L)+(PA(M,L)-PA(MM,L))*DELZS
      U4=UA(MM,JA)+(UA(M,JA)-UA(MM,JA))*DELZS
      V4=VA(MM,JA)+(VA(M,JA)-VA(MM,JA))*DELZS
      R4=RA(MM,JA)+(RA(M,JA)-RA(MM,JA))*DELZS
      P4=PA(MM,JA)+(PA(M,JA)-PA(MM,JA))*DELZS
      UAST=U1+(U3-U1)*DELZS
      VAST=V1+(V3-V1)*DELZS
      RAST=R1+(R3-R1)*DELZS
      PAST=P1+(P3-P1)*DELZS
      L5=JA-1
      IF(L.LT.JA) L5=JA+1
      U5=UA(MM,L5)+(UA(M,L5)-UA(MM,L5))*DELZS
      V5=VA(MM,L5)+(VA(M,L5)-VA(MM,L5))*DELZS
      P5=PA(MM,L5)+(PA(M,L5)-PA(MM,L5))*DELZS
      UYAST=FAC*(U2-U5)/DY2A+FAC*(U2+U5-2.0*U4)*(DELYS/DELYA)
      VYAST=FAC*(V2-V5)/DY2A+FAC*(V2+V5-2.0*V4)*(DELYS/DELYA)
      PYAST=FAC*(P2-P5)/DY2A+FAC*(P2+P5-2.0*P4)*(DELYS/DELYA)
      UZAST=(U1-U3)/DELZA
      VZAST=(V1-V3)/DELZA
      PZAST=(P1-P3)/DELZA
      CS=COS(DTHEST)
      SS=SIN(DTHEST)
      ALOC=GG*SQRT(EXP(0.5*(PAST-RAST)))
      ULOC=(VAST*CS+UAST*SS)*XCOS1-(UAST*CS-VAST*SS)*XSIN1
      VLOC=(UAST*CS-VAST*SS)*XCOS1+(VAST*CS+UAST*SS)*XSIN1
      ULOCZ=(VZAST*CS+UZAST*SS)*XCOS1-(UZAST*CS-VZAST*SS)*XSIN1
      ULOCY=(VYAST*CS+UYAST*SS)*XCOS1-(UYAST*CS-VYAST*SS)*XSIN1
     1+VLOC*(THETAB-THETAA)
      CAL=(SL*XSIN1-XI)/RSTAR
      SAL=(SL*XCOS1-ETA)/RSTAR
      VLOCZ=(UZAST*CS-VZAST*SS)*XCOS1+(VZAST*CS+UZAST*SS)*XSIN1
      VLOCY=(UYAST*CS-VYAST*SS)*XCOS1+(VYAST*CS+UYAST*SS)*XSIN1
     1-ULOC*(THETAB-THETAA)
```

```
      CSTAR=(BOYST*(ZAST-1.0)/DAST) -ZAST*SHYST/DAST
      ULOCR=ULOCZ/DAST
      VLOCR=VLOCZ/DAST
      PR=PZAST/DAST
      ULOCTH=ULOCZ*CSTAR+ULOCY/(THETAB-THETAA)
      VLOCTH=VLOCZ*CSTAR+VLOCY/(THETAB-THETAA)
      PTH=PZAST*CSTAR+PYAST/(THETAB-THETAA)
      UETA=SAL*ULOCR+CAL*ULOCTH/RSTAR
      VETA=SAL*VLOCR+CAL*VLOCTH/RSTAR
      PETA=SAL*PR+CAL*PTH/RSTAR
      VC=UAST*SIN(THETA1+DTHEST)+VAST*COS(THETA1+DTHEST)
      AFJ=(G*VC)/(1.0+RSTAR*SIN(THETA1+DTHEST))
      IF(MAXSY.NE.1) AFJ=0.0
      RHX=-(G*VETA+VLOC*PETA+AFJ-G*VLOC*UETA/ALOC)*DELT
      AAVER=(ALOC+AA)*0.5
      ALAP=ALOG(AP)
      AUU=AAVER*(ALAP-PAST-RHX)/G +ULOC
   71 DIF2(ME)=AUU-AU
      IF(MEE.NE.-1) GO TO 72
      MEE=0
      IF(DIF2(1)*DIF2(2)) 72,75,75
   72 IF(ABS(DIF2(ME)/AU).LT.EPS1.OR.IJK.GT.IJKMAX) GO TO 75
      GO TO (73,74),ME
   73 ME=2
      W1(2)=W(1)+0.001
      GO TO 54
   74 DIF=DIF2(2)-DIF2(1)
      IF(DIF2(2).EQ.DIF2(1)) GO TO 1072
      W1BAR=W1(1)-DIF2(1)*(W1(2)-W1(1))/DIF
      W1(1)=W1(2)
      DIF2(1)=DIF2(2)
      W1(2)=W1BAR
      GO TO 54
 1072 WRITE(2,1074)K,JA,DIF2(2),W1(2),W1(1),W1BAR
 1074 FORMAT(1X,15HSHOCK ITERATION,/,2I5,4E15.8)
   75 PNA(MM,JA)=ALOG(AP)
      RNA(MM,JA)=ALOG(AR)
      UNA(MM,JA)=AV*XCOS1-AU*XSIN1
      SNA(MM,JA)=PNA(MM,JA)-G*RNA(MM,JA)
      VNA(MM,JA)=AV*XSIN1+AU*XCOS1
      WNT(JA)=W1(ME)
   76 CONTINUE
      IF(ABS(WNT(3)).GE.ABS(WNT(2))) GO TO 77
       WNT(1)=2.0*WNT(2)-WNT(3)
      GO TO 2002
   77 WNT(1)=1.1*WNT(2)
 2002 CONTINUE
      UNA(MM,1)=2.0*UNA(MM,2)-UNA(MM,3)
      VNA(MM,1)=2.0*VNA(MM,2)-VNA(MM,3)
      RNA(MM,1)=2.0*RNA(MM,2)-RNA(MM,3)
      SNA(MM,1)=2.0*SNA(MM,2)-SNA(MM,3)
      PNA(MM,1)=SNA(MM,1)+G*RNA(MM,1)
C
CC    EVALUATION OF SHOCK POINT E
C
      SL=SH1(NNA)
      XCOS1=1.0/SH1(NNA)
      XSIN1=SQRT(1.0-XCOS1*XCOS1)
      SPSI=1.0
      CPSI=0.0
```

```
      ME=1
      W1(ME)=W(NNA)
      IJK=0
   78 IJK=IJK+1
   79 WS=W1(ME)*XSIN1
      VX=VINF*SPSI+WS
      VXX=VX*VX
      AU=(GM1*VXX+2.0*G)/(GP1*VX)-WS
      AR=VX/(AU+WS)
      AP=(GM1-GP1*AR)/(GM1*AR-GP1)
      AV=0.0
      AA=GG*SQRT(AP/AR)
      XI=(AA-AU)*DELT
      IF(XI.GT.0.0) GO TO 86
      IF(ME.EQ.1) GO TO 85
      MEE=1
      ZW1(1)=W1(1)
      IJZ=0
   80 IJZ=IJZ+1
      WS=ZW1(MEE)*XSIN1
      VX=VINF +WS
      AU=(GM1*VXX+2.0*G)/(GP1*VX) -WS
      AR=VX/(AU+WS)
      AP=(GM1-GP1*AR)/(GM1*AR-GP1)
      AV=0.0
      AA=GG*SQRT(AP/AR)
      XI=(AA-AU)*DELT
      ZDIF(MEE)=XI
      IF(ABS(ZDIF(MEE)).LT.0.000001.OR.IJZ.GT.20) GO TO 53
      GO TO (81,82),MEE
   81 MEE=2
      ZW1(2)=W1(2)
      GO TO 80
   82 W1BZ=ZW1(1)-ZDIF(1)*(ZW1(2)-ZW1(1))/(ZDIF(2)-ZDIF(1))
      ZW1(1)=ZW1(2)
      ZDIF(1)=ZDIF(2)
      ZW1(2)=W1BZ
      GO TO 80
   53 CONTINUE
      XI=ABS(XI)
      W1(2)=ZW1(MEE)
      MEE=-1
      GO TO 86
   85 W1(1)=W1(1)+0.00001*2.0**IJK
      GO TO 78
   86 CONTINUE
      XI=ABS(XI)
      RSTAR=SQRT(SL*SL+XI*XI-2.0*SL*XI*XSIN1)
      DTHEST=ASIN(XI*XCOS1/RSTAR)
      DELYS=DTHEST/(THETAC-THETAB)-YB(3)
      BOST=BOB(3)+((BOB(4)-BOB(2))/DY2B)*DELYS
     1+((BOB(4)+BOB(2)-BOB(3)*2.0)/DYSQB)*DELYS*DELYS*0.5
      SHXST=RSTAR
      BOYST=BOYB(3)+((BOYB(4)-BOYB(2))/DY2B)*DELYS
     1+((BOYB(4)+BOYB(2)-2.0*BOYB(3))/DYSQB)*DELYS*DELYS*0.5
      SHXYST=COS(THETAB+DTHEST)/((SIN(THETAB+DTHEST))
     1*(SIN(THETAB+DTHEST)))
      DAST=SHXST-BOST
      ZAST=1.0
      DELYS=ABS(DTHEST)/((THETAB-THETAA)*DELYA)
      U3=UA(M,NNA)+(UA(M,NNA1)-UA(M,NNA))*DELYS
      V3=VA(M,NNA)+(VA(M,NNA1)-VA(M,NNA))*DELYS
      UAST=UA(MM,NNA)+(UA(MM,NNA1)-UA(MM,NNA))*DELYS
      VAST=VA(MM,NNA)+(VA(MM,NNA1)-VA(MM,NNA))*DELYS
      RAST=RA(MM,NNA)+(RA(MM,NNA1)-RA(MM,NNA))*DELYS
      PAST=PA(MM,NNA)+(PA(MM,NNA1)-PA(MM,NNA))*DELYS
```

```
      UYAST=(UA(MM,NNA1)-UA(MM,NA))/DY2A
     1+(UA(MM,NA)+UA(MM,NNA1)-2.0*UA(MM,NNA))*(DELYS/DELYA)
      VYAST=(VA(MM,NNA1)-VA(MM,NA))/DY2A
     1+(VA(MM,NA)+VA(MM,NNA1)-2.0*VA(MM,NNA))*(DELYS/DELYA)
      UZAST=(UAST-U3)/DELZA
      VZAST=(VAST-V3)/DELZA
      CS=COS(DTHEST)
      SS=SIN(DTHEST)
      ALOC=GG*SQRT(EXP(0.5*(PAST-RAST)))
      ULOC=(VAST*CS+UAST*SS)*XCOS1-(UAST*CS-VAST*SS)*XSIN1
      VLOCZ=(UZAST*CS-VZAST*SS)*XCOS1+(VZAST*CS+UZAST*SS)*XSIN1
      VLOCY=(UYAST*CS-VYAST*SS)*XCOS1+(VYAST*CS+UYAST*SS)*XSIN1
     1-ULOC*(THETAB-THETAA)
      CSTAR=(BOYST*(ZAST-1.0)/DAST)-(ZAST*SHXYST/DAST)
      CAL=(SL*XSIN1-XI)/RSTAR
      SAL=(SL*XCOS1)/RSTAR
      VLOCR=VLOCZ/DAST
      VLOCTH=VLOCZ*CSTAR+VLOCY/(THETAB-THETAA)
      VETA=SAL*VLOCR+CAL*VLOCTH/RSTAR
      AFJ=VETA
      IF(MAXSY.NE.1) AFJ=0.0
      RHX=-(VETA+AFJ)*G*DELT
      AAVER=(ALOC+AA)*0.5
      ALAP=ALOG(AP)
      AUU=AAVER*(ALAP-PAST-RHX)/G +ULOC
      DIF2(ME)=AUU-AU
      IF(MEE.NE.-1) GO TO 87
      MEE=0
      IF(DIF2(1)*DIF2(2))87,90,90
   87 IF(ABS(DIF2(ME)/AU).LT.EPS1.OR.IJK.GT.IJKMAX) GO TO 90
      GO TO (88,89),ME
   88 ME=2
      W1(2)=W1(1)+0.001
      GO TO 78
   89 IF(DIF2(2).EQ.DIF2(1)) GO TO 90
      W1BAR=W1(1)-DIF2(1)*(W1(2)-W1(1))/(DIF2(2)-DIF2(1))
      W1(1)=W1(2)
      DIF2(1)=DIF2(2)
      W1(2)=W1BAR
      GO TO 78
   90 PNB(MM,2)=ALOG(AP)
      RNB(MM,2)=ALOG(AR)
      SNB(MM,2)=PNB(MM,2)-G*RNB(MM,2)
      UNB(MM,2)=-AU*XSIN1
      VNB(MM,2)=AU*XCOS1
      UNA(MM,NNA)=UNB(MM,2)
      VNA(MM,NNA)=VNB(MM,2)
      PNA(MM,NNA)=PNB(MM,2)
      RNA(MM,NNA)=RNB(MM,2)
      SNA(MM,NNA)=SNB(MM,2)
      WAXN=W1(ME)
      WNT(NNA)=W1(ME)
C
```

```
C     SEARCH FOR MINIMUM VELOCITY POINT ON THE BODY SURFACE
C
      QMINA=SQRT(UA(1,1)*UA(1,1)+VA(1,1)*VA(1,1))
      JAE=1
      DO 291 JA=1,NNA
      QA=SQRT(UA(1,JA)*UA(1,JA)+VA(1,JA)*VA(1,JA))
      IF(QA.LT.QMINA) JAE=JA
      IF(QA.LT.QMINA) QMINA=QA
  291 CONTINUE
      JBE=2
      QMINB=SQRT(UB(1,2)*UB(1,2)+VB(1,2)*VB(1,2))
      DO 293 JB=2,NNB
      QB=SQRT(UB(1,JB)*UB(1,JB)+VB(1,JB)*VB(1,JB))
      IF(QB.LT.QMINB) JBE=JB
      IF(QB.LT.QMINB) QMINB=QB
  293 CONTINUE
C
C     CALCULATION OF M.F.R.
C
      JB=NNB
      ALPHA=0.0
      CS=COS(ALPHA)
      SS=SIN(ALPHA)
      DO 211 IB=1,MM
      SMFR(IB)=1.0-(BOB(JB)+ZB(IB)*DB(JB))*CS
      AJ=2.0*SMFR(IB)
      IF(MAXSY.NE.1) AJ=1.0
      UBARUI=(UB(IB,JB)*SS+VB(IB,JB)*CS)/(GG*XMACH)
      DMFR(IB)=UBARUI*EXP(RB(IB,JB))*AJ
  211 CONTINUE
      CALL SIMP(SMFR,DMFR,MM,ACTMFR)
      ACTMFR=ABS(ACTMFR)
C
C     COMPUTATION OF AXIS POINTS (METHOD OF CHARACTERISTICS)
C
      DO 250 JB=3,NNB
      SHX1=SHX(JB)
      THETA2=THETAB+YB(JB)*(THETAC-THETAB)
      XSIN2=-SIN(THETA2)
      XCOS2=COS(THETA2)
C     FIRST STEP OF MACCORMACK SCHEME FOR POINTS ON AXIS OF SYMMETRY
      XVAX(JB)=UB(MM,JB)*XCOS2+VB(MM,JB)*XSIN2
      ETA=XVAX(JB)*DELT
      IF(JB.EQ.NNB) GO TO 215
      UYB=(UB(MM,JB+1)-UB(MM,JB))/DELYB
      VYB=(VB(MM,JB+1)-VB(MM,JB))/DELYB
      PYB=(PB(MM,JB+1)-PB(MM,JB))/DELYB
      E=EXP(PB(MM,JB)-RB(MM,JB))
      DXVETA=XSIN2*(UYB*XCOS2+VYB*XSIN2)/((THETAC-THETAB)*SHX1)
      APETA=(XSIN2*PYB)/(SHX1*(THETAC-THETAB))
      DXVDTAX(JB)=-(XVAX(JB)*DXVETA+E*APETA)
      BIGVN=XVAX(JB)+DXVDTAX(JB)*DELT
      UNB(MM,JB)=BIGVN*XCOS2
      VNB(MM,JB)=BIGVN*XSIN2
      DTHE=-ATAN((XSIN2*ETA)/(SHX1-XCOS2*ETA))
      DELYE=DTHE/(THETAC-THETAB)
      SYB=(SB(MM,JB+1)-SB(MM,JB-1))/DY2B
      SYYB=(SB(MM,JB+1)+SB(MM,JB-1)-2.0*SB(MM,JB))/DYSQB
      SNB(MM,JB)=SB(MM,JB)+SYB*DELYE+0.5*SYYB*DELYE*DELYE
  215 CONTINUE
      ME=1
```

```
      A1(ME)=GG*EXP(0.5*(PB(MM,JB)-RB(MM,JB)))
      IJK=0
  201 IJK=IJK+1
      XI=ABS(A1(ME))*DELT
      RSTAR=SQRT(SHX1*SHX1+ETA*ETA+XI*XI-2.0*SHX1*(XCOS2*ETA+XSIN2*XI))
      DTHEST=ATAN((XCOS2*XI-XSIN2*ETA)/(SHX1-(XCOS2*ETA+XSIN2*XI)))
      DELYS=DTHEST/(THETAC-THETAB)
      IF(JB.EQ.NNB) GO TO 208
      BOST=BOB(JB)+((BOB(JB+1)-BOB(JB-1))/DY2B)*DELYS
     1+((BOB(JB+1)+BOB(JB-1)-2.0*BOB(JB))/DYSQB)*0.5*DELYS*DELYS
      BOYST=BOYB(JB)+((BOYB(JB+1)-BOYB(JB-1))/DY2B)*DELYS
     1+((BOYB(JB+1)+BOYB(JB-1)-2.0*BOYB(JB))/DYSQB)*0.5*DELYS*DELYS
      GO TO 209
  208 CONTINUE
      BOST=BOB(NNB)+(BOB(NB1)-BOB(NNB))*(ABS(DTHEST)/DTHB)
      BOYST=BOYB(NNB)+(BOYB(NB1)-BOYB(NNB))*(ABS(DTHEST)/DTHB)
      DTHE=ATAN(ETA/SHX(NNB))
      SNB(MM,NNB)=SB(MM,NNB)+(SB(MM,NB1)-SB(MM,NNB))*(DTHE/DTHB)
  209 CONTINUE
      SHXST=-1.0/SIN(THETA2+DTHEST)
      SHXYST=COS(THETA2+DTHEST)/(SIN(THETA2+DTHEST)*SIN(THETA2+DTHEST))
      ZBST=(RSTAR-BOST)/(SHXST-BOST)
      DELZS=ZBST-ZB(M)
      DBST=SHXST-BOST
      CSTAR=(BOYST*(ZBST-1.0)/DBST)-((ZBST*SHXYST)/DBST)
      IF(ABS(DELYS).GT.DELYB.OR.ABS(DELZS).GT.DELZB) GO TO 255
      DELZS=(1.0-ZBST)/DELZB
      DELYS=DELYS/DELYB
      FAC=1.0
      L=JB+1
      IF(DELYS.LT.0.0) L=JB-1
      IF(DELYS.LT.0.0) FAC=-1.0
      DELYS=ABS(DELYS)
      U1=UB(MM,JB)+(UB(MM,L)-UB(MM,JB))*DELYS
      V1=VB(MM,JB)+(VB(MM,L)-VB(MM,JB))*DELYS
      R1=RB(MM,JB)+(RB(MM,L)-RB(MM,JB))*DELYS
      P1=PB(MM,JB)+(PB(MM,L)-PB(MM,JB))*DELYS
      U3=UB(M,JB)+(UB(M,L)-UB(M,JB))*DELYS
      V3=VB(M,JB)+(VB(M,L)-VB(M,JB))*DELYS
      R3=RB(M,JB)+(RB(M,L)-RB(M,JB))*DELYS
      P3=PB(M,JB)+(PB(M,L)-PB(M,JB))*DELYS
      U2=UB(MM,L)+(UB(M,L)-UB(MM,L))*DELZS
      V2=VB(MM,L)+(VB(M,L)-VB(MM,L))*DELZS
      R2=RB(MM,L)+(RB(M,L)-RB(MM,L))*DELZS
      P2=PB(MM,L)+(PB(M,L)-PB(MM,L))*DELZS
      U4=UB(MM,JB)+(UB(M,JB)-UB(MM,JB))*DELZS
      V4=VB(MM,JB)+(VB(M,JB)-VB(MM,JB))*DELZS
      R4=RB(MM,JB)+(RB(M,JB)-RB(MM,JB))*DELZS
      P4=PB(MM,JB)+(PB(M,JB)-PB(MM,JB))*DELZS
      UBST=U1+(U3-U1)*DELZS
      VBST=V1+(V3-V1)*DELZS
      RBST=R1+(R3-R1)*DELZS
      PBST=P1+(P3-P1)*DELZS
      IF(JB.EQ.NNB) GO TO 210
      L5=JB-1
      IF(L.LT.JB) L5=JB+1
      U5=UB(MM,L5)+(UB(M,L5)-UB(MM,L5))*DELZS
      V5=VB(MM,L5)+(VB(M,L5)-VB(MM,L5))*DELZS
      P5=PB(MM,L5)+(PB(M,L5)-PB(MM,L5))*DELZS
      UYBST=FAC*(U2-U5)/DY2B+FAC*(U2+U5-2.0*U4)*(DELYS/DELYB)
```

```
      VYBST=FAC*(V2-V5)/DY2B+FAC*(V2+V5-2.0*V4)*(DELYS/DELYB)
      PYBST=FAC*(P2-P5)/DY2B+FAC*(P2+P5-2.0*P4)*(DELYS/DELYB)
      GO TO 212
  210 CONTINUE
      UYBST=(U4-U2)/DELYB
      VYBST=(V4-V2)/DELYB
      PYBST=(P4-P2)/DELYB
  212 CONTINUE
      UZBST=(U1-U3)/DELZB
      VZBST=(V1-V3)/DELZB
      PZBST=(P1-P3)/DELZB
      CS=COS(DTHEST)
      SS=SIN(DTHEST)
      ALOC=GG*EXP(0.5*(PBST-RBST))
      ULOC=-(UBST*CS-VBST*SS)*XSIN2+(VBST*CS+UBST*SS)*XCOS2
      VLOC=(UBST*CS-VBST*SS)*XCOS2+(VBST*CS+UBST*SS)*XSIN2
      ULOCY=-(UYBST*CS-VYBST*SS)*XSIN2+(VYBST*CS+UYBST*SS)*XCOS2
     1+VLOC*(THETAC-THETAB)
      ULOCZ=-(UZBST*CS-VZBST*SS)*XSIN2+(VZBST*CS+UZBST*SS)*XCOS2
      VLOCY=(UYBST*CS-VYBST*SS)*XCOS2+(VYBST*CS+UYBST*SS)*XSIN2
     1-ULOC*(THETAC-THETAB)
      VLOCZ=(UZBST*CS-VZBST*SS)*XCOS2+(VZBST*CS+UZBST*SS)*XSIN2
      SAL=(SHX1*XCOS2-ETA)/RSTAR
      CAL=(SHX1*XSIN2-XI)/RSTAR
      ULOCR=ULOCZ/DBST
      VLOCR=VLOCZ/DBST
      PR=PZBST/DBST
      ULOCTH=ULOCZ*CSTAR+ULOCY/(THETAC-THETAB)
      VLOCTH=VLOCZ*CSTAR+VLOCY/(THETAC-THETAB)
      PTH=PZBST*CSTAR+PYBST/(THETAC-THETAB)
      UETA=SAL*ULOCR+CAL*ULOCTH/RSTAR
      VETA=SAL*VLOCR+CAL*VLOCTH/RSTAR
      PETA=SAL*PR+CAL*PTH/RSTAR
      VC=UBST*SIN(THETA2+DTHEST)+VBST*COS(THETA2+DTHEST)
      AFJ=(G*VC)/(1.0+RSTAR*SIN(THETA2+DTHEST))
      IF(MAXSY.NE.1) AFJ=0.0
      RHX=-(G*VETA+VLOC*PETA+AFJ-G*VLOC*UETA/ALOC)*DELT
      XXP=RHX-G*ULOC/ALOC+PBST
      XXR=(XXP-SNB(MM,JB))/G
      XXA=GG*EXP(0.5*(XXP-XXR))
      DIF3(ME)=(A1(ME)-0.5*(-XXA+ULOC-ALOC))*DELT
      IF(ABS(DIF3(ME)/XXA).LT.EPS2.OR.IJK.GT.IJKMAX) GO TO 230
      GO TO (205,206)ME
  205 ME=2
      A1(2)=0.5*(-XXA+ULOC-ALOC)
      GO TO 201
  206 ABAR=A1(1)-DIF3(1)*(A1(2)-A1(1))/(DIF3(2)-DIF3(1))
      A1(1)=A1(2)
      DIF3(1)=DIF3(2)
      A1(2)=ABAR
      GO TO 201
  230 PNB(MM,JB)=XXP
      RNB(MM,JB)=XXR
  250 CONTINUE
      GO TO 280
  255 WRITE(2,260)K,JB,IJK,DELYS,DELZS,RSTAR,DTHEST,SHXST,BOST
  260 FORMAT(/,1X,18HAXIS POINT FAILURE,/,1X,3I5,/,1X,6F15.7)
      GO TO 2001
  280 CONTINUE
C
```

```
C       EVALUATION OF BODY POINTS (MESH A)
C
        DO 450 JA=2,NNA
        BOL=BOA(JA)
        XSIN2=SBOA(JA)
        XCOS2=CBOA(JA)
C       FIRST STEP OF MACCORMACK SCHEME
        XVA(JA)=UA(1,JA)*XCOS2+VA(1,JA)*XSIN2
        UYA=(UA(1,JA+1)-UA(1,JA))/DELYA
        VYA=(VA(1,JA+1)-VA(1,JA))/DELYA
        PYA=(PA(1,JA+1)-PA(1,JA))/DELYA
        E=EXP(PA(1,JA)-RA(1,JA))
        DXVETA=(XSIN2*(UYA*XCOS2+VYA*XSIN2))/(BOA(JA)*(THETAB-THETAA))
        BPETA=(XSIN2*PYA)/(BOA(JA)*(THETAB-THETAA))
        DXVDTA(JA)=-(XVA(JA)*DXVETA+E*BPETA)
        BIGVN=XVA(JA)+DXVDTA(JA)*DELT
        UNA(1,JA)=BIGVN*XCOS2
        VNA(1,JA)=BIGVN*XSIN2
C       END OF FIRST STEP OF MACCORMACK SCHEME
        ETA=-XVA(JA)*DELT
        DTHE=ATAN((XSIN2*ETA)/(BOL+XCOS2*ETA))
        SNA(1,JA)=SA(1,JA)+(SA(1,JA)-SA(1,JA-1))*(DTHE/DTHA)
        ME=1
        A1(ME)=GG*EXP(0.5*(PA(1,JA)-RA(1,JA)))
        IJK=0
  401   IJK=IJK+1
        XI=ABS(A1(ME)*DELT)
        RSTAR=SQRT(BOL*BOL+ETA*ETA+XI*XI+2.0*BOL*(ETA*XCOS2+XI*XSIN2))
        DTHEST=ATAN((XSIN2*ETA-XCOS2*XI)/(BOL+XCOS2*ETA+XSIN2*XI))
        DELYS=DTHEST/(THETAB-THETAA)
        IF(JA.NE.NNA) GO TO 402
        IF(DTHEST.GT.0.0.AND.JA.EQ.NNA) GO TO 408
        DTHEST1=DTHA-ABS(DTHEST)
        BOST=BOA(NNA)+BOYA(NNA)*DTHEST+BOYYA(NNA)*DTHEST*DTHEST*0.5
        BOYST=BOYA(NNA)+BOYYA(NNA)*DTHEST
        SHST=SH(NA)+SHY(NA)*DTHEST1+SHYY(NA)*DTHEST1*DTHEST1*0.5
        SHYST=SHY(NA)+SHYY(NA)*DTHEST1
        DAST=SHST-BOST
        ZAST=(RSTAR-BOST)/(SHST-BOST)
        DELZS=ZAST-ZA(2)
        GO TO 403
  408   CONTINUE
        BOST=BOA(NNA)+BOYA(NNA)*DTHEST+BOYYA(NNA)*DTHEST*DTHEST*0.5
        BOYST=BOYA(NNA)+BOYYA(NNA)*DTHEST
        SHST=-(1.0/SIN(THETAB+DTHEST))
        SHYST=COS(THETAB+DTHEST)/(SIN(THETAB+DTHEST)*SIN(THETAB+DTHEST))
        DAST=SHST-BOST
        ZAST=(RSTAR-BOST)/DAST
        DELZS=ZAST-ZA(2)
        GO TO 403
  402   CONTINUE
        DELYS=(DTHEST/(THETAB-THETAA))
        BOST=BOA(JA)+((BOA(JA+1)-BOA(JA-1))/DY2A)*DELYS+0.5*((BOA(JA+1)+
       1BOA(JA-1)-2.0*BOA(JA))/DYSQA)*DELYS*DELYS
        BOYST=BOYA(JA)+((BOYA(JA+1)-BOYA(JA-1))/DY2A)*DELYS+0.5*DELYS*DELY
       1S*((BOYA(JA+1)+BOYA(JA-1)-2.0*BOYA(JA))/DYSQA)
        SHST=SH(JA)+((SH(JA+1)-SH(JA-1))/DY2A)*DELYS+0.5*DELYS*DELYS*
       1((SH(JA+1)+SH(JA-1)-2.0*SH(JA))/DYSQA)
        SHYST=SHY(JA)+((SHY(JA+1)-SHY(JA-1))/DY2A)*DELYS+0.5*DELYS*DELYS*
       1((SHY(JA+1)+SHY(JA-1)-2.0*SHY(JA))/DYSQA)
        ZAST=(RSTAR-BOST)/(SHST-BOST)
```

```
      DELZS=ZAST-ZA(2)
      DAST=SHST-BOST
  403 CONTINUE
      CSTAR=(BOYST*(ZAST-1.0)/DAST)-((ZAST*SHYST)/DAST)
      IF(ABS(DELZS).GT.DELZA.OR.ABS(DELYS).GT.DELYA) GO TO 4005
      GO TO 4025
 4005 WRITE(2,4010)
 4010 FORMAT(/,1X,22HBODY POINT FAILURE (A))
      WRITE(2,4015)K,JA,ME
 4015 FORMAT(3I3)
      WRITE(2,4020)DELZS,DELZA,DELYS,DELYA,RSTAR,DTHEST,BOST,SHST,A1(ME)
 4020 FORMAT(9F10.6)
      GO TO 2001
 4025 CONTINUE
      FAC=1.0
      L=JA+1
      DELZS=ZAST
      IF(DTHEST.LT.0.0) FAC=-1.0
      IF(DTHEST.LT.0.0) L=JA-1
      DELYS=ABS(DELYS)/DELYA
      U1=UA(1,JA)+((UA(2,JA)-UA(1,JA))/DELZA)*DELZS
      V1=VA(1,JA)+((VA(2,JA)-VA(1,JA))/DELZA)*DELZS
      R1=RA(1,JA)+((RA(2,JA)-RA(1,JA))/DELZA)*DELZS
      P1=PA(1,JA)+((PA(2,JA)-PA(1,JA))/DELZA)*DELZS
      U3=UA(1,L)+((UA(2,L)-UA(1,L))/DELZA)*DELZS
      V3=VA(1,L)+((VA(2,L)-VA(1,L))/DELZA)*DELZS
      R3=RA(1,L)+((RA(2,L)-RA(1,L))/DELZA)*DELZS
      P3=PA(1,L)+((PA(2,L)-PA(1,L))/DELZA)*DELZS
      U2=UA(1,JA)+(UA(1,L)-UA(1,JA))*DELYS
      V2=VA(1,JA)+(VA(1,L)-VA(1,JA))*DELYS
      R2=RA(1,JA)+(RA(1,L)-RA(1,JA))*DELYS
      P2=PA(1,JA)+(PA(1,L)-PA(1,JA))*DELYS
      U4=UA(2,JA)+(UA(2,L)-UA(2,JA))*DELYS
      V4=VA(2,JA)+(VA(2,L)-VA(2,JA))*DELYS
      R4=RA(2,JA)+(RA(2,L)-RA(2,JA))*DELYS
      P4=PA(2,JA)+(PA(2,L)-PA(2,JA))*DELYS
      L5=JA-1
      IF(L.LT.JA) L5=JA+1
      U5=UA(1,L5)+(UA(2,L5)-UA(1,L5))*(DELZS/DELZA)
      V5=VA(1,L5)+(VA(2,L5)-VA(1,L5))*(DELZS/DELZA)
      P5=PA(1,L5)+(PA(2,L5)-PA(1,L5))*(DELZS/DELZA)
      UYAST=FAC*(U3-U5)/DY2A+FAC*(U3+U5-2.0*U1)*(DELYS/DELYA)
      VYAST=FAC*(V3-V5)/DY2A+FAC*(V3+V5-2.0*V1)*(DELYS/DELYA)
      PYAST=FAC*(P3-P5)/DY2A+FAC*(P3+P5-2.0*P1)*(DELYS/DELYA)
      UZAST=(U4-U2)/DELZA
      VZAST=(V4-V2)/DELZA
      PZAST=(P4-P2)/DELZA
      UAST=U2+((U4-U2)/DELZA)*DELZS
      VAST=V2+((V4-V2)/DELZA)*DELZS
      RAST=R2+((R4-R2)/DELZA)*DELZS
      PAST=P2+((P4-P2)/DELZA)*DELZS
      SS=SIN(DTHEST)
      CS=COS(DTHEST)
      ULOC=-(UAST*CS-VAST*SS)*XSIN2+(VAST*CS+UAST*SS)*XCOS2
      VLOC= (UAST*CS-VAST*SS)*XCOS2+(VAST*CS+UAST*SS)*XSIN2
      ULOCY=-(UYAST*CS-VYAST*SS)*XSIN2+(VYAST*CS+UYAST*SS)*XCOS2
     1+VLOC*(THETAB-THETAA)
      ULOCZ=-(UZAST*CS-VZAST*SS)*XSIN2+(VZAST*CS+UZAST*SS)*XCOS2
      VLOCY=(UYAST*CS-VYAST*SS)*XCOS2+(VYAST*CS+UYAST*SS)*XSIN2
```

```
     1-ULOC*(THETAB-THETAA)
      VLOCZ=(UZAST*CS-VZAST*SS)*XCOS2+(VZAST*CS+UZAST*SS)*XSIN2
      SAL=(XCOS2*BOL+ETA)/RSTAR
      CAL=(XSIN2*BOL+XI)/RSTAR
      CSTAR=(BOYST*(ZAST-1.0)/DAST)-(ZAST*SHYST/DAST)
      ALOC=GG*SQRT(EXP(0.5*(PAST-RAST)))
      ULOCR=ULOCZ/DAST
      VLOCR=VLOCZ/DAST
      PR=PZAST/DAST
      ULOCTH=ULOCZ*CSTAR+ULOCY/(THETAB-THETAA)
      VLOCTH=VLOCZ*CSTAR+VLOCY/(THETAB-THETAA)
      PTH=PZAST*CSTAR+PYAST/(THETAB-THETAA)
      UETA=SAL*ULOCR+CAL*ULOCTH/RSTAR
      VETA=SAL*VLOCR+CAL*VLOCTH/RSTAR
      PETA=SAL*PR+CAL*PTH/RSTAR
      THETA1=THETAA+YA(JA)*(THETAB-THETAA)
      VC=UAST*SIN(THETA1+DTHEST)+VAST*COS(THETA1+DTHEST)
      AFJ=(G*VC)/(1.0+RSTAR*SIN(THETA1+DTHEST))
      IF(MAXSY.NE.1) AFJ=0.0
      RHX=-(G*VETA+VLOC*PETA+AFJ+G*VLOC*UETA/ALOC)*DELT
      XXP=PAST+G*ULOC/ALOC+RHX
      PNA(1,JA)=XXP
      RNA(1,JA)=(PNA(1,JA)-SNA(1,JA))/G
      XXA=GG*EXP(0.5*(XXP-RNA(1,JA)))
      DIF3(ME)=(A1(ME)-0.5*(ALOC+ULOC+XXA))*DELT
      IF(ABS(DIF3(ME)/XXA).LT.EPS2.OR.IJK.GT.IJKMAX) GO TO 450
      GO TO (405,406)ME
  405 ME=2
      A1(2)=0.5*(XXA+ALOC+ULOC)
      GO TO 401
  406 ABAR=A1(1)-DIF3(1)*(A1(2)-A1(1))/(DIF3(2)-DIF3(1))
      A1(1)=A1(2)
      DIF3(1)=DIF3(2)
      A1(2)=ABAR
      GO TO 401
  450 CONTINUE
      UNA(1,1)=2.0*UNA(1,2)-UNA(1,3)
      VNA(1,1)=2.0*VNA(1,2)-VNA(1,3)
      RNA(1,1)=2.0*RNA(1,2)-RNA(1,3)
      PNA(1,1)=2.0*PNA(1,2)-PNA(1,3)
      SNA(1,1)=2.0*SNA(1,2)-SNA(1,3)
C
CC    EVALUATION OF BODY POINTS (MESH B)
C
      DO 350 JB=2,NNB
      BOL=BOB(JB)
      XSIN2=SBOB(JB)
      XCOS2=CBOB(JB)
      XVB(JB)=UB(1,JB)*XCOS2+VB(1,JB)*XSIN2
      ETA=-XVB(JB)*DELT
      IF(JB.EQ.NNB) GO TO 355
      UYB=(UB(1,JB+1)-UB(1,JB))/DELYB
      VYB=(VB(1,JB+1)-VB(1,JB))/DELYB
      PYB=(PB(1,JB+1)-PB(1,JB))/DELYB
      E=EXP(PB(1,JB)-RB(1,JB))
      DXVETA=(XSIN2*(UYB*XCOS2+VYB*XSIN2))/(BOB(JB)*(THETAC-THETAB))
      BPETA=(XSIN2*PYB)/(BOB(JB)*(THETAC-THETAB))
      DXVDTB(JB)=-(XVB(JB)*DXVETA+E*BPETA)
      BIGVN=XVB(JB)+DXVDTB(JB)*DELT
      UNB(1,JB)=BIGVN*XCOS2
```

```
      VNB(1,JB)=BIGVN*XSIN2
  355 CONTINUE
      DTHE=ATAN((XSIN2*ETA)/(BOL+XCOS2*ETA))
      SNB(1,JB)=SB(1,JB)+(SB(1,JB)-SB(1,JB-1))*(DTHE/DTHB)
      ME=1
      A1(ME)=GG*EXP(0.5*(PB(1,JB)-RB(1,JB)))
      IJK=0
  301 IJK=IJK+1
      XI=ABS(A1(ME)*DELT)
      RSTAR=SQRT(BOL*BOL+ETA*ETA+XI*XI+2.0*BOL*(ETA*XCOS2+XI*XSIN2))
      DTHEST=ATAN((XSIN2*ETA-XCOS2*XI)/(BOL+XCOS2*ETA+XSIN2*XI))
      DELYS=DTHEST/(THETAC-THETAB)
      IF(JB.NE.2) GO TO 302
      IF(DTHEST.LT.0.0.AND.JB.EQ.2) GO TO 340
      YBST=DTHEST/(THETAC-THETAB)
      BOST=BOB(2)+((BOB(3)-BOB(2))*YBST)/DELYB
      BOYST=BOYB(2)+((BOYB(3)-BOYB(2))*YBST)/DELYB
      SHXST=SHX(2)+((SHX(3)-SHX(2))*YBST)/DELYB
      SHXYST=SHXY(2)+((SHXY(3)-SHXY(2))*YBST)/DELYB
      DBST=SHXST-BOST
      ZBST=(RSTAR-BOST)/(SHXST-BOST)
      DELZS=ZBST-ZB(2)
      GO TO 303
  340 CONTINUE
      BOST=BOB(2)+BOYB(2)*DTHEST+BOYYB(2)*DTHEST*DTHEST*0.5
      BOYST=BOYB(2)+BOYYB(2)*DTHEST
      SHXST=SH(NA)+SHY(NA)*(DTHA-ABS(DTHEST))+SHYY(NA)*(DTHA-ABS(DTHEST)
     1)*(DTHA-ABS(DTHEST))*0.5
      SHXYST=SHY(NA)+SHYY(NA)*(DTHA-ABS(DTHEST))
      DBST=SHXST-BOST
      ZBST=(RSTAR-BOST)/DBST
      DELZS=ZBST-ZB(2)
      GO TO 303
  302 CONTINUE
      IF(JB.EQ.NNB) GO TO 308
      BOST=BOB(JB)+((BOB(JB+1)-BOB(JB-1))/DY2B)*DELYS+((BOB(JB+1)+BOB(JB
     1-1)-2.0*BOB(JB))/DYSQB)*0.5*DELYS*DELYS
      BOYST=BOYB(JB)+((BOYB(JB+1)-BOYB(JB-1))/DY2B)*DELYS+0.5*DELYS*DELY
     1S*((BOYB(JB+1)+BOYB(JB-1)-2.0*BOYB(JB))/DYSQB)
      GO TO 309
  308 CONTINUE
      BOST=BOB(NNB)+(BOB(NB1)-BOB(NNB))*(ABS(DTHEST)/DTHB)
      BOYST=BOYB(NNB)+(BOYB(NB1)-BOYB(NNB))*(ABS(DTHEST)/DTHB)
  309 CONTINUE
      THETA2=THETAB+YB(JB)*(THETAC-THETAB)
      SHXST=-1.0/(SIN(THETA2+DTHEST))
      SHXYST=COS(THETA2+DTHEST)/(SIN(THETA2+DTHEST)*SIN(THETA2+DTHEST))
      DBST=SHXST-BOST
      ZBST=(RSTAR-BOST)/(SHXST-BOST)
      DELZS=ZBST-ZB(2)
  303 CONTINUE
      CSTAR=(BOYST*(ZBST-1.0)/DBST)-((ZBST*SHXYST)/DBST)
      IF(ABS(DELZS).GT.DELZB.OR.ABS(DELYS).GT.DELYB) GO TO 4030
      GO TO 4060
 4030 WRITE(2,4035)
 4035 FORMAT(/,1X,22HBODY POINT FAILURE (B))
      WRITE(2,4041)K,JB,ME
 4041 FORMAT(3I3)
      WRITE(2,4042)DELZS,DELZB,DELYS,DELYB,RSTAR,DTHEST,BOST,SHST,A1(ME)
 4042 FORMAT(9F10.6)
```

```
      GO TO 2001
 4060 CONTINUE
      FAC=1.0
      L=JB+1
      DELZS=ZBST
      IF(DTHEST.LT.0.0) FAC=-1.0
      IF(DTHEST.LT.0.0) L=JB-1
      DELYS=ABS(DELYS)/DELYB
      U1=UB(1,JB)+((UB(2,JB)-UB(1,JB))/DELZB)*DELZS
      V1=VB(1,JB)+((VB(2,JB)-VB(1,JB))/DELZB)*DELZS
      R1=RB(1,JB)+((RB(2,JB)-RB(1,JB))/DELZB)*DELZS
      P1=PB(1,JB)+((PB(2,JB)-PB(1,JB))/DELZB)*DELZS
      U3=UB(1,L)+((UB(2,L)-UB(1,L))/DELZB)*DELZS
      V3=VB(1,L)+((VB(2,L)-VB(1,L))/DELZB)*DELZS
      R3=RB(1,L)+((RB(2,L)-RB(1,L))/DELZB)*DELZS
      P3=PB(1,L)+((PB(2,L)-PB(1,L))/DELZB)*DELZS
      U2=UB(1,JB)+(UB(1,L)-UB(1,JB))*DELYS
      V2=VB(1,JB)+(VB(1,L)-VB(1,JB))*DELYS
      R2=RB(1,JB)+(RB(1,L)-RB(1,JB))*DELYS
      P2=PB(1,JB)+(PB(1,L)-PB(1,JB))*DELYS
      U4=UB(2,JB)+(UB(2,L)-UB(2,JB))*DELYS
      V4=VB(2,JB)+(VB(2,L)-VB(2,JB))*DELYS
      R4=RB(2,JB)+(RB(2,L)-RB(2,JB))*DELYS
      P4=PB(2,JB)+(PB(2,L)-PB(2,JB))*DELYS
      IF(JB.EQ.NNB) GO TO 310
      L5=JB-1
      IF(L.LT.JB) L5=JB+1
      U5=UB(1,L5)+(UB(2,L5)-UB(1,L5))*(DELZS/DELZB)
      V5=VB(1,L5)+(VB(2,L5)-VB(1,L5))*(DELZS/DELZB)
      P5=PB(1,L5)+(PB(2,L5)-PB(1,L5))*(DELZS/DELZB)
      UYBST=FAC*(U3-U5)/DY2B+FAC*(U3+U5-2.0*U1)*(DELYS/DELYB)
      VYBST=FAC*(V3-V5)/DY2B+FAC*(V3+V5-2.0*V1)*(DELYS/DELYB)
      PYBST=FAC*(P3-P5)/DY2B+FAC*(P3+P5-2.0*P1)*(DELYS/DELYB)
      GO TO 311
  310 CONTINUE
      UYBST=(U1-U3)/DELYB
      VYBST=(V1-V3)/DELYB
      PYBST=(P1-P3)/DELYB
  311 CONTINUE
      UBST=U2+((U4-U2)/DELZB)*DELZS
      VBST=V2+((V4-V2)/DELZB)*DELZS
      RBST=R2+((R4-R2)/DELZB)*DELZS
      PBST=P2+((P4-P2)/DELZB)*DELZS
      UZBST=(U4-U2)/DELZB
      VZBST=(V4-V2)/DELZB
      RZBST=(R4-R2)/DELZB
      PZBST=(P4-P2)/DELZB
      SS=SIN(DTHEST)
      CS=COS(DTHEST)
      ALOC=GG*EXP(0.5*(PBST-RBST))
      ULOC=-(UBST*CS-VBST*SS)*XSIN2+(VBST*CS+UBST*SS)*XCOS2
      VLOC=(UBST*CS-VBST*SS)*XCOS2+(VBST*CS+UBST*SS)*XSIN2
      ULOCZ=-(UZBST*CS-VZBST*SS)*XSIN2+(VZBST*CS+UZBST*SS)*XCOS2
      ULOCY=-(UYBST*CS-VYBST*SS)*XSIN2+(VYBST*CS+UYBST*SS)*XCOS2
     1+VLOC*(THETAC-THETAB)
      VLOCY=(UYBST*CS-VYBST*SS)*XCOS2+(VYBST*CS+UYBST*SS)*XSIN2
     1-ULOC*(THETAC-THETAB)
      VLOCZ=(UZBST*CS-VZBST*SS)*XCOS2+(VZBST*CS+UZBST*SS)*XSIN2
      SAL=(BOL*XCOS2+ETA)/RSTAR
      CAL=(BOL*XSIN2+XI)/RSTAR
```

```
      ULOCR=ULOCZ/DBST
      VLOCR=VLOCZ/DBST
      PR=PZBST/DBST
      ULOCTH=ULOCZ*CSTAR+ULOCY/(THETAC-THETAB)
      VLOCTH=VLOCZ*CSTAR+VLOCY/(THETAC-THETAB)
      PTH=PZBST*CSTAR+PYBST/(THETAC-THETAB)
      UETA=SAL*ULOCR+CAL*ULOCTH/RSTAR
      VETA=SAL*VLOCR+CAL*VLOCTH/RSTAR
      PETA=SAL*PR+CAL*PTH/RSTAR
      THETA2=THETAB+YB(JB)*(THETAC-THETAB)
      VC=UBST*SIN(THETA2+DTHEST)+VBST*COS(THETA2+DTHEST)
      AFJ=(G*VC)/(1.0+RSTAR*SIN(THETA2+DTHEST))
      IF(MAXSY.NE.1) AFJ=0.0
      RHX=-(G*VETA+VLOC*PETA+AFJ+G*VLOC*UETA/ALOC)*DELT
      XXP=PBST+G*ULOC/ALOC+RHX
      PNB(1,JB)=XXP
      RNB(1,JB)=(XXP-SNB(1,JB))/G
      XXA=GG*EXP(0.5*(XXP-RNB(1,JB)))
      DIF3(ME)=(A1(ME)-0.5*(ALOC+ULOC+XXA))*DELT
      IF(ABS(DIF3(ME)/XXA).LT.EPS2.OR.IJK.GT.IJKMAX) GO TO 330
      GO TO (305,306)ME
  305 ME=2
      A1(2)=0.5*(XXA+ALOC+ULOC)
      GO TO 301
  306 IF(DIF3(1).EQ.DIF3(2))WRITE(2,207)DIF3(1),A1(1),A1(2),ABAR,XXA,
     1K,JB
  207 FORMAT(1X,24HBODY POINT (B) ITERATION,/,1X,5E15.6,2I5)
      ABAR=A1(1)-DIF3(1)*(A1(2)-A1(1))/(DIF3(2)-DIF3(1))
      A1(1)=A1(2)
      DIF3(1)=DIF3(2)
      A1(2)=ABAR
      GO TO 301
  330 CONTINUE
  350 CONTINUE
C
C     EVALUATION OF SUBSONIC BOUNDARY POINTS
C
C     EVALUATION OF POINTS C AND F
      UNB(1,NNB)=0.0
      DTHE=ATAN(VB(1,NNB)*DELT/BOB(NNB))
      SNB(1,NNB)=SB(1,NNB)+(SB(1,NB1)-SB(1,NNB))*(DTHE/DTHB)
      RNB(1,NNB)=(PNB(1,NNB)-SNB(1,NNB))/G
      UNB(MM,NNB)=0.0
C
C     INTERIOR POINTS ON SUBSONIC BOUNDARY
      DO 850 IB=2,M
      RL=DB(NNB)*ZB(IB)+BOB(NNB)
      ME=1
      MES=1
      XXA=GG*EXP(0.5*(PB(IB,NNB)-RB(IB,NNB)))
      A1(ME)=UB(IB,NNB)+XXA
        AS(MES)=UB(IB,NNB)-XXA
      ETA=VB(IB,NNB)*DELT
      IJK=0
  801 IJK=IJK+1
C
C      INTEGRATION ALONG U+A CHARACTERISTICS
      XI=-A1(ME)*DELT
      RSTAR=SQRT(ETA*ETA+(RL+XI)**2)
      DTHEST=ASIN(ABS(ETA/RSTAR))
```

```
SHXST=(1.0/SIN(THETAC-DTHEST))
SHXYST=COS(THETAC-DTHEST)/(SIN(THETAC-DTHEST)*SIN(THETAC-DTHEST))
BOST=BOB(NNB)+(BOB(NB1)-BOB(NNB))*(DTHEST/DTHB)
BOYST=BOYB(NNB)+(BOYB(NB1)-BOYB(NNB))*(DTHEST/DTHB)
DBST=SHXST-BOST
ZBST=(RSTAR-BOST)/DBST
DELYS=ABS(DTHEST)/(THETAC-THETAB)
DELZS=ZBST-ZB(IB)
IF(ABS(DELYS).GT.DELYB.OR.ABS(DELZS).GT.DELZB) GO TO 855
CSTAR=(BOYST*(ZBST-1.0)-ZBST*SHXYST)/DBST
FAC=1.0
L=IB+1
IF(ZBST.LT.ZB(IB))L=IB-1
IF(ZBST.LT.ZB(IB)) FAC=-1.0
DELZS=ABS(DELZS)/DELZB
DELYS=ABS(DELYS)/DELYB
U1=UB(IB,NNB)+(UB(L,NNB)-UB(IB,NNB))*DELZS
V1=VB(IB,NNB)+(VB(L,NNB)-VB(IB,NNB))*DELZS
R1=RB(IB,NNB)+(RB(L,NNB)-RB(IB,NNB))*DELZS
P1=PB(IB,NNB)+(PB(L,NNB)-PB(IB,NNB))*DELZS
U3=UB(IB,NB1)+(UB(L,NB1)-UB(IB,NB1))*DELZS
V3=VB(IB,NB1)+(VB(L,NB1)-VB(IB,NB1))*DELZS
R3=RB(IB,NB1)+(RB(L,NB1)-RB(IB,NB1))*DELZS
P3=PB(IB,NB1)+(PB(L,NB1)-PB(IB,NB1))*DELZS
P6=PB(IB,NB)+(PB(L,NB)-PB(IB,NB))*DELZS
U6=UB(IB,NB)+(UB(L,NB)-UB(IB,NB))*DELZS
V6=VB(IB,NB)+(VB(L,NB)-VB(IB,NB))*DELZS
R6=RB(IB,NB)+(RB(L,NB)-RB(IB,NB))*DELZS
U2=UB(L,NNB)+(UB(L,NB1)-UB(L,NNB))*DELYS
V2=VB(L,NNB)+(VB(L,NB1)-VB(L,NNB))*DELYS
R2=RB(L,NNB)+(RB(L,NB1)-RB(L,NNB))*DELYS
P2=PB(L,NNB)+(PB(L,NB1)-PB(L,NNB))*DELYS
U4=UB(IB,NNB)+(UB(IB,NB1)-UB(IB,NNB))*DELYS
V4=VB(IB,NNB)+(VB(IB,NB1)-VB(IB,NNB))*DELYS
R4=RB(IB,NNB)+(RB(IB,NB1)-RB(IB,NNB))*DELYS
P4=PB(IB,NNB)+(PB(IB,NB1)-PB(IB,NNB))*DELYS
UBST1=U4+(U2-U4)*DELZS
VBST1=V4+(V2-V4)*DELZS
RBST1=R4+(R2-R4)*DELZS
PBST1=P4+(P2-P4)*DELZS
UZBST=FAC*(U2-U4)/DELZB
VZBST=FAC*(V2-V4)/DELZB
PZBST=FAC*(P2-P4)/DELZB
UYBST=(U1-U6)/DY2B+(U1+U6-2.0*U3)*((1.0-DELYS)/DELYB)
VYBST=(V1-V6)/DY2B+(V1+V6-2.0*V3)*((1.0-DELYS)/DELYB)
PYBST=(P1-P6)/DY2B+(P1+P6-2.0*P3)*((1.0-DELYS)/DELYB)
SS=SIN(DTHEST)
CS=COS(DTHEST)
ALOC1=GG*EXP(0.5*(PBST1-RBST1))
ULOC1=UBST1*CS+VBST1*SS
VLOC1=VBST1*CS-UBST1*SS
ULOCZ=UZBST*CS+VZBST*SS
VLOCZ=VZBST*CS-UZBST*SS
ULOCY=UYBST*CS+VYBST*SS+(THETAC-THETAB)*VLOC1
VLOCY=VYBST*CS-UYBST*SS-(THETAC-THETAB)*ULOC1
ULOCR=ULOCZ/DBST
VLOCR=VLOCZ/DBST
PR=PZBST/DBST
ULOCTH=ULOCY/(THETAC-THETAB)+ULOCZ*CSTAR
VLOCTH=VLOCY/(THETAC-THETAB)+VLOCZ*CSTAR
PTH=PYBST/(THETAC-THETAB)+PZBST*CSTAR
```

```
      UETA=(ULOCTH*CS)/RSTAR-ULOCR*SS
      VETA=(VLOCTH*CS)/RSTAR-VLOCR*SS
      PETA=(PTH/RSTAR)*CS-PR*SS
      AFJ=G*(-ULOC1)/(1.0-RSTAR*CS)
      IF(MAXSY.NE.1) AFJ=0.0
      RHX1=-(G*VETA+VLOC1*PETA+AFJ+(G*VLOC1*UETA)/ALOC1)*DELT
      ALOCA1=0.5*(ALOC1+XXA)
      RHS1=RHX1+PBST1+ULOC1*(G/ALOCA1)
C
C      INTEGRATION ALONG U-A CHARACTERISTICS
      XI=-AS(MES)*DELT
      RSTAR=SQRT(ETA*ETA+(RL+XI)**2)
      DTHEST=ASIN(ABS(ETA/RSTAR))
      SHXST=-(1.0/SIN(THETAC-DTHEST))
      SHXYST=COS(THETAC-DTHEST)/(SIN(THETAC-DTHEST)*SIN(THETAC-DTHEST))
      BOST=BOB(NNB)+(BOB(NB1)-BOB(NNB))*(DTHEST/DTHB)
      BOYST=BOYB(NNB)+(BOYB(NB1)-BOYB(NNB))*(DTHEST/DTHB)
      DBST=SHXST-BOST
      ZBST=(RSTAR-BOST)/DBST
      DELYS=ABS(DTHEST)/(THETAC-THETAB)
      DELZS=ZBST-ZB(IB)
      IF(ABS(DELYS).GT.DELYB.OR.ABS(DELZS).GT.DELZB) GO TO 855
      CSTAR=(BOYST*(ZBST-1.0)-ZBST*SHXYST)/DBST
      FAC=1.0
      L=IB+1
      IF(ZBST.LT.ZB(IB))L=IB-1
      IF(ZBST.LT.ZB(IB)) FAC=-1.0
      DELZS=ABS(DELZS)/DELZB
      DELYS=ABS(DELYS)/DELYB
      U1=UB(IB,NNB)+(UB(L,NNB)-UB(IB,NNB))*DELZS
      V1=VB(IB,NNB)+(VB(L,NNB)-VB(IB,NNB))*DELZS
      R1=RB(IB,NNB)+(RB(L,NNB)-RB(IB,NNB))*DELZS
      P1=PB(IB,NNB)+(PB(L,NNB)-PB(IB,NNB))*DELZS
      U3=UB(IB,NB1)+(UB(L,NB1)-UB(IB,NB1))*DELZS
      V3=VB(IB,NB1)+(VB(L,NB1)-VB(IB,NB1))*DELZS
      R3=RB(IB,NB1)+(RB(L,NB1)-RB(IB,NB1))*DELZS
      P3=PB(IB,NB1)+(PB(L,NB1)-PB(IB,NB1))*DELZS
      P6=PB(IB,NB)+(PB(L,NB)-PB(IB,NB))*DELZS
      U6=UB(IB,NB)+(UB(L,NB)-UB(IB,NB))*DELZS
      V6=VB(IB,NB)+(VB(L,NB)-VB(IB,NB))*DELZS
      R6=RB(IB,NB)+(RB(L,NB)-RB(IB,NB))*DELZS
      U2=UB(L,NNB)+(UB(L,NB1)-UB(L,NNB))*DELYS
      V2=VB(L,NNB)+(VB(L,NB1)-VB(L,NNB))*DELYS
      R2=RB(L,NNB)+(RB(L,NB1)-RB(L,NNB))*DELYS
      P2=PB(L,NNB)+(PB(L,NB1)-PB(L,NNB))*DELYS
      U4=UB(IB,NNB)+(UB(IB,NB1)-UB(IB,NNB))*DELYS
      V4=VB(IB,NNB)+(VB(IB,NB1)-VB(IB,NNB))*DELYS
      R4=RB(IB,NNB)+(RB(IB,NB1)-RB(IB,NNB))*DELYS
      P4=PB(IB,NNB)+(PB(IB,NB1)-PB(IB,NNB))*DELYS
      PBST2=P4+(P2-P4)*DELZS
      UBST2=U4+(U2-U4)*DELZS
      VBST2=V4+(V2-V4)*DELZS
      RBST2=R4+(R2-R4)*DELZS
      UZBST=FAC*(U2-U4)/DELZB
      VZBST=FAC*(V2-V4)/DELZB
      PZBST=FAC*(P2-P4)/DELZB
      UYBST=(U1-U6)/DY2B+(U1+U6-2.0*U3)*((1.0-DELYS)/DELY
      VYBST=(V1-V6)/DY2B+(V1+V6-2.0*V3)*((1.0-DELYS)/DE
```

```
      PYBST=(P1-P6)/DY2B+(P1+P6-2.0*P3)*((1.0-DELYS)/DELYB)
      SS=SIN(DTHEST)
      CS=COS(DTHEST)
      VLOC2=VBST2*CS-UBST2*SS
      ULOC2=UBST2*CS+VBST2*SS
      ALOC2=GG*EXP(0.5*(PBST2-RBST2))
      ULOCZ=UZBST*CS+VZBST*SS
      VLOCZ=VZBST*CS-UZBST*SS
      ULOCY=UYBST*CS+VYBST*SS+(THETAC-THETAB)*VLOC2
      VLOCY=VYBST*CS-UYBST*SS-(THETAC-THETAB)*ULOC2
      ULOCR=ULOCZ/DBST
      VLOCR=VLOCZ/DBST
      PR=PZBST/DBST
      ULOCTH=ULOCY/(THETAC-THETAB)+ULOCZ*CSTAR
      VLOCTH=VLOCY/(THETAC-THETAB)+VLOCZ*CSTAR
      PTH=PYBST/(THETAC-THETAB)+PZBST*CSTAR
      UETA=(ULOCTH*CS)/RSTAR-ULOCR*SS
      VETA=(VLOCTH*CS)/RSTAR-VLOCR*SS
      PETA=(PTH*CS)/RSTAR-PR*SS
      AFJ=G*(-ULOC2)/(1.0-RSTAR*CS)
      IF(MAXSY.NE.1) AFJ=0.0
      RHX2=-(G*VETA+VLOC2*PETA+AFJ-(G*VLOC2*UETA)/ALOC2)*DELT
      ALOCA2=0.5*(ALOC2+XXA)
      RHS2=RHX2+PBST2-ULOC2*(G/ALOCA2)
      UNB(IB,NNB)=(RHS1-RHS2)*(ALOCA1*ALOCA2)/(G*(ALOCA1+ALOCA2))
      PNB(IB,NNB)=RHS1-(G/ALOCA1)*UNB(IB,NNB)
C
C     INTEGRATION ALONG U CHARACTERISTIC
      XI=-UNB(IB,NNB)*DELT
      RSTAR=RL+XI
      ZBST=(RSTAR-BOB(NNB))/DB(NNB)
      DELZS=ZBST-ZB(IB)
      L=IB+1
      FAC=1.0
      IF(ZBST.LT.ZB(IB)) L=IB-1
      IF(ZBST.LT.ZB(IB)) FAC=-1.0
      DELZS=ABS(DELZS)/DELZB
      S1=SB(IB,NNB)+(SB(L,NNB)-SB(IB,NNB))*DELZS
      VLOC=VB(IB,NNB)+(VB(L,NNB)-VB(IB,NNB))*DELZS
      S2=SB(IB,NB1)+(SB(L,NB1)-SB(IB,NB1))*DELZS
      SZBST=FAC*(SB(L,NNB)-SB(IB,NNB))/DELZB
      SYBST=(S1-S2)/DELYB
      CSTAR=(BOYB(NNB)*(ZBST-1.0)-ZBST*SHXY(NNB))/DB(NNB)
      SZBST=(SB(L,NNB)-SB(IB,NNB))*(FAC/DELZB)
      STH=SYBST/(THETAC-THETAB)+SZBST*CSTAR
      SETA=STH/RSTAR
      SNB(IB,NNB)=S1-(VLOC*SETA)*DELT
      RNB(IB,NNB)=(PNB(IB,NNB)-SNB(IB,NNB))/G
      XXA=GG*EXP(0.5*(PNB(IB,NNB)-RNB(IB,NNB)))
      IF(ME.EQ.1) GO TO 805
      ER1=(PNB(IB,NNB)-PNB1)/PNB1
      ER2=(UNB(IB,NNB)-UNB1)/UNB1
      IF(ABS(ER1).LT.EPS3.AND.ABS(ER2).LT.EPS3) GO TO 830
      IF(IJK.GT.IJKMAX) GO TO 830
      PNB1=PNB(IB,NNB)
      UNB1=UNB(IB,NNB)
      GO TO 801
  805 ME=2
      MES=2
      A1(2)=0.5*(ULOC1+ALOC1+XXA+UNB(IB,NNB))
      AS(2)=0.5*(UNB(IB,NNB)-XXA+ULOC2-ALOC2)
      PNB1=PNB(IB,NNB)
```

```
      UNB1=UNB(IB,NNB)
      GO TO 801
  830 CONTINUE
  850 CONTINUE
      GO TO 860
  855 WRITE(2,865)
  865 FORMAT(/,5X,25HSUBSONIC BOUNDARY FAILURE)
      WRITE(2,4042)DELZS,DELZB,DELYS,DELYB,RSTAR,DTHEST,BOST,SHXST,A1(ME
     1)
      WRITE(2,4041) K,IB,ME
      GO TO 2001
  860 CONTINUE
C
C     EVALUATION OF AXIAL VELOCITY ON THE SUBSONIC BOUNDARY
C
      IF(MAXSY.EQ.1) GO TO 218
      DO 217 IB=1,MM
      SMFR(IB)=1.0-(DB(NNB)*ZB(IB)+BOB(NNB))
      AJ=2.0*SMFR(IB)
      IF(MAXSY.NE.1) AJ=1.0
      DMFR(IB)=AJ*(EXP(RNB(IB,NNB)))/(XMACH*GG)
  217 CONTINUE
      CALL SIMP(SMFR,DMFR,MM,VBSUB1)
      VBSUB1=ABS(VBSUB1)
      VBSUB=AMFR/VBSUB1
  218 CONTINUE
      DO 213 IB=1,MM
      VNB(IB,NNB)=VBSUB
  213 CONTINUE
C
C     INTERIOR POINTS   (MESH A)
      DO 448 JA=2,NNA
      WT=(WNT(JA)-W(JA))/DELT
      YA1=YA(JA)
      SHY1=SHY(JA)*SIGA
      BOYA1=BOYA(JA)*SIGA
      BOYYA1=BOYYA(JA)*(SIGA*SIGA)
      WY=YW(JA)
      DYA=SHY1-BOYA1
      SINA=SIN(SIGA*YA1+THETAA)
      COSA=COS(SIGA*YA1+THETAA)
      SHYY1=SHYY(JA)*SIGA*SIGA
      DTA=(SHY(JA)-BOYA(JA))*SIGTA*YA1+W(JA)
      DO 449 IA=2,M
      RLA=ZA(IA)*DA(JA)+BOA(JA)
      ZA1=ZA(IA)
      RLZA=DA(JA)
      RLYA=ZA1*DYA+BOYA1
      RLTA=ZA1*DTA+BOYA(JA)*SIGTA*YA1
      CALL DERIV(IA,JA,UA,VA,RA,PA,DZ2A,DZSQA,DY2A,DYSQA,DYDZA,UYA,VYA,
     1RYA,PYA,UZA,VZA,RZA,PZA,UYYA,VYYA,RYYA,PYYA,UZZA,VZZA,RZZA,PZZA,
     2UYZA,VYZA,RYZA,PYZA)
      SZA=PZA-G*RZA
      SZZA=PZZA-G*RZZA
      SYA=PYA-G*RYA
      SYYA=PYYA-G*RYYA
      SYZA=PYZA-G*RYZA
      AAA=(VA(IA,JA)/RLA-YA1*SIGTA)/SIGA
      AZA=(VZA-VA(IA,JA)*RLZA/RLA)/(RLA*SIGA)
```

```
      AYA=(VYA-VA(IA,JA)*RLYA/RLA-RLA*SIGTA)/(RLA*SIGA)
      CA=(ZA1-1.0)*BOYA(JA)-ZA1*SHY(JA)
      CZA=BOYA(JA)-SHY(JA)
      CYA=(ZA1-1.0)*SIGA*BOYYA(JA)-ZA1*SIGA*SHYY(JA)
      CTA=(ZA1-1.0)*(BOYA(JA)*SIGTA*YA1)-ZA1*WY/SIGA
      BA=(-W(JA)*ZA1+UA(IA,JA)+VA(IA,JA)*CA/RLA)/DA(JA)
      BZA=(-W(JA)+UZA+(VA(IA,JA)*CZA+CA*VZA-VA(IA,JA)*CA*RLZA/RLA)/RLA)
     1/DA(JA)
      BYA=(-ZA1*WY+UYA+(VA(IA,JA)*CYA+CA*VYA-VA(IA,JA)*CA*RLYA/RLA)/RLA-
     1BA*DYA)/DA(JA)
      EA=EXP(PA(IA,JA)-RA(IA,JA))
      FA=0.0
      FZA=0.0
      FYA=0.0
      IF(MAXSY.NE.1) GO TO 446
      FA=(UA(IA,JA)*SINA+VA(IA,JA)*COSA)/(1.0+RLA*SINA)
      FZA=((UZA-FA*RLZA)*SINA+VZA*COSA)/(1.0+RLA*SINA)
      FYA=((UYA-VA(IA,JA)*SIGA-FA*RLYA)*SINA+(VYA+UA(IA,JA)*SIGA-FA*RLA*
     1SIGA)*COSA)/(1.0+RLA*SINA)
  446 CONTINUE
      UTA=-(BA*UZA+AAA*UYA-VA(IA,JA)*VA(IA,JA)/RLA+EA*PZA/DA(JA))
      VTA=-(BA*VZA+AAA*VYA+UA(IA,JA)*VA(IA,JA)/RLA+PZA*EA*CA/(RLA*DA(JA)
     1)+PYA*EA/(RLA*SIGA))
      RTA=-(BA*RZA+AAA*RYA+UZA/DA(JA)+CA*VZA/(RLA*DA(JA))+VYA/(RLA*SIGA)
     1+UA(IA,JA)/RLA+FA)
      STA=-(BA*SZA+AAA*SYA)
      PTA=STA+G*RTA
      ATA=(VTA-VA(IA,JA)*RLTA/RLA-RLA*YA1*SIGTTA-(VA(IA,JA)-RLA*YA1*SIGT
     1A)*(SIGTA/SIGA))/(SIGA*RLA)
      BTA=(-ZA1*WT+UTA+(VA(IA,JA)*CTA+CA*VTA-VA(IA,JA)*CA*RLTA/RLA)/RLA
     1-BA*DTA)/DA(JA)
      FTA=((UTA-VA(IA,JA)*YA1*SIGTA-FA*RLTA)*SINA
     1+(VTA+UA(IA,JA)*YA1*SIGTA-RLA*YA1*FA*SIGTA)*COSA)/(1.0+RLA*SINA)
      IF(MAXSY.NE.1) FTA=0.0
      RZTA=-((BA*RZZA+BZA*RZA)+(AAA*RYZA+AZA*RYA)+UZZA/DA(JA)
     1+VZZA*CA/(RLA*DA(JA))+VZA*(CZA-CA*RLZA/RLA)/(RLA*DA(JA))+
     2(VYZA-RLZA*VYA/RLA)/(RLA*SIGA)+(UZA-UA(IA,JA)*RLZA/RLA)/RLA+FZA)
      RYTA=-(BA*RYZA+BYA*RZA+AAA*RYYA+AYA*RYA+(UYZA-DYA*UZA/DA(JA))/DA
     1(JA)+(CA/(RLA*DA(JA)))*VYZA+VZA*(CYA-(CA/(RLA*DA(JA)))*(RLA*DYA+
     2DA(JA)*RLYA))/(RLA*DA(JA))+(VYYA-RLYA*VYA/RLA)/(RLA*SIGA)+(UYA-
     3(UA(IA,JA)/RLA)*RLYA)/RLA+FYA)
      UZTA=-(BA*UZZA+BZA*UZA+AAA*UYZA+AZA*UYA
     1-(VA(IA,JA)/RLA)*(2.0*VZA-(VA(IA,JA)/RLA)*RLZA)
     2+EA*(PZZA+PZA*PZA-PZA*RZA)/DA(JA))
      UYTA=-(BA*UYZA+BYA*UZA+AAA*UYYA+AYA*UYA-(2.0*VYA-VA(IA,JA)*RLY
     1A/RLA)*VA(IA,JA)/RLA+(PYZA+PZA*PYA-PZA*RYA-DYA*PZA/DA(JA))*EA/DA(J
     2A))
      VZTA=-(BA*VZZA+BZA*VZA+AAA*VYZA+AZA*VYA+(UA(IA,JA)*VZA+VA(IA,JA)*
     1UZA-(UA(IA,JA)*VA(IA,JA)/RLA)*RLZA)/RLA+
     2(CA*EA/(RLA*DA(JA)))*(PZZA+PZA*PZA-PZA*RZA)
     3+(PZA*EA/(RLA*DA(JA)))*(CZA-(CA/RLA)*RLZA)
     4+(EA/(RLA*SIGA))*(PYZA+PZA*PYA-RZA*PYA-RLZA*PYA/RLA))
      VYTA=-(BA*VYZA+BYA*VZA+AAA*VYYA+AYA*VYA+(UA(IA,JA)*VYA+VA(IA,JA)
     1*UYA-UA(IA,JA)*VA(IA,JA)*RLYA/RLA)/RLA+CA*EA*(PYZA+PZA*PYA-PZA*RLY
     2A-DYA*PZA/DA(JA))/(RLA*DA(JA))+EA*PZA*(CYA-CA*RLYA/RLA)/(RLA*DA(JA
     3))+EA*(PYYA+PYA*PYA-PYA*RYA-RLYA*PYA/RLA)/(RLA*SIGA))
      SZTA=-(BA*SZZA+BZA*SZA+AAA*SYZA+AZA*SYA)
      SYTA=-(BA*SYZA+BYA*SZA+AAA*SYYA+AYA*SYA)
      PYTA=SYTA+G*RYTA
      PZTA=SZTA+G*RZTA
```

```
      RTTA=-(BA*RZTA+BTA*RZA+AAA*RYTA+ATA*RYA+(UZTA-DTA*UZA/DA(JA))/DA(
     1JA)+CA*VZTA/(RLA*DA(JA))+(CTA-CA*(RLA*DTA+DA(JA)*RLTA)/(RLA*DA(JA)
     2))*VZA/(RLA*DA(JA))+(VYTA-RLTA*VYA/RLA)/(RLA*SIGA)-SIGTA*VYA/(RLA
     3*SIGA*SIGA)+(UTA-UA(IA,JA)*RLTA/RLA)/RLA+FTA)
      UTTA=-(BA*UZTA+BTA*UZA+AAA*UYTA+ATA*UYA
     1-VA(IA,JA)*(2.0*VTA-VA(IA,JA
     1)*RTA/RLA)/RLA+(EA/DA(JA))*(PZTA+PTA*PZA-RTA*PZA-DTA*PZA/DA(JA)))
      VTTA=-(BA*VZTA+BTA*VZA+AAA*VYTA+ATA*VYA+(UA(IA,JA)*VTA+VA(IA,JA)*
     1UTA-UA(IA,JA)*VA(IA,JA)*RLTA/RLA)/RLA+(CA*EA/(RLA*DA(JA)))*(PZTA+
     2PTA*PZA-RTA*PZA-DTA*PZA/DA(JA))+(PZA*EA/(RLA*DA(JA)))*(CTA-CA*RL
     3TA/RLA)+(EA/(RLA*DA(JA)))*(PYTA+PTA*PYA-RTA*PYA-RLTA*PYA/RLA)
     4-EA*PYA*SIGTA/(RLA*SIGA*SIGA))
      STTA=-(BA*SZTA+BTA*SZA+AAA*SYTA+ATA*SYA)
      UNA(IA,JA)=UA(IA,JA)+UTA*DELT+0.5*UTTA*DELT*DELT
      VNA(IA,JA)=VA(IA,JA)+VTA*DELT+0.5*VTTA*DELT*DELT
      RNA(IA,JA)=RA(IA,JA)+RTA*DELT+0.5*RTTA*DELT*DELT
      SNA(IA,JA)=SA(IA,JA)+STA*DELT+0.5*STTA*DELT*DELT
      PNA(IA,JA)=SNA(IA,JA)+G*RNA(IA,JA)
  449 CONTINUE
  448 CONTINUE
      DO 447 IA=2,M
      UNA(IA,1)=2.0*UNA(IA,2)-UNA(IA,3)
      VNA(IA,1)=2.0*VNA(IA,2)-VNA(IA,3)
      RNA(IA,1)=2.0*RNA(IA,2)-RNA(IA,3)
      SNA(IA,1)=2.0*SNA(IA,2)-SNA(IA,3)
      PNA(IA,1)=SNA(IA,1)+G*RNA(IA,1)
  447 CONTINUE
C
C     INTERIOR POINTS (MESH B)
C
      SIGB=THETAC-THETAB
      SIGTB=-THBT
      SIGTTB=-THBTT
      DO 550 JB=2,NB1
      YB1=YB(JB)
      SHXY1=SHXY(JB)*SIGB
      SHXYY1=SHXYY(JB)*SIGB*SIGB
      BOYB1=BOYB(JB)*SIGB
      BOYYB1=BOYYB(JB)*SIGB*SIGB
      DYB=SHXY1-BOYB1
      SINB=SIN(SIGB*YB1+THETAB)
      COSB=COS(SIGB*YB1+THETAB)
      DTB=(SHXY(JB)-BOYB(JB))*SIGTB*(YB1-1.0)
      DO 549 IB=2,M
      ZB1=ZB(IB)
      RLB=ZB1*DB(JB)+BOB(JB)
      RLYB=ZB1*DYB+BOYB1
      RLZB=DB(JB)
      RLTB=ZB1*DTB+BOYB(JB)*SIGTB*(YB1-1.0)
      CALL DERIV(IB,JB,UB,VB,RB,PB,DZ2B,DZSQB,DY2B,DYSQB,DYDZB,UYB,VYB,
     1RYB,PYB,UZB,VZB,RZB,PZB,UYYB,VYYB,RYYB,PYYB,UZZB,VZZB,RZZB,PZZB,
     2UYZB,VYZB,RYZB,PYZB)
      SYB=PYB-G*RYB
      SYYB=PYYB-G*RYYB
      SYZB=PYZB-G*RYZB
      SZZB=PZZB-G*RZZB
      SZB=PZB-G*RZB
      AAB=(VB(IB,JB)/RLB-(1.0-YB1)*SIGTB)/SIGB
      AZB=(VZB-(VB(IB,JB)/RLB)*RLZB)/(RLB*SIGB)
      AYB=(VYB-(VB(IB,JB)/RLB)*RLYB)/(RLB*SIGB)-SIGTB/SIGB
```

```
      CB=(ZB1-1.0)*BOYB(JB)-ZB1*SHXY(JB)
      CZB=BOYB(JB)-SHXY(JB)
      CYB=(ZB1-1.0)*SIGB*BOYYB(JB)-ZB1*SIGB*SHXYY(JB)
      BB=(UB(IB,JB)+VB(IB,JB)*CB/RLB)/DB(JB)
      BZB=(UZB+(VB(IB,JB)*CZB+CB*VZB-(VB(IB,JB)*CB/RLB)*RLZB)/RLB)/DB(JB
     1)
      BYB=(UYB+(VB(IB,JB)*CYB+CB*VYB-(VB(IB,JB)*CB/RLB)*RLYB)/RLB
     1-BB*DYB)/DB(JB)
      FB=0.0
      FZB=0.0
      FYB=0.0
      IF(MAXSY.NE.1) GO TO 546
      FB=(UB(IB,JB)*SINB+VB(IB,JB)*COSB)/(1.0+RLB*SINB)
      FZB=((UZB-FB*RLZB)*SINB+VZB*COSB)/(1.0+RLB*SINB)
      FYB=((UYB-VB(IB,JB)*SIGB-FB*RLYB)*SINB+(VYB+UB(IB,JB)*SIGB-FB*RLB
     1*SIGB)*COSB)/(1.0+RLB*SINB)
  546 CONTINUE
      RTB=-(BB*RZB+AAB*RYB+UZB/DB(JB)+(CB/(RLB*DA(JB)))*VZB+VYB/(RLB*
     1SIGB)+UB(IB,JB)/RLB +FB)
      EB=EXP(PB(IB,JB)-RB(IB,JB))
      UTB=-(BB*UZB+AAB*UYB-VB(IB,JB)*VB(IB,JB)/RLB+EB*PZB/DB(JB))
      VTB=-(BB*VZB+AAB*VYB+(UB(IB,JB)*VB(IB,JB)/RLB)+
     1(CB*EB/(RLB*DB(JB)))*PZB+(EB/(RLB*SIGB))*PYB)
      STB=-(BB*SZB+AAB*SYB)
      ATB=(VTB-(VB(IB,JB)/RLB)*RLTB-VB(IB,JB)*SIGTB/SIGB)/(RLB*SIGB)
     1-(1.0-YB1)*(-SIGTTB+SIGTB*SIGTB/SIGB)/SIGB
      CTB=(ZB1-1.0)*BOYB(JB)*(YB1-1.0)*SIGTB-ZB1*SHXY(JB)*(YB1-1.0)*SIGT
     1B
      BTB=(UTB+(VB(IB,JB)*CTB+CB*VTB-(VB(IB,JB)*CB/RLB)*RLTB)/RLB-BB*DT
     1B)/DB(JB)
      FTB=((UTB+VB(IB,JB)*(1.0-YB1)*SIGTB-FB*RLTB)*SINB+(VTB-UB(IB,JB)*(
     11.0-YB1)*SIGTB+RLB*(1.0-YB1)*FB*SIGTB)*COSB)/(1.0+RLB*SINB)
      IF(MAXSY.NE.1) FTB=0.0
      RZTB=-(BB*RZZB+BZB*RZB+AAB*RYZB+AZB*RYB+UZZB/DB(JB) +
     1(CB/(RLB*DB(JB)))*VZZB+VZB*(CZB-(CB/RLB)*RLZB)/(RLB*DB(JB))+
     2(VYZB-RLZB*VYB/RLB)/(RLB*SIGB)+(UZB-(UB(IB,JB)/RLB)*RLZB)/RLB+FZB)
      RYTB=-(BB*RYZB+BYB*RZB+AAB*RYYB+AYB*RYB+
     1(UYZB-DYB*UZB/DB(JB))/DB(JB)+(CB/(RLB*DB(JB)))*VYZB+
     2(CYB-(CB/(RLB*DB(JB)))*(RLB*DYB+DB(JB)*RYB))*VZB/(RLB*DB(JB))+
     3(VYYB-RLYB*VYB/RLB)/(RLB*SIGB)+(UYB-(UB(IB,JB)/RLB)*RLYB)/RLB
     4+FYB)
      UZTB=-(BB*UZZB+BZB*UZB+AAB*UYZB+AZB*UYB-(VB(IB,JB)/RLB)*(2.0*VZB
     1-(VB(IB,JB)/RLB)*RLZB)+(EB/DB(JB))*(PZZB+PZB*PZB-PZB*RZB))
      SZTB=-(BB*SZZB+BZB*SZB+AAB*SYZB+AZB*SYB)
      SYTB=-(BB*SYZB+BYB*SZB+AAB*SYYB+AYB*SYB)
      STTB=-(BB*SZTB+BTB*SZB+AAB*SYTB+ATB*SYB)
      PZTB=SZTB+G*RZTB
      PYTB=SYTB+G*RYTB
      PTB=STB+G*RTB
      UYTB=-(BB*UYZB+BYB*UZB+AAB*UYYB+AYB*UYB-(VB(IB,JB)/RLB)*(2.0*VYB-
     1(VB(IB,JB)/RLB)*RLYB)+(EB/DB(JB))*(PYZB+PZB*PYB-PZB*RLYB-DYB*PZB/
     1DB(JB)))
      VYTB=-(BB*VYZB+BYB*VZB+AAB*VYYB+AYB*VYB
     1+(UB(IB,JB)*VYB+VB(IB,JB)*UYB-(UB(IB,JB)*VB(IB,JB)/RLB)*RLYB)/RLB+
     2(CB*EB/(RLB*DB(JB)))*(PYZB+PZB*PYB-PZB*RYB-DYB*PZB/DB(JB))
     3+(EB*PZB/(RLB*DB(JB)))*(CYB-(CB/RLB)*RLYB)
```

```
     4+(EB/(RLB*SIGB))*(PYYB+PYB*PYB-PYB*RYB-RLYB*PYB/RLB))
      VZTB=-(BB*VZZB+BZB*VZB+AAB*VYZB+AZB*VYB+(UB(IB,JB)*VZB+VB(IB,JB)*
     1UZB-(UB(IB,JB)*VB(IB,JB)/RLB)*RZB)/RLB+(EB*CB/(RLB*DB(JB)))*(PZZB+
     2PZB*PZB-PZB*RZB)+(PZB*EB/(RLB*DB(JB)))*(CZB-(CB/RLZB)*RLZB)+
     3(EB/(RLB*SIGB))*(PYZB+PZB*PYB-RZB*PYB-RLZB*PYB/RLB))
      RTTB=-(BB*RZTB+BTB*RZB+AAB*RYTB+ATB*RYB
     1+(UZTB-DTB*UZB/DB(JB))/DB(JB)+CB*VZTB/(RLB*DB(JB))
     2+(CTB-(CB/(RLB*DB(JB)))*(RLB*DTB+DB(JB)*RLTB))*VZB/(RLB*DB(JB))
     3+(VYTB-RLTB*VYB/RLB)/(RLB*SIGB)
     4-SIGTB*VYB/(RLB*SIGB*SIGB)
     5+(UTB-(UB(IB,JB)/RLB)*RLTB)/RLB+FTB)
      UTTB=-(BB*UZTB+BTB*UZB+AAB*UYTB+ATB*UYB-(VB(IB,JB)/RLB)*(2.0*VTB-
     1(VB(IB,JB)/RLB)*RLTB)+(EB/DB(JB))*(PZTB+PTB*PZB-RTB*PZB-DTB*PZB
     2/DB(JB)))
      VTTB=-(BB*VZTB+BTB*VZB+AAB*VYTB+ATB*VYB+(UB(IB,JB)*VTB+VB(IB,JB)*
     1UTB-(UB(IB,JB)*VB(IB,JB)/RLB)*RLTB)/RLB+(EB*CB/(RLB*DB(JB)))*(PZTB
     2+PTB*PZB-RTB*PZB-DTB*PZB/DB(JB))+(EB*PZB/(RLB*DB(JB)))*(CTB-(CB/
     3RLB)*RLTB)+(EB/(RLB*SIGB))*(PYTB+PTB*PYB-RTB*PYB-(RLTB*PYB/RLB))
     4-(EB/(RLB*SIGB*SIGB))*PYB*SIGTB)
      UNB(IB,JB)=UB(IB,JB)+UTB*DELT+0.5*UTTB*DELT*DELT
      VNB(IB,JB)=VB(IB,JB)+VTB*DELT+0.5*VTTB*DELT*DELT
      RNB(IB,JB)=RB(IB,JB)+RTB*DELT+0.5*RTTB*DELT*DELT
      SNB(IB,JB)=SB(IB,JB)+STB*DELT+0.5*STTB*DELT*DELT
      PNB(IB,JB)=SNB(IB,JB)+G*RNB(IB,JB)
  549 CONTINUE
  550 CONTINUE
C
C     SECOND STEP OF THE MACCORMACK SCHEME FOR THE AXIS OF SYMMETRY
C
      DO 251 JB=3,NB1
      SHX1=SHX(JB)
      THETA2=THETAB+YB(JB)*(THETAC-THETAB)
      XSIN2=-SIN(THETA2)
      XCOS2=COS(THETA2)
      XV=UNB(MM,JB)*XCOS2+VNB(MM,JB)*XSIN2
      VYB=(VNB(MM,JB)-VNB(MM,JB-1))/DELYB
      UYB=(UNB(MM,JB)-UNB(MM,JB-1))/DELYB
      PYB=(PNB(MM,JB)-PNB(MM,JB-1))/DELYB
      E=EXP(PNB(MM,JB)-RNB(MM,JB))
      DXVETA=XSIN2*(UYB*XCOS2+VYB*XSIN2)/((THETAC-THETAB)*SHX1)
      APETA=(XSIN2*PYB)/(SHX1*(THETAC-THETAB))
      DXVDT=-(XV*DXVETA+E*APETA)
      VMSS(JB)=XVAX(JB)+(DXVDTAX(JB)+DXVDT)*0.5*DELT
  251 CONTINUE
      DO 252 JB=3,NB1
      THETA2=THETAB+YB(JB)*(THETAC-THETAB)
      XSIN2=-SIN(THETA2)
      XCOS2=COS(THETA2)
      UNB(MM,JB)=VMSS(JB)*XCOS2
      VNB(MM,JB)=VMSS(JB)*XSIN2
  252 CONTINUE
      DO 451 JA=2,NNA
      BOL=BOA(JA)
      XSIN2=SBOA(JA)
      XCOS2=CBOA(JA)
      XV=UNA(1,JA)*XCOS2+VNA(1,JA)*XSIN2
      UYA=(UNA(1,JA)-UNA(1,JA-1))/DELYA
      VYA=(VNA(1,JA)-VNA(1,JA-1))/DELYA
      PYA=(PNA(1,JA)-PNA(1,JA-1))/DELYA
      E=EXP(PNA(1,JA)-RNA(1,JA))
      DXVETA=(XSIN2*(UYA*XCOS2+VYA*XSIN2))/(BOA(JA)*(THETAB-THETAA))
      BPETA=(XSIN2*PYA)/(BOA(JA)*(THETAB-THETAA))
```

```
      DXVDT=-(XV*DXVETA+E*BPETA)
      VMSS(JA)=XVA(JA)+(DXVDTA(JA)+DXVDT)*0.5*DELT
  451 CONTINUE
      DO 452 JA=2,NNA
      VNA(1,JA)=VMSS(JA)*SBOA(JA)
  452 UNA(1,JA)=VMSS(JA)*CBOA(JA)
      VNA(1,1)=2.0*VNA(1,2)-VNA(1,3)
      UNA(1,1)=2.0*UNA(1,2)-UNA(1,3)
C     LINEAR INTERPOLATION FOR THE INTERMESH POINT OF BODY B AT THE
C     SECOND STEP OF THE MACCORMACK SCHEME.
      D2=1.0-(DTHB/(THETAB-THETAA))
      LA=NA
      IF(D2.LT.YA(NA)) LA=NA-1
      DELYSA=D2-YA(LA)
      UYA=(UNA(1,LA+1)-UNA(1,LA))/DELYA
      VYA=(VNA(1,LA+1)-VNA(1,LA))/DELYA
      RYA=(RNA(1,LA+1)-RNA(1,LA))/DELYA
      PYA=(PNA(1,LA+1)-PNA(1,LA))/DELYA
      UNB(1,1)=UNA(1,LA)+UYA*DELYSA
      VNB(1,1)=VNA(1,LA)+VYA*DELYSA
      RNB(1,1)=RNA(1,LA)+RYA*DELYSA
      PNB(1,1)=PNA(1,LA)+PYA*DELYSA
      SNB(1,1)=PNB(1,1)-G*RNB(1,1)
C     THE SECOND STEP OF THE MACCORMACK SCHEME FOR BODY B.
      DO 453 JB=2,NB1
      BOL=BOB(JB)
      XSIN2=SBOB(JB)
      XCOS2=CBOB(JB)
      XV=UNB(1,JB)*XCOS2+VNB(1,JB)*XSIN2
      UYB=(UNB(1,JB)-UNB(1,JB-1))/DELYB
      VYB=(VNB(1,JB)-VNB(1,JB-1))/DELYB
      PYB=(PNB(1,JB)-PNB(1,JB-1))/DELYB
      E=EXP(PNB(1,JB)-RNB(1,JB))
      DXVETA=(XSIN2*(UYB*XCOS2+VYB*XSIN2))/(BOL*(THETAC-THETAB))
      BPETA=(XSIN2*PYB)/(BOB(JB)*(THETAC-THETAA))
      DXVDT=-(XV*DXVETA+E*BPETA)
      VMSS(JB)=XVB(JB)+(DXVDTB(JB)+DXVDT)*0.5*DELT
  453 CONTINUE
      DO 454 JB=2,NB1
      UNB(1,JB)=VMSS(JB)*CBOB(JB)
      VNB(1,JB)=VMSS(JB)*SBOB(JB)
  454 CONTINUE
C     END  OF MACCORMACK SCHEME  FOR BODY AND AXIS OF SYMMETRY POINTS
C
C  AVERAGING VALUES ALONG INTERFACE BOUNDARY  (INTERIOR POINTS)
C
      DO 506 I=1,M
      UNA(I,NNA)=0.5*(UNA(I,NNA)+UNB(I,2))
      VNA(I,NNA)=0.5*(VNA(I,NNA)+VNB(I,2))
      RNA(I,NNA)=0.5*(RNA(I,NNA)+RNB(I,2))
      PNA(I,NNA)=0.5*(PNA(I,NNA)+PNB(I,2))
      SNA(I,NNA)=PNA(I,NNA)-G*RNA(I,NNA)
      UNB(I,2)=UNA(I,NNA)
      VNB(I,2)=VNA(I,NNA)
      RNB(I,2)=RNA(I,NNA)
      PNB(I,2)=PNA(I,NNA)
      SNB(I,2)=SNA(I,NNA)
  506 CONTINUE
C
```

```
C
C     RESET VALUES FOR NEW TIME STEP
C
      THETAB=THETABN
      THBT=THBTN
      CALL BODYA
      CALL BODYB
      DO 605 JA=1,NNA
      DO 600 IA=1,MM
      UA(IA,JA)=UNA(IA,JA)
      VA(IA,JA)=VNA(IA,JA)
      RA(IA,JA)=RNA(IA,JA)
      SA(IA,JA)=SNA(IA,JA)
      PA(IA,JA)=PNA(IA,JA)
  600 CONTINUE
  605 CONTINUE
      DO 615 JB=2,NNB
      DO 610 IB=1,MM
      UB(IB,JB)=UNB(IB,JB)
      VB(IB,JB)=VNB(IB,JB)
      RB(IB,JB)=RNB(IB,JB)
      PB(IB,JB)=PNB(IB,JB)
      SB(IB,JB)=SNB(IB,JB)
  610 CONTINUE
  615 CONTINUE
      DO 620 JA=1,NNA
      W(JA)=WNT(JA)
      SH(JA)=SH1(JA)
      XCOT(JA)=XCOT1(JA)
  620 CONTINUE
C
C     LINEAR INTERPOLATION AT INTERFACE POINTS
      DO 3034 I=1,MM
      D1=(DTHA/(THETAC-THETAB))-YB(2)
      D2=1.0-(DTHB/(THETAB-THETAA))
      LB=2
      LA=NA
      IF(D1.GT.YB(3)) LB=3
      IF(D2.LT.YA(NA)) LA=NA-1
      DELYSB=D1-YB(LB)
      DELYSA=D2-YA(LA)
      UYB=(UB(I,LB+1)-UB(I,LB))/DELYB
      VYB=(VB(I,LB+1)-VB(I,LB))/DELYB
      RYB=(RB(I,LB+1)-RB(I,LB))/DELYB
      PYB=(PB(I,LB+1)-PB(I,LB))/DELYB
      VYA=(VA(I,LA+1)-VA(I,LA))/DELYA
      UYA=(UA(I,LA+1)-UA(I,LA))/DELYA
      RYA=(RA(I,LA+1)-RA(I,LA))/DELYA
      PYA=(PA(I,LA+1)-PA(I,LA))/DELYA
      UA(I,NNA1)=UB(I,LB)+UYB*DELYSB
      VA(I,NNA1)=VB(I,LB)+VYB*DELYSB
      RA(I,NNA1)=RB(I,LB)+RYB*DELYSB
      PA(I,NNA1)=PB(I,LB)+PYB*DELYSB
      SA(I,NNA1)=PA(I,NNA1)-G*RA(I,NNA1)
      UB(I,1)=UA(I,LA)+UYA*DELYSA
      VB(I,1)=VA(I,LA)+VYA*DELYSA
      RB(I,1)=RA(I,LA)+RYA*DELYSA
      PB(I,1)=PA(I,LA)+PYA*DELYSA
      SB(I,1)=PB(I,1)-G*RB(I,1)
 3034 CONTINUE
C
```

```
C       INTERMEDIATE OUTPUT ON LINE PRINTER
C
      IF(K.EQ.KMAX) GO TO 5050
      IF((K/JK)*JK.LT.K) GO TO 5010
 5050 CONTINUE
      CALL WRTBOD
      WRITE(2,3040)
 3040 FORMAT(//,1X,29HEXTRA MESH POINTS FOR A AND B)
      WRITE(2,3045)
 3045 FORMAT(/,6X,2HPA,13X,2HMA,13X,2HUA,13X, 2HVA,13X,2HRA,13X,2HSA)
      DO 3050 I=1,MM
      P=EXP(PA(I,NNA1))
      R=EXP(RA(I,NNA1))
      AM1= UA(I,NNA1)*UA(I,NNA1)+VA(I,NNA1)*VA(I,NNA1)
      AM=SQRT(AM1/(G*P/R))
      WRITE(2,3055)P,AM,UA(I,NNA1),VA(I,NNA1),RA(I,NNA1),SA(I,NNA1)
 3055 FORMAT(6F15.7)
 3050 CONTINUE
      WRITE(2,3060)
 3060 FORMAT(/,6X,2HPB,13X,2HMB,13X,2HUB,13X,2HVB,13X,2HRB,13X,2HSB)
      DO 3065 I=1,MM
      P=EXP(PB(I,1))
      R=EXP(RB(I,1))
      AM1=UB(I,1)*UB(I,1)+VB(I,1)*VB(I,1)
      BM=SQRT(AM1/(G*P/R))
      WRITE(2,3070)P,BM,UB(I,1),VB(I,1),RB(I,1),SB(I,1)
 3070 FORMAT(6F15.7)
 3065 CONTINUE
      WRITE(2,2003)
 2003 FORMAT(/,1X,12HSHOCK POINTS,/,6X,2HPA,13X,7HMACH NO,8X,2HRA,13X,
     12HSA,13X,2HUA,13X,2HVA,13X,2HSH,13X,1HW)
      DO 2009 JA=1,NNA
      AP=EXP(PA(MM,JA))
      AR=EXP(RA(MM,JA))
      AM=SQRT(G*AP/AR)
      AM=(SQRT(UA(MM,JA)*UA(MM,JA)+VA(MM,JA)*VA(MM,JA)))/AM
      WRITE(2,2004)AP,AM,AR,SA(MM,JA),UA(MM,JA),VA(MM,JA),SH(JA),W(JA)
 2004 FORMAT(8E15.7)
 2009 CONTINUE
      WRITE(2,2010)
 2010 FORMAT(//,1X,29HVARIABLES ON AXIS OF SYMMETRY)
      WRITE(2,2015)
 2015 FORMAT(//,6X,3HPNB,13X,5HMAXIS,13X,3HUNB,13X,3HVNB,13X,3HRNB,13X,
     13HSNB)
      DO 2025 JB=2,NNB
      PW=EXP(PB(MM,JB))
      RW=EXP(RB(MM,JB))
      AMAX=UB(MM,JB)*UB(MM,JB)+VB(MM,JB)*VB(MM,JB)
      AMAXIS=SQRT(AMAX/(G*PW/RW))
      WRITE(2,2020)PW,AMAXIS,UB(MM,JB),VB(MM,JB),RW,SB(MM,JB)
 2020 FORMAT(6F15.7)
 2025 CONTINUE
      WRITE(2,3000)
 3000 FORMAT(//,1X,22HBODY POINTS FOR MESH A)
      WRITE(2,3005)
 3005 FORMAT(/,6X,3HPNA,13X,2HMA,13X,3HUNA,13X,3HVNA,13X,3HRNA,13X,3HSNA
     1)
      DO 3010 JA=1,NNA
      P=EXP(PA(1,JA))
      R=EXP(RA(1,JA))
      AM1=UA(1,JA)*UA(1,JA)+VA(1,JA)*VA(1,JA)
      AM=SQRT(AM1/(G*P/R))
```

```
      WRITE(2,3015)P,AM,UA(1,JA),VA(1,JA),R,SA(1,JA)
 3015 FORMAT(6F15.7)
 3010 CONTINUE
      WRITE(2,3020)
 3020 FORMAT(//,1X,22HBODY POINTS FOR MESH B)
      WRITE(2,3025)
 3025 FORMAT(/,6X,3HPNB,13X,2HMB,13X,3HUNB,13X,3HVNB,13X,3HRNB,13X,3HSNB
     1)
      DO 3035 JB=2,NNB
      P=EXP(PB(1,JB))
      R=EXP(RB(1,JB))
      AM1=UB(1,JB)*UB(1,JB)+VB(1,JB)*VB(1,JB)
      BM=SQRT(AM1/(G*P/R))
      WRITE(2,3030)P,BM,UB(1,JB),VB(1,JB),R,SB(1,JB)
 3030 FORMAT(6F15.7)
 3035 CONTINUE
      WRITE(2,8000)
 8000 FORMAT(/,9X,30HVARIABLES ON SUBSONIC BOUNDARY,//,
     19X,3HPNB,13X,4HMSUB,13X,3HUNB,10X,3HVNB,10X,3HRNB,10X,3HSNB)
      DO 8010 IB=1,MM
      PE=EXP(PB(IB,NNB))
      RE=EXP(RB(IB,NNB))
      QBS=UB(IB,NNB)*UB(IB,NNB)+VB(IB,NNB)*VB(IB,NNB)
      AMSUB=SQRT(QBS/(G*PE/RE))
      WRITE(2,8030)PE,AMSUB,UB(IB,NNB),VB(IB,NNB),RE,SB(IB,NNB)
 8030 FORMAT(6F15.7)
 8010 CONTINUE
      WRITE(2,9051) DELT,ACCT
 9051 FORMAT(/,1X,5HDELT=,F12.8,5X,5HACCT=,F11.6)
      CALL SECOND(CPU)
      WRITE(2,599)CPU
  599 FORMAT(/,5X,4HCPU=,F12.3)
      RTHAOB=DTHA/DTHB
      WRITE(2,5000)RTHAOB
 5000 FORMAT(/,1X,7HRTHAOB=,F10.6)
      WRITE(2,2030)ACTMFR
 2030  FORMAT(/,1X,23HACTUAL MASS FLOW RATIO=,F10.6)
C
C     EVALUATION OF DRAG COEFFIENTS,PRESSURE RECOVERY AND CONCRIT.
C
      JSTAG=JAE
      IF(QMINB.LT.QMINA) JSTAG=NNA+(JBE-2)
      CDFAC=(2.0)/(G*XMACH*XMACH)
      JMAX=NNA+NNB-2
      DO 510 JA=1,NNA
      J=JA
      CP(J)=CDFAC*(EXP(PA(1,JA))-1.0)
      T(J)=(THETAB-THETAA)*YA(JA)+THETAA
      AJ=(BOA(JA)*SIN(T(J))+1.0)*2.0
      IF(MAXSY.NE.1)AJ=1.0
      SPSI=-(SBOA(JA)*COS(T(J))+CBOA(JA)*SIN(T(J)))
      CPSI=SIN(T(J))*SBOA(JA)-COS(T(J))*CBOA(JA)
      STMS=SIN(T(J))*CPSI-COS(T(J))*SPSI
      DRAG(J)=CP(J)*AJ*BOA(JA)*(SPSI/STMS)
  510 CONTINUE
      DO 511 JB=2,NNB
      J=NNA+JB-2
      CP(J)=CDFAC*(EXP(PB(1,JB))-1.0)
      T(J)=(THETAC-THETAB)*YB(JB)+THETAB
      SPSI=-(SBOB(JB)*COS(T(J))+CBOB(JB)*SIN(T(J)))
```

```
      CPSI=SIN(T(J))*SBOB(JB)-COS(T(J))*CBOB(JB)
      AJ=(BOB(JB)*SIN(T(J))+1.0)*2.0
      IF(MAXSY.NE.1) AJ=1.0
      STMS=SIN(T(J))*CPSI-COS(T(J))*SPSI
      DRAG(J)=CP(J)*AJ*BOB(JB)*(SPSI/STMS)
  511 CONTINUE
      WRITE(2,3026)
 3026 FORMAT(/,5X,5HTHETA,6X,2HCP)
      DO 3028 J=1,JMAX
      THETA1=T(J)*PPYE
      WRITE(2,3027)THETA1,CP(J)
 3027 FORMAT(5X,2F10.6)
 3028 CONTINUE
      CALL SIMP(T,DRAG,JSTAG,CDEXT1)
      CALL SIMP(T,DRAG,JMAX,CDCOWL)
      CDADD1=CDCOWL-CDEXT1
      POIPI=(1.0+(GM1/2.0)*(XMACH**2))**RALEX2
      DO 513 I=1,MM
      IB=MM+1-I
      AJX(I)=1.0-ZB(IB)*DB(NNB)-BOB(NNB)
      AJ=2.0*AJX(I)
      IF(MAXSY.NE.1) AJ=1.0
      DRAG(I)=CDFAC*AJ*(EXP(PB(IB,NNB))-1.0)
     1+CDFAC*AJ*EXP(RB(IB,NNB))*(VB(IB,NNB)**2)
      QCF=SQRT(UB(IB,NNB)*UB(IB,NNB)+VB(IB,NNB)*VB(IB,NNB))
      XMCF=QCF/(GG*EXP(0.5*(PB(IB,NNB)-RB(IB,NNB))))
      POP=(1.0+(GM1/2.0)*(XMCF**2))**RALEX2
      PRY(I)=POP*EXP(PB(IB,NNB))/POIPI
  513 CONTINUE
      PRNS=RAL/POIPI
      CALL SIMP(AJX,PRY,MM,PRA1)
      PRA=PRA1/DB(NNB)
      WRITE(2,512)PRA,PRNS
  512 FORMAT(/,5X,18HPRESSURE RECOVERY=,F10.6,5X,
     122HNORMAL SHOCK RECOVERY=,F10.6)
      CALL SIMP(AJX,DRAG,MM,CDADD2)
      CDADD=CDADD1+CDADD2-2.0*(ACTMFR**(MAXSY+1))
      CDEXT=CDEXT1+CDADD
      WRITE(2,514)CDEXT,CDADD,CDCOWL,CDEXT1,CDADD1,CDADD2
  514 FORMAT(/,3X,5HCDEXT,5X,5HCDADD,5X,6HCDCOWL,4X,6HCDEXT1,
     14X,6HCDADD1,4X,6HCDADD2,/,6F10.6)
      DO 555 JA=1,NNA
      T(JA)=ABS(W(JA))
  555 CONTINUE
      CALL SIMP(YA,T,NNA,WAVEG)
      CONCRIT=WAVEG*DELT
      WRITE(2,556)CONCRIT
  556 FORMAT(/,5X,8HCONCRIT=,F12.8)
 5010 CONTINUE
C
C     OUTPUT ON MAGNETIC TAPE
C
      IF(MAGW.NE.1) GO TO 7050
      IF(K.EQ.KMAX) GO TO 7045
      IF((K/MP)*MP.LT.K) GO TO 7050
 7045 CONTINUE
      MAGR=1
      WRITE(3)M,NA,NB,JK,KJ,MP,IJKMAX,K,KRUN,MAGR,MAGW,MAXSY,NRUN
      WRITE(3)THETAA,THETAB,THETAC,XMACH,ACCT,AELPS,BELPSU,BELPSL
      WRITE(3)G,EPS1,EPS2,EPS3,ENTBOD,RAL,THBT,AMFR
      WRITE(3)(SH(JA),W(JA),XCOT(JA),JA=1,NNA)
```

```
      WRITE(3)((UA(IA,JA),VA(IA,JA),RA(IA,JA),
     1PA(IA,JA),SA(IA,JA),IA=1,MM),JA=1,NNA1)
      WRITE(3)((UB(IB,JB),VB(IB,JB),RB(IB,JB),
     1PB(IB,JB),SB(IB,JB),IB=1,MM),JB=1,NNB)
 7050 CONTINUE
      IF(K.EQ.KMAX) GO TO 5075
      IF((K/KJ)*KJ.LT.K) GO TO 45
 5075 CONTINUE
C
      WRITE(2,6000)
 6000 FORMAT(/,5X,6HMESH A)
      WRITE(2,5030) K
 5030  FORMAT(//,1X,17HNO OF TIME STEPS=,I4)
      WRITE(2,6005)
 6005 FORMAT(/,6X,2HPA,13X,7HMACH NO,10X,2HRA,13X,2HUA,13X,2HVA,13X,2HSA
     1)
      DO 6010 JA=1,NNA
      DO 6015 IA=1,MM
      PW=EXP(PA(IA,JA))
      RW=EXP(RA(IA,JA))
      AMACH=SQRT((UA(IA,JA)*UA(IA,JA)+VA(IA,JA)*VA(IA,JA))/(G*PW/RW))
      WRITE(2,6020)PW,AMACH,RW,UA(IA,JA),VA(IA,JA),SA(IA,JA)
 6020 FORMAT(1X,6E15.7)
 6015 CONTINUE
 6010 CONTINUE
      WRITE(2,6030)
 6030 FORMAT(1H1,5X,6HMESH B)
      WRITE(2,6035)
 6035 FORMAT(/,6X,2HPB,13X,7HMACH NO,10X,2HRB,13X,2HUB,13X,2HVB,13X,2HSB
     1)
      DO 4050 JB=2,NNB
      DO 4045 IB=1,MM
      PW= EXP(PB(IB,JB))
      RW=EXP(RB(IB,JB))
      BMACH=SQRT((UB(IB,JB)*UB(IB,JB)+VB(IB,JB)*VB(IB,JB))/(G*PW/RW))
      WRITE(2,4040)PW,BMACH,RW,UB(IB,JB),VB(IB,JB),SB(IB,JB)
 4040 FORMAT(1X,6E15.7)
 4045 CONTINUE
 4050 CONTINUE
      IF(K.LT.KMAX) GO TO 45
      GO TO 2051
C
C     VARIABLES IN MESH A AND MESH B ARE PRINTED AND THE EXECUTION OF
C     THE PROGRAM STOPPED IF AN INSTABILITY IS DETECTED AT THE AXIS
C     OF SYMMETRY OR INLET SURFACE NODE POINTS.
 2001 CONTINUE
      DO 94 JA=1,NNA1
      DO 98 IA=1,MM
      PA(IA,JA)=EXP(PA(IA,JA))
      RA(IA,JA)=EXP(RA(IA,JA))
   98 CONTINUE
   94 CONTINUE
      DO 96 JB=1,NNB
      DO 97 IB=1,MM
      RB(IB,JB)=EXP(RB(IB,JB))
      PB(IB,JB)=EXP(PB(IB,JB))
   97 CONTINUE
   96 CONTINUE
      WRITE(2,6000)
```

```
      WRITE(2,4043)((UA(IA,JA),VA(IA,JA),RA(IA,JA),PA(IA,JA),IA=1,MM),
     1JA=1,NNA1)
      WRITE(2,6030)
      WRITE(2,4043)((UB(IB,JB),VB(IB,JB),RB(IB,JB),PB(IB,JB),IB=1,MM),
     1JB=1,NNB)
 4043 FORMAT(4E15.7)
 2051 CONTINUE
      STOP
      END
C
      SUBROUTINE WRTBOD
      COMMON/AAA/BOA(27),BOYA(27),BOYYA(27),YA(27),NNA,XNA,DTHA,SBOA(27)
     1,CBOA(27),NNA1,NA
      COMMON/BBB/BOB(27),BOYB(27),BOYYB(27),YB(27),NNB,XNB,DTHB,SBOB(27)
     1,CBOB(27),NB
      COMMON/TTT/THETAA,THETAB,THETAC
      COMMON/INTG/K
      COMMON/ELLIPSE/AELPS,BELPSU,BELPSL
      WRITE(2,5030) K
 5030  FORMAT(//,1X,17HNO OF TIME STEPS=,I4)
      WRITE(2,8000)
 8000 FORMAT(/,1X,2HJA,8X,5HTHETA,8X,1HX,8X,7HBOA(JA),8X,8HBOYA(JA),
     18X,9HBOYYA(JA))
      DO 8020 JA=1,NNA
      XJA=JA-1
      THETA1=THETAA+DTHA*XJA
      X=BOA(JA)*COS(THETA1)
      THETA1=THETA1*(180.0/3.14159265)
      WRITE(2,8010)JA,THETA1,X,BOA(JA),BOYA(JA),BOYYA(JA)
 8010 FORMAT(1X,I2,3X,F10.6 ,6X,F9.6,6X,F6.4,6X,F6.4,6X,F6.4)
 8020 CONTINUE
      WRITE(2,8015)
 8015 FORMAT(//,1X,2HJB,8X,5HTHETA,8X,1HX,8X,7HBOB(JB),8X,8HBOYB(JB),
     18X,9HBOYYB(JB))
      DO 8025 JB=2,NNB
      XJB=JB-2
      THETA2=THETAB+DTHB*XJB
      X=BOB(JB)*COS(THETA2)
      THETA2=THETA2*(180.0/3.14159265)
      WRITE(2,8030)JB,THETA2,X,BOB(JB),BOYB(JB),BOYYB(JB)
 8030 FORMAT(1X,I2,3X,F10.6,6X,F9.6,6X,F6.4,6X,F6.4,6X,F6.4)
 8025 CONTINUE
      WRITE(2,8035)AELPS,BELPSU,BELPSL
 8035 FORMAT(/,1X,6HAELPS=,F10.6,5X,7HBELPSU=,F10.6,5X,7HBELPSL=,F10.6)
      RETURN
      END
C
```

```
      SUBROUTINE DERIV(I,J,U,V,R,P,DZ2,DZSQ,DY2,DYSQ,DYDZ,UY,
     1VY,RY,PY,UZ,VZ,RZ,PZ,UYY,VYY,RYY,PYY,UZZ,VZZ,RZZ,PZZ,UYZ,VYZ,RYZ,
     2PYZ)
      DIMENSION U(16,27),V(16,27),R(16,27),P(16,27)
      UY=(U(I,J+1)-U(I,J-1))/DY2
      VY=(V(I,J+1)-V(I,J-1))/DY2
      RY=(R(I,J+1)-R(I,J-1))/DY2
      PY=(P(I,J+1)-P(I,J-1))/DY2
      UZ=(U(I+1,J)-U(I-1,J))/DZ2
      VZ=(V(I+1,J)-V(I-1,J))/DZ2
      RZ=(R(I+1,J)-R(I-1,J))/DZ2
      PZ=(P(I+1,J)-P(I-1,J))/DZ2
      UYY=(U(I,J+1)+U(I,J-1)-2.0*U(I,J))/DYSQ
      VYY=(V(I,J+1)+V(I,J-1)-2.0*V(I,J))/DYSQ
      RYY=(R(I,J+1)+R(I,J-1)-2.0*R(I,J))/DYSQ
      PYY=(P(I,J+1)+P(I,J-1)-2.0*P(I,J))/DYSQ
      UZZ=(U(I+1,J)+U(I-1,J)-2.0*U(I,J))/DZSQ
      VZZ=(V(I+1,J)+V(I-1,J)-2.0*V(I,J))/DZSQ
      RZZ=(R(I+1,J)+R(I-1,J)-2.0*R(I,J))/DZSQ
      PZZ=(P(I+1,J)+P(I-1,J)-2.0*P(I,J))/DZSQ
      UYZ=(U(I+1,J+1)-U(I+1,J-1)-U(I-1,J+1)+U(I-1,J-1))/DYDZ
      VYZ=(V(I+1,J+1)-V(I+1,J-1)-V(I-1,J+1)+V(I-1,J-1))/DYDZ
      RYZ=(R(I+1,J+1)-R(I+1,J-1)-R(I-1,J+1)+R(I-1,J-1))/DYDZ
      PYZ=(P(I+1,J+1)-P(I+1,J-1)-P(I-1,J+1)+P(I-1,J-1))/DYDZ
      RETURN
      END
C
      SUBROUTINE BODYA
      COMMON/AAA/BOA(27),BOYA(27),BOYYA(27),YA(27),NNA,XNA,DTHA,SBOA(27)
     1,CBOA(27),NNA1,NA
      COMMON/TTT/THETAA,THETAB,THETAC
      COMMON/ELLIPSE/AELPS,BELPSU,BELPSL
      A=AELPS
      B=BELPSU
      DTHA=(THETAB-THETAA)/XNA
      DO 1 JA=1,NNA
      THETA=(THETAB-THETAA)*YA(JA)+THETAA
      CS=COS(THETA)
      SS=SIN(THETA)
      IF(THETA.GT.3.14159265) B=BELPSL
      DENOM=B*B*CS*CS+A*A*SS*SS
      BOA(JA)=(A*B)/SQRT(DENOM)
      BOYA(JA)=BOA(JA)*CS*SS*(B*B-A*A)/DENOM
      XNUM=3.0*BOYA(JA)*(B*B*CS*SS-A*A*CS*SS)
     1-BOA(JA)*(A*A-B*B)*(CS*CS-SS*SS)
      BOYYA(JA)=XNUM/DENOM
      BBOYA=BOYA(JA)/BOA(JA)
      SBOA(JA)=1.0/SQRT(1.0+BBOYA*BBOYA)
  194 CBOA(JA)=BBOYA*SBOA(JA)
    1 CONTINUE
      RETURN
      END
C
```

```
      SUBROUTINE BODYB
      COMMON/BBB/BOB(27),BOYB(27),BOYYB(27),YB(27),NNB,XNB,DTHB,SBOB(27)
     1,CBOB(27),NB
      COMMON/TTT/THETAA,THETAB,THETAC
      COMMON/ELLIPSE/AELPS,BELPSU,BELPSL
      A=AELPS
      B=BELPSL
      DTHB=(THETAC-THETAB)/XNB
      DO 1 JB=2,NNB
      THETA=(THETAC-THETAB)*YB(JB)+THETAB
      CS=COS(THETA)
      SS=SIN(THETA)
      DENOM=B*B*CS*CS+A*A*SS*SS
      BOB(JB)=(A*B)/SQRT(DENOM)
      BOYB(JB)=BOB(JB)*CS*SS*(B*B-A*A)/DENOM
      XNUM=3.0*BOYB(JB)*(B*B*CS*SS-A*A*CS*SS)
     1-BOB(JB)*(A*A-B*B)*(CS*CS-SS*SS)
      BOYYB(JB)=XNUM/DENOM
      BBOYB=BOYB(JB)/BOB(JB)
      SBOB(JB)=1.0/SQRT(1.0+BBOYB*BBOYB)
      CBOB(JB)=BBOYB*SBOB(JB)
    1 CONTINUE
      RETURN
      END
C
```

```
      SUBROUTINE SIMP(X,Y,NN,AREA)
      DIMENSION X(201),Y(201),AI(201)
      J=1
      N=1
      AI(1)=0.0
  112 N=N+1
      A1=X(J+1)-X(J)
      A2=X(J+2)-X(J+1)
      A3=X(J+2)-X(J)
      B1=Y(J+1)-Y(J)
      B2=Y(J+2)-Y(J+1)
      B3=Y(J+2)-Y(J)
      C1=((((ABS(A3))**2.0))/3.0)*(((B3*A1)-(B1*A3))/((A1*A2)))
      C2=(((ABS(A3))**2.0)/2.0)*((B3/A3)-(((B3*A1)-(B1*A3))/(A1*A2)
      C3=Y(J)*A3
      AI(N)=C1+C2+C3
      AI(N)=AI(N)+AI(N-1)
      J=J+2
      IF((J+2).GT.NN) GO TO 1007
       IF(J-NN)112,1006,1006
 1006 AREA=AI(N)
      GO TO 1008
 1007 AREA=AI(N)+(X(NN)-X(NN-1))*0.5*(Y(NN)+Y(NN-1))
 1008 CONTINUE
      RETURN
      END
****
```